DOCTOR OF PHILOSOPHY

The corrosion protection of aluminium

Roberts, Erica Wyn

Award date:
2008

Awarding institution:
Bangor University

The Corrosion Protection of Aluminium

A thesis presented to the University of Wales Bangor

In candidature of the degree of

Doctor of Philosophy

By

Erica W. Roberts

Prifysgol Cymru • University of Wales

Bangor

Table of Contents

Abstract

This thesis is concerned with the corrosion protection of aluminium. Specifically, it investigates alternatives to chromate containing conversion coatings for aluminium extrusions of alloy 6063, used in architectural applications, and also examines these coatings on sheet alloy 3105.

A huge financial cost is incurred due to corrosion damage each year. Chromate conversion coatings have been applied successfully to aluminium extrusions before subsequent powder coatings for decades, achieving a high standard of corrosion protection and paint adhesion. However the toxic and potentially carcinogenic nature of hexavalent chromium compounds has led to a drive towards environmentally friendly conversion or coating systems.

This thesis discusses the corrosion protection of aluminium, describing the processes undertaken to produce a novel corrosion protection pretreatment. The introduction describes the importance of aluminium, the different alloys types and the classification system, the detrimental effects of corrosion upon aluminium, current protection systems in place, and some of the systems that are being investigated as alternatives.

Chapter 2 looks in detail at two the aluminium alloy types that have been used throughout this thesis, aluminium alloys 3105 and 6063. These are important commercial alloys but their behaviour under etching conditions has been less well studied to date. On this basis, investigations into alloy morphology in the as received condition and following etching prior to the pretreatment step have been carried out.

These have direct consequence to the subsequent application of the chrome-free pretreatment coatings described in Chapter 3 and in later chapters.

Chapter 3 analyses the novel chrome free pretreatments based around a *pseudo*-sol gel process involving the use or zirconium and/or titanium precursors. These initial coatings have been analysed in plan view using SEM/EDX. Selected coatings have also been powder coated, exposed to Lockheed testing and then ultramicrotomed so that cross-sections can be analysed using TEM and EDX. The microscopy data have been compared to ascertain surface coverage and to gain a qualitative understanding of adhesion between the different layers. The addition of polymers to the pretreatments showed an improvement in some of the pretreatments, with the concentration playing an important part. Good surface coverage was obtained with two pretreatments in particular.

Chapter 4 discusses the results of industry-standard, accelerated corrosion testing and adhesion testing for each of the pretreatments described in Chapter 3. The data from Chapters 3 and 4 have then been considered together to try to establish understanding which can be used to develop suitable coatings that may be optimized for commercial use. In agreement with Chapter 3, the addition of polymer showed an improvement in the pretreatment performance. Three of the pretreatments showed excellent corrosion resistance, with two of these also exhibiting excellent adhesion.

In Chapter 5, electrochemistry, academically favoured over the accelerated corrosion testing described in Chapter 4, is utilized to assess the resistance to potential of some of the pretreatments. These data have been considered in the light of the conclusions

drawn in Chapters 3 and 4, and suggests a different mechanism of corrosion protection in the new pretreatments compared to that observed on chrome based systems.

Chapter 6 looks at the development of a novel technique for qualitative screening of potential alloy pretreatments in a short period of time. The aim here is to develop a rapid test which can identify suitable candidates for more detailed corrosion testing and analysis.

Chapter 7 presents the details of all the experimental detail of the research carried out, while Chapter 8 brings together conclusions from the thesis and also discusses future work that stems from this research.

Cydnabyddiaeth / Acknowledgement

Hoffwn fynegi fy niolchgarwch i nifer fawr o bobl sydd wedi fy helpu a'm cefnogi yn ystod cyfnod llunio'r thesis hwn.

I ddechrau, hoffwn ddiolch i Dr Peter Holliman, a fu'n goruchwylio'r thesis hwn yn ddiflino, ac sydd wedi bod yn gefnogaeth fawr. Rwy'n gwerthfawrogi ei amser, ei amynedd, ei sylw i fanylion a'i frwdfrydedd parhaus yn fawr.

Bu Mr Ian Rogers a Mr Brian Tomkins hefyd yn hael iawn eu cefnogaeth, ac yn barod eu cyngor, gan gynnig atebion i broblemau'n barhaus.

Yn ogystal, mae Dr X Zhou, o Ganolfan Diogelu Cyrydiad, Prifysgol Manceinion wedi rhoi o'i amser i lunio'r dadansoddiad TEM a gyflwynwyd yn y thesis hwn, a rhoddodd gefnogaeth a chyngor hefyd. Rwyf hefyd yn ddiolchgar i Geoff Scamans, Innoval Technology, sydd wedi cynnal profion Lockheed testing, ac a fu eto'n ffynhonnell werthfawr iawn o gyngor a chefnogaeth.

Hoffwn ddiolch hefyd i'r grŵp Electrogemeg am gael defnyddio'u hoffer, ac yn benodol i Chris, am eu cymorth, cyngor, amser a'u hamynedd.

Hoffwn ddiolch i'r holl staff technegol, ac yn benodol John Charles, Alan, Mike, Glyn, Kevin, Gwynfor a Dennis, am eu holl gymorth a'u cefnogaeth dros y blynyddoedd, a hefyd i Andrew Davies a John Cambridge am eu cymorth a'u cyngor ar SEM ac AFM. Bu'r merched yn y swyddfa, yn yr Adran Gemeg ac yn Almetron, hefyd yn ffynhonnell

wych o gymorth, felly hefyd fy nghydweithwyr yn Almetron, ac yn benodol Stephen Brown am y profion ASS. Hoffwn ddiolch hefyd i Dr Lorrie Murphy am ei chefnogaeth barhaus.

Diolch hefyd i Almetron a Kawneer am ddefnyddio'u cyfleusterau a rhoi samplau o fetelau a chemegau i mi.

Mae fy nghydweithwyr wedi sicrhau bod y profiad o wneud y gwaith ymchwil hwn yn un gwerthfawr ac maent yn sicr yn ffrindiau bore oes; Alison, Arthur, Bea, Catherine, Connie, Deiniol, Enlli, Iestyn (write up buddy), Kev, Sarah, Max, Mark D, Mark F. Mae fy nheulu a'm ffrindiau hefyd wedi bod yn ffynhonnell gyson o gefnogaeth ac anogaeth.

I gloi, ni fyddai wedi bod yn bosibl i mi wneud y gwaith ymchwil hwn heb gymorth ariannol EPSRC ac Almetron Ltd, ac felly rwy'n ddiolchgar iawn i'r ddau ohonynt.

My gratitude extends to many, many people whom have helped and supported me during this thesis.

Firstly, I would extend my gratitude Dr Peter Holliman, who tirelessly supervised this thesis, and has been a tremendous support. His time, patience, attention to detail, and perpetual enthusiasm are very greatly appreciated.

Mr Ian Rogers and Mr Brian Tomkins, have also been a constant source of support, advice and always have solutions to problems.

In addition, Dr X Zhou, of the Corrosion Protection Center, Manchester University has very kindly given his time to producing the TEM analysis presented in this thesis, and has also provided support and advice. I am also indebted to Geoff Scamans, Innoval Technology, who has conducted the Lockheed testing, and again has been an invaluable source of advice and support.

I would also like to thank the Electrochemistry group for use of equipment, and in particular Chris, for their help, advice, time and patience.

I would like to thank all the technical staff, in particular John Charles, Alan, Mike, Glyn, Kevin, Gwynfor and Dennis, for all their help and support over the years, and also Andrew Davies and John Cambridge for their help and advice on the SEM and AFM. The ladies in the office, both at the Chemistry Dept and Almetron, have also been a great source of help, as have my fellow colleagues at Almetron, in particular Stephen Brown for ASS testing. I would also like Dr Lorrie Murphy for her continued support.

Thanks also go to Almetron and Kawneer for use of facilities and gifting of metal samples and chemicals.

My fellow colleagues have helped make my research such a great experience and have become friends for life; Alison, Arthur, Bea, Catherine, Connie, Deiniol, Enlli, Iestyn (write up buddy), Kev, Sarah, Max, Mark D, Mark F. My family and friends have also been a constant source of support and encouragement.

Finally, this research would not have been possible without the financial support of EPSRC and Almetron Ltd, and therefore I am very grateful to both.

1. Introduction

Aluminium is often called the metal of the future as its properties are exploited for use in an increasing number of functions and its sustainability is realised.[1-4] It is the third most abundant element in the Earth's crust, and is the most abundant metallic material.[5,6] It's use as an economic engineering material began at the end of the 19th century, [7] and it is being employed in more and more applications as further benefits of its use are realised.[4] Some of the commercially desirable properties of aluminium include:

- high thermal and electrical conductivity[8,9] (237 W mK^{-1}, 37×10^6 S m^{-1} at 300 K)[10]
- ease of forming and shaping: aluminium can be cast, rolled, forged and extruded into almost any shape with clean edges, corners and fine detailing and can be joined through methods such as welding, mechanical joining or adhesion[3,11]
- resistance to progressive corrosion: the exposed surface of aluminium reacts with oxygen to form an inert barrier film of aluminium oxide which prevents further oxidation. Unlike iron rust, this film does not flake off to reveal further unreacted metal to oxidise[7]
- impermeability: the thinnest foil, 0.006 mm, forms a 100 % barrier to light, oxygen, moisture, odour and taste[4]
- non toxic and colourless corrosion products:[9,12] the aluminium oxide layer formed on the surface of aluminium is colourless, transparent and also non toxic
- reflectivity:[8] aluminium efficiently reflects radiant energy, visible light, radiant heat, and electromagnetic waves, or can be treated to be reflective or absorbing[7]
- magnetic neutrality:[8,9] important in the electrical and electronic industries
- suitability for recycling

However, aluminium's greatest commercial advantage is its strength to weight ratio of its alloys. A variety of physical and mechanical properties can developed ranging from high purity to complex alloys, with more than 300 alloy compositions commonly recognized.[7] These properties make aluminium particularly suitable to many applications, encompassing architectural and structural applications, beverage and food packaging, chemical equipment, aerospace and increasingly the automotive industry, resulting in it being one of the most utilised metals in the world.[13]

Additionally, aluminium has a capacity to be formed and cast by virtually all known processes, common examples being rolling, extrusion, pressure die, gravity die, pressure mold, impactings and sintering.[7] Certain alloys are particularly suitable for extruding, which is used to produce complex seamless configurations, used extensively in architectural applications which are finished with a powder coating, Figure 1.1.

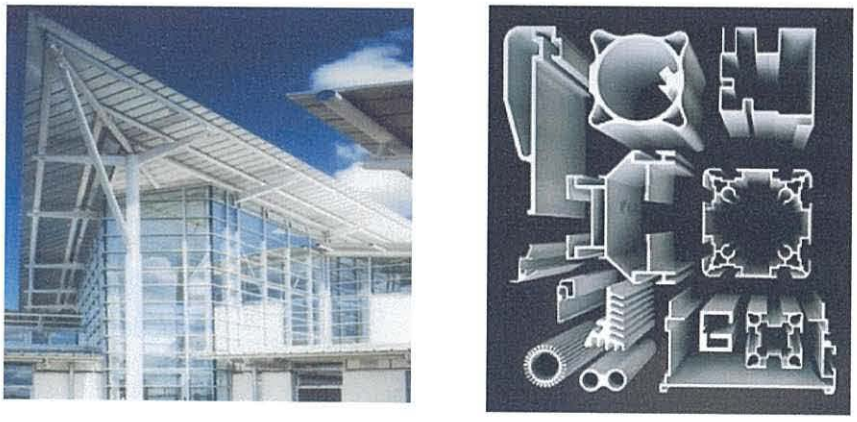

Figure 1.1 Examples of aluminium use[13,14]

Aluminium is often powder coated;[15] this is a type of paint that is applied for aesthetic purposes, and also to apply a barrier type coating which prevents corrosion when intact. Powder coating is a specialist process utilising an electrostatic spraying system to apply a colour-stable powder to metal components which are subsequently heat cured.[16] The technology provides a single coat of paint which is hard, stable, durable and which is

chemically bonded to the surface. However, adhesion relies on correct pretreatment of the metal.[13] The powder coatings generally consist of resins – polyester being most widely used in architectural applications, as well as pigments and various additives, and a great advantage is that no solvents are involved.[17] The powders are thermosetting, fusing into a continuous film upon curing at *ca.* 200 °C for up to 30 min, to provide a coating 40-150 μm in thickness.[17]

The powder coatings are available in a large range of colours, shades and gloss levels.[13] Aesthetic appearance is an important requirement for architectural applications, with a minimum expectation of 25 years without any impairment to the surface appearance. Several organisations, e.g. Qualicoat, have been established who set comprehensive quality requirements and technical specifications relating to the quality of lacquering, painting and coating on aluminium and its alloys for architectural applications. Suppliers of coating systems who meet these criteria are awarded "approval" from these organisations, which is recognised as a label of quality worldwide, and gains the confidence of industry.

The 6063 alloy is widely used for architectural extrusions, as it provides good extrudability and a high quality surface finish. It is produced in standard and custom architectural shapes, and also tube and pipe forms.

Almetron Ltd, whom are sponsoring this study, specialise in pretreatments for AA6063, and as such the focus of this research will be aimed at this alloy. This thesis describes studies using the extruded 6063 alloy and also sheet alloy 3105 which is of greater purity than the 6063 alloy. This will enable assessment of novel pretreatments with surface impurities being a much reduced variable. It should be noted that the industrial

co-sponsor of this EPSRC CASE award (Almetron) have been awarded Qualicoat approval for their current chromate pretreatment system and hence any novel chromate-free system aimed at the architectural industry developed in this thesis would also need to satisfy the Qualicoat criteria, to demonstrate the quality of product to industry. The requirements of gaining approval involve passing a number of tests including the acetic acid salt spray weathering test, and adhesion tests, which will be discussed further in Chapter 4.

Production of Aluminium

Aluminium's primary ore is bauxite, which is composed of hydrated aluminium oxides which make up a number of different minerals.[5,8] Bauxite deposits are produced through the weathering of rocks where surface water has caused leaching of the more soluble compounds such as the alkalis, silica, lime and magnesia, leaving minerals containing aluminium and iron, which are less soluble, as residues.[5] Bauxite consists of three main minerals; gibbsite, α $Al_2O_3.3H_2O$, boehmite, α $Al_2O_3.H_2O$, and diaspore, β $Al_2O_3.3H_2O$. In general, the aluminium oxide content of bauxite ranges from around 30 to 55 %, and it is believed that the reserves of bauxite are sufficient to last for several hundred years at the current production rate.[5]

Production of aluminium oxide is from bauxite by means of the Bayer Process.[5] Bauxite is ground to powder before being purified by dissolving in sodium hydroxide and reprecipitated using carbon dioxide.[6] Aluminium hydrates dissolve in the hot sodium hydroxide, leaving behind impurities such as iron oxide and titanium oxide. Unfortunately, the presence of silica can lead to sodium alumino-silicate precipitates causing yield losses, which makes ores with over 7 % silica uneconomic.[5,11,18] The

aluminium containing solution is then filtered and cooled before being calcined at 1000-1100 °C to drive off the water of the trihydrate to produce Al_2O_3.[5]

The aluminium oxide is then dissolved in cryolite (Na_3AlF_6) at 800-1000 °C in an electrolytic cell or 'pot' according to the Hall-Heroult process.[6] The electrolytic cell is lined with carbon, which forms the cathode, and a carbon anode is lowered into the aluminium oxide/cryolite electrolyte. Electrical current flows between the cathode and anode, producing molten aluminium at the cathode. The process can be represented by the following simplified overall reaction:

$$4Al^{3+} + 3O^{2-} + 3C \longrightarrow 4Al + 3CO_2\,(g)$$

In general, approximately four tonnes of bauxite produce approximately two tonnes of alumina, which yields one tonne of aluminium.[5]

Recycling

Although the production of aluminium is highly energy intensive and costly, (around 13 kWh / kg) its low melting point (660° C) means that the re-melting process requires typically 5 % of the original energy investment.[5,19] Aluminium's resistance to corrosion also enables it to retain a high metal value after use. Indeed, the recycling of aluminium dates back to 1908, driven by the need to reduce the unit price and make aluminium competitive compared for instance with steel.[8]

The processing of scrap aluminium results in virtually 100 % recovery. However, end-of-life material is both recycling infrastructure and product sensitive. For instance, aluminium can recycling rates vary from a few percent to almost 80 % in different European countries, whilst aluminium foil is almost unrecoverable.[5] Whilst it has been estimated that 70 % of aluminium is recycled in total, this quantity is only sufficient to

meet 30 % of today's demand,[7] and consequently current aluminium production rates remain high.

Red mud is the term for the waste generated during the processing of bauxite. This waste material has been studied for a wide field of application for catalytic reactions such as hydrogenation, hydroliquefaction, oxidation, etc.[20] It consists of a mixture of compounds originally present in the bauxite and those introduced during the Bayer process, with ferric oxide (Fe_2O_3) generally being the major constituent which gives it its characteristic brick red colour.

Aluminium's capacity as a recyclable material is an environmentally positive attribute, and many of its applications have derived from reduced energy consumption benefits, which are becoming increasingly important in the drive towards becoming more energy efficient.[21] It is one of the few metals which has sufficient abundance to last several hundred years and which is also suitable for a sustainable society,[7] which is a further distinct advantage of the use of aluminium.

Alloys

In its pure state, aluminium is a relatively soft and ductile metal, which tends to self anneal and lose strength.[8] It has a yield strength of 34.5 MPa and a tensile strength of 90 MPa (compared with structural steel which has a yield strength of 250 MPa and tensile strength of 400 MPa). However, these properties can be greatly enhanced by alloying with other treatments and using heat treatments. For example, the high strength alloy used for aircraft, 7075, has a yield strength of 57 MPa and a tensile strength of 490 MPa.[8] It is this capacity, together with its light density (2.69 g/cm^3) which is one third that of steel (7.83 g/cm^3),[5,8] that gives aluminium a high weight to strength ratio.

Alloys may be cast or wrought. Cast alloys are cast directly to final or near final form without any mechanical treatment, while wrought alloys may be cast as ingot or billet and then worked mechanically by a process such as rolling, extrusion, forging or cast to final form.[13,22,23] The wrought alloys may be divided into those which may be hardened and strengthened by mechanical working alone, and those which may be heat treated.[12] Work hardening involves deformation at room or slightly elevated temperatures, whilst solution heat treatment involves soaking of the metal at temperatures between 450°C and 550°C, followed by quenching, and then ageing at temperatures between 20°C and 175°C.[23] The alloys 6063 and 3105 are both wrought; AA6063 is typically extruded whilst AA3105 is rolled into sheets.

Copper, magnesium, silicon, manganese, zinc, nickel, and chromium are the main elements used in aluminium alloys.[24] A designation system is used to classify the various alloys into groups, initially according the principal alloying elements, denoted by the first digit,[22] e.g. series 1xxx represents the commercially pure aluminium series. The second digit refers to a particular variation of the alloy (where this is zero there is no variation).[5] In the case of wrought alloys, the third and fourth digits are of no significance but are unique to the alloy. Series 1xxx ranges from AA1100, which is > 99.00 % aluminium, to the purer AA1175, which is > 99.75 % aluminium. The document Aluminium Alloy, Selection and Applications,[22] describes the alloy designation system in further detail, and discusses the various types, properties and characteristics of the aluminium alloys. A brief summary of this information relating to the wrought alloys is presented to demonstrate the benefits of the alloying elements. However, in the context of corrosion, these additional impurities can also cause significant problems.

As described above, commercially pure aluminium alloys (> 99.00% minimum aluminium) form the 1xxx series and these alloys show high formability, corrosion resistance and electrical conductivity. Their key benefits are extremely high corrosion resistance, formability and electrical conductivity, and typical applications would be foil and strip for packaging, electrical applications, chemical equipment, truck bodies and sheet metal work. Although they may be strain hardened, they are not heat treatable and have low strength.

Alloy, %		**1xxx**	**1350**
Si		.006-.7	.1
Fe		.006-.7	.4
Cu		.006-.1	.05
Mn		.002-.05	.01
Mg		.006-.05	-
Cr		<.03	.01
Ni		-	-
Zn		.006-.1	.05
Ti		.002-.03	.03
Ga		<.03	.03
V		.05	
Specified other elements		B <.05	B .05, V+Ti .02
Unspecified Others	Each	<.03	.03
	Total	<.05	10
Al min		99.00	99.50

Table 1.1 Composition of the 1xxx series aluminium alloy and selected example AA1350. Alloy 1350 is used is electrical applications as it has low impurities, and impurities may affect conductivity

In the 2xxx series, copper is used to increase the strength of the alloys. Toughness, and in some alloys, weldability, are also benefits, however poor corrosion resistance results in the need for painting or cladding. These alloys are used in the aircraft and transportation applications.

The alloys of the 3xxx series are used in the bodies of beverage cans. The addition of manganese to this alloy results in a strain hardenable, corrosion resistant material suitable for welding, brazing, and soldering. They are used in heat transfer applications, packaging and equipment for food, chemicals, and building, and roofing. The aluminium alloy 3105 is typically produced in sheet form for roofing and exhibits high filiform corrosion resistance.[25] In this thesis, the development of a chromate-free corrosion protection system will be described for alloy 3105.

Alloy, %		**2xxx**	**2014**
Si		.1-1.3	.5-1.2
Fe		.12-1.2	.70
Cu		1-6.8	3.9-5.0
Mn		.05-1.3	.40-1.2
Mg		.02-1.8	.20-0.8
Cr		<.02	.10
Ni		<2.3	-
Zn		.1-.8	.25
Ti		.02-.3	.15
Ga		<.05	
V		.15	
Specified other elements		Bi, Pb, Sn Zr	Zr + Ti .2
Unspecified Others	Each	<.1	.05
	Total	<.15	.15
Al min		rem	99.50

Table 1.2 Composition of the 2xxx series aluminium alloy and selected example AA2014. Aircraft internal structure includes extrusions and plate of 2xxx and 7xxx alloys like 2024, 2124 and 2618. rem refers to the remainder of the alloy composition

Alloy, %		3xxx	3105
Si		.08-1.8	.60
Fe		.1-.80	.70
Cu		05-.50	.30
Mn		.05-1.3	.3-.8
Mg		.05-1.8	.20-0.8
Cr		<.4	.20
Ni		<.05	-
Zn		.05-10	.40
Ti		.03-.10	.10
Ga		<.05	-
V		<.05	-
Specified other elements		Zr Be	
Unspecified Others	Each	0.5	0.5
	Total	<.15	<.15
Al min		rem	rem

Table 1.3 Composition of the 3xxx series aluminium alloy and selected example AA3105. Alloy 3105 is used in roofing

Good flow characteristics afforded by high silicon content make the 4xxx series suitable for complex shaped forgings such as aircraft pistons, and weld wires.

Alloy, %		4xxx	4043
Si		.08-13.5	4.5-6
Fe		.09-1	.8
Cu		.1-4.7	.30
Mn		.03-1.3	.05
Mg		.05-2	-
Cr		<.2	-
Ni		<1.3 .05-.25	-
Zn		.05-.25	.1
Ti		.04-.2	.2
Ga		-	-
V		-	-
Specified other elements		Be Bi Co Cd	.0003 max Be
Unspecified Others	Each	0.5	0.05
	Total	<.15	<.15
Al min		rem	rem

Table 1.4 Composition of the 4xxx series aluminium alloy and selected example AA4043. Alloy 4043 is one of the most widely used weld wires

The 5xxx series exhibit excellent corrosion resistance, even in salt water, due to their low manganese content.[26] Their high magnesium content gives moderate strength and high toughness down to cryogenic temperatures, and they are readily welded by a variety of techniques, resulting in a wide application in building and construction, automotive, cryogenic and marine applications. Increasing magnesium content results in higher strength, however care must be taken with alloys of greater than 3 % magnesium content where the alloys are exposed to continuous exposure of above 100°C, as susceptibility to stress corrosion cracking may occur.[22]

Alloy, %		**5xxx**	**5083**
Si		.08-.70	.40-.7
Fe		.10-.8	.40
Cu		.03-.25	.10
Mn		.01-1.2	.40-.10
Mg		.02-5.6	4.0-4.9
Cr		.03-.35	.05-.25
Ni		<.05	-
Zn		05-2.8	.25
Ti		.04-.2	.15
Ga		<.05	-
V		<.05	-
Specified other elements		Be Zr Mn Cr	-
Unspecified Others	Each	0.5	.05
	Total	.10-.15	.15
Al min		rem	rem

Table 1.5 Composition of the 5xxx series aluminium alloy and selected example AA5083. Alloy 5083 is one of the higher strength alloys, with a higher Mg content

Alloy, %		6xxx	6063
Si		.20-1.8	.20-.6
Fe		.08-1.0	.35
Cu		.03-1.2	.10
Mn		.03-1.0	.10
Mg		.35-1.5	.45-.9
Cr		.03-.35	-
Ni		<.20	-
Zn		.03-2.4	0.5
Ti		.08-.2	.10
Ga		-	-
V		<.20	-
Specified other elements		Bi Zr Pb	-
Unspecified Others	Each	0.5	.05
	Total	.10-.15	.15
Al min		rem	rem

Table 1.6 Composition of the 6xxx series aluminium alloy and selected example AA6063. Alloy 6063 is one of the first choice alloys for architectural and structural members

A unique feature of the 6xxx series is their extrudability, which coupled with their high strength, makes them particularly suitable for load bearing architectural and structural applications. These alloys contain both magnesium and silicon, are heat treatable and exhibit good corrosion resistance. As well as providing good extrudability alloy 6063 can be heat treated, resulting good resistance to general corrosion and stress corrosion cracking.[7] In this thesis, the development of a chromate-free corrosion protection system will be described for alloy AA6063.

The 7xxx series contain zinc and provide the highest strength of the Al-Zn-Mg-Cu alloys and are used in the aerospace and automotive industry. They are not considered weldable and hence are riveted. They do not exhibit good corrosion resistance and as such are normally coated or used in Alclad®. Alclad® is a trademark of Alcoa used as a generic term to describe aluminium sheet formed from high-purity aluminium surface layers, metallurgically bonded to high strength aluminium alloy core material. These sheets commonly used by the aircraft industry.[27]

Alloy, %		7xxx	7075
Si		.10-.6	.40
Fe		.10-.7	.6
Cu		.05-2.6	1.2-2.0
Mn		.02-.8	.30
Mg		.10-3.7	2.1-2.9
Cr		.04-.35	.18-.28
Ni		<.03	-
Zn		.08-8.7	5.1-6.1
Ti		.03-.2	.20
Ga		<.03	-
V		<.05	-
Specified other elements		Zr Pb Ag	Zr Bi Sn
Unspecified Others	Each	0.03-.05	.05
	Total	.10-.15	.15
Al min		rem	rem

Table 1.7 Composition of the 7xxx series aluminium alloy and selected example AA7075. Alloy 7075 is one of the principle alloys used for aircraft structures

The lesser used alloying elements are classified within the 8xxx series, and include iron, nickel, and lithium. Iron and nickel add strength without impairing the electrical conductivity, whilst lithium is added for exceptional strength and modulus.

Alloy, %		8xxx	8017
Si		.03-1.1	.10
Fe		.15-2.0	.55-.8
Cu		.005-2.2	.10-.20
Mn		<.01	-
Mg		.02-1.4	.01-.05
Cr		<.20	-
Ni		<1.3	-
Zn		.03-1.8	.05
Ti		<.07	-
Ga		<.03	-
V		<.05	-
Specified other elements		B Li Zr Sn	.04 B, .003 Li
Unspecified Others	Each	.02-.05	.03
	Total	.10-.15	.10
Al min		rem	rem

Table 1.8 Composition of the 8xxx series aluminium alloy and selected example AA8017. Alloy 8017 is used for conductors

Natural Corrosion Resistance

The term 'corrosion' derives from the Latin word '*rodere*', which means 'to gnaw' in the context of rats, and 'corrodere' meaning 'to gnaw to pieces'.[28] Although the term is commonly mistaken to mean rust, which is the product of the corrosion of iron, it is a largely destructive phenomenon that is suffered by the majority most metals.[28] The cost of corrosion in the UK alone exceeds £2,000 million and, in addition to financial costs, corrosion can be inconvenient, dangerous, and wasteful as it weakens structures making them unsafe, in need of monitoring, and requiring eventual replacement.

In their natural state most metals are found chemically combined with oxygen or other elements as ores.[29] This is a result of thermodynamic laws, which state that high energy states favour lower energy states.[29] The ores are generally of lower energy states than the chemically pure metal, and in order to separate a pure metal from its ores, a large amount of energy is required, as discussed in the production of aluminium. It is this tendency to recombine with species in the environment (most usually atmospheric oxygen) that, along with the thermodynamic driving forces, leads to corrosion, oxidizing the metal into a cation, through an electrochemical reaction. The reactions are spontaneous in the thermodynamic sense.

In this context aluminium is thermodynamically active and has a high affinity for oxygen, resulting in a thin oxide layer of Al_2O_3 forming on its surface instantly.[6,8,9,28] This, in itself, can be considered a corrosion process. However, the oxide layer is thermodynamically stable, and also acts as a barrier to further species in the environment, Figure 1.2.

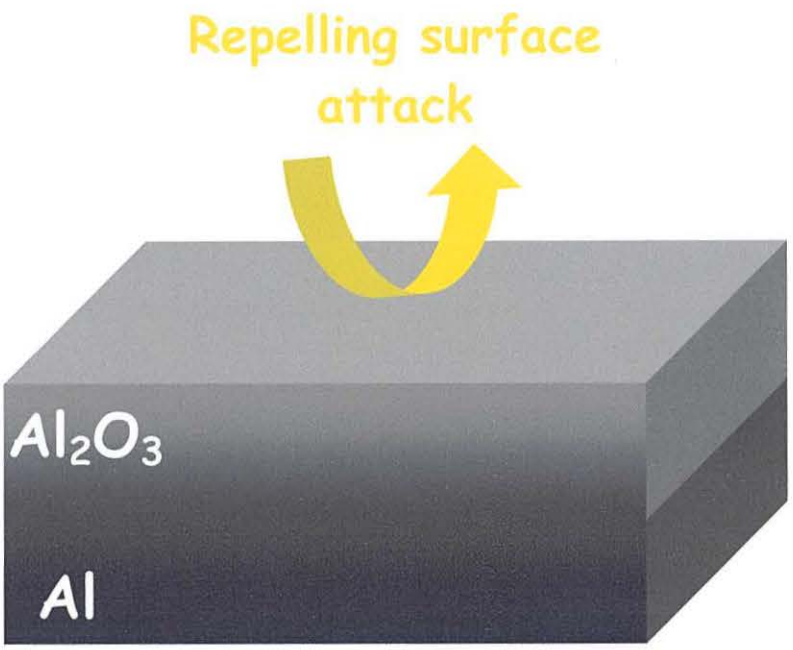

Figure 1.2 The oxide film acts as a barrier against the environment, protecting against corrosion

Most metals undergo similar processes that render them less susceptible to further corrosion, and this process is termed passivation. For instance, steel is made stainless by alloying with chromium which forms chromium oxide on the surface,[29-32] and titanium forms titanium oxide which is a very protective oxide film.[33-35] However, when iron corrodes to form rust, the discoloured corrosion product is permeable to air and water, allowing the metal to continue to corrode, even after a surface layer of rust has formed. With sufficient hydration, the iron can eventually convert entirely to rust and disintegrate.[36] Some metals do not corrode under normal conditions, such as gold. In this case, the reaction with water and oxygen to form $Au(OH)_3$ would not be a spontaneous reaction.[29] Thus, the overall energy state would not decrease.

Oxidation of exposed aluminium is effectively instantaneous and the thickness of the resulting oxide coating is *ca.* 1 nm thick (10 Å),[37] and is colourless and transparent. In

normal atmospheres, the coating will grow to between 20 and 200 nm thick and is composed of two layers, an inner continuous and compact, amorphous oxide layer, and a thicker, more permeable, porous outer layer of hydrated oxide.[37] The inner oxide coating is referred as the "barrier layer" and it's thickness is determined solely by temperature; in dry air it would be the only coating formed. In the presence of moisture, the oxide is hydrated.

The oxide film controls the rate of corrosion and protects the substrate metal. However, corrosion is very rapid if the film is damaged. This can result from mechanical rupture or from chemical attack from ions such as chloride.[23] Repair of the damaged coating is instant in most cases, and is accompanied by oxygen reduction or hydrogen evolution depending on the moisture content of the environment.

Evidence suggests that flaws can exist in the oxide film, which act as nucleation sites for film breakdown. In solution, these reports suggest that further flaws develop and are repassivated, but the presence of aggressive ions hinders the repassivation step, allowing pits to nucleate.[23]

Aluminium oxide also exhibits amphoteric behaviour, and is susceptible to both acids and alkalis. In acid solutions of pH less than 4 or alkaline solutions with pH greater than 10 the oxide layer dissolves. This exposes the aluminium metal which react to produce $[Al(OH_2)_6]^{3+}$ in acid, and $[Al(OH)_4]^-$ in alkali.[38] The Pourbaix Diagram illustrates aluminium behaves at different pH and potential values, Figure 1.3.

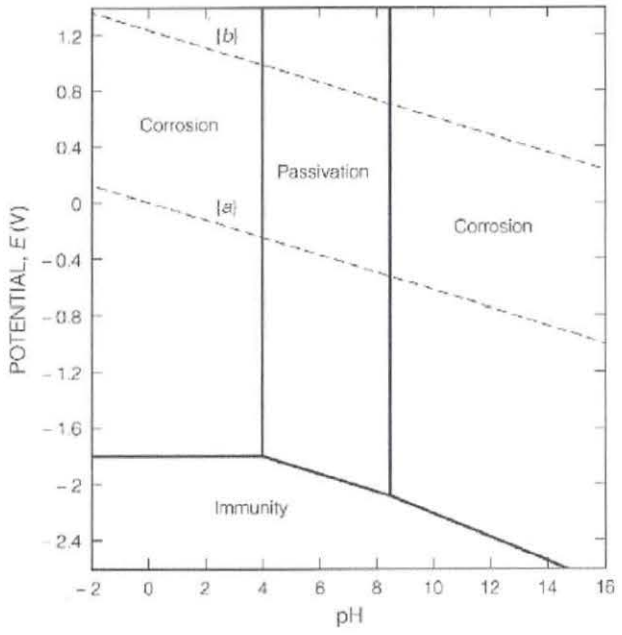

Figure 1.3 The Pourbaix Diagram for aluminium indicating the pH and potential values where corrosion and passivation occur for aluminium

Factors affecting Corrosion

The purification of aluminium involves solidification from a melt, in which the metal atoms are loosely packed in random order. During solidification, the atoms begin to become ordered. At a given temperature, an ordered arrangement is formed, which is accompanied by a release of energy called the latent heat of fusion.[39] In pure metals, this release of energy will maintain a constant temperature within the metal for the duration of the solidification process, compensating for the natural susceptibility of the system to cool down to the temperature of the surroundings.

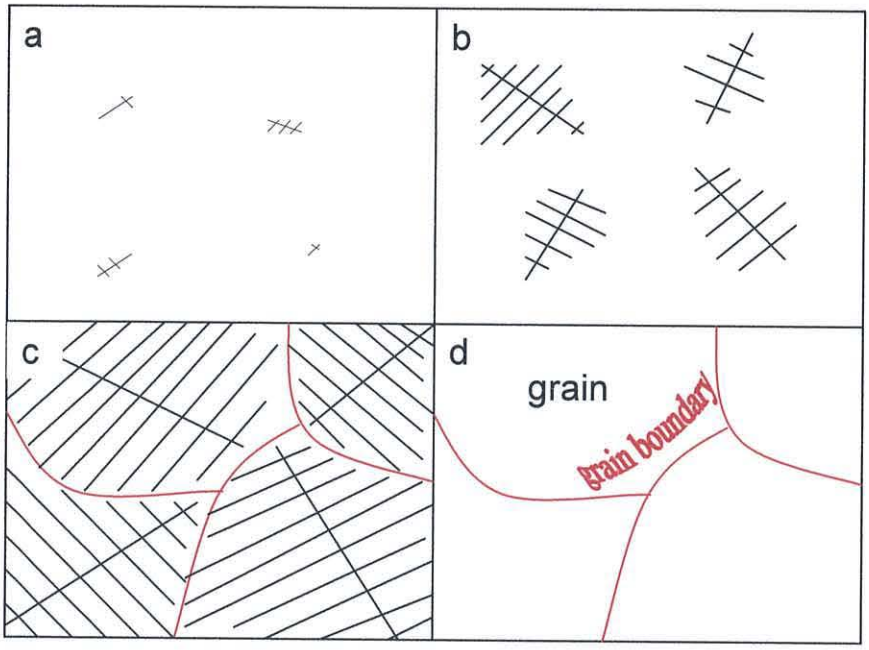

Figure 1.4 Solidification showing dentric growth: a) nucleation of crystals in the melt, b) growth of crystals into dentrites, c) complete solidification, final grain structure redrawn from [28,39]

The cooling process causes nucleation sites within the liquid, Figure 1.4a. The rate of cooling can affect the number of crystals that nucleate, rapid cooling causing many sites, and thus more grain boundaries, and more potential corrosion sites, whilst slow cooling produces a few slow growing crystals. Upon formation of a crystal, further solidification will develop to form an array, Figure 1.4b. The rate of cooling is faster from the corners of the crystal than the edges, and faster from the edges than faces. Growth will therefore develop from the corners into branches termed dentrites, the braches developing with solid material as growth from the edges and faces eventually draw near. The orientation of the dentrites at this stage is random. When their growth has developed to the extent that they meet other dentrites, movement becomes restricted, fixing the random orientations. The remaining liquid between the branches then solidifies, cooling continuing in the solid state, Figure 1.4c. When in the solid state, the crystals are referred to as grains, and area between different grains the grain

boundary, Figure 1.4d, which is less thermodynamically and electrochemically stable than the lattice sites. As the rate of cooling affects the size of the crystals and hence the size of the grains it is significant in determining the mechanical properties and affects the corrosion process.

In addition, dislocations can result from the rolling process, which are defined as defects either within or between the crystal lattices of individual crystallites. These tend to occur in arrays varying from subgrains with ragged boundaries, to high density configurations of 'forests' and slip bands.[39] The 3xxx and 5xxx series alloys are the main work hardening alloy groups, whilst the 2xxx, 6xxx, and 7xxx series are heat treatable alloys.[23] Both dislocations and grain boundaries are cathodic with respect to the surrounding matrix due to accumulations of impurities.[40]

Although aluminium and its alloys exhibit relatively good corrosion resistance, localised forms of corrosion can occur, and the addition of alloying elements serve to decrease aluminium's resistance to corrosion. Whilst magnesium has little effect, copper lowers the resistance more than the other elements.[23] Thus, the addition of alloying elements and any alloy processing can have significant effects on the corrosion behaviour of that material. For instance, during the soaking process of solution heat treatment the alloying elements are taken into solid solution and then partly released during ageing. The matter released remains consistent with the matrix, with the exception of the grain boundary, and strengthens the alloy. Prolonged or raised temperature ageing can result in break down of this consistency, which decreases strength. The ageing process is more advanced at the grain boundary, causing precipitation of incoherent particles.

Types of Corrosion

The types and severity of corrosion attack are dependent upon the type and aggressiveness of the environment, and the chemical and metallurgical structure of the aluminium. pH, temperature, dissolved oxygen levels, flow rates and pollutants are all determining factors, and damage may only be apparent years after corrosion is initiated.[41-44] Primary corrosion mechanisms which apply to all aluminium alloys include general corrosion; bimetallic or galvanic corrosion; localised attack such as grain boundary attack, dealloying, exfoliation, pitting, crevice attack, corrosion fatigue; and flow induced corrosion such as erosion, impingement, fretting.

The corrosion mechanisms causing greatest concern in the field of aluminium are described as follows. Corrosion of pure aluminium in the passive range as defined by the Pourbaix Diagram to be between pH 4 and 8.5, is localised, and is evident by the random formation of pits. This is the most common form of corrosion in natural environments.[23] It is believed that the initiation of these corrosion processes occur at various sites at the aluminium surface where there are defects in the oxide film,[42,45] the corrosion resulting in a roughened and less reflective surface caused by the development of numerous pits.[43] Pitting corrosion is most commonly produced by attack from halide ions, in particular chloride, in the open air. This is because, in the presence of oxygen, aluminium in halide solutions is readily polarised to its pitting potential, which is the potential in a particular solution above which pits initiate. In aluminium, the corrosion reaches a limiting value, which is well established and can be predicted.

Intergranular or intercrystalline corrosion is a selective attack of grain boundaries and immediately adjacent areas without attack of the grains themselves. It occurs due to the precipitation of alloying elements, which causes the grain boundary to be less

thermodynamically and electrochemically stable than at perfect lattice sites, giving rise to accelerated attack at these more vulnerable sites.[23,46] In high strength aluminium used for aircraft, such as the 7xxx series, material strength is determined by controlling the precipitates both at the grain boundaries and within the grain. Thus, $CuAl_2$ and $FeAl_3$ are common precipitates which are cathodic to the surrounding metal, compared to Mg_5Al_8 and $MgZn_3$ which are anodic.[46] The presence of such intermetallics creates minute localized galvanic cells when an electrolyte is present. Corrosion may then occur where, if the intermetallic is cathodic, the surrounding metal is attacked, or if anodic, the intermetallics dissolve to leave a porous metal. By comparison, the 6xxx series generally resist this type of corrosion, and when it does occur in this alloy series it is no more severe than pitting corrosion, however, it is involved in stress corrosion cracking in some alloys.[37] This is due to their composition, with copper limited to small amounts, and the magnesium and silicon contents balanced to form Mg_2Si, which has a negligible effect on electrode potential.

An insidious form of corrosion attack on aluminium is that of stress corrosion. This is the propagation of intergranular cracking of a material whilst elastically loaded at stress concentrations. Stress corrosion requires a combination of residual or applied tensile stress, a corrosive environment (particularly containing chloride ions), and a directional microstructure allowing easy crack propagation. Al-Cu, Al-Mg, Al-Zn-Mg and Al-Li alloys are sensitive to this type of corrosion.[17,37]

Stress also plays a part in exfoliation, or Lamellar, corrosion, which is another hazardous form of attack as large amounts of metal can be destroyed. In this case, corrosion proceeds along grain boundaries parallel to the metal surface, the resulting corrosion product creating sufficient stress to force open the intervening material. This

type of corrosion is most likely to occur with Al-Cu and Al-Zn-Mg-Cu alloys in marine environments but is also found in most heat treatable alloys and in work hardening Al-Mn and Al-Mg alloys, but is contained through the fabrication process.[17]

Filiform corrosion

Filiform corrosion occurs under protective coatings[47] and it is the primary corrosion mechanism for powder coated aluminium.[48] It resembles worm like filaments that travel under the paint, lifting it off, in some cases with the appearance of white corrosion products and blistering.[49,50]

It has been reported that the initiation of the filiform attack is at coating defects or cut edges[47,51] enabling attack of the underlying aluminium, with occurring linearly, predominantly in the working direction.[23] Most cases occur near the sea and mainly at joints and fabrications, with the main controlling parameters being water permeability and elasticity of the coating, oxygen diffusion paths, presence of salts, and substrate chemical composition.[15,47,49,52]

Filiform corrosion does not weaken or destroy metallic components.[52] It affects only the surface appearance, causing loss of paint adhesion and degradation of visual appearance, and as a result is considered a cosmetic type of attack.[47,48,51] However, it is a major obstacle in the architectural, aircraft and automotive industry and remains an important commercial issue. Whilst filiform corrosion is almost unheard of in the UK in the context of architectural aluminium, a number of incidents have been recorded in work carried out by mainland European processors,[13] with a number of issues on painted architectural extrusions and sheet reported in Northern Europe in the 1990's.[23] Although the precise cause in unknown, it is possible that its prevention of this type of

corrosion could be related to the degree of etching prior to the application of the conversion coating. For instance, the typical etch rate in the UK is 50 g/m^2, as opposed to 2 g/m^2 in Europe where predominantly different pretreatments are used.[53] Thermo-mechanical processing also has contributing effects toward filiform corrosion, with heat treatment resulting in enhanced secondary precipitation of intermetallic particles on alloy 3005, and described as the main contributing factor to the observed poor filiform corrosion.[15,49,54,55] By comparison, good corrosion resistance was obtained by removing the surface layer of metal, either by etching or mechanical polishing.

Corrosion Protection

In architectural applications the appearance of the aluminium is expected to survive several years without any impairment and with little maintenance, and in most cases a surface finish is applied which has a dual function; to provide a decorative finish, and to also improve the corrosion resistance of the substrate.

For aesthetic and cosmetic reasons, the finish is one of the most important visual elements of any building.[13] Aluminium and its alloys are frequently used where durability and low maintenance are desirable. A failure can lead not only to deterioration of appearance, but also high costs. Anodising and powder coating are two of the most widely used processes for enhancing corrosion protection, and are also used to impart coloured or textured finishes. Anodising is an electrolytic process that deposits a chemically stable oxide layer on the surface of the aluminium, sometimes referred to as anodic oxidation.[13]

Anodising is an electrolytic process that is commercially unique to aluminium, resulting in a thickened oxide layer, by a factor more than one thousand,[5] and which can also be coloured.[56-61]

Another common surface treatment of aluminium is the formation of a conversion coating. This process has been considered as a controlled corrosion process to give a superficial layer of substrate metal oxides, chromates, phosphates or other compounds that are chemically bonded to the surface. This layer protects the substrate from corrosion by acting as an insulating barrier of low solubility between the metal surface and the environment and/or by containing corrosion inhibiting compounds.[62]

Conversion coatings are characterized by direct participation of the metal through the reaction of the external atomic layers with anions of suitably selected medium occurs through an intricate process involving electrochemical, physiochemical and chemical reactions, simplified by the following equation:

$$mM + nA^{z-} \longrightarrow M_mA_n + nze$$ [62]

where

M = metal reaction with medium

A = the medium anion.

Conversion coatings have found extensive applications, for example as lubricants in cold working metals, decreasing friction and allowing the application of higher loads,[62] but their main use is for the purpose of corrosion protection and improved adhesion of a subsequent organic layer, typically a powder coating, Figure 1.5. Corrosion protection of aluminium and its alloys by conversion coatings dates back to the 1920's.[62]

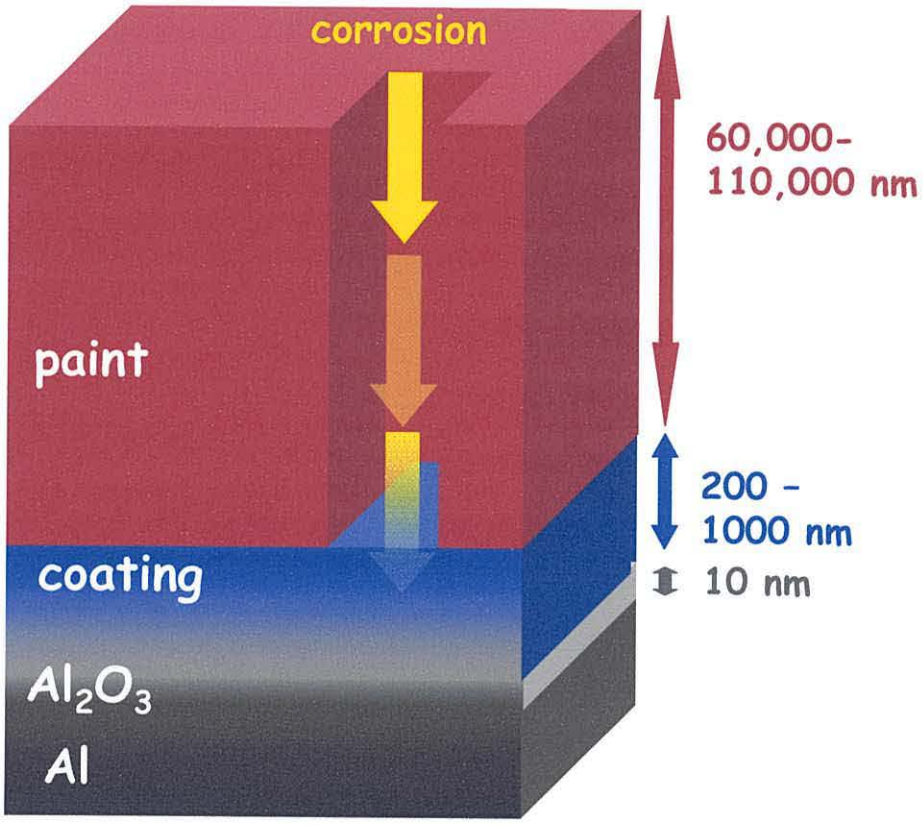

Figure 1.5 Schematic of the main components of an aluminium surface which has been subjected to a conversion coating followed by powder coating

Generally, chromate conversion coatings are considered to give the best improvement in corrosion behaviour of the aluminium alloys and, for instance, it is only films formed in chromate solutions which meet the stringent corrosion resistance requirements of the military specifications MIL-C-81706.[56,63] The chromate conversion coatings provide the advantages of good paint adhesion, low cost, and ease of application, and are the most widely used conversion coatings for aluminium surfaces prior to painting.[64] However, the production, storage, and application of chromate solutions cause significant environmental and health related problems, as they contain hexavalent chromium compounds that have several toxic effects and are potential carcinogens.[56,63] These problems, along with changes in legislation, have lead to the need to develop

chromium free systems, which are less hazardous and which are environmentally friendly. This has in resulted in a great interest in understanding the effective chromate system, in order to apply and/or develop the science to new coatings. Therefore, the development of a chromium-free system for aluminium is essential and is the subject of this PhD.

Chromates

Chromate conversion coatings on aluminium are amorphous.[40] Such coatings are produced from acidic solutions containing hexavalent chromium and fluoride. It is generally accepted that the structure of the resulting coating can be sub-divided into three parts: the outer or external surface, bulk coating, and interface region between the bulk and the alloy. The bulk layer is relatively thick and porous, composed of spheres with a diameter of the order of tens of nanometers. It has large defects and is nonuniform, and has a morphology resembling the cracking of mud on the micrometer level Chapter 3, Figure 3.72, Figure 3.74.[40,65] By comparison, reports of the intact inner layer, which is believed to consist of aluminium oxyfluoride where fluoride is present, is thin and dense and acts as a barrier.[66,67]

It is believed that the mechanism of the chromate conversion coating involves destabilisation of the passive aluminium oxide film by fluoride, until electron tunnelling is possible,[40] Figure 1.6. When the aluminium comes in contact with an acid environment a chemical attack of the oxide, followed by an electrochemical attack of the aluminium, takes place.[63] In the presence of halogen acids this results in severe corrosion due to formation of soluble compounds:

$$2Al^{0} + 6H^{+} \rightarrow 2Al^{3+} + 3H_2 \qquad \textbf{Equation 1.1}$$

$$Al^{3+} + 3F^{-} \rightarrow AlF_3 \qquad \textbf{Equation 1.2}$$

$$Al^{3+} + 6F^{-} \rightarrow AlF_6^{3-} \qquad \textbf{Equation 1.3}$$

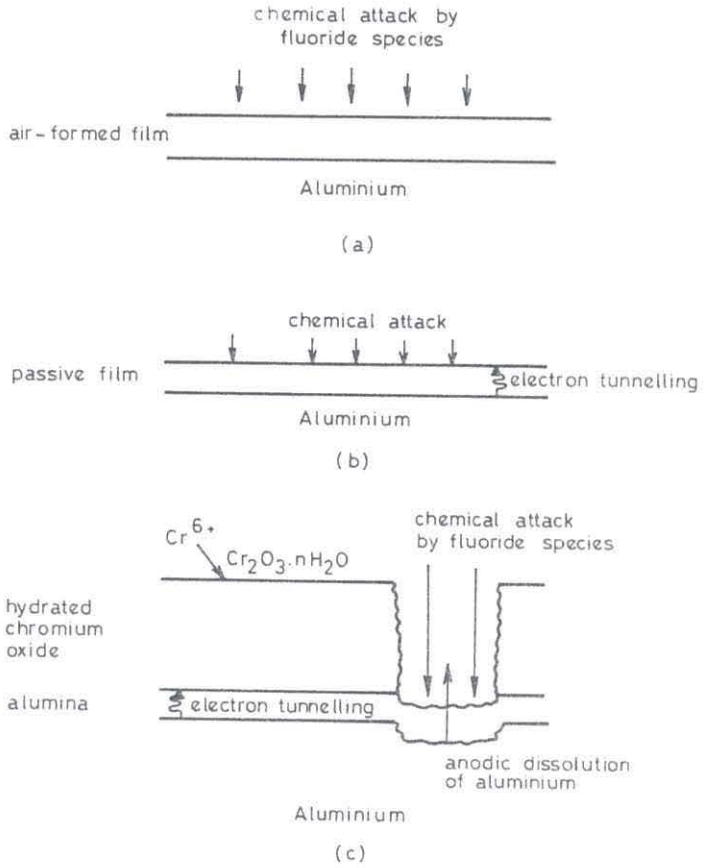

Figure 1.6 Schematic diagram of the development of the chromate conversion coating on high purity aluminium.[66]

In a chromate conversion coating, these steps are followed by reduction of the chromate by the exposed aluminium, to produce a chromate containing coating. It has been reported that the hydration state and speciation of the resulting chromium species can vary with conditions and is not clearly understood. Some possibilities include chromium hydroxide, and a hydrated chromium oxide gel.[40,68,69]

$$Cr_2O_7^{2+} + 2Al^0 + 8H^+ \rightarrow 2Cr(OH)_3 \downarrow + 2AlOOH \downarrow \quad \textbf{Equation 1.4}$$

$$Cr_2O_7^{2+} + 2Al^0 + 2H^+ + H_2O \rightarrow 2CrOOH \downarrow + 2AlOOH \downarrow \quad \textbf{Equation 1.5}$$

The AlOOH which is believed to be produced as a by-product of chromate reduction can be dissolved by HF, allowing further reaction of Cr^{6+} at the aluminium interface, resulting on further deposition of chromate.[40]

Based on a combination of open circuit potential measurements and surface analysis techniques one theory for the mechanism of the coating formation has been proposed to take place in three stages: activation of the surface, initiation of the coating formation, and growth of the conversion layer.[65] This mechanism suggests that, during activation the aluminium oxide film is partially dissolved by the fluoride, leading to an increase in electron tunnelling probability and electric field, and enabling the migration of Al^{3+} ions. This step was described as rate determining and dependant on both the initial oxide thickness and bath composition, both determining the morphology and structure of the conversion layer. It was also suggested that dissolution of the aluminium oxide film is fundamental to both the nucleation and subsequent growth of the chromate conversion coating.[65]

The reduction of the chromate takes place in the next step, and nucleation is brought about by the resulting increase in Cr^{3+} concentration and pH between the bulk solution and aluminium surface, with supersaturation enabling precipitation of the chromate species.[65] Again, this step is dependant on the initial oxide thickness and bath composition. Growth of the film develops through changes in the location of precipitation sites, and is a porous layer consisting of small spherical particles, with

aluminium dissolution and Cr^{6+} reduction still occurring through this film and depositing further chromate. This process has been studied and found to be initially a linear function of time, Figure 1.7.[65] The role of fluoride has again been found to be important here for continued dissolution of aluminium. For instance, without the addition of NaF to a chromium phosphate conversion bath, a non-uniform distribution of chromium and phosphate on top of the oxide layer was observed, but no chromium phosphate conversion layer.[70]

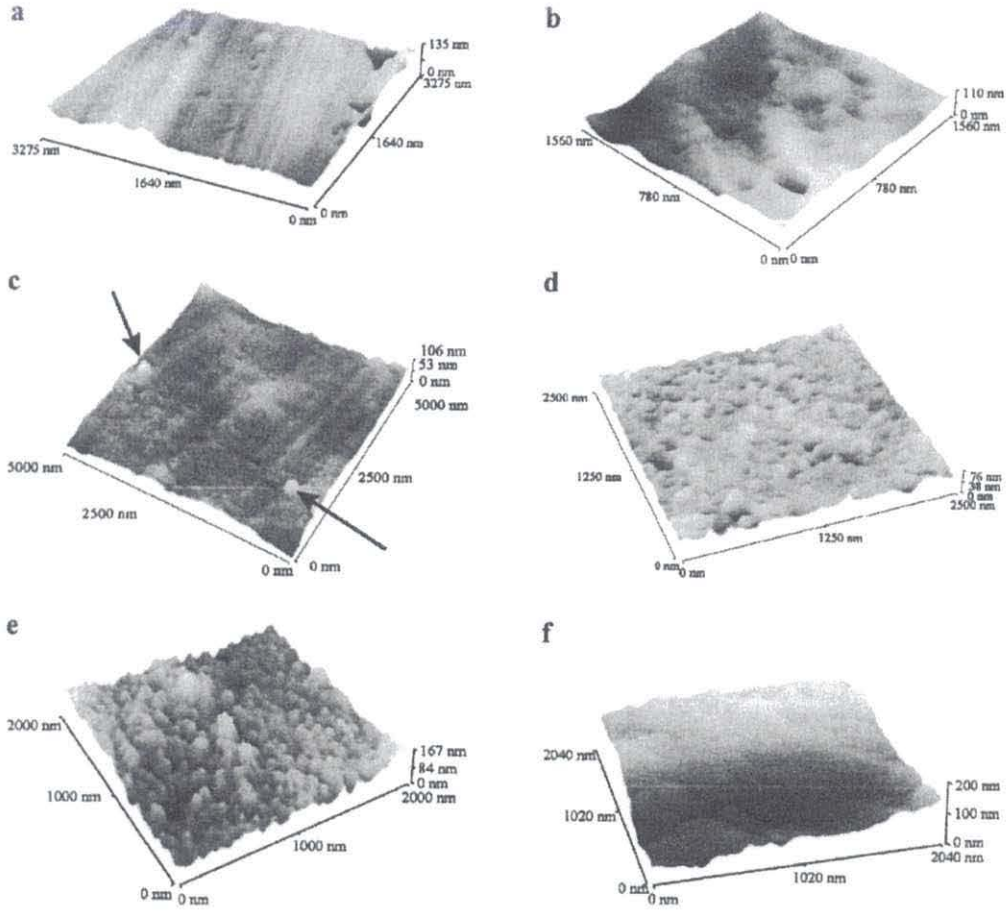

Figure 1.7 AFM topographic images for a) uncoated AA1050, and coated AA1050 in a solution of 0.03 M chromium oxide for immersion times of b) 2, c) 5, d) 12, e) 30, f) 60 seconds. The arrows indicate deposits, attributed to the precipitation of chromium hydroxide/oxide[65]

A sol-gel perspective has also been considered alongside the above theory. In this case, the nucleation, through hydrolysis and condensation of the chromium ions are believed to form polymeric species, which then develop into to colloidal particles and eventually coagulate to form a gel.[65]

A different view for the mechanism of chromate coating formation considers the cathodic flaw sites of the aluminium grain, dependent on the purity or pretreatment of the substrate.[66] Thus, these workers have considered the case of relatively pure aluminium (99.98 %) and have described it as comprising of a cellular structure, developed through solidification. Where the cellular structure intersects the surface, impurities such as iron, silicon and copper, are described to concentrate locally, providing preferred cathodic sites for the reduction of Cr^{6+}. Following this, deposits are thought to spread from these cathodic flaw sites until the surface is covered by the conversion coating, which prevents Al^{3+} egression and the continued anodic reaction, terminating the growth of the coating which is non-uniform and dependent on the orientation of the aluminium grain.

By comparison, these workers have described that on high purity aluminium (99.99967 %) there is no preferential growth and the coating is relatively uniform with occasional random holes where the chromium containing material is absent, Figure 1.8.[66] This is reported to be due to the absence of cathodic sites on the high purity aluminium. Thus, in this case, the coating proceeds by growing at sites where electron tunnelling is increasingly probable due to dissolution by fluoride where the local aluminium oxide coating is thinnest due to local fluctuations.

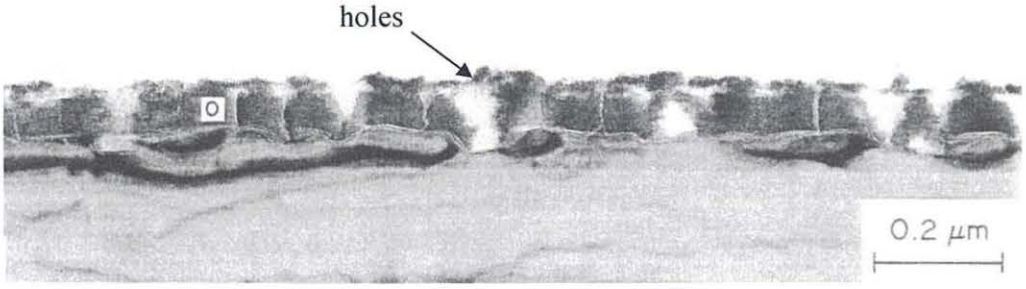

Figure 1.8 TEM of ultramicrotomed sections of high-purity aluminium and attached conversion coating[66]

Continuing with this mechanism, it has been stated that, as the coating development, and hence the cathodic area, increases, so does the potential of the specimen surface, which in turn is balanced by local thickening of the oxide at uncoated regions, resulting in less or negligible tunnelling of electrons, and therefore uncoated areas. As such these areas act as fixed anodic sites during the coating growth, where growth of aluminium oxide, and its subsequent dissolution by fluoride takes place to produce pitting. Here, the probability of electron tunnelling decreases, and coating deposition is hindered, resulting in the afore mentioned holes.[66]

Interestingly, EDX analysis of ultramicrotomed sections[66] and XPS measurements[40] indicated the presence of only chromium and oxygen within the conversion coating. The absence of aluminium and fluoride suggests that the dissolution of aluminium through the already formed conversion coating is unlikely, supporting the proposed mechanism of deposition of chromate due to reduction of Cr^{6+} by electron tunnelling,[66] which is evidence against theories suggesting that aluminium ions diffuse through the coating to the coating-solution interface, where the reduction of dichromate and dissolution of aluminium proceed concurrently.

The preparation of a substrate prior to coating is also reported to be key in affecting the nucleation and growth of the conversion coating and therefore the associated protective properties.[63] Etching the surface increases the surface area which can improve adhesion by providing a mechanical keying action. It has been reported there is significant correlation between surface micro roughness and adhesion, and therefore corrosion resistance.[71] The increase in surface area was also reported to also lead to the formation of a denser conversion coating resulting in improved protection.

Knudsen *et al.* have also studied the etching process and have stated that the type of etching process undertaken can also affect the reactivity of the surface, whereby samples of aluminium pretreated with different procedures showed significant differences in microstructure and morphology. [63] For instance, an extra step consisting of immersion in nitric–hydrofluoric acid solution for 30 s carried out after immersion in sulfuric–phosphoric acid solution resulted in a more etched, but less reactive surface. These workers ascribed this to the removal of a large amount of cathodic sites, mainly related to Al_Fe_Si precipitates present in the clad, Figure 1.9. A similar effect, but on a smaller scale, was noted with increased time of immersion in sulphuric–phosphoric acid solution. It has been stated that the removal of these cathodic sites gives rise to a more homogeneous nucleation of the chromate conversion coating on the surface of the aluminium, resulting in a denser, less porous chromate film with fewer defects which is more protective, Figure 1.10.[67] The surface preparation will be discussed further in Chapter 2.

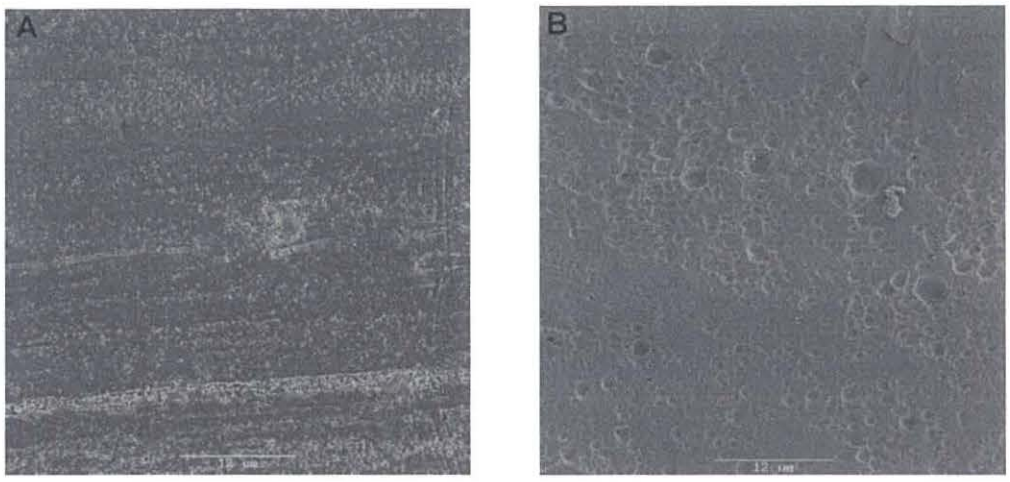

Figure 1.9 SEM micrographs A: sample treated 5 min in the H_3PO_4–H_2SO_4 solution, B: sample treated 5 min in the H_3PO_4–H_2SO_4 solution and 30 s in the HNO_3–HF solution (2000×magnification)[63]

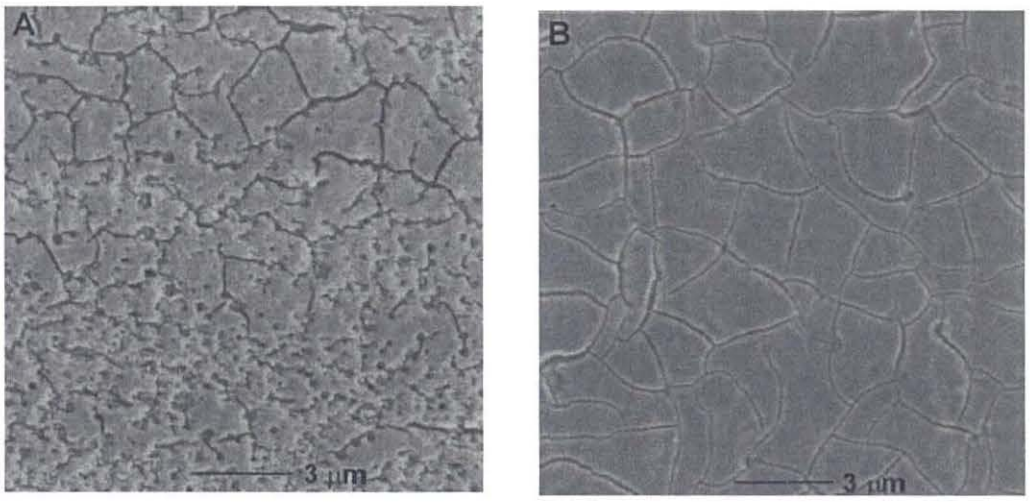

Figure 1.10 SEM micrographs of different pretreatments after chromating. A: sample treated 5 min in the H_3PO4–H_2SO_4 solution, B: sample treated 5 min in the H_3PO4–H_2SO_4 solution and 30 s in the HNO_3–HF solution (2000× magnification)[63]

Ion beam analysis (Rutherford backscattering, elastic recoil detection), XPS and AES were performed on a chromate coating by Yu *et al*[72] and these workers suggested that the major component of the coating is γ-CrOOH.*n*H2O. They also stated that this phase underwent structural transformation at 310°C to Cr_2O_3. Evidence of Cr^{6+} was only found on the outer layer, which is in agreement with Hughes, Taylor and Hinton,[40] who

found the external surface to consist of 70 % chromium hydroxide and 6 % chromate, and the bulk of the coating to consist of both Cr_2O_3 and CrOOH (by XPS and SEM). XANES conducted by Lytle *et al* on the surface layer of a chromate coating found 23% Cr^{6+} in tetrahedral coordination, with the remaining chromium as Cr^{3+} in octahedral coordination.[73] These workers found that the corresponding EXAFS analysis, to find the Cr-O coordination, was in agreement with this determination.

Proposed mechanisms for the corrosion protection offered by the chromate conversion coating include an increase in the electrical resistance of the coating, or blocking of pores and/or dynamic repair of newly created breaks and defects in the film.[74] The latter would involve the reduction of Cr^{6+} to Cr^{3+} in the event of coating damage, a theory supported by the minimal corrosion of chromated panels during salt spray testing, which involves a scribe through the coating to the metal substrate. Currently, this is one of the widely accepted mechanisms of the chromate conversion coating's corrosion protection, known as the "self healing" ability of the chromate.

To investigate the corrosion protection offered by chromate coatings, Zhao *et al* [74] conducted experiments using coated and uncoated specimens, separated by a 1.8 mm thick layer of 0.1 M NaCl. After 96 h hours, a lack of significant corrosion on the uncoated, sandwiched against a chromate coating alloy was observed, with only a few pits formed, while in the control experiment, with two uncoated specimens, severe pitting and general corrosion was exhibited. Samples prepared in a similar manner were investigated by XPS, which indicated the presence of both chromium and fluoride on the previously uncoated specimens, which had been sandwiched against a chromate coating, demonstrating that chromium in some from had migrated from the coated specimen to the uncoated one. In support of this assertion, the pits formed in these

samples contained product which gave Raman spectra similar to that of the chromate conversion coating. Overall it was concluded that chromate was released from the coating into the salt solution and that this was able to migrate to protect a neighbouring region of exposed or unprotected alloy. Furthermore, there seemed to be evidence that the mobility of the Cr^{6+} species in aqueous solution is selective for corrosion sites, accumulating at susceptible areas. Thus the chromate, or its reduction product, was desribed as an effective cathodic passivator that inhibits the rate of cathodic reaction.

SEM investigations of chromated panels subjected to salt spray testing (SST) revealed that the panels generally appeared the same as before being subjected to the salt spray, with a few small pits in some samples.[66] Before salt spray testing the edges of the "cracked mud" type morphology were sharp. However, these became smoothed and thinned following dissolution by the SST, *ca.* 500 Å of the surface being eroded away (2000 Å to 1 μm originally). Aluminium and other elements, previously undetected in the surface layer, were detected by XPS after SST. XANES spectra revealed that the effect of SST was to decrease the amount of total Cr and Cr^{6+} in the surface and total layer, with as little as ~7 % of Cr^{6+} remaining in tetrahedral coordination in the surface layer. Considerable Cr^{6+} was reduced to Cr^{3+}, and considerable Cr^{3+} removed from the oxide layer. Auger analysis was in agreement with these findings. It was concluded that the chromium stabilised surface oxide on aluminium is a very dynamic system which responds to its environment, and that the mobility of the chromium ions could be due to partial hydration, and that the presence of the water of hydration is essential for the protective activity of chromium. The results were believed to be consistent with a model previously described, in which Cr^{6+} is reduced to Cr^{3+} upon contact with metallic aluminium and then form a hydrated chromium oxide layer. The remaining Cr^{6+} in the layer acts as a reservoir against further exposure of bare aluminium, where it would

react with the aluminium and form a plug of hydrated Cr_2O_3 in the flaw to prevent further attack.

Tan, Bailey and Kinsella[69] also suggested that the presence of water is required for protection of aluminium by chromate. They stated that there is no intact barrier film, but that the porous chromate layer becomes protective only after ageing in the environment. This was based on electrochemical noise resistance findings which showed that corrosion rates of treated species were similar to those of untreated specimens at the very beginning of exposure tests, but dropped significantly with time suggesting some form of surface change and enhancement of corrosion protection during exposure to the corrosive environment. Ageing treatment also lowered corrosion rates and provided better protection during extended exposure, Figure 1.11.

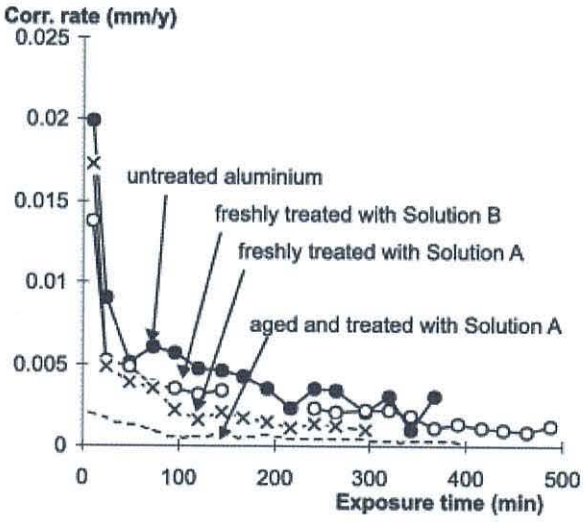

Figure 1.11 Exposure tests of untreated, freshly treated and aged aluminium electrodes in 0.1 M NaCl solution Solution A is a commercial chrome oxide treatment, solution B, a commercial chrome phosphate treatment[69]

The explanation put forward by Tan, Bailey and Kinsella discusses the possibility that an initial porous corrosion product layer forms, and upon exposure to air, a water layer forms due to the capillary action of the pores, Figure 1.12. Corrosion inhibitors in the

coating are then believed to dissolve in the water layer to form an inhibiting film. The results support the theory that chromate conversion coating formation is not simply a solution process, but more likely involves enhancement during exposure to the environment. Alternatively, the anodic pores sites become covered by a corrosion inhibiting substance during the ageing period due to migration of a Cr^{6+} species to pore sites and subsequent blocking of corrosion.

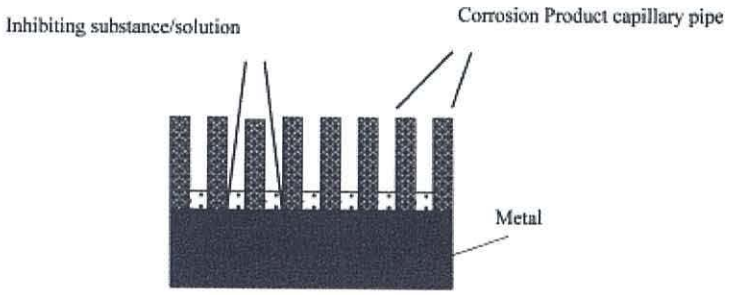

Figure 1.12 A model showing the mechanism of corrosion protection by a porous CCC film[69]

Electrochemical measurements by Hughes, Taylor and Hinton[40] also indicated an improvement in corrosion protection by ageing the chromate conversion coating. Improvements were observed during the first 40 hours of ageing, which was in laboratory air, 55 % humidity, 20°C. After this the coating deteriorated, and at 165 hours the performance approached that of an untreated sample.[40] SEM of the coated surfaces also indicated changes during ageing. Isolated cracks in a fresh coating developed into a continuous network, with the aged sample showing much more texture. From XPS analysis, it was proposed that this was due to dehydration of the coating.[40] The eventual deterioration of the coating was attributed to the limited Cr^{6+} ions available to repair the growing network of cracks in the process in which plugs of hydrated chromium oxide form at the base of the cracks.

In summary, it is generally accepted that the deposition of chromate proceeds through the reduction of Cr^{6+} to Cr^{3+} either at cathodic sites of impurities, or at areas of reduced aluminium oxide thickness where electron tunnelling is possible. Although the exact composition of the conversion layer formed is not known there is evidence to support the presence of Cr^{6+} species which is believed to be responsible for the corrosion protection of aluminium, even during coating damage. This protection is often called the "self healing" ability. Associated with this, there is evidence that the Cr^{6+} species is mobile in aqueous solutions, and is selective for corrosion sites, accumulating at susceptible areas,[74] and also evidence of a reduced amount of Cr^{6+} and increase in Cr^{3+} during exposure to corrosive environments.[66] Thus, part of the reason for the difficulty in assessing a precise composition for the chromate coating is that it has been shown to be an highly dynamic structure which ages upon exposure to different environmental conditions. Ageing treatments show improved corrosion protection, and explanations put forward suggest the need for water to be present for a protective layer to form, either to fill the porous layer with a film[69] or to form a hydrated chromium oxide layer.[66] The presence of water may also be required for the migration of Cr^{6+} - mobile in aqueous solutions - to defects in the initially formed coating, such as the holes in the coating mentioned by Brown *et al.*[66]

Chrome Free Systems

There are several chrome free coatings discussed in literature or presented in patents which have been developed with varying success, although some may not strictly be considered as true conversion coatings. They include coatings based on the group IVB metals, rare earth metals, phosphates, oxyanion analogues, cobalt, hydrated metal salts, lithium inhibited hydrotalcites, lubricating oils, silanes and titanates, and self assembling molecules.[75] Typically, in these chrome free systems, inorganic molecules

react with the oxidised aluminium surface in some manner to form mixed oxides which can act as a barrier to corrosion. It has been suggested that because titanium and zirconium prefer hexavalent coordination in aqueous solution, and the 4+ oxidation state in general, that this makes them ideal adhesion promoters, as two valences remain after forming the mixed aluminium/titanium or aluminium/zirconium oxide.[76] It has further been suggested that molybdates, vandates and silicates are film forming oxides which should also cover the surface and improve adhesion. In addition, in attempts to mimic the "self-healing" properties of the chromate coating, it was suggested that other metals may able to oxidize the metal surface following coating damage and reproduce the chromate system. Considering organic materials, it has been suggested that polymers with a high capacity for aluminium surfaces block active surface centres and cover the surface with a thin organic coating. However, more recent trends in the development of chrome-free coatings for aluminium have tended to use a mixture of organic and inorganic treatments and additions to provide more than one type of protection, such as a zirconium based system combined with a sealant polymer, Figure 1.13, or cerium with molybdenum.[75] In these cases, the inorganic additions have been reported to protect the substrate in the event of a breakdown in the coating, e.g. by the reduction of Mo^{6+} during anodic attack, whilst the corresponding organic additions are reported to strengthen the metal/paint interface, increase resistance of the interface to hydration and under film corrosion, and improve adhesion of the paint. Within this, developments in polymer technology, usually based on acrylic acid copolymers (as opposed to homopolymers) have been reported to have led to consistent paint adhesion properties and greater bath stability.[75]

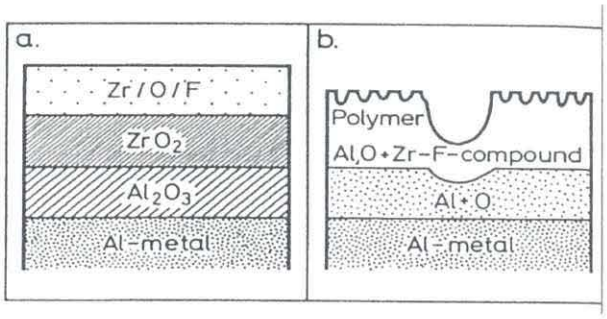

Figure 1.13 Proposed models of the layer structures of the zirconium based conversion layers a) without and b) with a polymer compound[75]

It is also worth noting that cleaning requirements for the substrate are often more rigorous with non-chrome coatings.[75] This is because the chromate bath is oxidising, and therefore contributes somewhat to the surface preparation of the substrate, i.e. the bath is etching as well as depositing. Some of the non-chrome coatings which do not act as oxidizing agents do not have this ability, and therefore adequate surface preparation is of greater importance. The control parameters are also often more complex, as there are no simple measurements to verify depletion of the coating bath. Chrome based systems require only a titration against ammonium iron (II) sulfate to ensure chromate levels are within specified limits, and use of a fluoride meter to confirm fluoride levels. But, for one commercial chrome free silane treatment for example, bath control is carried out by monitoring bath pH and an acid/base titration to determine alkaline silane concentration.[77] However actual silane concentration can only be determined by ICP. Also, an additional benefit of the chromate based system is that the coating deposited is coloured, and the coating can be visualised. Thus, problems can be identified as soon as the coating has dried. Chrome coating weights should also be around 1 g/m^2 which can be measured for a 0.1 x 0.1 m panel. Silane coating weight would need to be quantified by XRF.

The pretreatment bath is one of many in the process of treating the aluminium. For instance, for an acid etch process there are typically five baths required – etch, rinse, chromate, rinse, rinse (rinse meaning a water bath) – and seven to ten for an alkaline etch (desmut and a warm rinse are also required after an alkaline etch). A simplified schematic of these two processes is presented in Chapter 2, Figure 2.1. As a result "no-rinse" or "dried in place" processes, where the application of a coating is followed immediately by dry off with no rinsing, have also been developed in the drive for more environmentally friendly systems. Their main benefits are reduced water consumption and treatment, and reduced floor space as a result of a reduction in the number of baths. The coil coating industry have achieved virtually 100 % coating chemical utilisation by using roll coaters to apply the coating, or a squeegee to remove excess chemical applied by spray or immersion.[75] However, these techniques are often not suitable for aluminium extrusions due to their frequently complex shapes. Most non-rinse products have two components; an inorganic component to react with the aluminium surface and form what is termed "a non-reactive" corrosion resistant layer, and an organic compound to form a film (frequently a polymer) which will improve adhesion by forming a bond with the paint. The resulting coating is typically clear and of 0.1 to 0.27 g m^{-2} in weight, with coatings in excess of this showing poor adhesion, and those short providing inadequate protection.

Self Assembling Molecules

Self assembling molecules (SAM) are described by Chemetall GmbH, an industry leader, as aqueous solutions of bifunctional organic molecules corresponding to the general formula $X\text{-}(CH_2)_n\text{-}Y$.[77] It is reported that they can form a strong Al-O-P bond with a functional group, X, which has a high affinity to the activated surface, both anchoring and aligning themselves perpendicular to the substrate whilst a second

functional group, Y, has a correspondingly high affinity to the paint system. It has been suggested that SAMs can provide excellent corrosion results in combination with paint, however, thorough cleaning and several rinse steps are reported to be required, possibly to prevent contamination of the SAM bath.[77] An emphasis on subsequent painting for effective protection suggests that problems may become apparent if paint damage occurs, such as filiform corrosion. This hypothesis is supported by Knudsen, Bjørgum, and Tanem,[48] whom conducted a comparative study of chrome, anodizing and chrome free processes including SAM, cerate and zirconium/titanium systems, Figure 1.14. To investigate filiform corrosion, corrosion was initiated by putting droplets of hydrochloric acid (16 % wt) into a scribe on the powder coating for 1-2 minutes, before placing samples in a climate cabinet. These workers reported that all process gave good resistance to filiform corrosion when a powder coating with good adhesion properties (superior paint quality) was applied. However, none of the chrome free systems gave comparable results to chromating and anodising, which provide resistance through the conversion coating itself regardless of the powder coating. As adhesion promoters rather than corrosion resistive coatings, SAM coatings can only improve corrosion resistance through strengthening the adhesion of the organic coating. They do not provide corrosion resistance themselves, but act to improve the adhesion of the subsequent paint coating, relying on this paint coating to provide protection.

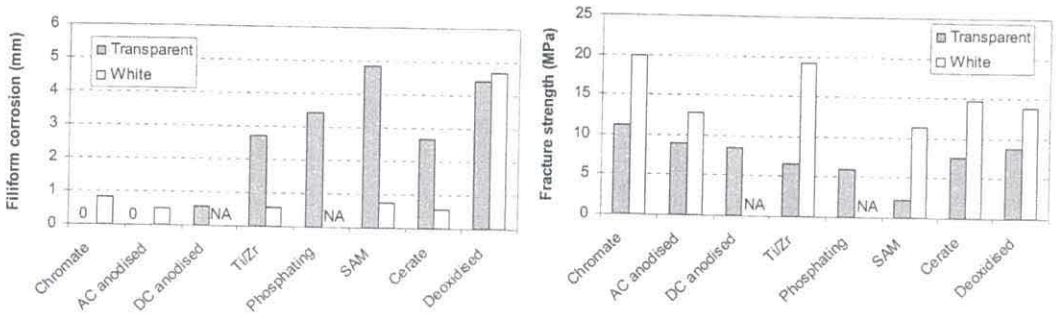

Figure 1.14 Filiform corrosion and fracture strength data for a range of treatments: chromate, anodised – ac and dc, titanium and zirconium based treatment, phosphate, SAM, cerate, and deoxidised, using both white and transparent paint[48]

Cerate

A cerate containing process gave better adhesion results and better filiform resistance than the SAM in the same tests by Knudsen, Bjørgum, and Tanem.[48] However, performance was poor compared to chromate with the inferior, transparent, powder coating. Cerate bath solutions generally consist of three components; Ce^{3+} salt, a mineral acid, and peroxide.[75] An accelerator is also sometimes required. Several electrochemical or redox reactions are reported to take place when aluminium is placed in this solution, resulting in the reduction of the peroxide and protons, oxidation of aluminium and cerium, and thus dissolution of Al to Al^{3+} and formation of Ce^{4+}.[77] An increase in pH also leads to the formation and subsequent precipitation of aluminium and cerium hydroxide, and an overall coating consisting of Al^{3+}/Ce^{4+} hydroxide/oxide is produced, with a yellow colour caused by the Ce^{4+}.

$$2Al \rightarrow 2Al^{3+} + 6e^- \qquad \textbf{Equation 1.6}$$

$$O_2 + 2H_2O + 2e^- \rightarrow H_2O_2 + 2OH^- \qquad \textbf{Equation 1.7}$$

$$2Ce^{3+} + 2OH^- + H_2O_2 \rightarrow 2Ce(OH)_2^{2+} \qquad \textbf{Equation 1.8}$$

$$2Ce(OH)_2^{2+} + 4OH^- \rightarrow 2CeO_2 + 4H_2O \qquad \textbf{Equation 1.9}$$

$$2Ce^{3+} + 4OH^- + O_2 + 2e^- \rightarrow 2CeO_2 + 2H_2O \qquad \textbf{Equation 1.10}[78]$$

SEM analysis has been reported which has shown a cerium rich (species not specified) homogeneous surface film with some isolated cracks and local changes in morphology. At high magnification, the coating was reported to have an amorphous appearance.[79] The same workers stated that XPS depth profiling indicated a coating thickness of 0.1 to 0.2 μm which was suggested to be possibly bilayered, with a cerium rich layer over a hydrated aluminium oxide layer.

In a different study, the corrosion protection afforded by the cerate coating was believed to be the result of suppression of the cathodic oxygen reduction reaction, by a cerium oxide barrier preventing either oxygen to, or electrons from, the metal, resulting in the delay of the overall corrosion rate.[79,80] The preparation of the surface with a sulphuric acid solution of Ce^{4+}, termed a "deoxidation" was found to be critical in the performance of the coating,[81] as was an additional sealing by immersion in a silicate layer, which improved performance in a salt spray test (ASTM B-117), and although the requirements of the test were exceeded, performance was not as good as a chromate comparison.[79]

Another approach has been reported which used an acidic "seeded" etch containing cerium chloride heptahydrate, coupled with a post etch treatment of immersion in deionised water at 90-95°C for five minutes prior to the cerium containing conversion coating.[82] This post etch treatment was reported to have changed the surface morphology, the surface pits appearing smoother with rounder surface features. The cerium was also claimed to have been chemically altered, with the Ce^{3+}/ Ce^{4+} in a ratio of 10:1 after post etch treatment, compared to 1:8 without.

Cerium–molybdenum coatings are also reported to give good corrosion protection, and a more uniform distribution of cerium was obtained following a post-heat treatment given to such coatings.[78] However, with all the cerate based treatments there is a very narrow operating scope for the pH, which is required to be between 1.9 and 2.2. In addition, particular cleaning steps must be performed to prevent pitting.

Zirconium and Titanium

Many alternatives to chromate processes use titanium and/or zirconium oxide based systems, some incorporating a polymer to promote adhesion of the subsequent paint layer. Preferential nucleation and growth was found on and around α-Al(Fe,Mn)Si particles (AA6060 model analogues were made from aluminium and alloying elements, one with the specific particles grown from melts) from an acidic fluorotitanate/-zirconate based solution, but complete coverage was not obtained, Figure 1.15, Figure 1.16.[83] These surface particles were reported to act as local cathodes.

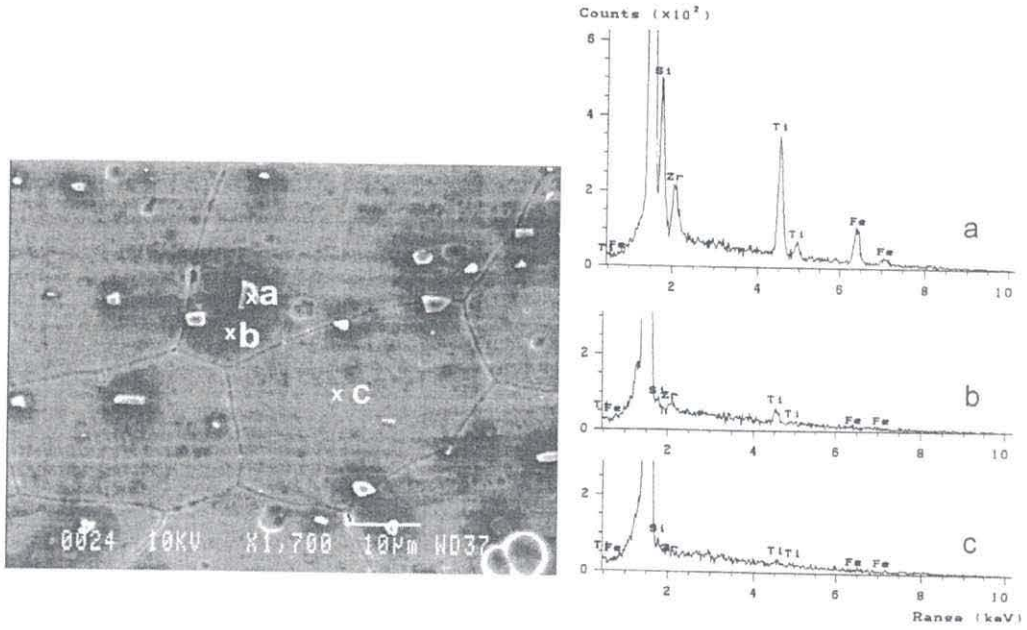

Figure 1.15 SEM image of AA6060 with relatively thick conversion layer. X-ray EDS analysis on particle at a) showed strong titanium and zirconium signals, which also detected in the dark areas surrounding the particle b) but not in the lighter areas some distance away c)[83]

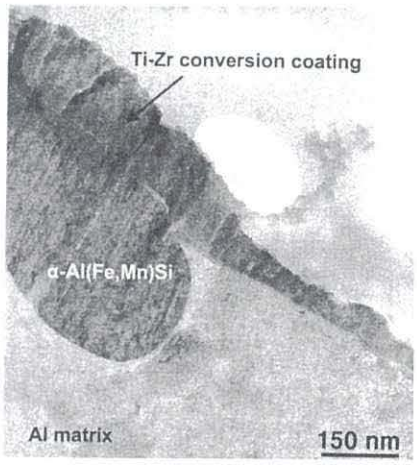

Figure 1.16 TEM of ultramicrotomed section of Ti-ZR treated AA6060 surface[83]

The non-uniform coating observed after this pretreatment step was believed to be controlled by local pH variations on the aluminium surface. The aluminium oxide layer was dissolved by fluoride ions and was believed to result in the formation of complexes – Equations 1.11-1.15. Cathodic reactions occurring on the α-Al(Fe,Mn)Si particles were reported as oxygen reduction and hydrogen evolution, which resulted in an alkaline diffusion layer which favoured precipitation of a titanium and zirconium containing oxide conversion film.

$$Al^{3+} + TiF_6^{2-} \rightarrow AlF_6^{3-} + Ti^{4+} \qquad \textbf{Equation 1.11}$$

$$O_2 + 2H_2O + 4e^- \rightarrow 4OH^- \qquad \textbf{Equation 1.12}$$

$$2H^+ + 2e^- \rightarrow H_2 \qquad \textbf{Equation 1.13}$$

$$Ti^{4+} + 3H_2O \rightarrow TiO_2.H_2O + 4H^+ \qquad \textbf{Equation 1.14}$$

$$Zr^{4+} + 3H_2O \rightarrow ZrO_2.H_2O + 4H^+ \qquad \textbf{Equation 1.15}$$

Treatment on particle free AlMg0.5Si0.4 alloy resulted in no visible conversion layer formation.[83] Increasing the pH from 2.9 to 4 enhanced deposition. Convection of the

solution also played a significant effect on deposition, an increase in agitation resulting in reduced deposition.

The apparently uncoated areas, upon closer examination, exhibited a high density of small particles of about 50 nm in diameter, which were also found present on the particle free AlMg0.5Si0.4 alloy.[83] Too small to analyse by SEM, the particles were assumed to be of the same composition as that of the coating; a titanium-rich oxide.

Furthermore, these workers reported that the fluorotitanate/-zirconate based process was inferior to chromate in terms of adhesion and resistance to filiform corrosion, although there was improvement in the durability of epoxy bonded AA6060 aluminium joints relative to an alkaline etch and deoxidation step. The consistency of the treatment on different alloys was also stated to be questionable if the extent of deposition is dependant on intermetallic particles.

The same proprietary acidic fluorotitanate/-zirconate based solution was also used in the comparative study by Knudsen, Bjørgum, and Tanem[48] mentioned previously, Figure 1.14. Of the chrome free systems these workers studied, it performed in best in the adhesion and along with cerate, was the best in filiform corrosion protection, but performed poorly with the inferior powder coating compared to chromating and anodizing. In a different comparitive study of chromate, chrome phosphate, fluorotitanate, phosphate-fluorotitanate, fluorozirconate and chromate-zirconate, it was indicated that the fluorozirconate performed as well as the chrome phosphate in terms of resistance to filiform corrosion.[47]

Sol-Gel Processes

The use of sol-gel based surface treatments and coatings for the protection of aluminium alloys have being investigated by several researchers and such chrome-free coatings have been are reported to offer great promise.[84] For instance, the mild preparation conditions which can be used has been quoted as one advantage, but low density of the deposited coating has posed problems. To avoid this problem, thermal treatments have been used to increase density. However, these can cause cracking due to the shrinkage phenomenon and the mismatch of thermal coefficients between metallic substrate and ceramic coating. This problem has been overcome by the addition of organic groups linked to the inorganic backbone, reducing the densification temperatures significantly.[84]

Some silane pretreatments have been found to provide greater protection than chromates whilst also improving adhesion.[77,85] Their application conditions include at room temperature, no rinsing, and they are reported to perform even when unpainted. The pretreatments are the product of complex hydrolysis and condensation reactions. Commonly used silane coupling agents have the structure $X_3Si(CH_2)_nY$, where X is a hydrolysable group such as methoxy or ethoxy, and Y an organofunctional group such as chlorine, amine, epoxy, or mercapto group.[85] These are called organofunctional silanes and are used as coupling agents across the organic-inorganic interface. Non-functional silanes have hydrolysable Si-O-C bonds on both ends and are better known as cross linking agents. One example, bis-1,2-(triethoxysilyl)ethane (BTSE) was found to give excellent corrosion protection on both painted and unpainted alloys, especially after a second processing step consisting of a vinyl trimethoxy silane dip. These samples were tested using ASTM B-117 salt spray tests amongst others (specified by the aircraft industry).[85] However, these workers suggested that the application

procedure needs to be strictly controlled; the BTSE had to be stirred for 24 h prior to use, and the pH maintained between 4.5 and 5. It should also be noted that the ASTM B-117 test does not specify the requirement of a score to the treated panel, and that corrosion in the event of paint damage is not considered.

The sol-gel technique has also been used to deposit zirconium oxide films with good results being obtained.[84] For instance, the acetic acid salt testing showed only small blisters on the score after 40 days. The workers used zirconium n-butoxide in acetic acid and anhydrous n-butanol to produce a film on aluminium which then underwent curing at 150-300°C. It was shown that the withdrawal speed, which defined the thickness by solid content and liquid viscosity, was a significant factor in applying the coating. Higher withdrawal rates gave thicker coatings, Figure 1.17. However, the cracks present became wider than those observed at lower withdrawal rates and detachment of the coating was sometimes observed due to the high shrinkage of the thick sol-gel layer during the hydrolysis and curing process.

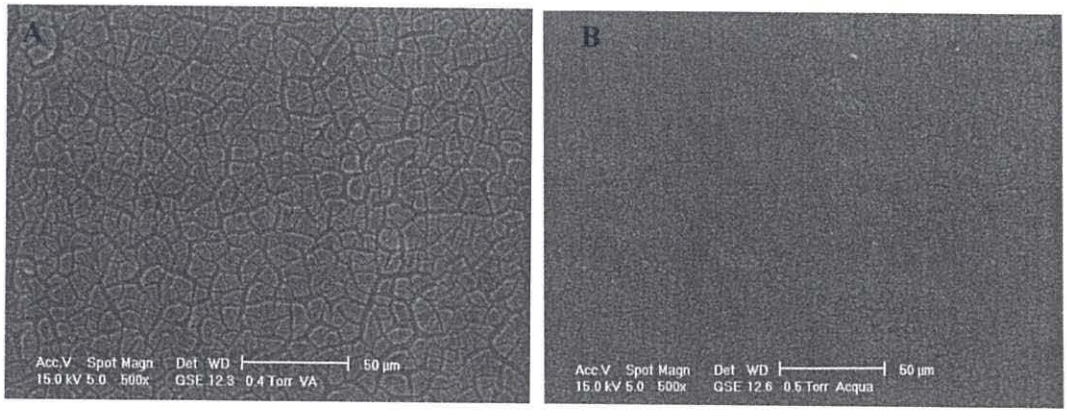

Figure 1.17 ESEM images of coating morphology obtained from withdrawal rates of A: 0.3 cm/s and B: 0.06 cm/s[84]

It was also shown that hydrolysis of the sample in boiling water for one minute rather than air also gave rise to a better coating. This could be due to cross linking which

might have occurred in the boiling water. A long etch time proved detrimental, with a large flake off of the sol-gel coating, and poor paint adhesion in trials, Figure 1.18. This was explained by the fact that the alkoxide should react with the hydroxyl groups present on the oxide layer on the metal, forming oxygen bridges. A thicker coating was obtained by increasing the number of coating layers i.e. applying the coating three times. From a commercial perspective, the high curing temperatures and hydrolysis temperatures may not be suitable.

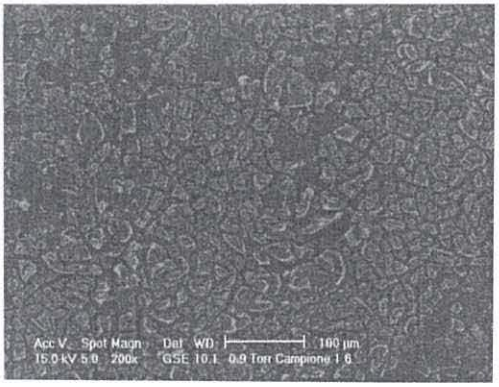

Figure 1.18 SEM of the coating morphology obtained from a long etch time prior to coating[84]

The addition of zirconia powders to increase the roughness of the sol-gel layer produced significant blistering during acetic acid salt testing which was reasoned by reduction in local organic coating thickness favouring water absorption and coating delamination.

Polymers

Conducting polymers have also been used increasingly in recent years as corrosion resistant coatings, with particular interest in polypyrrole due to its high chemical and physical stability. However its application has been considered unfavourable as it involves either anodic oxidation of the monomer or blending with another polymer. [86] A novel approach for depositing a polypyrrole containing film has been based on the development of an aqueous solution containing partially neutralised fluorozirconic and

titanic acids, resulting in a process typical of inorganic conversion coating. The acids were diluted in water and neutralised ZnO and/or aluminium powder, and additional water and the polypyrrole were added when the solution became transparent. The formation of the coating was based on the chemisorption of the monomer and/or oligomer on the ZrO_2 and TiO_2. Polymerisation was reported to then take place *via* the reduction of the Zn^{2+} or O_2. It was claimed that the coating exhibited advanced corrosion resistance and excellent adhesion properties but the nature of the testing was unclear.

Polyacrylic acid has also been investigated as a pretreatment on aluminium, and was found to improve dry adhesion but showed no corrosion protection properties, performing inferior to the uncoated aluminium panel.[87] One possible mode of interaction between the acid and the alloy is a chemical interaction between COO^- and Al^{3+}. A combination of a "special" polyacrylic acid and fluorozirconic acid has been approved by Qualicoat and is commercially available from Henkel under the trade name Alodine 4830/4831.[76] A second solution by Henkel, again approved by Qualicoat, is based on fluorotitanic acid and tannic acids.

Conclusion

This introduction has attempted to illustrate both the importance of aluminium alloys but also their corrosion resistance. Furthermore, it has described the main aluminium alloys and the current chromate-based conversion coatings used to protect aluminium. It has also described some examples of studies investigating the nature of the corrosion barrier properties and finally has listed the main selected examples of chrome free corrosion protection coatings; the latter being the main aim of this thesis.

References

(1) In *http://www.buildingtalk.com/news/pyr/pyr100.html* July 2007.
(2) In *http://www.rusal.com* June 2007.
(3) In *http://www.netshapeeng.com/profile.htm* February 2008.
(4) In *Aluminium - a metal with a bright future, www.sapagroup.com;* Sapa Technology, SE-612 81 Finspång, Sweden: August 2005.
(5) *Course Material: Aluminium and its Alloys*; EPSRC Engineering Doctorate Centre in Steel Technology, Materials Research Centre, Swansea, 2003.
(6) Cotton, F. A., Wilkinson, G. *Advanced Inorganic Chemistry*; 5th ed.; John Wiley and Sons, pg 210.
(7) In *General Introduction, Aluminium and Aluminium Alloys*; 5th ed.; Davies, J. R., Ed.; ASM International: 2002, p 1-18.
(8) Wernick, S., Pinner, R. In *Chapter 1, The Surface Treatment and Finishing of Aluminium and its alloys*; 3rd ed.; Draper: 1964.
(9) Luan, B.; Le, T.; Nagata, J. *Surface and Coatings Technology* **2004**, *186*, 431-443.
(10) *Handbook for Chemistry and Physics*; 82nd ed.; CRC Press, 2001.
(11) Chuanbing, H.; Yuhua, W. *Separation and Purification Technology* **2008**, *59*, 299-303.
(12) *About Aluminium*; 7th ed.; Alcan Ltd, 1976.
(13) In *Finishing Aluminium - A Guide For Architects*; The Aluminium Finishing Association: 1999.
(14) In *http://www.indiamart.com/aluminiumandaluminium/pcat-gifs/homepage/alui.jpg* June 2007.
(15) Yfantis, A. D., et al, *Aluminium Surface Science and Technology proceedings* **2000**, 295-298.
(16) Rankin *Inst Metal Finishing*, *58*, 158-160.
(17) Wernick, S., Sheasby, P.G., Pinner, R. *Chapter 14, The Surface Treatment and Finishing of Aluminium and its Alloys*; 6th ed.; Draper, 2001; Vol. 2.
(18) Ou, L.; Feng, Q.; Chen, Y.; Lu, Y.; Zhang, G. *Minerals Engineering* **2007**, *20*, 200-203.
(19) Hoyle, G. *Resources, Conservation and Recycling* **1995**, *15*, 181-191.
(20) Sushil, S.; Batra, V. S. *Applied Catalysis B: Environmental, In Press, Corrected Proof.*
(21) Westenbarger, D.; Boyd, R.; Jung, C. *Resources Policy* **1991**, *17*, 332-341.
(22) In *Aluminium Alloy, Selection and Applications, The Aluminium Association, Inc, 1998, www.aluminium.org* July 2007.
(23) Wernick, S., Sheasby, P.G., Pinner, R. *Chapter 1, The Surface Treatment and Finishing of Aluminium and its Alloys*; Draper, 2001; Vol. 1.
(24) *Alcan Industries Ltd: Properties of Alloys*; Cheney &Sons Ltd: Banbury, Oxon, 1968.
(25) Afseth, A.; Nordlien, J. H.; Scamans, G. M.; Nisancioglu, K. *Corrosion Science* **2001**, *43*, 2359-2377.
(26) Scamans, G., Critical Issues for Chrome-free Pretreatment of Aluminium Alloys, unpublished work.
(27) Snodgrass, J., Moran J., In *Corrosion Resistance of Aluminum Alloys. In Corrosion: Fundamentals, Testing and Protection, ASM Handbook.*; ASM: 2003; Vol. 13a.
(28) Trethewey, K. R., Chamberlain, J. In *Chapter 1, Corrosion for Science and Engineering*; 2nd ed.; Longman: 1996.

(29) Trethewey, K. R., Chamberlain, J. In *Chapter 4, Corrosion for Science and Engineering*; 2nd ed.; Longman: 1996.
(30) In http://www.worldstainless.org/About+stainless/What+is/Intro/ March 2008.
(31) In http://chemistry.about.com/cs/metalsandalloys/a/aa071201a.htm March 2008.
(32) In http://www.bssa.org.uk/about_stainless_steel.php March 2008.
(33) Gurrappa, I. *Materials Characterization* **2003**, *51*, 131-139.
(34) Al-Mayouf, A. M.; Al-Swayih, A. A.; Al-Mobarak, N. A.; Al-Jabab, A. S. *Materials Chemistry and Physics* **2004**, *86*, 320-329.
(35) Gurrappa, I.; Reddy, D. V. *Journal of Alloys and Compounds* **2005**, *390*, 270-274.
(36) In http://en.wikipedia.org/wiki/Rust March 2008.
(37) In *Corrosion Behaviour, Aluminium and Aluminium Alloys*; Davies, J. R., Ed.; ASM International: 2002, p 579-622.
(38) Shriver, D. F., Atkins, P.W. , Langford, C H., *Inorganic Chemistry*; 2nd ed.; Oxford Uni. Press, 1995.
(39) Trethewey, K. R., Chamberlain, J. In *Chapter 2, Corrosion for Science and Engineering*; 2nd ed.; Longman.
(40) Hughes, A. E., Tayor, R.J., Hinton. B.R.W., *Surface and Interface Analysis* **1997**, *25 (4)*, 223-234.
(41) Trethewey, K. R., Chamberlain, J. In *Chapter 11, Corrosion for Science and Engineering,*; 2nd ed.; Longman: 1996.
(42) Van Gheem, E.; Vereecken, J.; Le Pen, C. *Journal of Applied Electrochemistry* **2002**, *32*, 1193-1200.
(43) Van Gils, S.; Melendres, C. A.; Terryn, H.; Stijns, E. *Thin Solid Films*
The 3rd International Conference on Spectroscopic Ellipsometry **2004**, *455-456*, 742-746.
(44) Na, K.-H.; Pyun, S.-I. *Corrosion Science* **2007**, *49*, 2663-2675.
(45) Metikos/-e-Hukovica, M., Babica, R., Grubac, Z,. *Journal of Applied Electrochemistry* **1998**, *28*, 433-439.
(46) Trethewey, K. R., Chamberlain, J. In *Chapter 6, Corrosion for Science and Engineering,*; 2nd ed.; Longman: 1996.
(47) Fedrizzi, L.; Deflorian, F.; Rossi, S. *Aluminium Surface Science and Technology proceedings* **1997**, 243-248.
(48) Knudsen, O. O., Bjorgum A., Tanem, B.S. *Aluminium Surface Science and Technology proceedings* **2003**, 175-180.
(49) Delplancke, J. L.; Berger, S.; Lefebvre, X.; Maetens, D.; Pourbaix, A.; Heymans, N. *Progress in Organic Coatings* **2001**, *43*, 64-74.
(50) Kayes, A. P. e. a. *Aluminium Surface Science and Technology proceedings* **1997**, 249-254.
(51) Mol, J. M. C. *Aluminium Surface Science and Technology proceedings* **2000**, 237-242.
(52) Fedrizzi, L.; Bianchi, A.; Deflorian, F.; Rossi, S.; Bonora, P. L. *Electrochimica Acta* **2002**, *47*, 2159-2168.
(53) Communication with Brian Tomkins, MD, Almetron Ltd.
(54) Afseth, A.; Nordlien, J. H.; Scamans, G. M.; Nisancioglu, K. *Corrosion Science* **2002**, *44*, 2491-2506.
(55) Afseth, A.; Nordlien, J. H.; Scamans, G. M.; Nisancioglu, K. *Corrosion Science* **2002**, *44*, 2529-2542.
(56) Knudsen, O. O.; Tanem, B. S.; Bjorgum, A.; Mardalen, J.; Hallenstvet, M. *Corrosion Science* **2004**, *46*, 2081-2095.
(57) Bartolomé, M. J.; del Río, J. F.; Escudero, E.; Feliu Jr., S.; López, V.; Otero, E.; González, J. A. *Surface and Coatings Technology* **2008**, *202*, 2783-2793.

(58) Knudsen, O. Ø.; Tanem, B. S.; Bjørgum, A.; Mårdalen, J.; Hallenstvet, M. *Corrosion Science* **2004**, *46*, 2081-2095.
(59) López, V.; González, J. A.; Otero, E.; Escudero, E.; Morcillo, M. *Surface and Coatings Technology* **2002**, *153*, 235-244.
(60) Moutarlier, V.; Gigandet, M. P.; Ricq, L.; Pagetti, J. *Applied Surface Science* **2001**, *183*, 1-9.
(61) Leth-Olsen, H.; Nisancioglu, K. *Corrosion Science* **1998**, *40*, 1179-1194.
(62) Biestek, T., Weber, J. *Electrolytic and Chemical Conversion Coatings by T. Biestek and J.Weber*; Portcullis Press Ltd., Redhill, Surrey, 1976.
(63) Campestrini, P.; van Westing, E. P. M.; de Wit, J. H. W. *Electrochimica Acta* **2001**, *46*, 2553-2571.
(64) Spring, S., Woods, K. In *Metal Finishing* June 1981, p 49.
(65) Campestrini, P., GOEMINNE, G.,TERRYN, H. , VEREECKEN, J. , DE WIT, J. H. W., *Journal of the Electrochemical Society* **2004**, *151 (2)*, B59-B70.
(66) Brown, G. M.; Shimizu, K.; Kobayashi, K.; Thompson, G. E.; Wood, G. C. *Corrosion Science* **1993**, *34*, 1045-1054.
(67) Campestrini, P.; van Westing, E. P. M.; de Wit, J. H. W. *Electrochimica Acta* **2001**, *46*, 2631-2647.
(68) Zhao, J.; Xia, L.; Sehgal, A.; Lu, D.; McCreery, R. L.; Frankel, G. S. *Surface and Coatings Technology* **2001**, *140*, 51-57.
(69) Tan, Y.-J.; Bailey, S.; Kinsella, B. *Corrosion Science* **2002**, *44*, 1277-1286.
(70) Goeminne, G.; Terryn, H.; Vereecken, J. *Electrochimica Acta* **1998**, *43*, 1829-1838.
(71) Unpublished work, Almetron Ltd.
(72) Yu, Z.; Ni, H.; Zhang, G.; Wang, Y.; Dong, S.; Zhao, G. *Applied Surface Science* **1992**, *62*, 217-221.
(73) Lytle, F. W.; Greegor, R. B.; Bibbins, G. L.; Blohowiak, K. Y.; Smith, R. E.; Tuss, G. D. *Corrosion Science* **1995**, *37*, 349-369.
(74) Zhao, J., Frankel, G., McCreery, R.L., *J. Electrochem. Soc,* **1998**, *145 (7)*, 2258-2264.
(75) Baugh, L. M., Unpublished work, Alcan International, 2001.
(76) Roland, W. A., Kresse, J., Chemetall GmbH *Aluminium Surface Science and Technology proceedings* **1997**, 88-89.
(77) Schmidt-Hansberg, T., Schubach, P., *Aluminium Surface Science and Technology proceedings* **2003**, 9-14.
(78) Rangel, C. M., Paiva, T.I., *Aluminium Surface Science and Technology proceedings* **2000**, 301-306.
(79) Hinton, B. *Aluminium Surface Science and Technology proceedings* **1997**, 165-168.
(80) Sun, X., Thompson, G.E., Furneaux, R.C., *Aluminium Surface Science and Technology proceedings* **2000**, 515-520.
(81) Trueman, A. R., et al, *Aluminium Surface Science and Technology proceedings* **2000**, 270-276.
(82) Kimpton, H. J., et al *Aluminium Surface Science and Technology proceedings* **2000**, 467-472.
(83) Lunder, O., et al *Aluminium Surface Science and Technology proceedings* **1997**, 412-419.
(84) Fedrizzi, L. D. M., R; Rossi, S; Leonardelli, L. *Aluminium Surface Science and Technology proceedings* **2003**, 15-21.
(85) Van Ooij, W. J., Song, J., Subramanian, V., *Aluminium Surface Science and Technology proceedings* **1997**, 137-142.

(86) Yfantis, A. D., et al, *Aluminium Surface Science and Technology proceedings* **2000**, 527-532.
(87) Mirabedini, S. M., et al, *Aluminium Surface Science and Technology proceedings* **2000**, 485-490.

2. Alloy Preparation

This chapter describes the treatment of the aluminium alloys 3105 and 6063 in preparation for a corrosion protection coating and subsequent powder coating, which involves prior surface preparation of the metal surface. As mentioned in the introduction, the nature of the surface preparation is an extremely important process and can often play a crucial role in achieving a successful deposition of a corrosion protection coating, in particular with respect to good coverage and adhesion.[1,2] Referred to as chemical cleaning, the process can involve degreasing, deoxidizing, acid and alkaline etching and desmutting.[3] Degreasing is carried out to physically clean the surface of solid dirt and grease, leaving the surface "physically clean", whilst an etching process is required to remove the natural aluminium oxide formed on the surface, and contaminants such as silicon.[1] The aluminium oxide layer itself is also considered a contaminant as it can be detrimental to subsequent coating processes. The desmut stage is to remove the insoluble products which can form and deposit in the surface of the aluminium during the etch process.[4]

The parameters of each step of the cleaning process can result in modifications to the morphology and microstructure of the surface and also the sub-surface layer in some instances.[5,2] These modifications arise from the removal of surface material and key examples are discussed in the following introductory section to this chapter and then in further detail when considering the experimental data on the 3105 and 6063 alloys.

A typical commercial process for the surface preparation of architectural aluminium extrusions is shown in Figure 2.1. This typically involves an alkaline etch, which is a fairly easy and cheap method of etching but one which actually involves complex

chemistry.[3] Commercially, the process is based on sodium hydroxide. This might produce a black surface smut if the alloy contains a high percentage of impurities such as copper, manganese or silicon, which form oxides and intermetallics that are insoluble in the alkaline solution.[4]

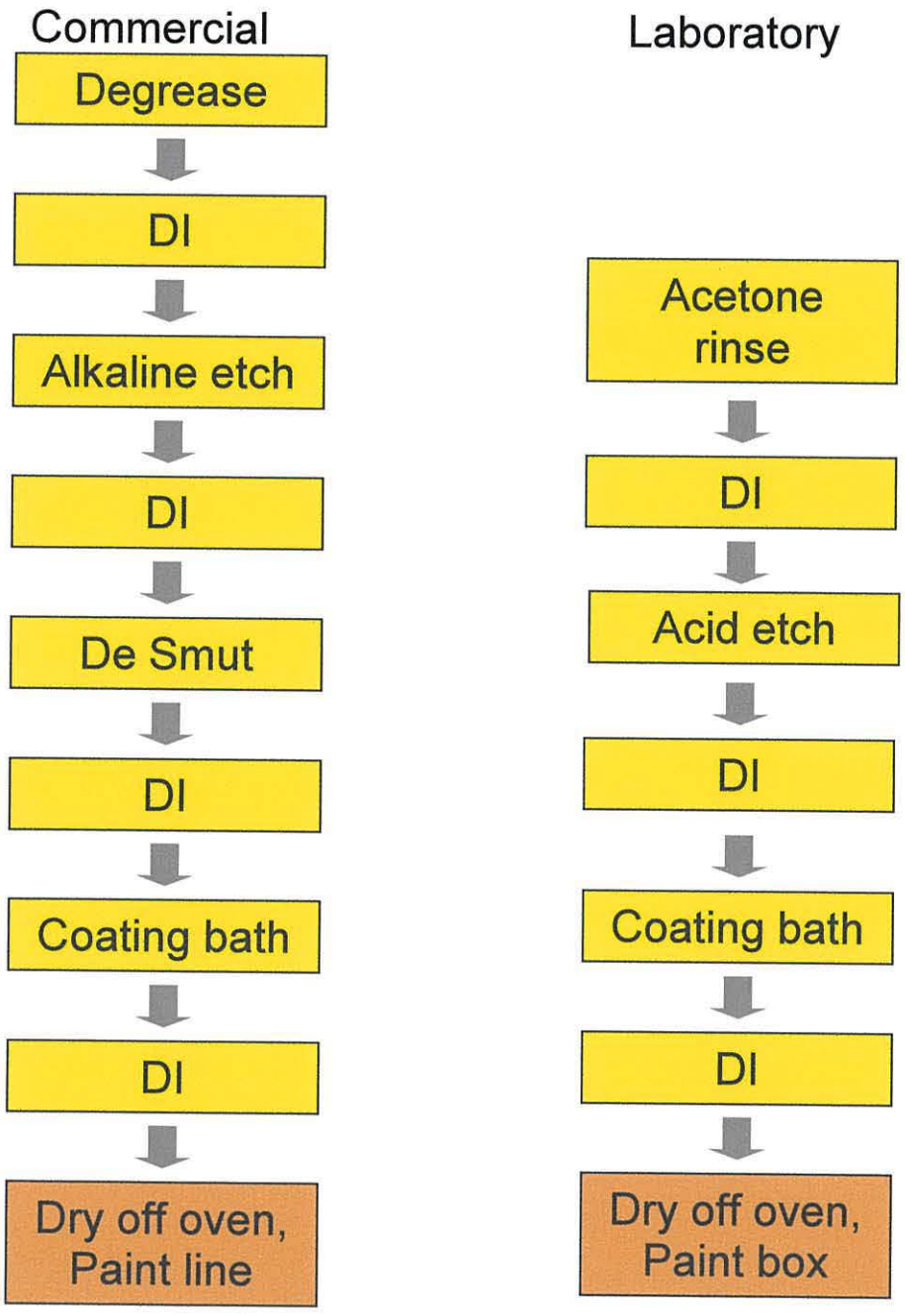

Figure 2.1 An example of a typical commercial alkaline etch process for the corrosion protection of aluminium, and the laboratory etch method used in this thesis to prepare samples for subsequent coating, deionised water (DI)

Following a deionised water rinse (DI), smut is generally removed with a nitric acid containing bath, termed a de-smut bath. The aluminium is then rinsed again with water, before being treated with the corrosion protecting coating. Within the discussions in this thesis, the addition of the corrosion protection coating will be referred to as the pretreatment step. Depending on the type of pretreatment step used, a further subsequent rinse may be required following the pretreatment. In a commercial process, the coated substrate is then oven dried in preparation for powder coating on a paint line, to remove moisture which is detrimental to the powder coating process.

In an alternative industrial process, an acid etch, or a deoxidising bath, may be used in place of the alkaline etch, and this is generally based on sulphuric, phosphoric, and/or chromic acid. These acid etch solutions may also contain fluoride.[6] Compared to the alkaline etch, an advantage is that the process is shorter as no desmut is required.

In a laboratory process, designed to mimic a commercial line, the physical dirt and grease coming into contact with the aluminium is limited, and thus the degreasing step is generally not required and can be substituted by an acetone rinse prior to the etch. An acid etch can also be used as it is a shorter process, requiring less baths than the alkaline etch process. A paint box is used in order to replicate the paint line. This process is illustrated in Figure 2.1 and constitutes the experimental design used in this thesis.

A review of published literature on the surface preparation of aluminium alloys shows that in a paper presented by Zhou *et al.*[7], the surface preparation of alloy 5005 sheet has been investigated by TEM analysis of ultramicrotomed cross sections. The data show that a near surface layer approximately 300 nm thick was visible on the as-rolled alloy, which was characterised by very fine grains, indicated by I on Figure 2.2a , and which

was generated through thermo-mechanical processes. The paper reported that the altered layer was removed completely by alkaline etching, which instead left a layer of etch product of thickness 20-30 nm on the surface - shown by II on Figure 2.2b. A further desmut step in HNO_3, removed the etch products, and left a scalloped surface, shown by III on Figure 2.2c, with a relatively uniform surface oxide film formed in air, and which was less than 10 nm in thickness. By comparison, when an acid cleaner was used, a combination of sulphuric acid and hydrogen fluoride, this did not completely remove the altered layer – indicated by IV - in the example given, Figure 2.2d.

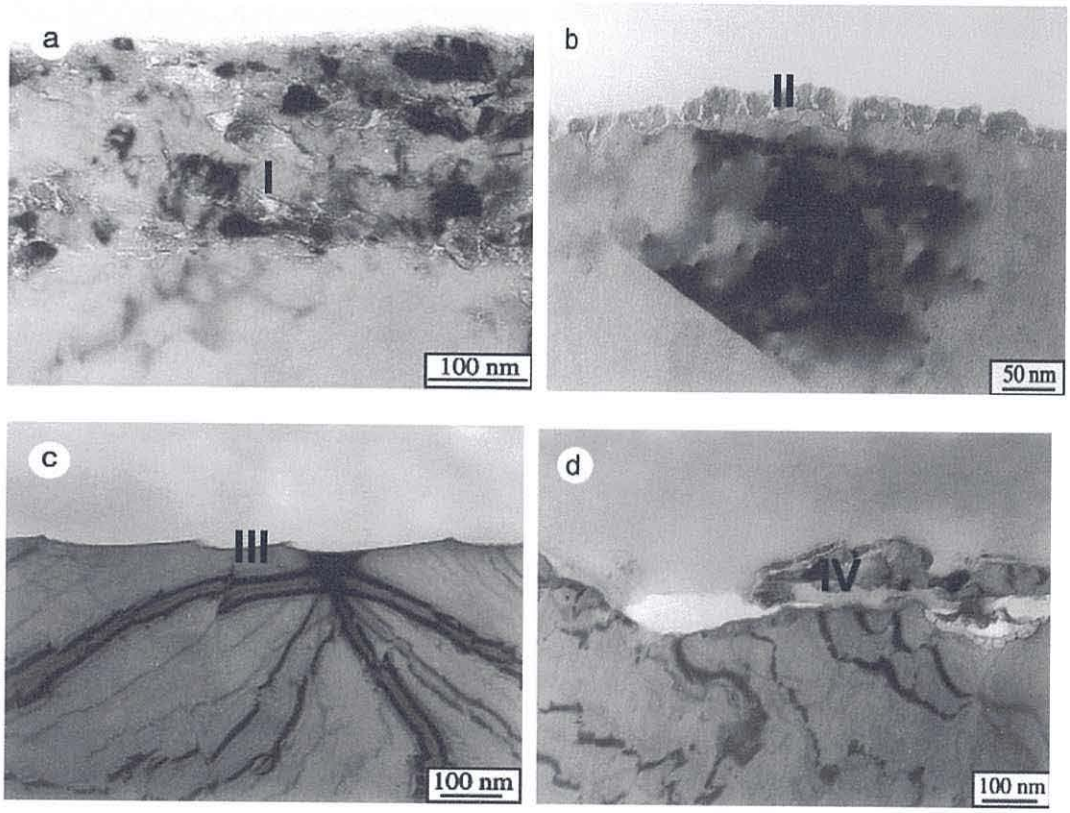

Figure 2.2 Transmission electron micrographs of ultramicrotomed cross sections of the 5005 H14 aluminium alloy: (a) as-rolled; (b) caustic etched; (c) caustic etched and desmutted; (d) acid cleaned.[7]

Papers presented by Lunder and co workers[8,9] have discussed the plan views of the extruded alloy 6060 by SEM, Figure 2.3a. The paper reports that alkaline etching was reported to remove around 5 μm depth of metal and much of the extrusion

directionality, leaving significant amounts of smut on the surface, Figure 2.3b.[8] X-ray EDS analysis of the smut found this to be rich in magnesium hydroxide, which was expected by these researchers as magnesium oxides and hydroxides (e.g. brucite) would be expected to be stable in the high pH solutions used in these studies. Other elements which also showed enrichment in the surface smut were silicon, and to a lesser extent iron and manganese.

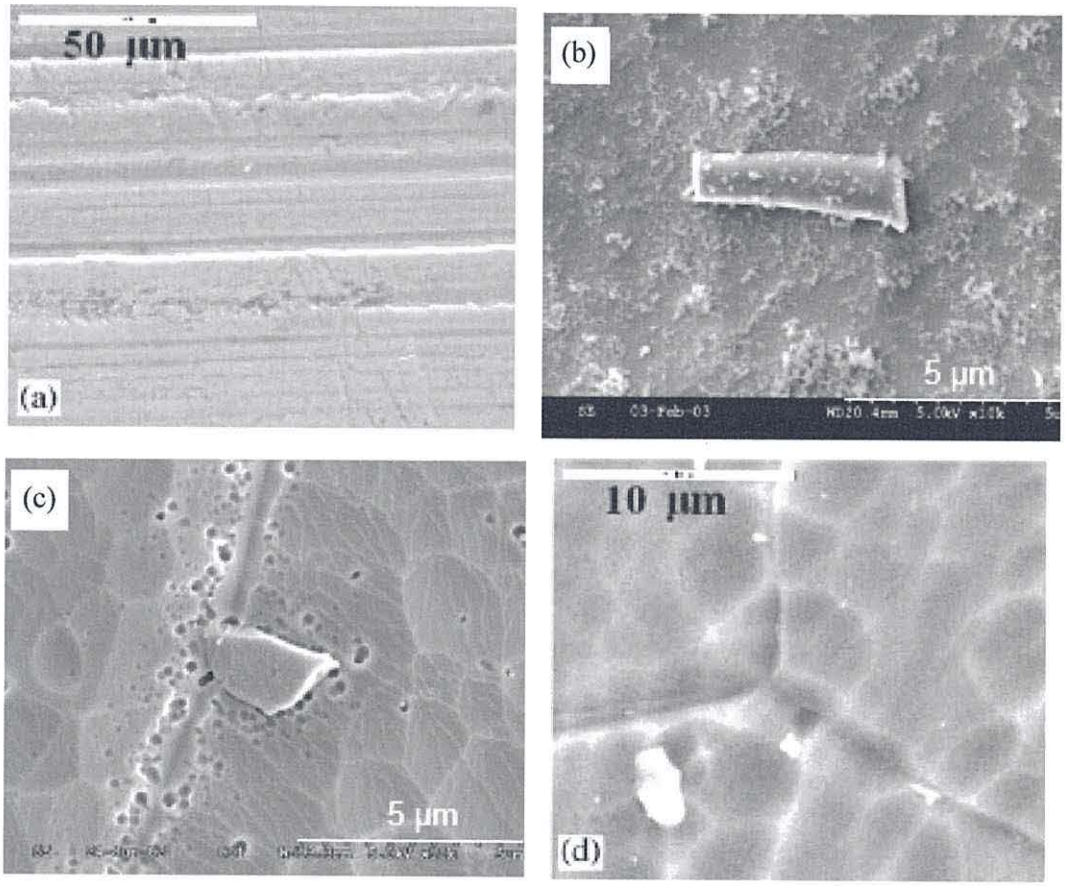

Figure 2.3 SEM micrographs of extruded aluminium alloy 6060: a) degreased,[8] b) NaOH etched,[9] c) NaOH etched and deoxidised in fluoride/sulphuric/phosphoric acid based solution,[9] d) NaOH etched and desmutted in nitric acid.[8]

Subsequent deoxidation in a fluoride-sulphuric-phosphoric acid based solution was shown to remove this smut layer to reveal a scalloped topography, with the scallops *ca* 0.5-2.5 µm in diameter and these features have been reported to have developed during the alkaline etching, Figure 2.3c.[9,10] Glow discharge optical emission spectroscopy

(GDOES) analysis revealed a reduction in magnesium content on the surface following the desmut stage. A number of sub-micron crystallographic etch pits, in particular along the grain boundary, were also noted. Desmutting in nitric acid revealed a similar scalloped topography, of slightly larger diameter, *ca.* 1-3 μm in diameter but no pitting was noted, Figure 2.3d.[8] The topography was also examined by AFM, Figure 2.4.

In studies by Critchlow and co workers,[11] a chromic acid-sulphuric acid etch, and a dichromate-sulphuric acid-hydrofluoric acid etch were reported to give a characteristic scalloped texture, with rolling lines removed, on alloy 2024-T3 clad (T3 refers to the temper of the alloy). The scallops were approximately 0.5-1 μm in diameter, and were reported to be probably related to the cellular structure of the alloy, with ridges developing where sub-grains intersected the surface of the alloy. It was suggested that the size of the scallops may have been related to both the solution and the alloy type.

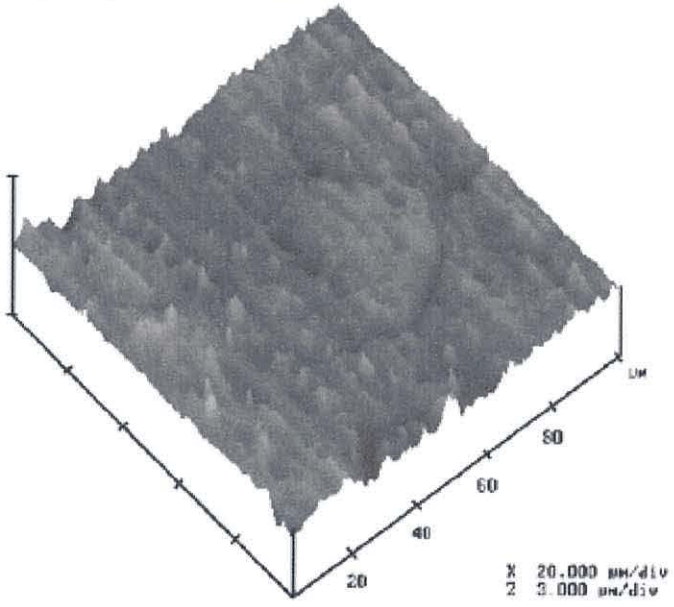

Figure 2.4 AFM image of extruded aluminium alloy 6060: NaOH etched and desmutted in nitric acid.[8]

Critchlow and co workers also reported that the thickness of the oxide following the chromic-sulphuric acid etch was *ca.* 20 nm. By comparison, a dichromate-sulphuric-

hydrofluoric acid etch left a thicker oxide, 40 nm, with evidence of fluoride present in the oxide. Other commercial chrome free cleaners and etches were investigated, e.g. Pyrene 10-21 – a highly alkaline etch cleaner, which showed slight scalloping but left some debris on the surface, suggesting inadequate rinsing or cleaning power. Another etch from the same manufacturer, Pyrene 14-19 – an acid cleaner, gave high scalloping with high debris, again suggesting poor rinsing or a more powerful deoxidiser required.[11] An oxide thickness of 5 nm was observed by Auger electron spectroscopy (AES) depth profile data. The thin oxide layer was considered to be caused by the formation of insoluble phosphates, which inhibited the formation of other oxides. The researchers also showed that another Pyrene acid etch, Pyrene 14-73, which contained 9 times the fluoride content of Pyrene 14-19, gave a scalloped surface similar to that of the chromic-sulphuric acid etch. A further non-chromated deoxidising etch, Chemcid, left a partial film on the surface of the substrate.

Thus it is evident from these studies that different reagents produce different morphologies on the surface of the aluminium. In the following sections, data will be presented from experimental investigations of the as received and etched surfaces of the 3105 and 6063 alloys by SEM, AFM and optical microscopy, which have not been studied previously in this manner. The etch used will be the same used throughout the research in this thesis, a phosphoric acid based, fluoride-containing etch which is a commercial product of Almetron, the Company co-sponsoring this CASE award. The aim is to use these data to aid the evaluation of the alloy surfaces following the coating depositions, which will be discussed in Chapter 3.

Alloy 3105

The aluminium alloy 3105 is a cold rolled, hard temper material which has a tendency to exhibit high filiform corrosion resistance.[12] In the "as received" condition (following acetone degreasing), SEM shows that rolling lines and defects are evident on the surface of the material, Figure 2.7a, b, c, d, which are also evident in the optical microscope image, Figure 2.8. A number of particles of less than 1 μm and *ca.* 2 μm in diameter are also apparent, Figure 2.7c, d. It has been reported that the intermetallic particles present in alloys of this specification generally have the compositions corresponding to one or both of two different phases, the binary phase $(Mn,Fe)Al_6$, or the ternary α-$(Mn,Fe)_3SiAl_{12}$.[13,14,15,16] EDX analysis of a large area of the surface at 60 x magnification shows the presence of aluminium and oxygen but did not indicate the presence of iron and manganese, Figure 2.5. Point analysis of the particle labelled 1 in Figure 2.7c and d clearly does show evidence of the presence of manganese, iron and silica, Figure 2.6.

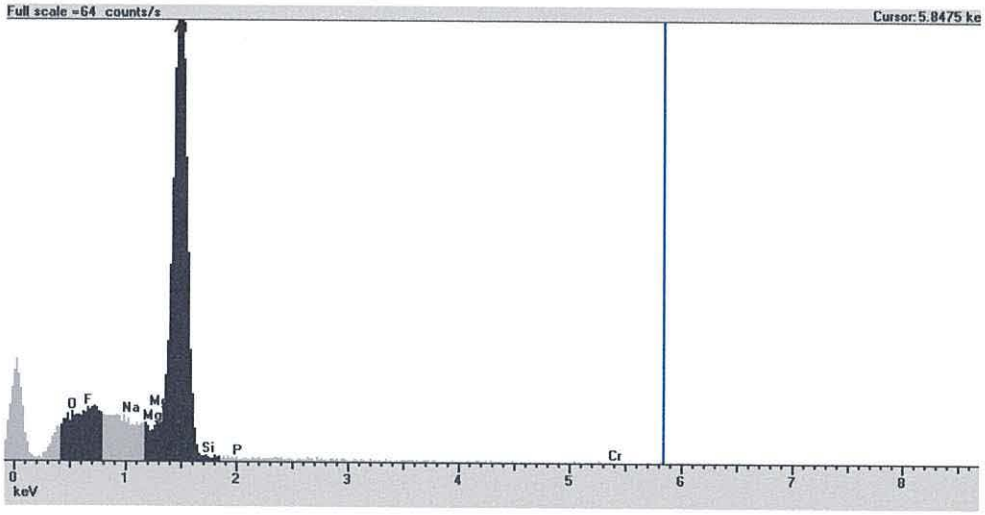

Figure 2.5 EDX analysis of a the matrix of the as received alloy 3105 (at 60x magnification)

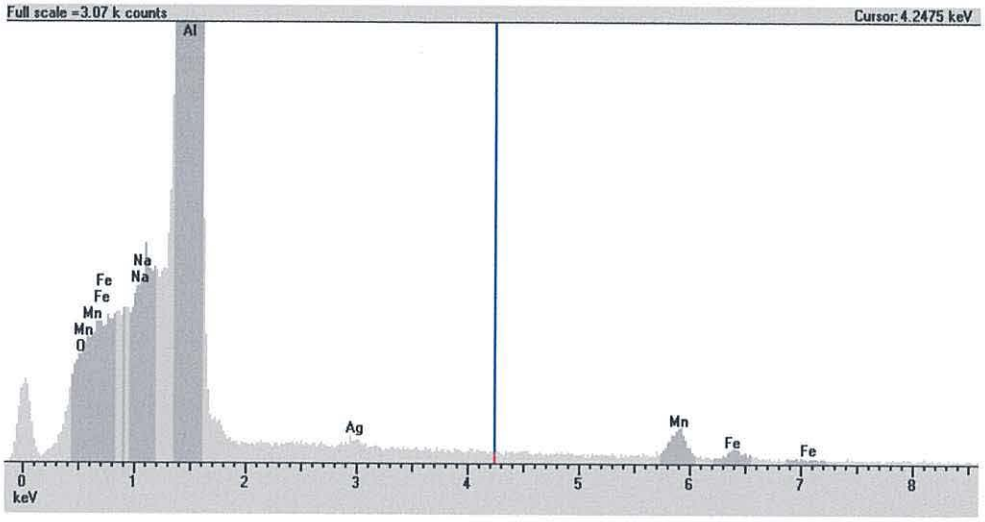

Figure 2.6 EDX point analysis of the particle labelled 1 in Figure 2.7, on the as received alloy 3105

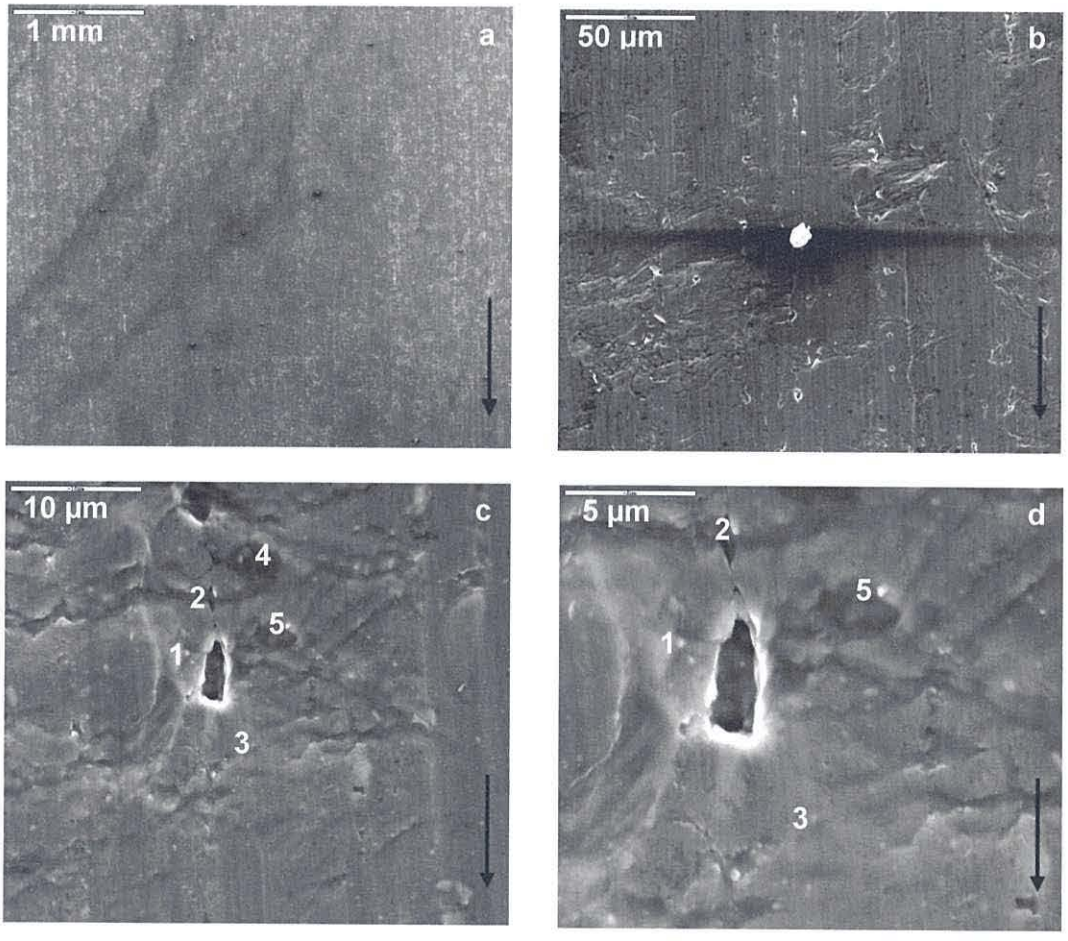

Figure 2.7 SEM images of acetone degreased alloy 3105. The arrow indicates the rolling direction. EDX analysis of the labelled particle 1 is shown in Figure 2.6

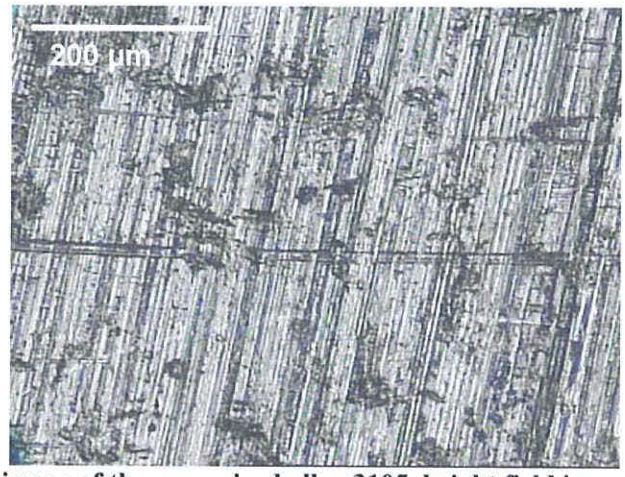

Figure 2.8 Optical image of the as received alloy 3105, bright field image

Samples of the as received 3105 alloy have also been analysed by AFM. AFM operates in an entirely different mode to SEM, typically measuring height differences between the AFM tip and the surface in tapping mode. It is these differences in height that produce the topography data, rather than *via* a narrowed electron beam as in the SEM. Thus AFM provides surface topographic data over a range of scan areas (25 x 25 µm and 50 x 50 µm shown in this thesis) often at nanometre scale resolution. AFM data can therefore effectively show data at higher resolution than SEM. The surface morphology shown, for alloy 3105, is the result of the manufacturing process which involves semi-fabricating the metal to rectangular cross sections followed by rolling,[17] Figure 2.9. The AFM images clearly show the rolling lines on the surface of the alloy in its as received condition, Figure 2.9a,b. These appear at intervals of *ca.* 5 µm apart in the image shown, with a depth of *ca.* 50 µm, Figure 2.9c. The data also confirm the presence of particles on the surface, e.g. at I in Figure 2.9a,b. From these data, it is possible to approximate the depth of the rolling lines to be *ca.* 50 nm below the surface (red), whilst the defect visible in the image has a depth of *ca.* 270 nm (blue), Figure 2.9b,c.

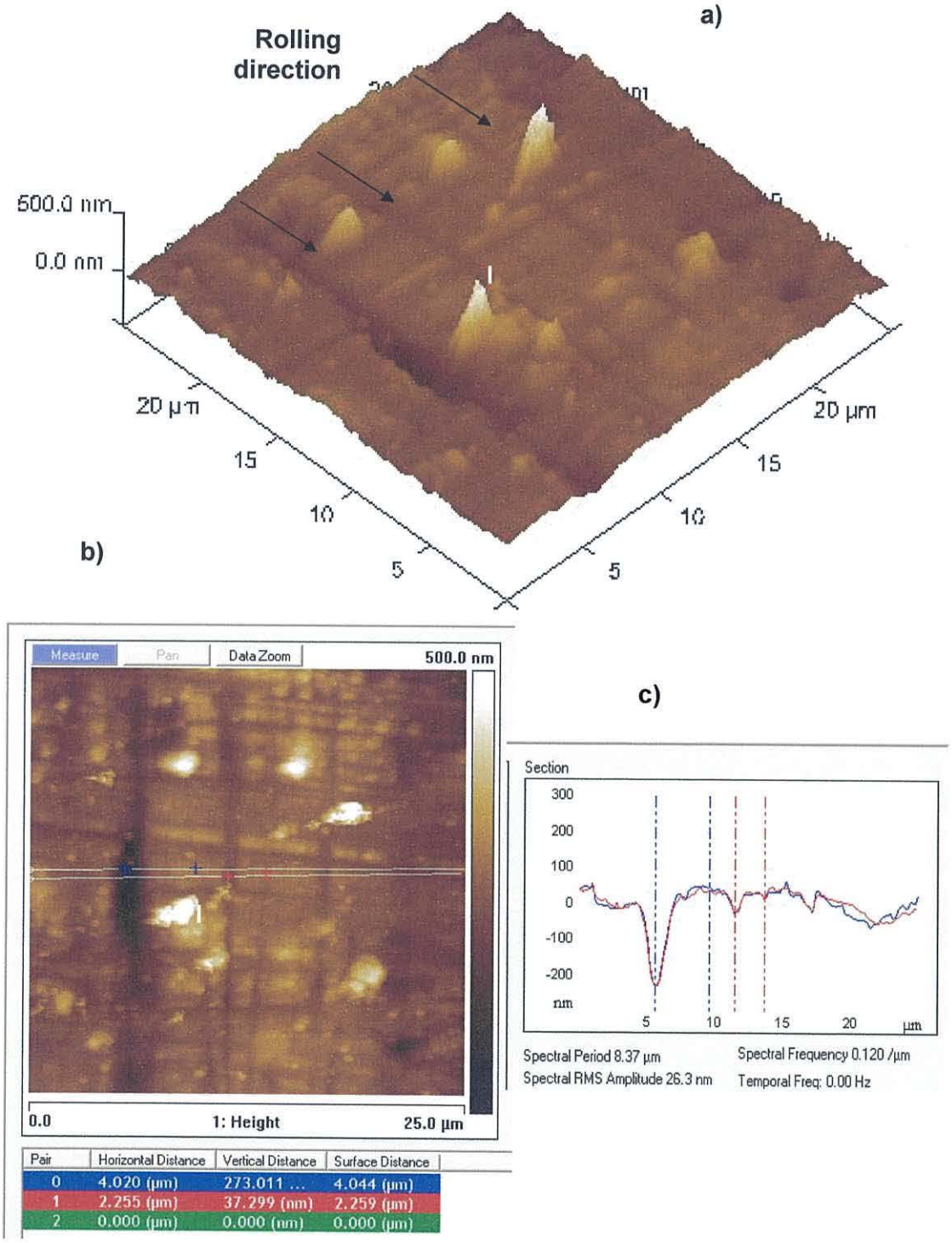

Figure 2.9 AFM images of acetone degreased alloy 3105. a) and b) show the morphology of the surface, b) showing the plan view of 3D image a). Shown on image a) is the rolling line, indicated by the arrows, and a particle is labelled I in a) and b). Also shown on b) is the location of the line analysis which is presented at c), the blue indicating the defect and the red indicating a rolling line.

Etched alloy 3105

Following an etching process of 6 minutes in AC133, a phosphoric acid cleaner containing fluoride, the SEM data show a pitted morphology on the 3105 alloy, with the surface particles described on the as received alloy less evident, Figure 2.10. Three types of holes are noted which are differentiated by size and/or shape; spherical pores ranging from 0.25 to 1.5 μm in diameter; larger pits of spherical and elliptical shapes, from 1.5 to 40 μm across and with charging observed around the pit edges by SEM; and developed pits where the etch attack appears more severe, causing more than one pit to merge. These largest pits range widely in size but are greater than 1.5 μm. These largest pits also contain some sharp edged morphology which may be indicative of crystalline material, and deposits are observed within some, as indicated by I on Figure 2.10d,f.

Figure 2.10 also shows that although the lines caused by the rolling process are no longer visible by SEM, the direction of the rolling process remains apparent, as the ellipsoidal shaped pits are longitudinal in the rolling direction. This suggests preferential etching in this direction, which may be due to the surface modification of the alloy during the rolling process.

EDX analysis of the surface matrix at lower magnification does not show significant changes from that of the as received alloy, Figure 2.11. Point EDX analysis of the particle labelled 1 in Figure 2.10 clearly shows high levels of iron compared to the background, Figure 2.12. Traces of fluoride, chloride and phosphorous are also evident, with phosphorus possibly residue from the etch bath, which may indicate that some insoluble phosphate material has formed on this sample.

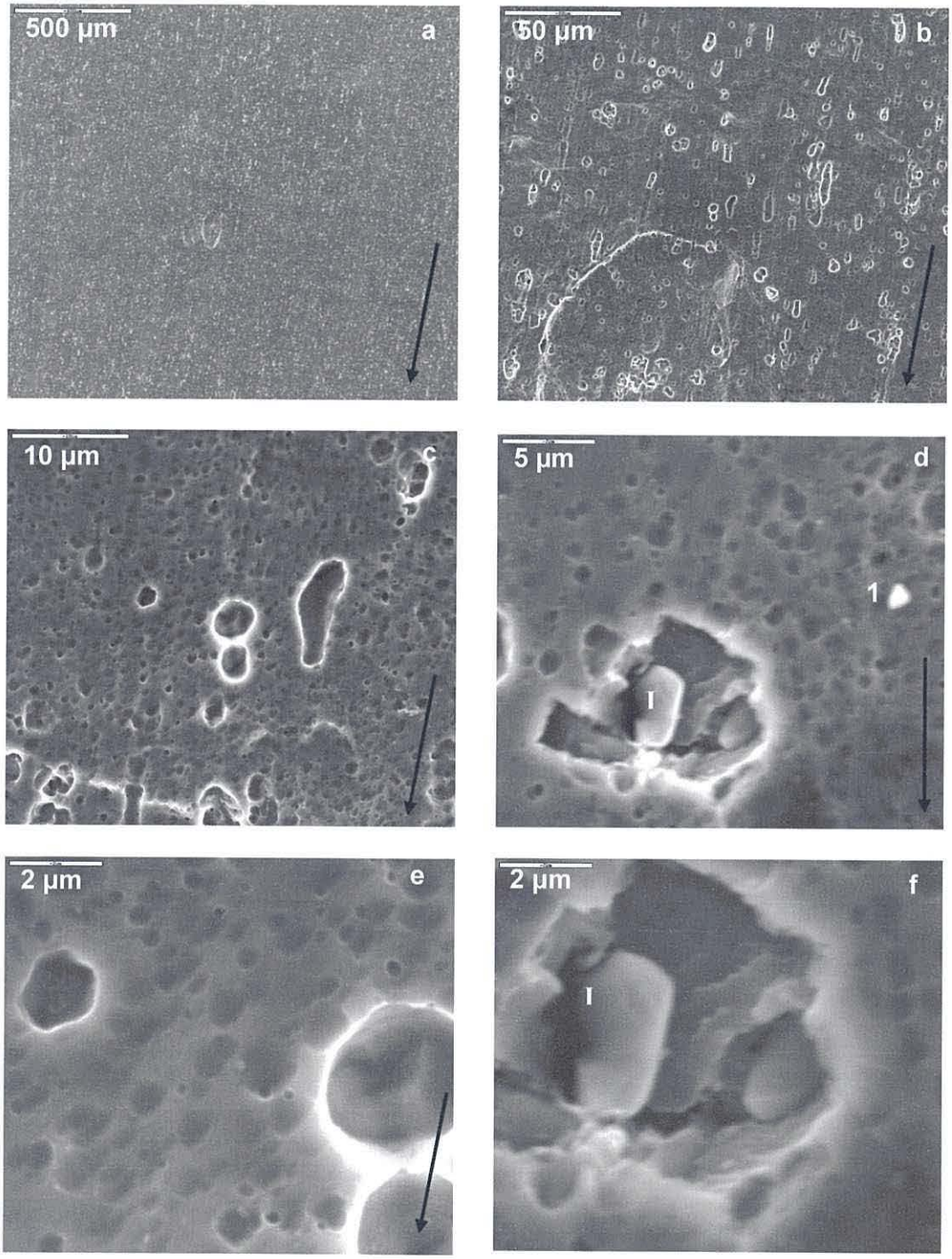

Figure 2.10 SEM images of alloy 3105 etched in AC133 for 6 min. 1 indicates the particle analysed by EDX in Figure 2.6. I indicates the deposits described. The arrows indicate the rolling direction

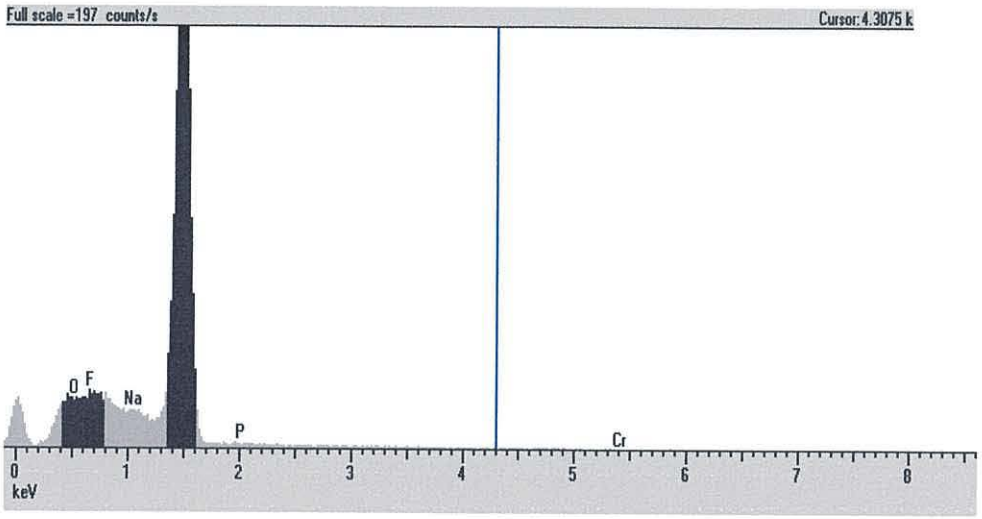

Figure 2.11 EDX analysis of a the matrix of the etched alloy 3105

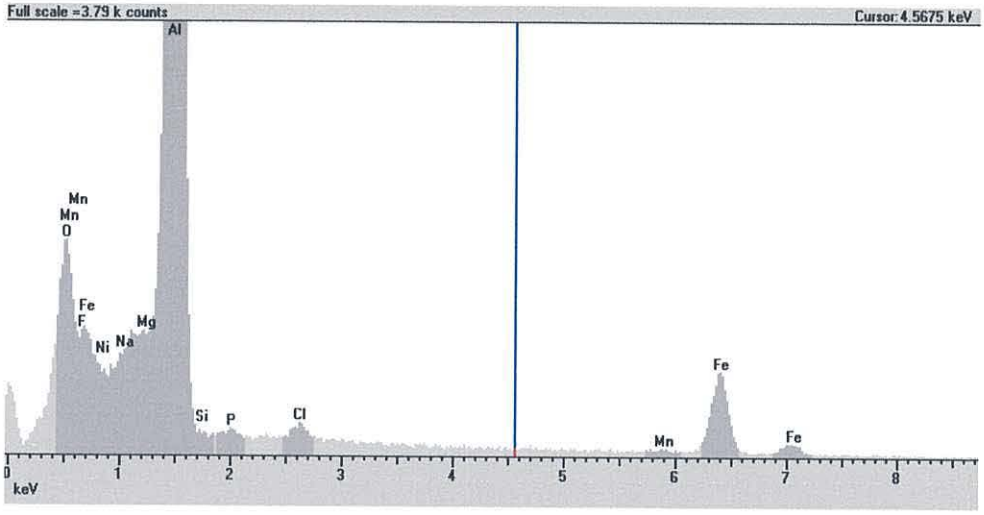

Figure 2.12 EDX analysis of the etched alloy 3105: the particle labelled 1 in Figure 2.10

The AFM data for the etched 3105 alloy, Figure 2.13a,b, showing a greater sample size analysed than the as received alloy, also clearly show a change in morphology of the alloy surface compared to that of the as received alloy, with a much rougher, textured morphology now visible in contrast with the previously as received surface which appeared smooth with periodic rolling lines. Thus, the AFM data show that the majority of the fine rolling lines of the bare surface have been etched away, leaving a coarse surface with few lines and a number of defects. In this case, the defects on the

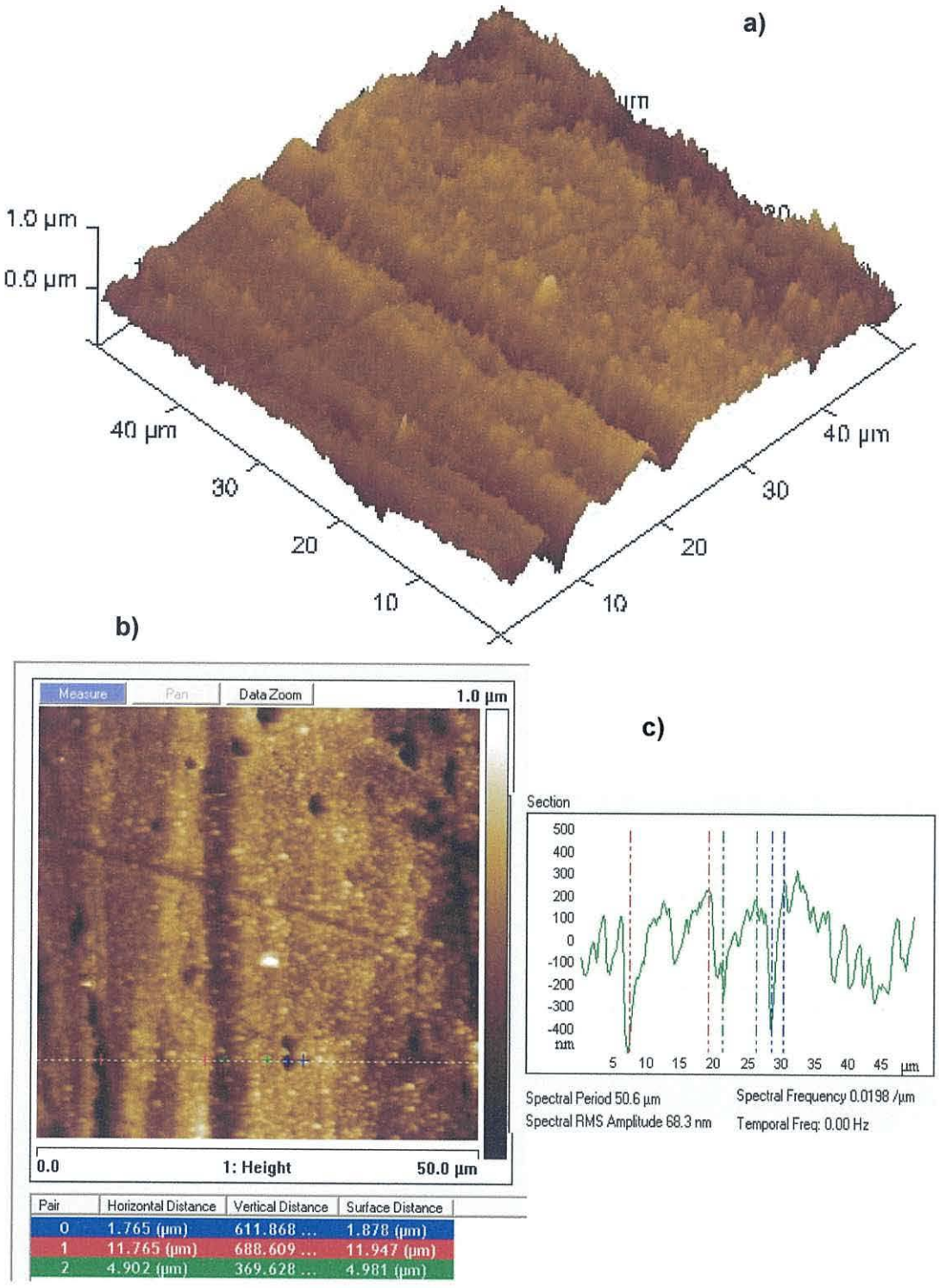

Figure 2.13 AFM 3D images of etched alloy 3105. a) and b) show the morphology of the surface, b) showing the plan view of 3D image a). Shown on b) is the location of the line analysis which is presented at c) the blue indicating the pit depth and the red and green indicating crevices and/or grain boundaries.

etched alloy are much deeper than those on the bare surface, and appear as deep crevices and pits on the surface. In the as received condition, a periodic variance of ± 50 nm in height every 5 μm was apparent from the line profile. On the etched 3105 alloy a periodic variance of 200 nm every 2.5 μm horizontally with 2 crevices of *ca* 600 nm depth in a 50 μm line analysis are evident, Figure 2.13b,c. The crevices may correspond to the grain boundary edges where preferential etching has resulted in the crevice depth observed. This confirms that etching of the surface results in an increased surface area, which can subsequently improve adhesion. The particles identified on the as received alloy appear less frequent on the etched alloy.

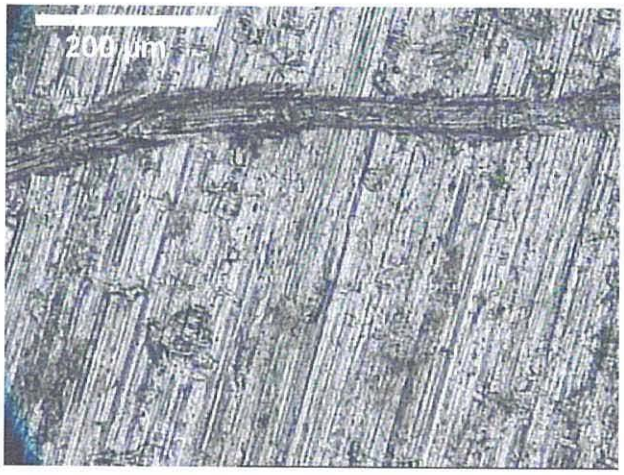

Figure 2.14 Optical image of etched alloy 3105

Although the AFM data shows the surface to be much rougher, the surface appears smoother than the as received alloy by optical microscopy, Figure 2.14. This is ascribed to the different scales of analysis of these two techniques. Thus, the roughness caused by the AC133 etch is too fine to be observed by optical microscopy.

24 h etch in ammonium bifluoride, 3105 alloy

A prolonged etch (24 h) of the 3105 alloy in an ammonium bifluoride solution gives a different morphology to that following the 6 minute AC133 etch, leaving a scalloped rather than a pitted surface, Figure 2.16a,b,c. The scalloped surface is indicated by I, and some residual matter was noted, indicated by II, Figure 2.16c. No rolling lines are apparent at all on the surface of the sample suggesting complete removal of the uppermost layer. The surface more closely resembles that of those discussed from the literature previously in this Chapter,[7-11] rather than the AC133 etched surface. It is possible that the scalloped surface is the result of fluoride, or a prolonged or aggressive etch. Thus, by comparison with the previous data, the etch action of the AC133 may either not be long enough, or aggressive enough to produce such a surface, or the composition, based on phosphoric acid, may inhibit such a topography developing. EDX analysis of the matrix is similar to the analysis of the 3105 alloy in its as received and etched states, Figure 2.15.

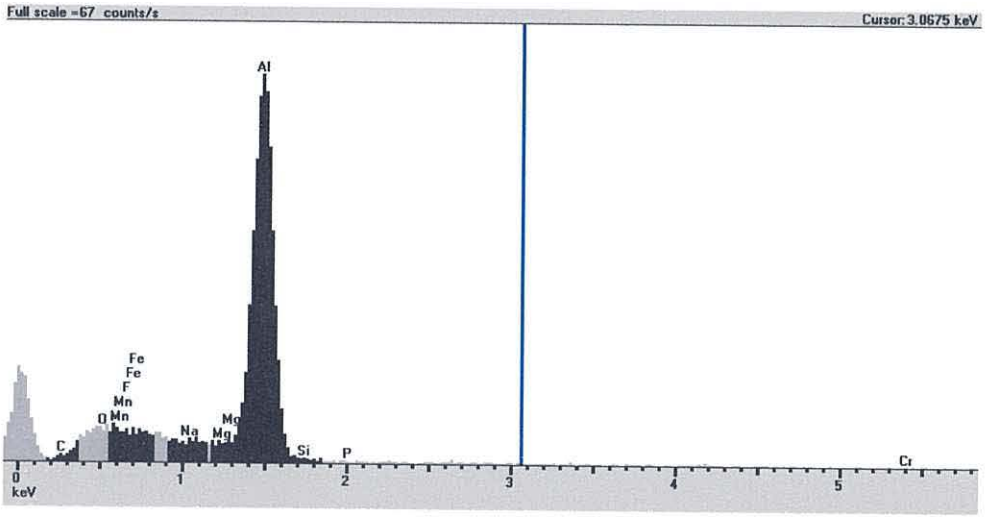

Figure 2.15 EDX spectra of the general matrix of alloy 3105 following 24 h etch in ammonium bifluoride (3000 x magnification)

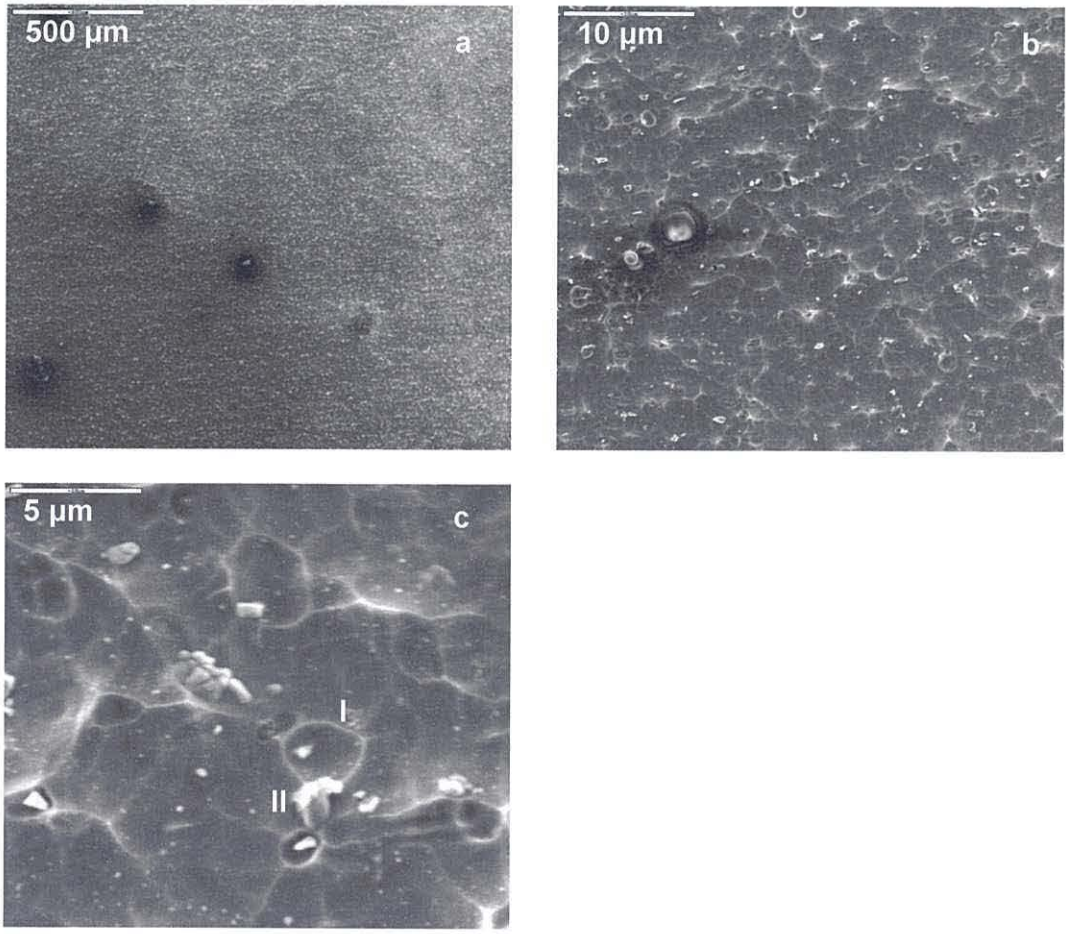

Figure 2.16 SEM images of alloy 3105 etched for 30 min in ammonium bifluoride. I indicates the scalloping, while II indicates some residual matter

Alloy 6063

Following analysis of alloy 3105, similar analysis of alloy 6063 has been carried out. An extruded sample of alloy 6063, following acetone degreasing, appears to exhibit less surface roughness than that of the 3105 alloy at lower magnification. Evident are grain boundaries and areas of dark colouration, Figure 2.17a, which are also noted later during pretreatment. Greater magnification reveals die lines, which are the result of the extrusion process, and a downy morphology Figure 2.17b,c,d. A number of spherical shaped particles are also evident, of less than 2 µm, Figure 2.17c. These have been found to contain iron, manganese and silica, Figure 2.18, Figure 2.19. EDX analysis of

the dark areas did not reveal any differences in composition to the bulk of the matrix, Figure 2.20.

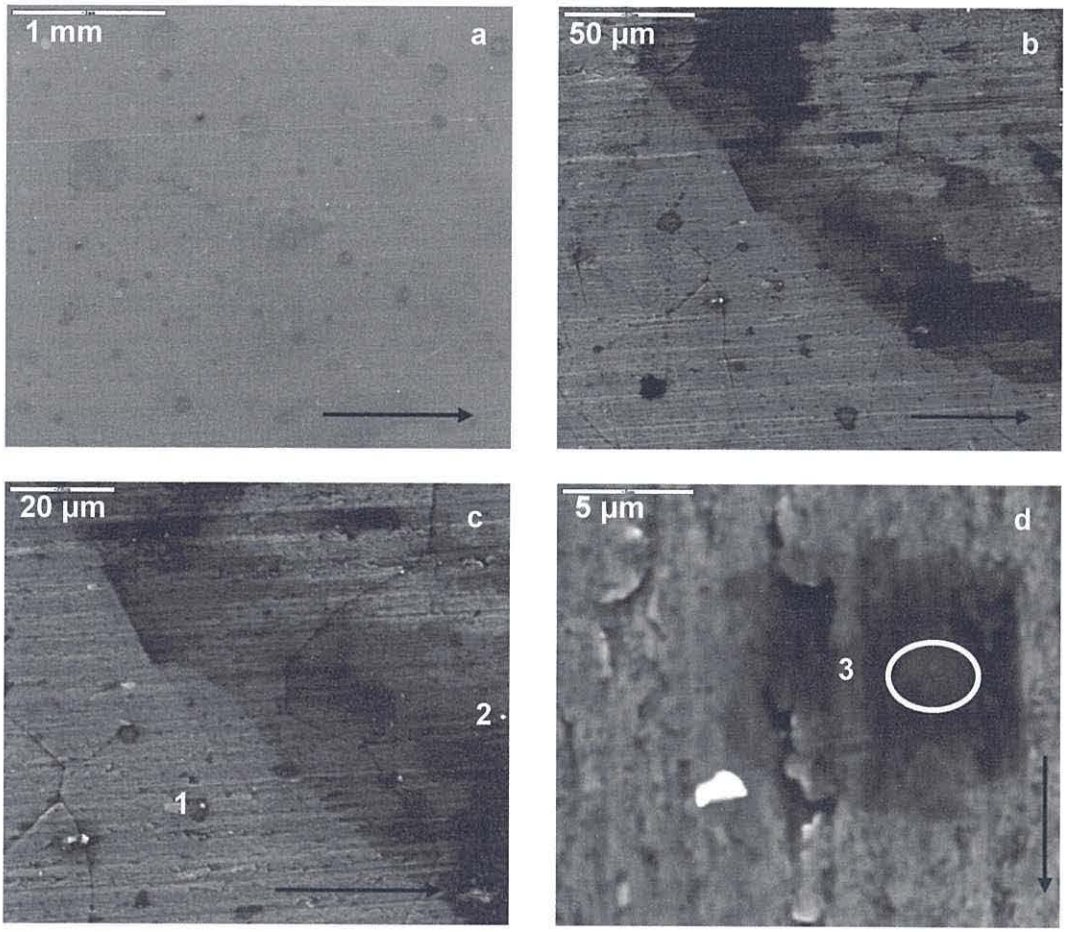

Figure 2.17 SEM images of acetone degreased alloy 6063. The black arrow indicates the rolling direction. The particles labelled 1 and 2 in image c, and area identified as 3 in image d have been analysed by EDX, see Figure 2.19, Figure 2.20

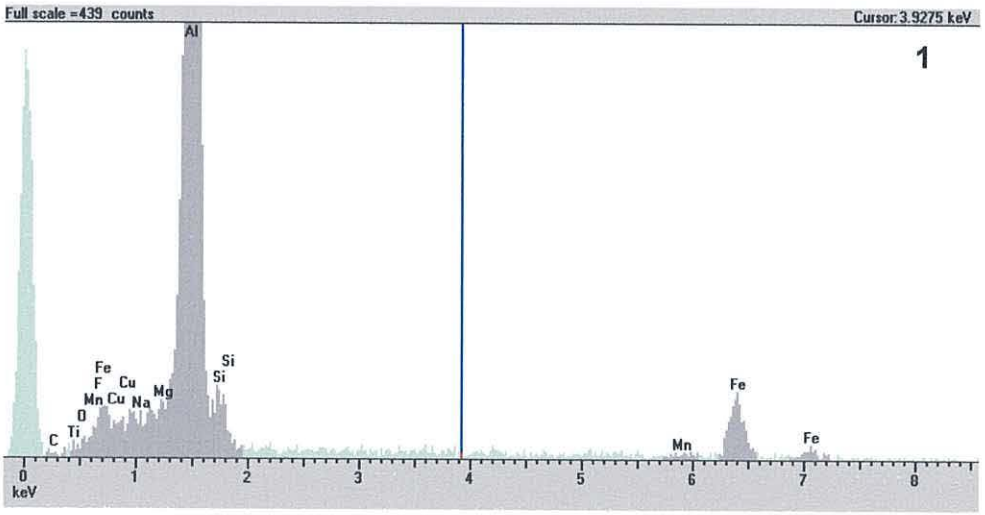

Figure 2.18 EDX analysis of the particles labelled 1 in Figure 2.17

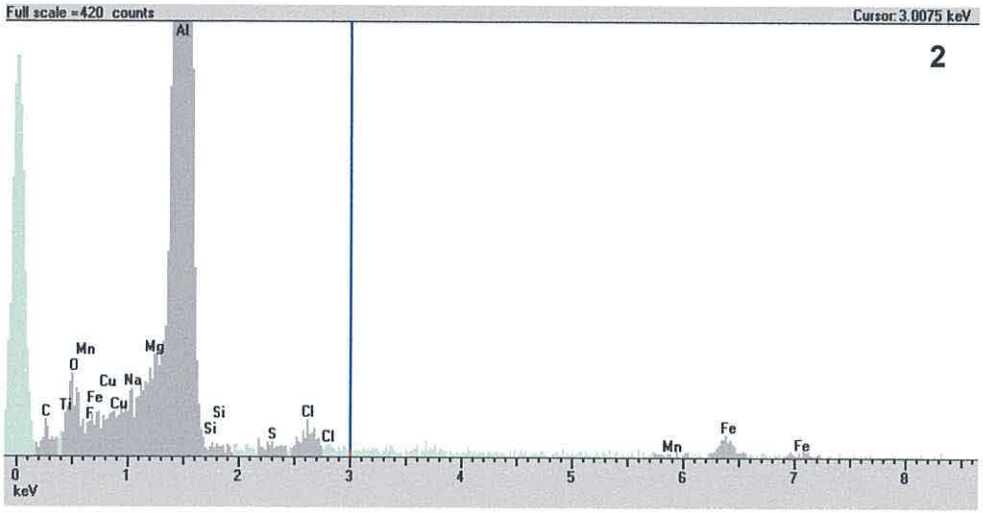

Figure 2.19b EDX analysis of the particles labelled 2 in Figure 2.17

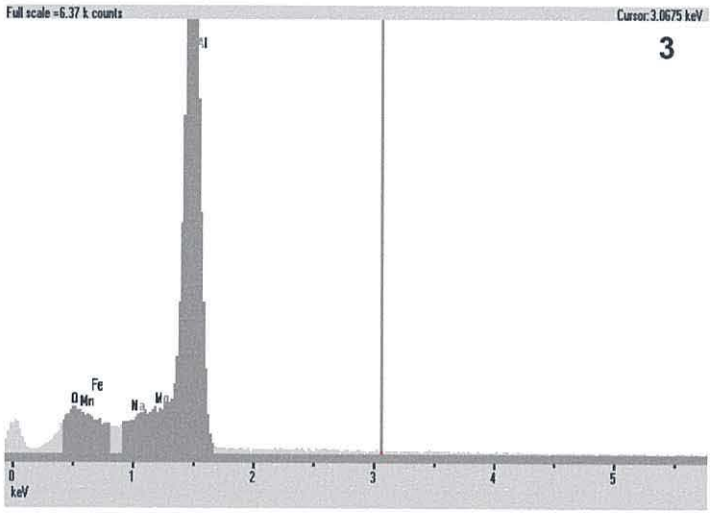

Figure 2.20 EDX analysis of the dark patch identified as 3 in image Figure 2.17d of alloy 6063 (Note the different scales)

The AFM data very clearly shows the extrusion die lines, and indicates some surface artefacts which may be intermetallic particles, indicated by I at Figure 2.21a. The surface of this as received 6063 extruded alloy is much rougher than that of the equivalent as received 3105 sheet alloy, which may be attributed to the different manufacturing processes for sheet and extrusion aluminium. Whilst showing a very rough surface, the AFM data suggest a broad periodicity on the extrusion lines of 5 μm horizontally, Figure 2.21. From one peak to the next trough, the depth is generally 300 nm with one very deep trough *ca.* 300 nm below the nominal surface. Indeed, such is

the degree of surface roughness on the as received 6063 alloy, it is similar to that observed on the etched 3105 alloy.

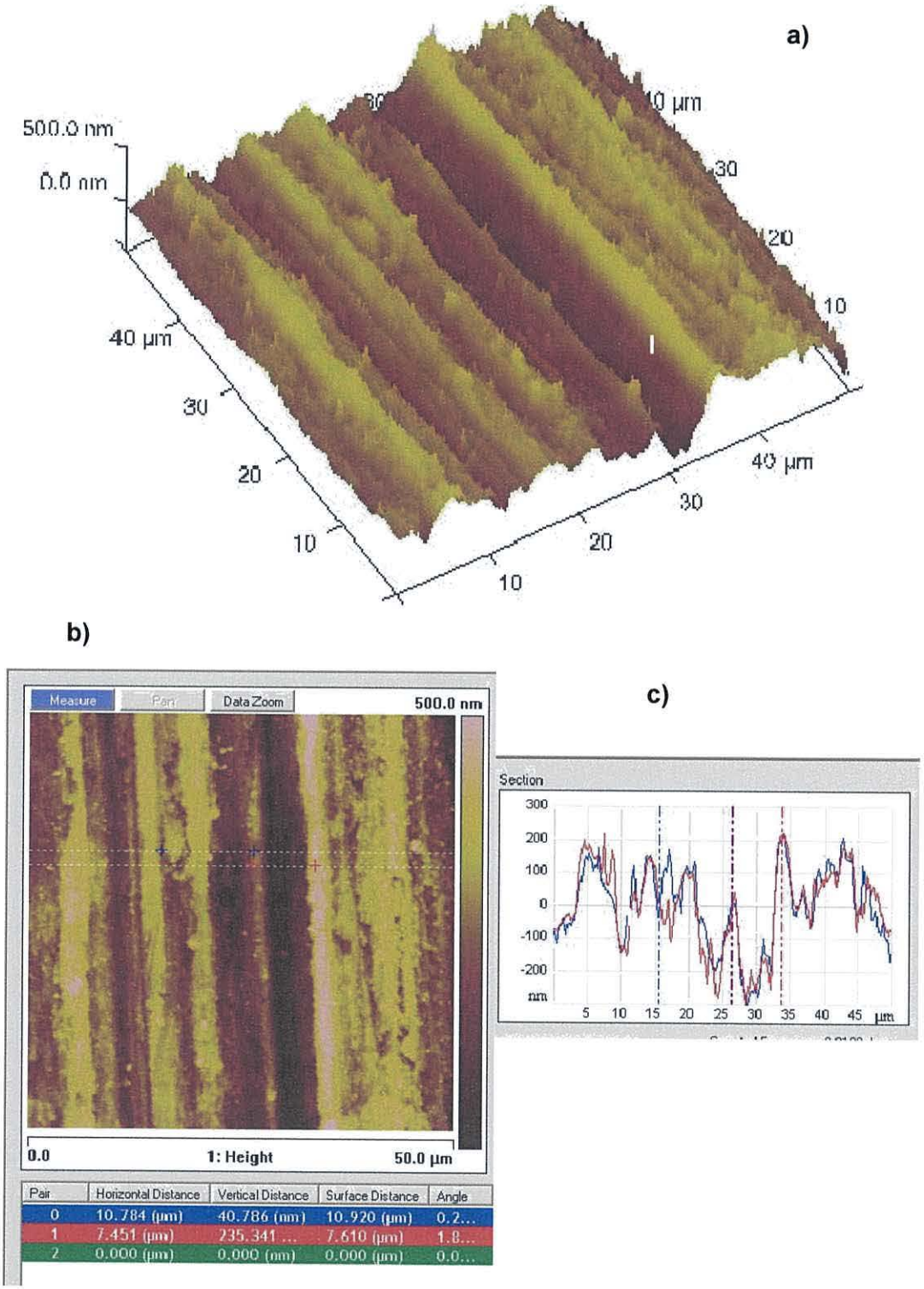

Figure 2.21 AFM images of acetone degreased alloy 6063. a) and b) show the morphology of the surface, b) showing the plan view of 3D image a). Shown on image a) is a particle labelled I and b) shows the location of the line analysis which is presented at c) - both blue and red indicating the extrusion lines

Etched alloy 6063

The SEM images of the AC133 etched 6063 alloy show that the extrusion die lines remain apparent after a 6 minute exposure. The grain boundaries appear much more defined, Figure **2.23**, with pits often found within the grain boundary of *ca.* 1 μm in diameter. As well as the spherical particles observed on the as received alloy, a number of rectangular particles are observed, of *ca.* 4 μm in length, as indicated by 1-4 on Figure **2.23**d. EDX analysis confirmed these intermetallic particles contained Si and Fe, Figure 2.22, indicating that they are intermetallic particles.

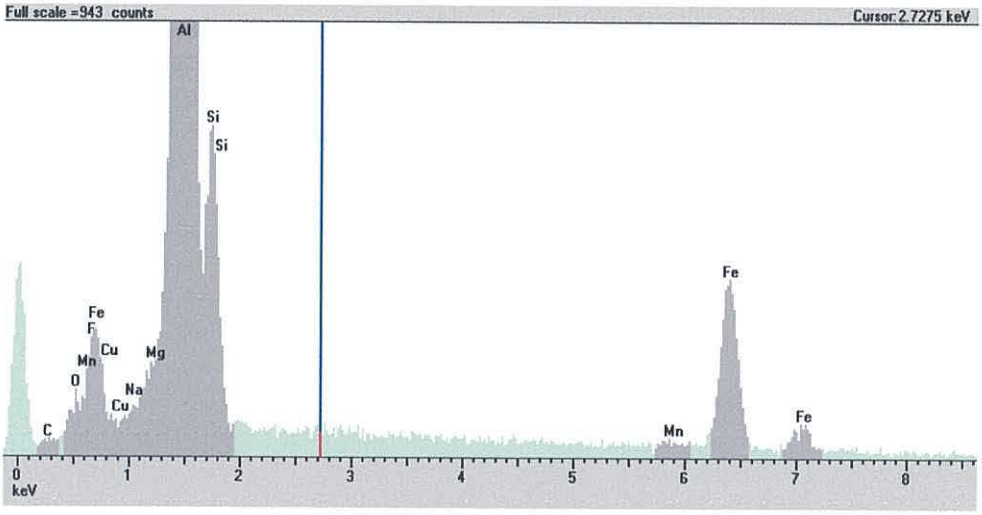

Figure 2.22 EDX analysis of the particle labelled 4 in Figure 2.23d

The AFM data the etched 6063 alloy again clearly show a change in morphology of the alloy surface. A fine surface roughness is visible, along with intermetallic particles, identified by I on Figure 2.24a,b. The horizontal periodicity of 5 μm, due to the extrusion lines remains evident, with the depth from peak to trough reduced to around 250 nm. The grain boundaries are now clearly visible, evident on the line analysis at a depth of 300 nm to the nominal surface. A scratch on the surface is also visible, which has a depth of 200 nm. The cross sectional surface is still very rough in comparison to the 3105 alloy, however the depth of the defects has reduced from 300 nm to around

250 nm overall, in line with the etching process removing the uppermost layers of the surface.

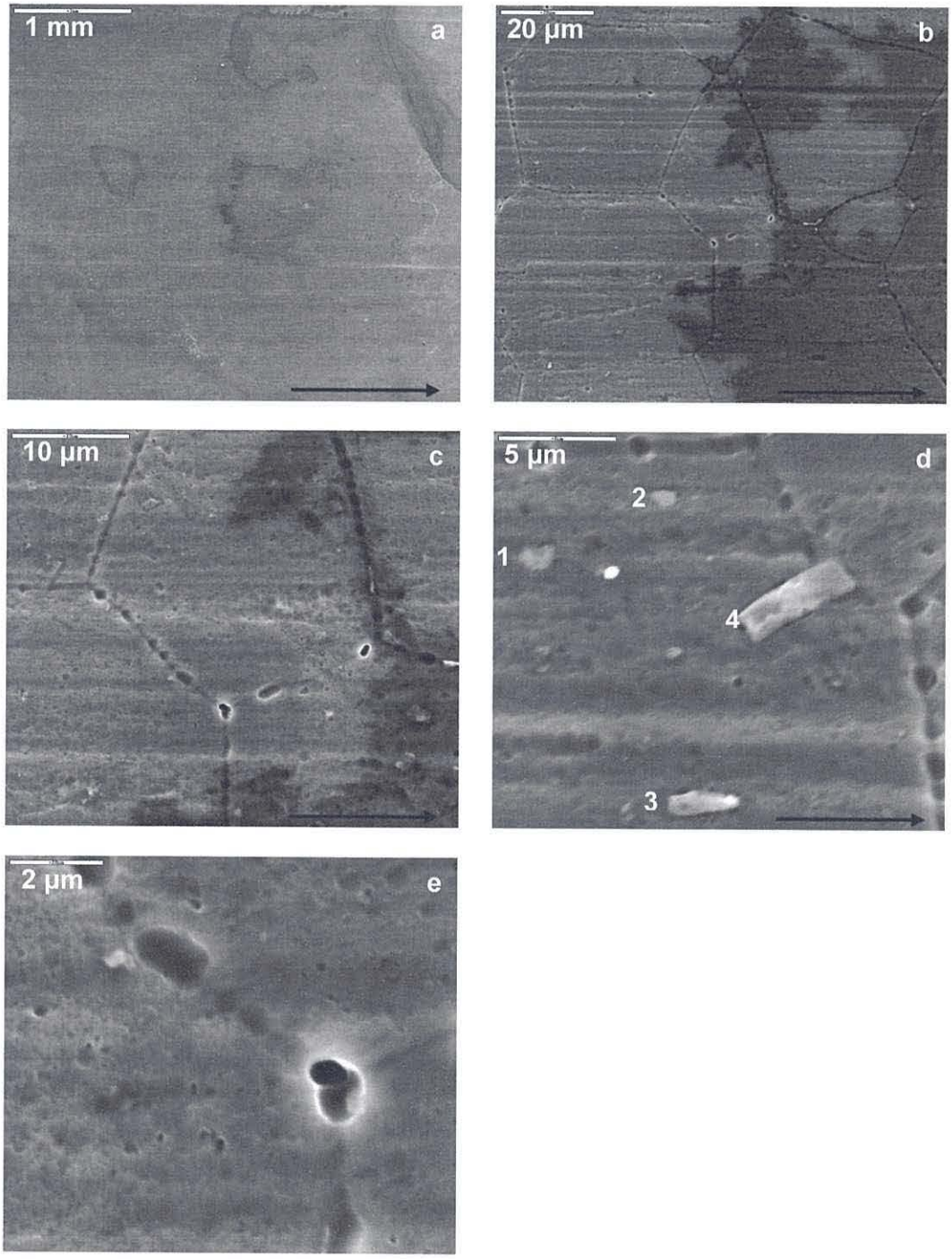

Figure 2.23 SEM images of alloy 6063 etched in AC133 for 6 min. The arrow indicates the extrusion direction, and numbers 1-4 identify some of the intermetallic particles

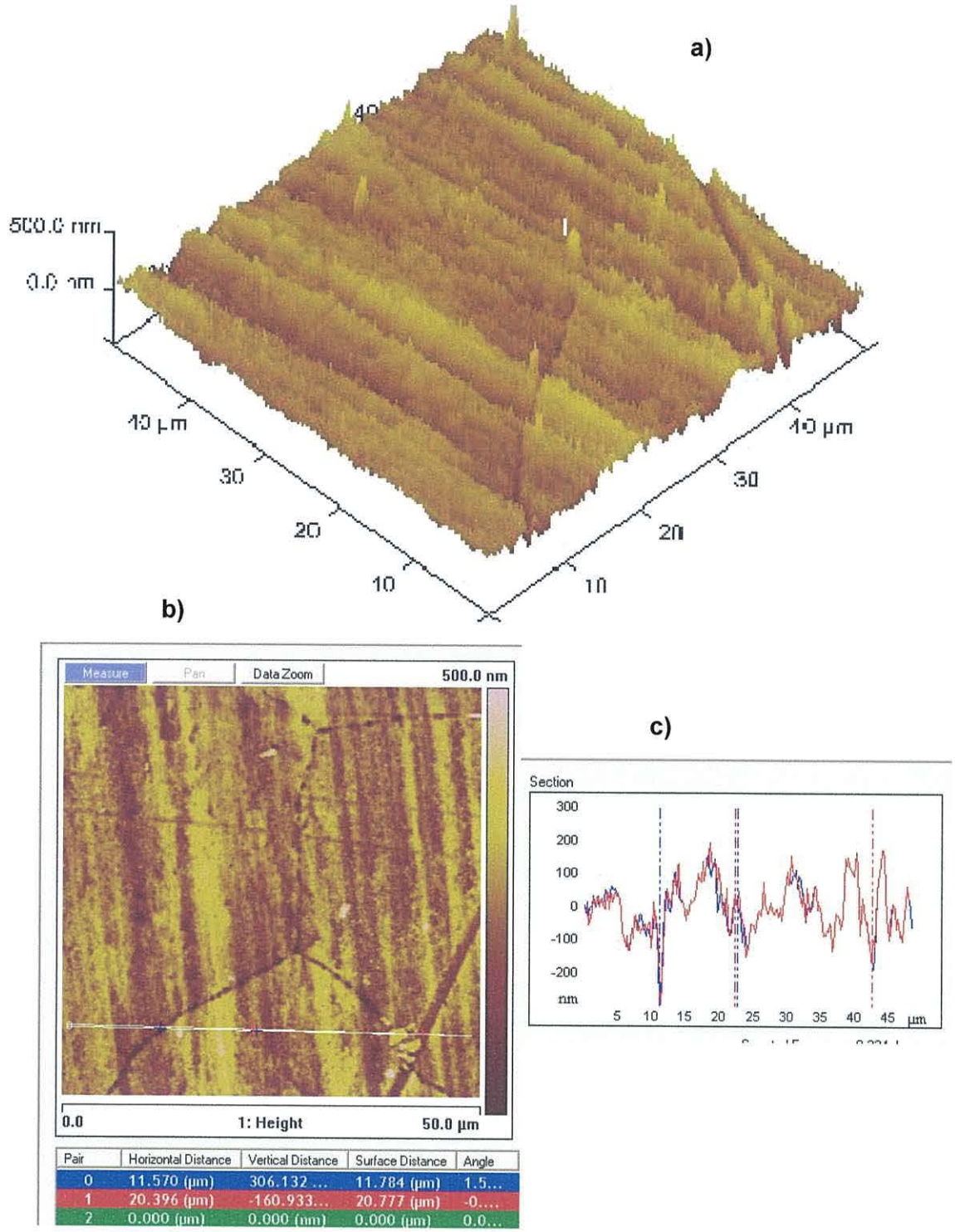

Figure 2.24 AFM images of etched alloy 6063. a) and b) show the morphology of the surface, b) showing the plan view of 3D image a). Shown on image on image a) is a particle labelled I and b) shows the location of the line analysis which is presented at c) - the blue indicates the depth of the grain boundary while the red indicates a scratch

Considering the as received and 6 minute etched surfaces of both the alloys, although the as received alloy 3105 initially appears to be the less textured surface, the difference in depth of the periodicity is less, and the periodicity is more consistent in the 6063 alloy in both conditions.

30 min etch (AC133), alloy 6063

A longer etch time of 30 minutes in AC133 led to a similarly pitted morphology as that of the 6 minute AC133 etched 3105 alloy. However, extrusion die lines were still visible after this longer etch period Figure 2.26b,c,d. Images from optical microscopy show particularly well how the die lines diminish with the greater etch time, whilst the grain boundaries become more pronounced, Figure 2.27. The intermetallic particles discussed earlier on the 6 minute etched surface appear to have been removed. In addition, although the 6 minute etch does not alter the composition of the matrix compared to that of the as received, acetone degreased surface, the 30 min etch shows a significant variation, suggesting enrichment of the surface with the contaminating iron and manganese.

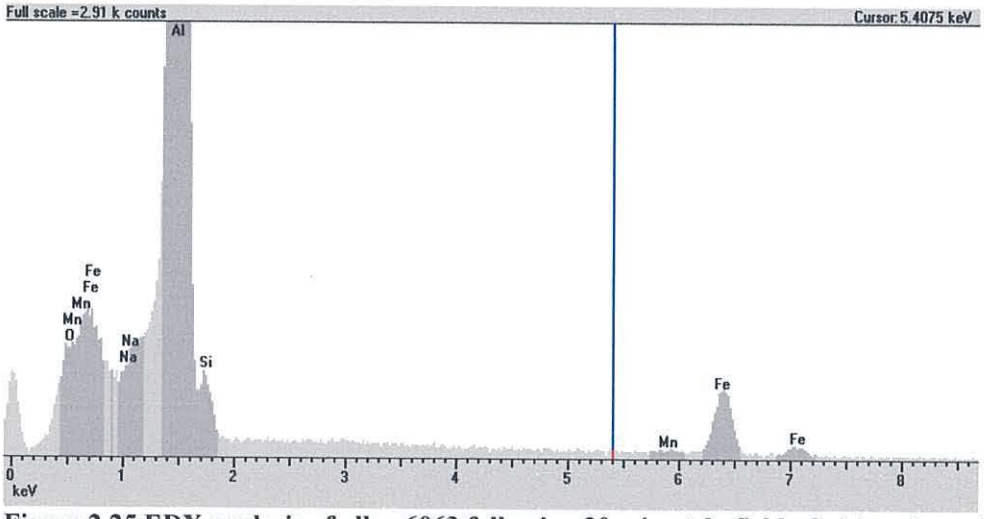

Figure 2.25 EDX analysis of alloy 6063 following 30 min etch, field of vision shown in Figure 2.26c

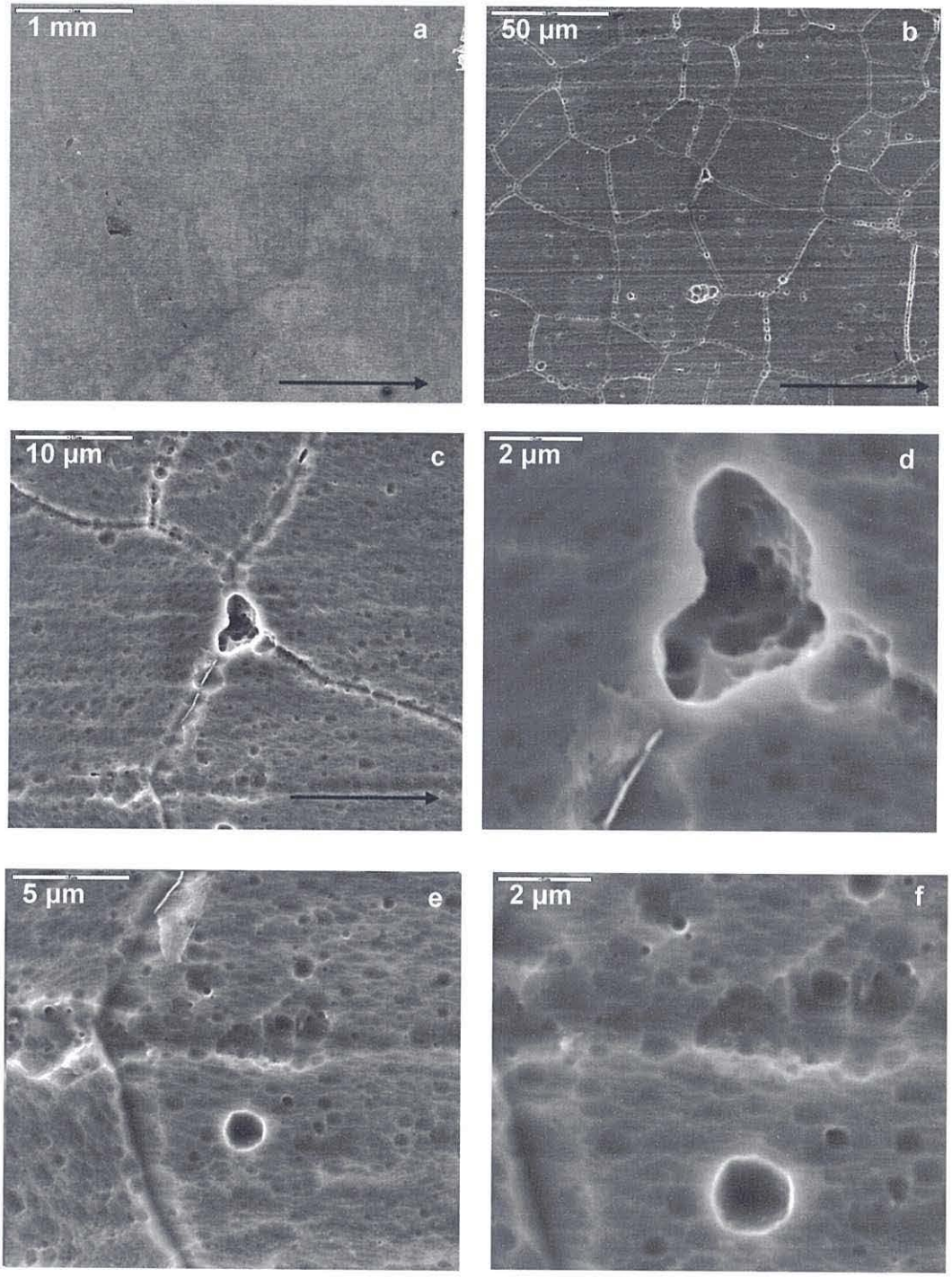

Figure 2.26 SEM images of alloy 6063 etched in AC133 for 30 min. The arrow indicates the rolling extrusion direction

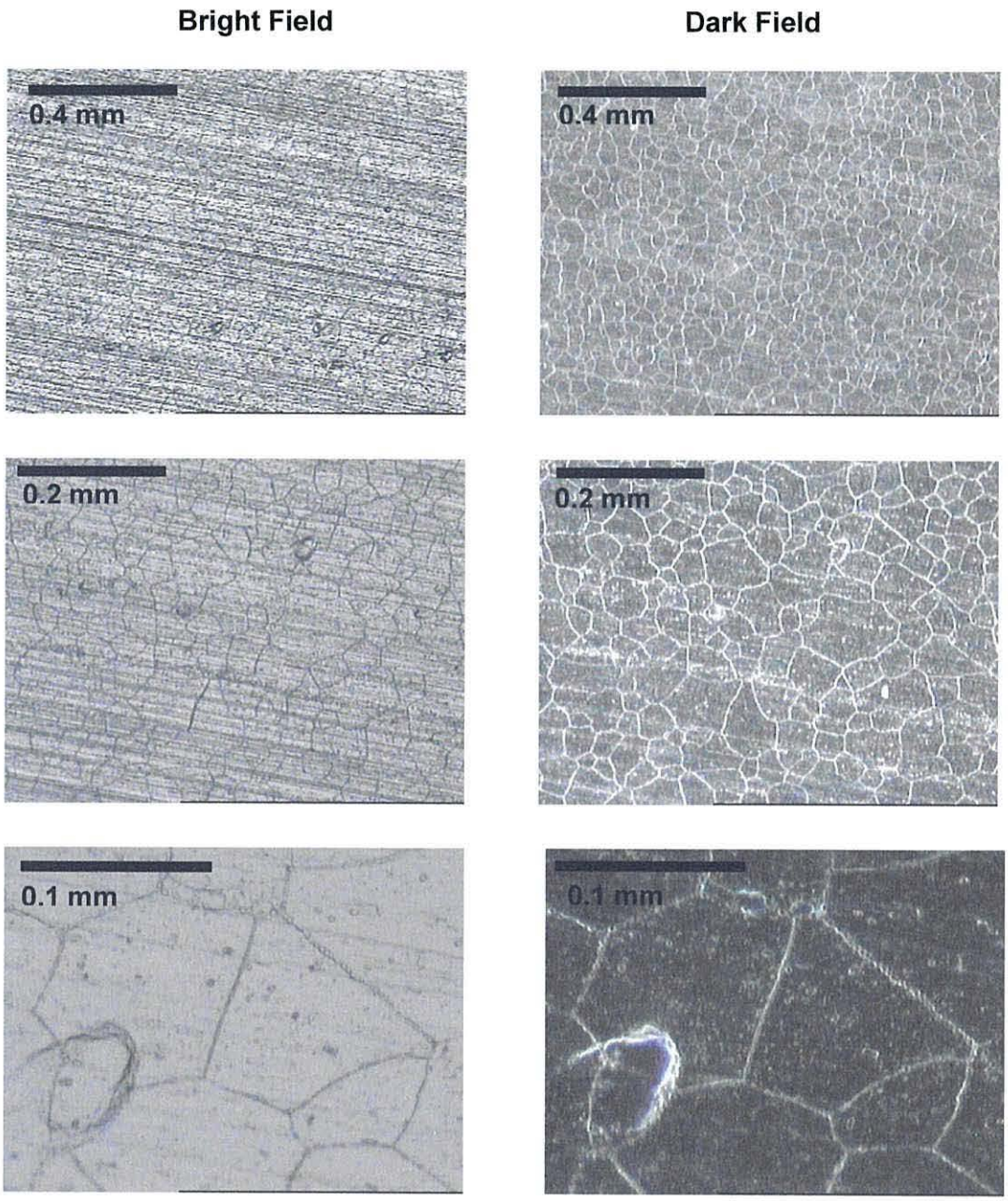

Figure 2.27 Optical image of the as received alloy 6063, bright field image: top x5, second x10, bottom x50 magnification (with internal magnification of 2), left bright field, right dark

Conclusions

The data for the 3105 alloy show that the AC133 etch appears to be an effective etching agent for this alloy even after only 6 minutes exposure with removal of the rolling lines and the formation of pits both evident. This pitted morphology is at variance with that reported for similar etched alloys in the literature. However, it may be that this pitted

morphology improves the adhesion of any post-etching coating technology. Interestingly, an extended etch of AA3105 with ammonium bifluoride solution over 24 hours produces a scalloped topography which has been previously observed in the literature and this may indicate the importance of fluoride within the etching process.

For the 6063 alloy, a 6 minute etch with AC133 showed less visible surface attack than for the 3105 alloy, but some pitting was evident along the grain boundaries. However, a 30 minute etch with AC133 showed similar levels of pitting to that of the 6 minute etched 3105 alloy, although extrusion lines were still evident, attributed to the original depth of the these indentations. It is hoped that the resulting etched morphology observed gives rise to an improved post-etch adhesion of any subsequent coating technology in the same way for the 3105 alloy.

References

(1) Luan, B.; Le, T.; Nagata, J. *Surface and Coatings Technology* **2004**, *186*, 431-443.
(2) Campestrini, P.; van Westing, E. P. M.; de Wit, J. H. W. *Electrochimica Acta* **2001**, *46*, 2553-2571.
(3) S Wernick, P. G. S., R. Pinner *The Surface Treatment and Finishing of Aluminium and its Alloys*; Draper, 2001; Vol. 1.
(4) S Wernick, R. P. *The Surface Treatment and Finishing of Aluminium and its alloys*; 3rd ed.; Draper, 1964.
(5) Digby, R. P.; Packham, D. E. *International Journal of Adhesion and Adhesives* **1995**, *15*, 61-71.
(6) In *Aluminium and Aluminium Alloys*; Davies, J. R., Ed.; ASM International: 2002, 5th ed.
(7) Zhou, X.; Thompson, G. E.; Scamans, G. M. *Corrosion Science* **2003**, *45*, 1767-1777.
(8) Lunder, O.; Olsen, B.; Nisancioglu, K. *International Journal of Adhesion and Adhesives* **2002**, *22*, 143-150.
(9) Lunder, O.; Lapique, F.; Johnsen, B.; Nisancioglu, K. *International Journal of Adhesion and Adhesives* **2004**, *24*, 107-117.
(10) Lunder, O.; Walmsley, J. C.; Mack, P.; Nisancioglu, K. *Corrosion Science* **2005**, *47*, 1604-1624.
(11) Critchlow, G. W.; Yendall, K. A.; Bahrani, D.; Quinn, A.; Andrews, F. *International Journal of Adhesion and Adhesives* **2006**, *26*, 419-453.
(12) Afseth, A.; Nordlien, J. H.; Scamans, G. M.; Nisancioglu, K. *Corrosion Science* **2001**, *43*, 2359-2377.
(13) Afseth, A.; Nordlien, J. H.; Scamans, G. M.; Nisancioglu, K. *Corrosion Science* **2002**, *44*, 2543-2559.
(14) Gras, C.; Meredith, M.; Hunt, J. D. *Journal of Materials Processing Technology* **2005**, *167*, 62-72.
(15) Davoodi, A.; Pan, J.; Leygraf, C.; Norgren, S. *Electrochimica Acta ELECTROCHEMICAL METHODS IN CORROSION RESEARCH Selection of papers from the 9th International Symposium (EMCR 2006) 18-23 June 2006, Dourdan, France* **2007**, *52*, 7697-7705.
(16) Alexander, D. T. L.; Greer, A. L. *Acta Materialia* **2002**, *50*, 2571-2583.
(17) In *General Introduction, Aluminium and Aluminium Alloys*; 5th ed.; Davies, J. R., Ed.; ASM International: 2002, p 1-18.

3. Coating Analysis

The etching of alloys 3105 and 6063, has been described in Chapter 2. Several chrome free coatings for corrosion resistance have been applied to the etched surfaces of these two alloys and will be discussed in this Chapter. Following the application of these coatings, a further layer of paint has been applied by powder coating to replicate the typical commercial process, and also in order to carry out detailed testing and analysis of the whole system. In this chapter, the data from these coated surfaces, both painted and unpainted, have been examined by SEM, TEM, and EDX, and these data are described. These data have been used to investigate coating morphology, coverage, bonding and composition. In particular, SEM provides information in plan view to help ascertain the surface coverage, morphology and topography prior to painting whilst TEM has been used in cross section (Figure 3.1).

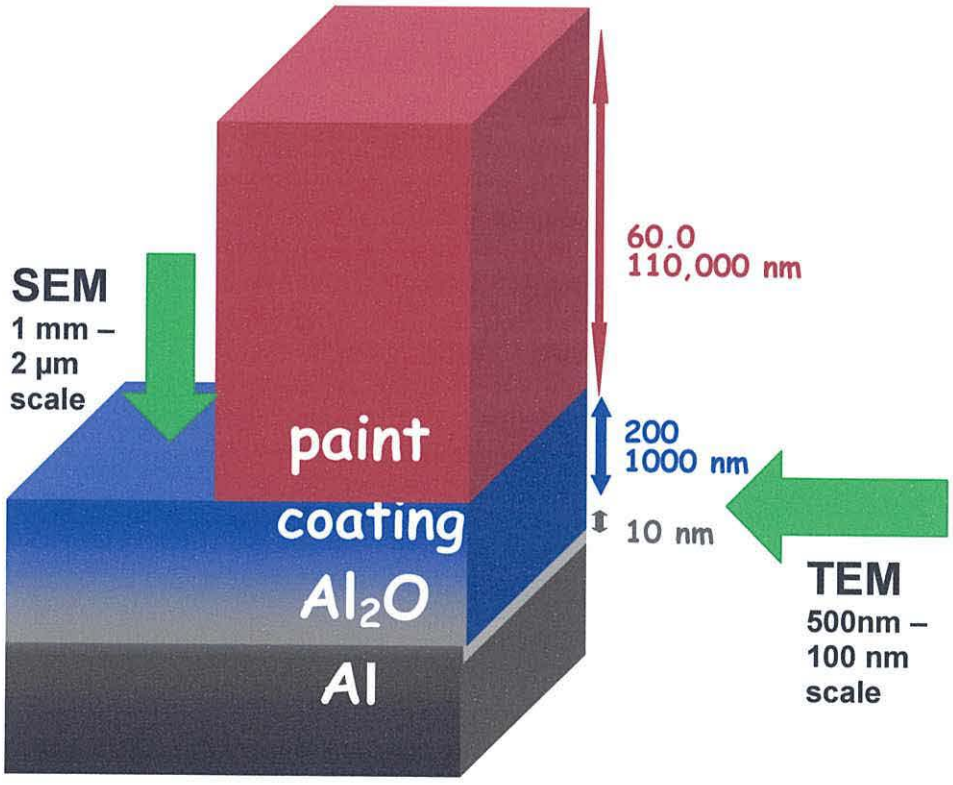

Figure 3.1 Schematic image showing SEM (plan) and TEM (cross-sectional) analyses of the coated /and painted substrate

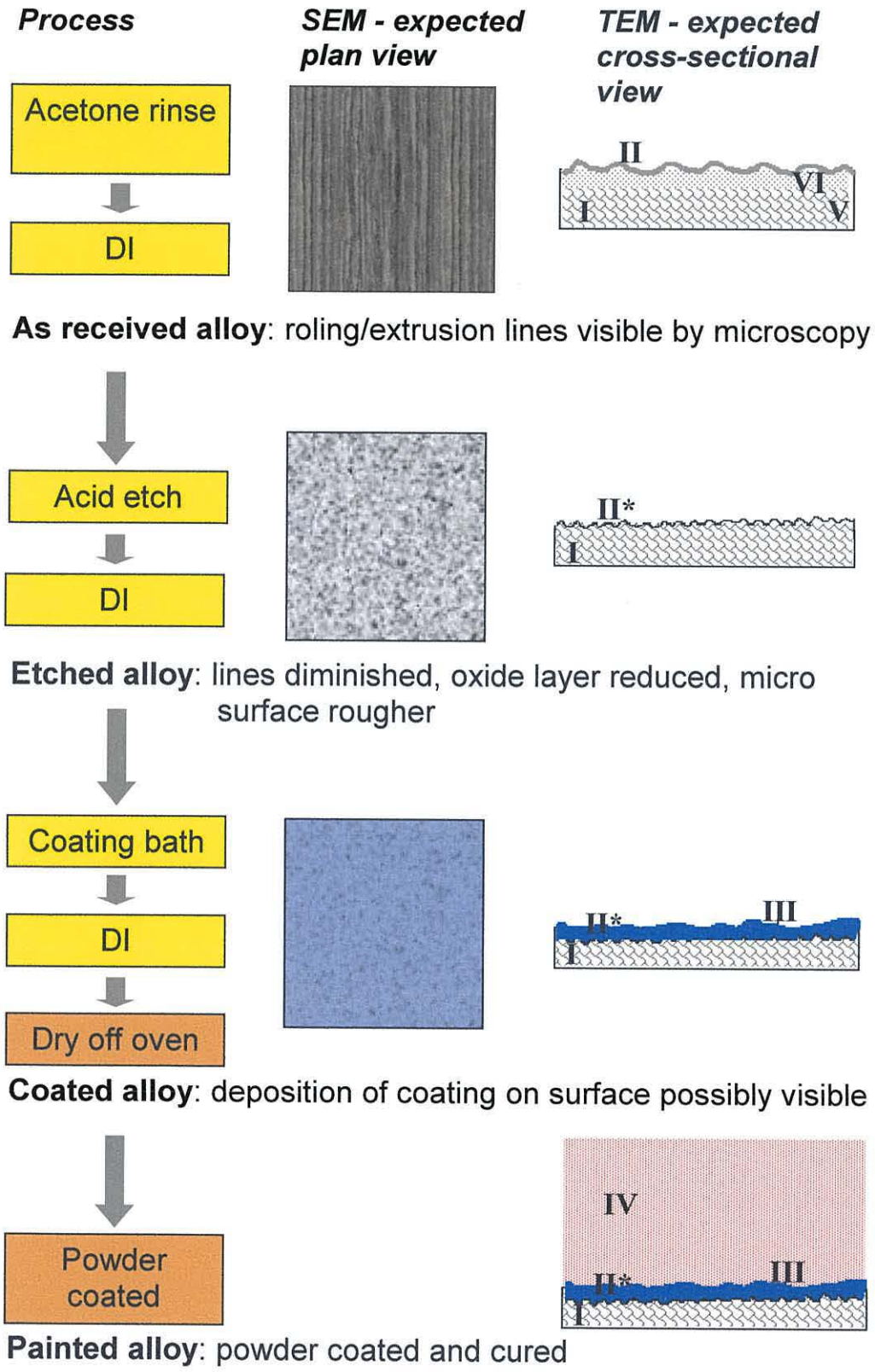

Figure 3.2 Schematic diagram of the plan and cross-sectional views of the coated /and painted substrate using SEM and TEM techniques. The various layers represent I - aluminium substrate, II - aluminium oxide, II* - reformed oxide, III – coating, IV - paint, V - large grain defects of the bulk material and artefacts caused by ultramicrotoming process, VI - nanograined surface layer caused by rolling/extrusion

In detail, TEM has been used alongside SEM to give a more complete description of the coatings. Thus, TEM has been used to carry out cross-sectional analysis of the coating and subsequent paint layer on the substrate surface at sub-nanometer scale resolution, Figure 3.1, Figure 3.2. Figure 3.2 shows the manner in which the alloys have been treated and analysed, and also shows generalisations of typical expected data for clarity of the experimental data presented later in this Chapter.

EDX analysis has been conducted in both SEM and TEM analyses (i.e. both plan and cross sectional analysis) to analyse the coating composition at the surface regions of the samples, and also to ascertain how the surface may vary with depth from the aluminium oxide through to the paint layer. These microscopic analyses have been further complemented by the use of electrochemistry to ascertain resistance to oxidation, physical tests to examine adhesion, and salt spray and humidity testing to examine resistance to corrosion to gain as complete a picture as possible of these new chrome-free coatings. The latter data will be discussed in Chapters 4, 5 and 6 of this thesis.

As described in Chapter 2, the etching process is known to remove the aluminium surface oxide and also sub-surface defects.[1] Thus, the use of the AC133 etchant which has been used in the studies described in this Chapter results in a finely textured surface, at the sub-micron level, which it is hoped should promote deposition and adhesion of the subsequent coating. In this thesis, as is typical in the commercial treatment for architectural aluminium, due to the intricate shapes produced by extruding aluminium, the chrome-free coatings have been applied through dip coating i.e. submerging in a bath of solution, followed de-ionised water rinsing. Dip coating has also been chosen in this thesis as this is preferred to spray coating to ensure an even coating is achieved and that the coating is applied within crevices and corners which are typical in the

commercial use of 6063 alloy extrusions. Rinsing has also been preferred to a no-rinse system in the experimental design used here, to prevent product build up in corners and crevices where the coating might settle.

The pretreatmed samples have then been oven dried to remove any moisture, and sub-divided into three groups for detailed analysis. The first group of samples have been investigated by SEM and EDX analysis whilst the second and third groups have been further treated by a successive process of powder coating. In detail, the second group of samples were powder coated with a clear lacquer, and were then sent for independent Lockeed testing by Innoval Technology Ltd. For the Lockheed test, an accelerated corrosion test lasting 1000 h, the panels were scribed, both parallel and perpendicular to the rolling direction, before being inoculated with HCl and placed in a cabinet of 85 % relative humidity. The samples were removed and visually examined and scanned/photographed at intervals of 24, 250, 500 h, and at the end of the test at 1000 h. The results of this test will be discussed in Chapter 4. Following the Lockheed testing, sections of the panels were then ultramicrotomed and cross-sections were analysed by TEM and EDX by Manchester University, Corrosion and Protection Centre. These TEM data are presented as part of this Chapter. Finally, the third group of coated panels have been powder coated with a beige polyester powder, and have been subjected to physical and accelerated corrosion tests which will be discussed in Chapter 4.

The chrome-free coating compositions studied within this Chapter are shown in Table 3.1, and the analyses carried out on the samples are indicated in Table 3.2. The compositions of the coatings have been chosen based around the use of hexafluorotitanic or hexafluorozirconic acids. Aqueous solutions of these acids have

Pretreatment/gl^{-1}	H_2F_6Zr	H_2F_6Ti	NH_4HF_2	PAA	PVA	$NiSO_4$	pH
1	7.56						1.85
2		8.375					0.76
3	3.48	8.375					0.88
4	3.48	8.375		0.17			0.94
5	0.348	0.8375		0.02			1.41
6	2.52		0.4	0.19			1.97
7	2.52	5.25	0.4	0.19			1.78
8	2.52	5.25	0.4	1			1.93
9	2.52	5.25		0.25	0.1		2.11
10	2.52	5.25				3.5	2.09

Table 3.1 Composition of coatings.

	3105			6063		
Pretreatment	SEM +EDX	TEM	EDAX TEM	SEM+ EDX	TEM	TEM EDX
1	6		6	6	6	6
2	3/6		6		6	6
3	3/6		6		6	6
4	3/6	6	6		6	6
5	3/6	6	6		6	6
6	6			6		
7	6			6		
8	6			6		
9	6			6		
10	6			6		

Table 3.2 Analysis carried out on the various coatings on both alloys. The number refers to the coating time in minutes

been chosen because it was hoped that they would act upon aluminium metal to produce a pseudo-conversion coating layer; i.e. that they would form a protective oxide layer on the aluminium surface to reduce corrosion but also that that layer would contain titanium or zirconium oxide within it. Furthermore, it was hoped that the fluoride within the acids would act in an etch-deposition mode, thereby covering the whole aluminium surface at an atomic scale. The other chemicals within the composition were considered as follows:- ammonium bifluoride to increase etching power, polymers (PVA and PAA) were added to study their effects on coating adhesion, and nickel sulphate to provide colour to aid visual observation.

Pretreatment 1 – Fluorozirconic acid

SEM analysis in plan view has been carried out following a 6 min coating on alloy 3105 following an etching process, which was described in Chapter 2. This coating is referred to as Pretreatment 1 and is based on fluorozirconic acid. In plan view, the coating appears to give a uniform coverage, Figure 3.4a. Similar characteristics to that of the etched surface are observed, but with a greater population density of holes and pits, Figure 3.4b,c. The rolling direction is also apparent in the images. Although the coated surface appears to have a higher number of pits than that of the etched surface, they of are a smaller size - around 5 μm in length, Figure 3.4e,f, - to those of the etched only surface, Chapter 2, and less pores are apparent. The holes on the coated surface also appear less "clean" or sharp than those on the etched surface, with less charging from the electron beam evident. The presence of additional pitting of the metal surface suggests that the fluorozirconc acid is acting both as an etchant and as a precursor to coating deposition. The latter is further supported by the presence of small deposits, as indicated by the arrow in Figure 3.4e. EDX analysis confirms the presence of zirconium, Figure 3.3.

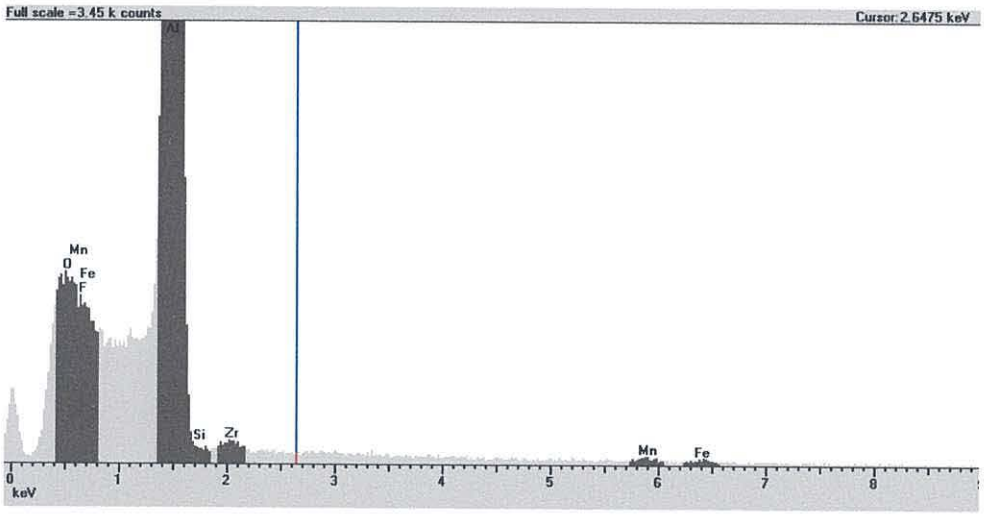

Figure 3.3 EDX analysis of alloy 3105 coated with Pretreatment 1 for 6 minutes, identifying the presence of zirconium, field of vision shown in Figure 3.4e

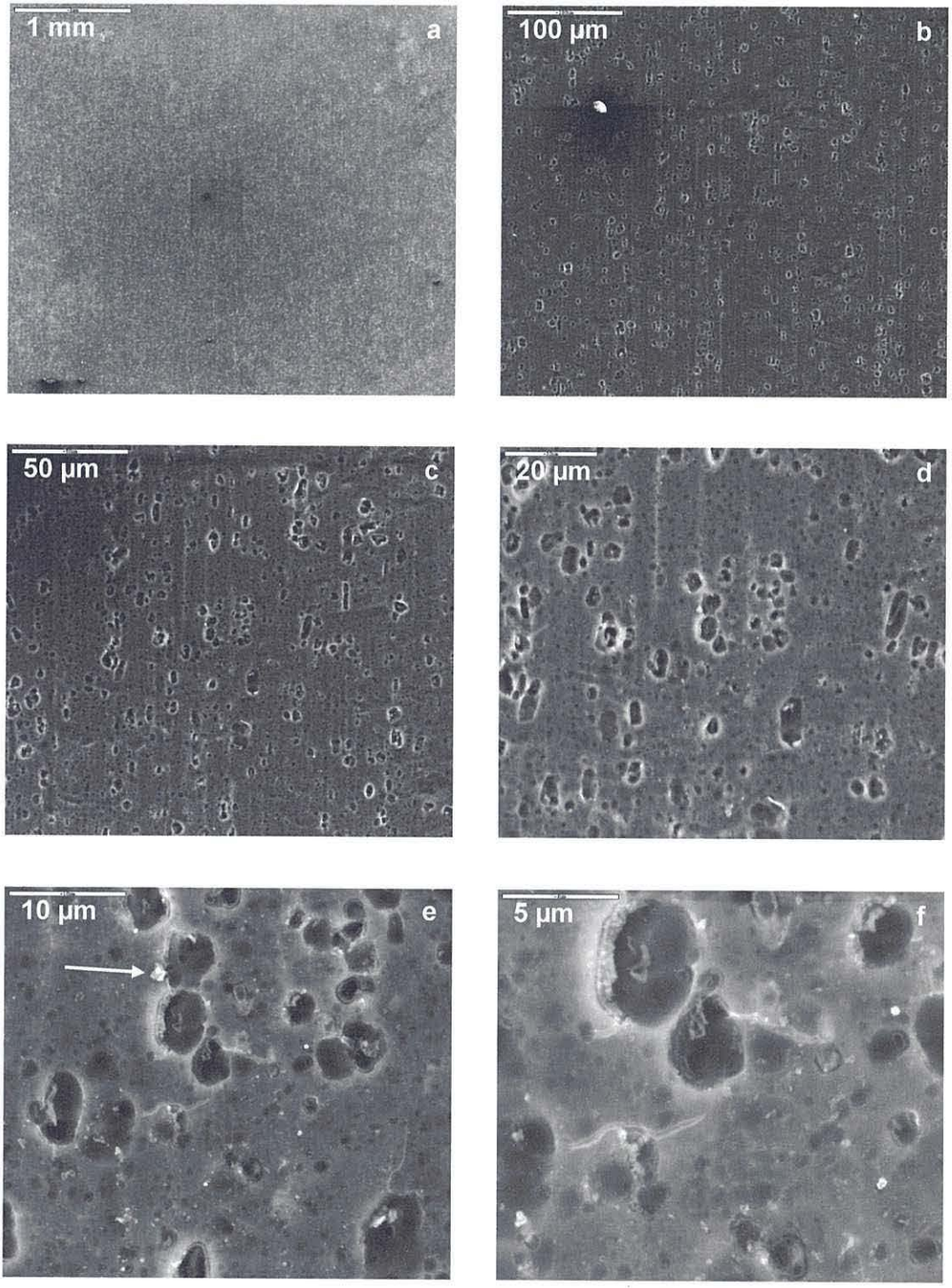

Figure 3.4 SEM images of alloy 3105 coated with Pretreatment 1 for 6 minutes. The arrow indicates an example of deposit

SEM analysis has also been carried out using Pretreatment 1 for 6 min on alloy 6063. The SEM data show that the coverage visible at macroscopic scale (1mm scale bar) is not uniform, but that a number circular patterns are visible, similar to a rippling effect, Figure 3.5a. Closer inspection at higher magnification shows the grain boundary lines and a number of intermetallic particles, Figure 3.5b-f. The extrusion lines are less prominent on the coated surface compared to that of the etched surface for the same alloy, discussed in Chapter 2, and, at the microscopic level (< 5 μm), the surface appears more scalloped. Similar, scalloped surface topographies have been reported by Lunder and co workers[2,3] and Critchlow and co workers,[4] discussed in Chapter 2. These workers ascribed their formation to the presence of fluoride in the etchant solution. These observations are in line with the data here where, as stated for the 3105 alloy, fluorozirconic acid is believed to act both as an etchant and as a coating deposition precursor. No notable difference in morphology between the darker and lighter regions is evident, however the difference in contrast may suggest a thicker coating for the former. Although quantitative analysis is difficult using EDX in an SEM, the analysis carried out suggests that a greater amount of zirconium may have been deposited in the darker region, Figure 3.6a,b, which supports the assertion that the difference in contrast is due to a thicker coating deposition. The frequency of intermetallic particles also appears to be greater on the coated surface than the etched surface, with the immediate area surrounding the particles darker. This could be due the surrounding darker area making the intermetallic particles more apparent.[5] Analysis of these particles indicates manganese and iron, and high zirconium content compared with analysis of the matrix, Figure 3.6c. It would be expected that these would be cathodic sites,[6] and that preferential etching of these cathodic particles or the area surrounding these may have caused a geometry that has resulted in the trapping of a more coating, or the nature of the particles may have attracted a better deposition.[7]

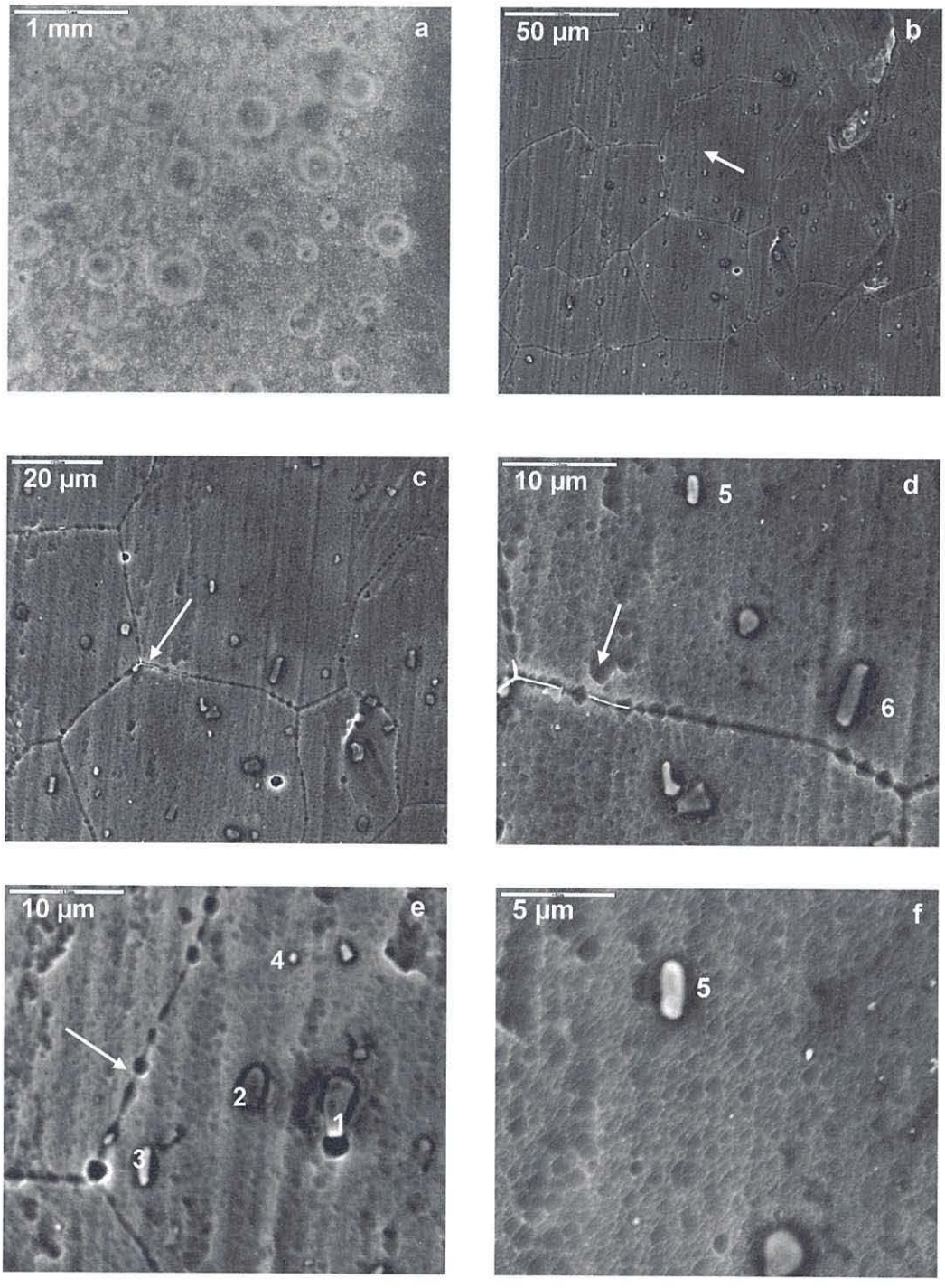

Figure 3.5 SEM images of alloy 6063 coated with Pretreatment 1 for 6 minutes, the numbers refer to intermetallic particles, whilst the arrows show the grain boundaries

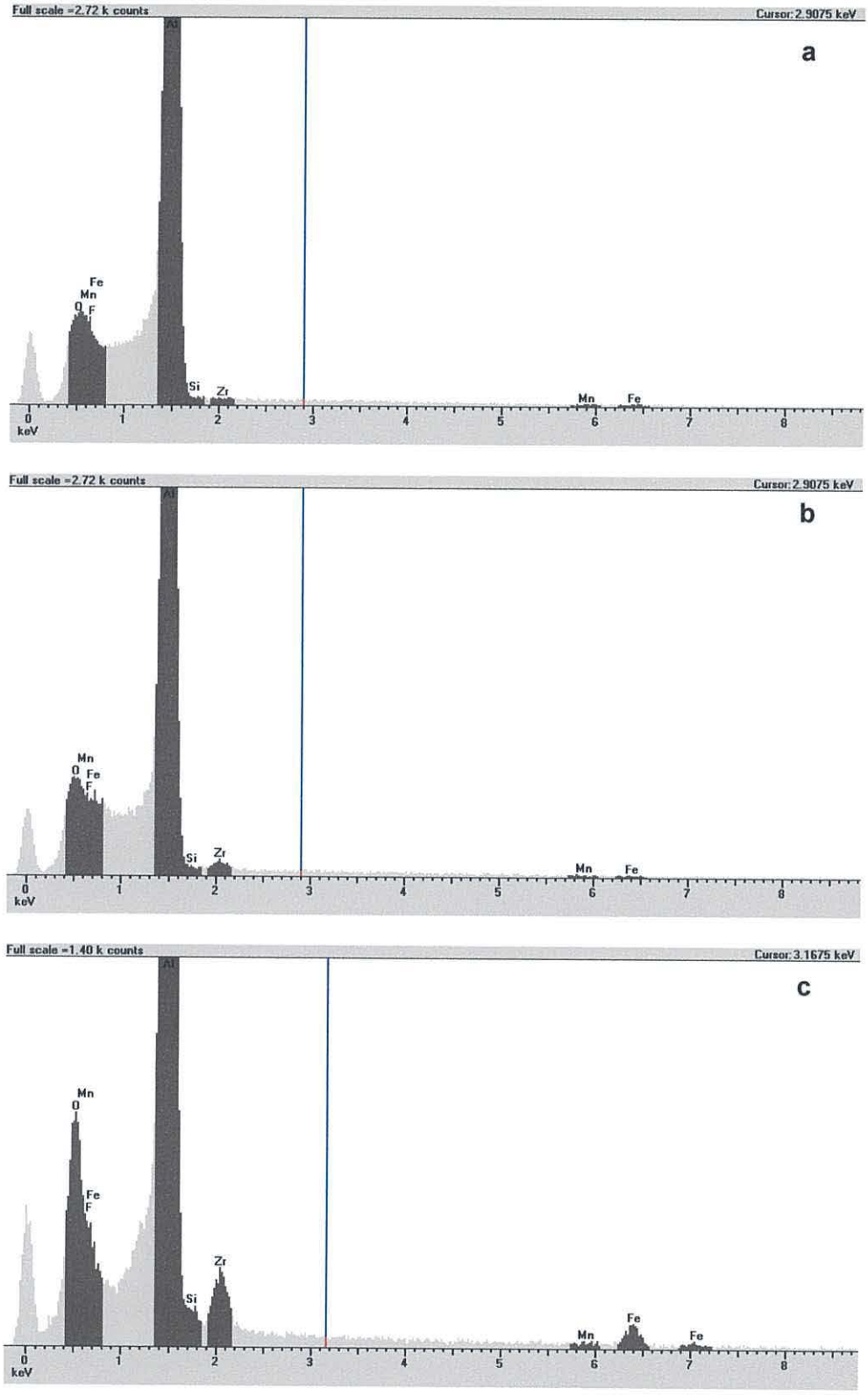

Figure 3.6 EDX analysis of alloy 6063 coated with Pretreatment 1 for 6 minutes a) lighter area shown in Figure 3.5e, b) darker area of same size (not shown), and c) particle 6 identified in Figure 3.5d

In general, from EDX analysis and comparing the zirconium to the background reading, it can be concluded that zirconium has been deposited in some form on the surface of the substrate on both alloys. From microscopic observations, a foam-like uniform coating has been deposited on the 3105 alloy, possibly also depositing within in the etch pits, resulting in the reduction of their appearance both in terms of size and morphology.

By comparison, deposition on the 6063 alloy, which has greater alloying elements, does not appear uniform, but the greater prominence of the intermetallic particles, and higher zirconium levels on darker regions, suggests preferential deposition at these sites. The scalloped morphology may be due to the etch action of the pretreatment at the other (lighter) sites. During these pretreatment processes, it is expected that the etching and depositing processes are competing reactions at the oxide surface. Thus, coating formation requires deposition to be favourable.

A subsequent group of alloy 6063 samples, following coating with Pretreatment 1, have been analysed by TEM. This group of samples were dried and powder coated, before being sent for Lockheed testing, which will be discussed in Chapter 4. Following 10 weeks of Lockheed testing, the samples were prepared by ultramicrotoming before being analysed by TEM. The micrographs, Figure 3.7, Figure 3.8a,b, show ultramicrotomed cross sections of alloy 6063 treated with Pretreatment 1, and then powder coated. A general description of the data is given here. To aid comparison with subsequent micrographs, all TEM data are presented in the same format i.e. the aluminium substrate at the bottom of the image, and the paint layer at the top. Figure 3.8a shows a multi-layer system, which can be described from the bottom to the top of the image as: the aluminium substrate **I**, a thin reformed aluminium oxide layer **II**, a thin layer of paint – exclusive to this sample **IV***, the pretreatment layer **III**, and the

main paint layer **IV**. The characteristics and sub-structure defects of the microstructure can be seen in the aluminium substrate (e.g. at **V**), and there may also be the presence of artefacts which may have been caused by the ultramicrotoming process, similar to that of the bulk microstructure described for other alloys.[8] It should be noted that some of the images may be distorted and may show some features caused through nature of the ultramicrotoming process necessary to obtaining the TEM data e.g. compression resulting in a rippling effect, giving the appearance of scalloping. Where it is clear that such artefacts are present, these will be discussed.

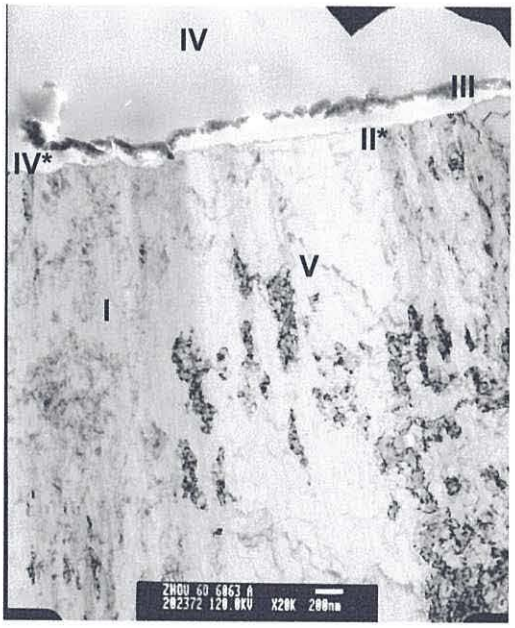

Figure 3.7 TEM of an ultramicrotomed cross section of alloy 6063 coated with Pretreatment 1 for 6 minutes and subsequently powder coated, and Lockheed tested. The various layers represent I - aluminium substrate, II* - reformed oxide, III – coating, IV - paint, V - defects of the bulk material and artefacts caused by ultramicrotoming process

In considering the processes the sample has been exposed to, prior to TEM analysis, firstly the natural oxide layer formed on the surface of the aluminium substrate would have been removed during the etching process. Thus, the approximately 10 nm thick oxide layer visible on the micrograph, **II** is the oxide layer reformed in air, which has developed during the minutes between etch and pretreatment processes. This is

expected for aluminium given the very high electropositivity of the element, which has been discussed in the introduction.

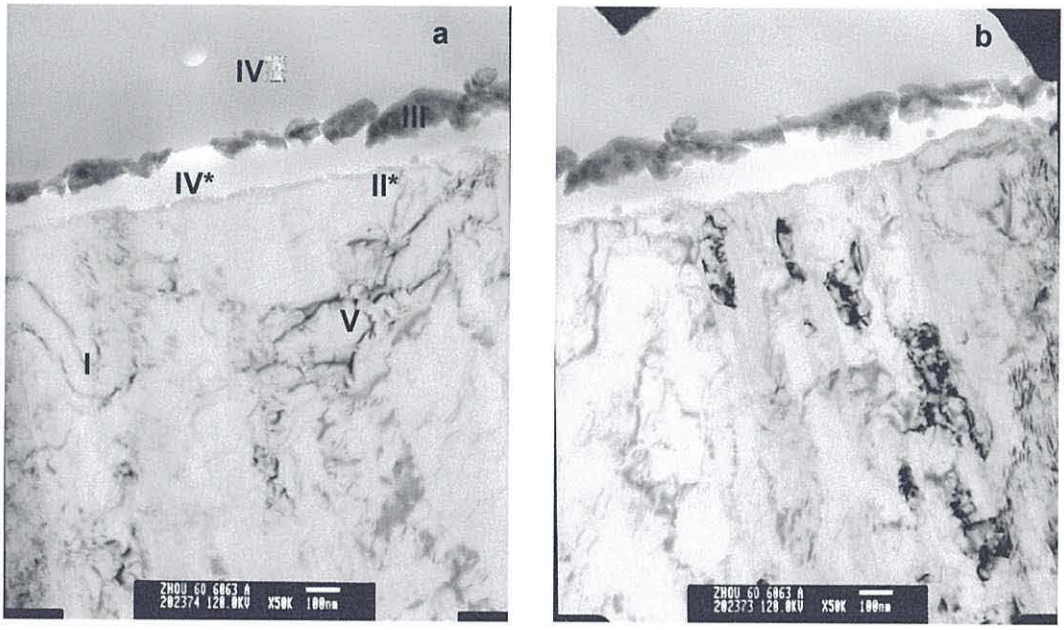

Figure 3.8 TEM at higher magnifications of the ultramicrotomed cross section shown in Figure 3.7, alloy 6063 coated with Pretreatment 1 for 6 minutes and subsequently powder coated and Lockheed tested. The various layers represent I - aluminium substrate, II* - reformed aluminium oxide, III – coating, IV - paint, V - defects of the bulk material and artefacts caused by ultramicrotoming process

The absence of near-surface defects suggests that the outermost surface of aluminium has been successfully etched away, indicating that the use of Almetron's AC133 acid etch is an efficient process in terms of near-surface layer removal In the paper by Zhou,[9] previously discussed in Chapter 2, the altered layer found on alloy 5005 sheet was 300 nm, and the sulphuric acid/hydrogen fluoride cleaner used in this previous study failed to completely remove the deformed layer, leaving approximately 100 nm behind.

Towards, the top of the TEM micrograph, the white layer above the oxide (IV*) is a thin paint layer, which has penetrated through the pretreatment layer (III), visible between the paint layers. The pretreatment layer appears to have a number of defects

through which the paint may have permeated, and varies in thickness from around 20 to 140 nm. This paint permeation in all probability occurred during the paint application and/or curing process, although this cannot be stated with absolute certainty due to the number of processes the sample has undergone prior to TEM analysis. In further analysis of the same sample, significant delamination of the pretreatment layer to the oxide layer is also evident, Figure 3.9a,b,c,d, which may have been caused by the ultramicrotoming process, during testing of the sample, or may not have been attached at all. Although the cause of the paint penetration, and detachment of the pretreatment layer may not be certain, the key information from this data is that adhesion of the pretreatment layer to the substrate is not sufficiently strong for this to be a viable coating process for corrosion protection.

It can be concluded that although SEM and EDX analyses indicate deposition of a zirconium-based coating on the surface prior to powder coating, as a complete system, with a paint layer, TEM analysis suggests that Pretreatment 1 does not provide a coating that shows adequate adhesion to the substrate surface. The delamination of the coating and paint ingression suggests that the coating would not afford the desired long term corrosion resistance.

Whilst in the TEM, EDX analysis of the coatings on the ultramicrotomed section was also carried out for alloy 6063, Figure 3.10. EDX analysis of an ultramicrotomed section of alloy 3105 was also carried out, Figure 3.11a, b. Analysis of the coating on alloy 3105 was carried out in the following areas; the inner region – the region of coating closest to the aluminium alloy, and the outer region – that furthest from the alloy.

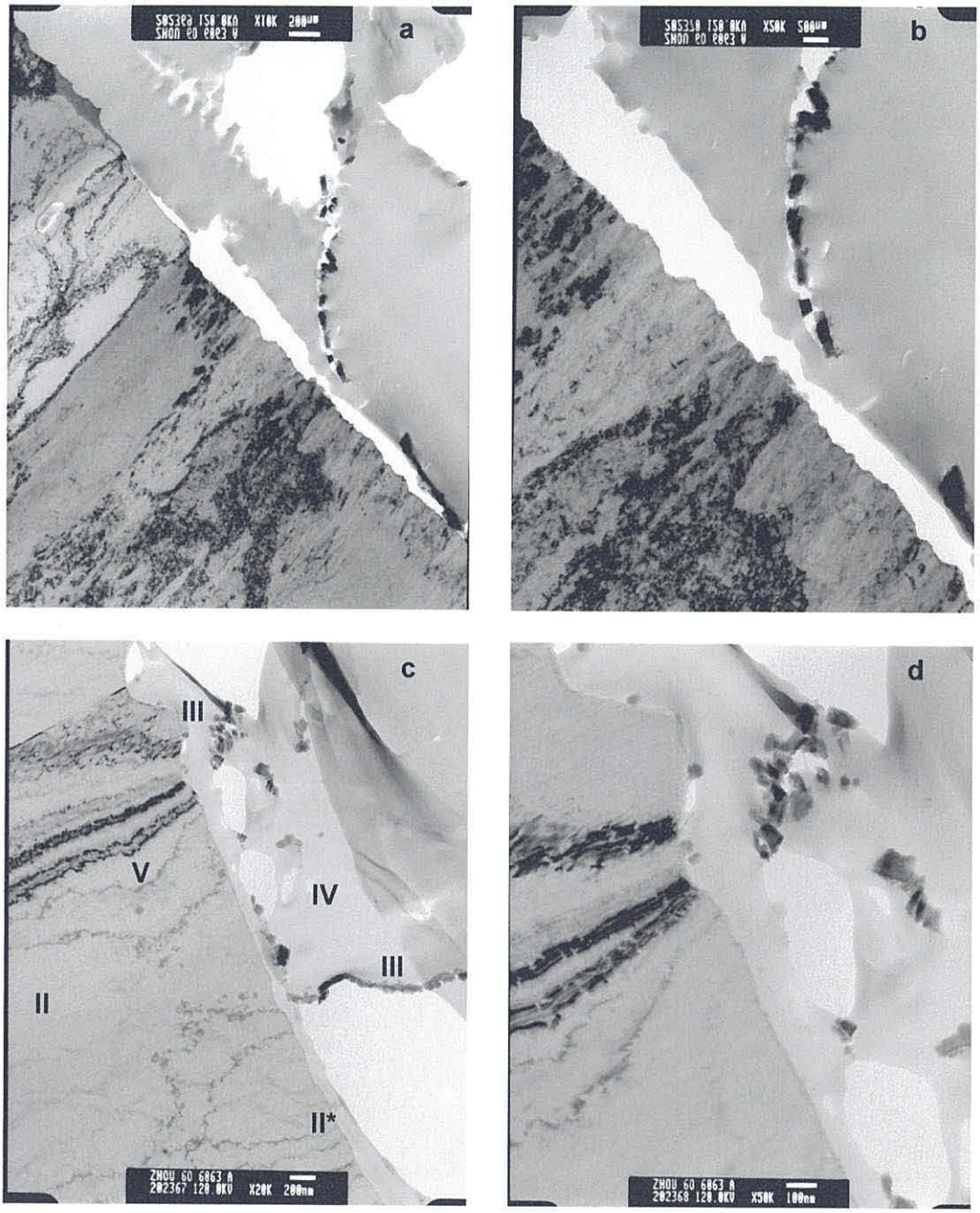

Figure 3.9 Further TEM of an ultramicrotomed cross section of alloy 6063 coated with Pretreatment 1 for 6 minutes and subsequently powder coated, and Lockheed tested. The various layers represent I - aluminium substrate, II - aluminium oxide, II* - reformed oxide, III – coating, IV - paint, V - large grain defects of the bulk material and artefacts caused by ultramicrotoming process

The presence of zirconium is clearly visible for both alloys 3105 and 6063. Also apparent is the presence of oxygen, which is similar in ratio for the for both the inner and outer region analysis for the 3105 alloy. However, a far greater proportion of

oxygen, relative to the zirconium seems to be present in the analysis of the coating on the 6063 alloy. Thus, the presence of aluminium in the same layer as zirconium suggests that the coating layer formed has one of the characteristics of a conversion coating. However, the fact that it appears to delaminate suggests that the coating is an additional layer which forms on the top of the surface which would not be in line with a conversion coating. The aluminium in the coating could be from dissolved aluminium in solution, from the etching action of the pretreatments. On the basis of these data, further studies investigated both the use of fluorotitanic acid and also the issue of coating delamination. It should be noted that the presence of nickel and copper peaks are due to the specimen holder.

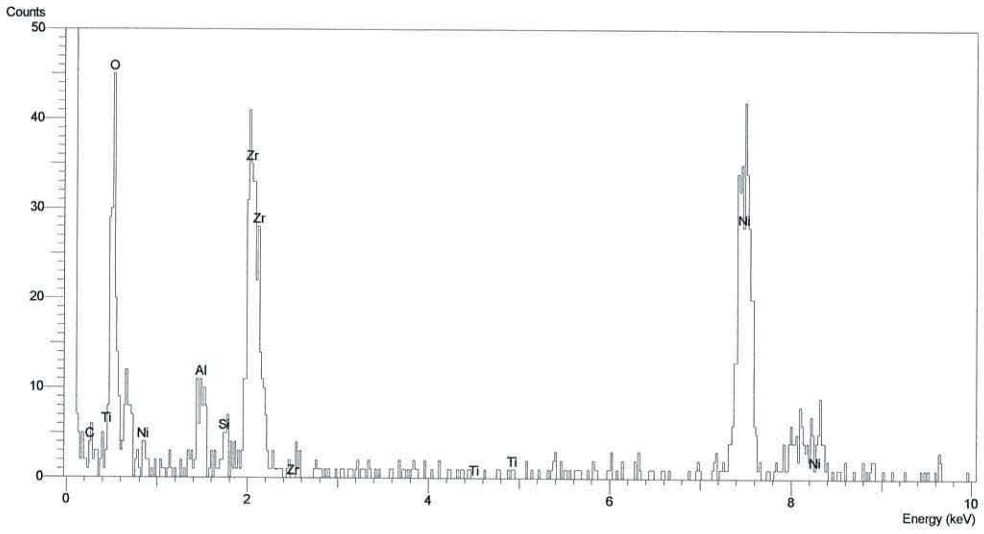

Figure 3.10 EDX analysis of the ultramicrotomed cross sections of alloy 6063 coated with Pretreatment 1 for 6 minutes and subsequently powder coated, and Lockheed tested

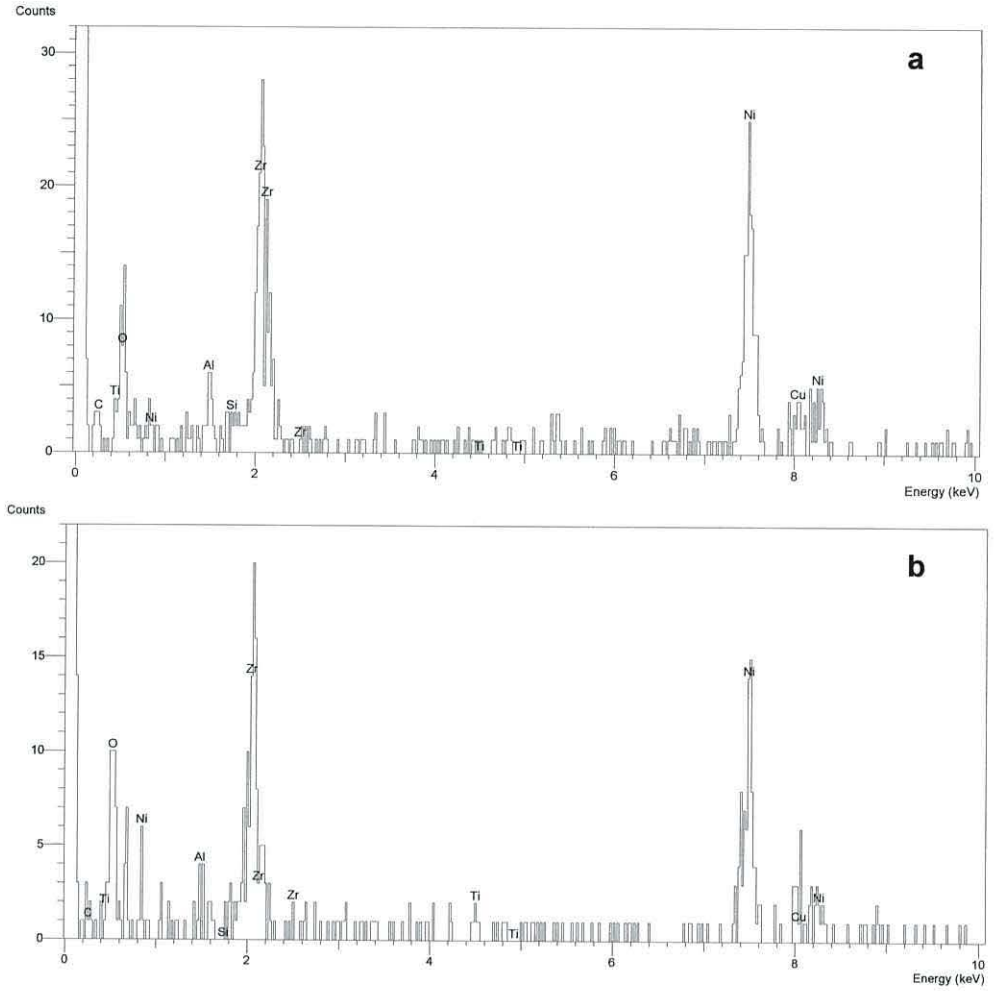

Figure 3.11 EDX analysis of the ultramicrotomed cross sections of alloy 3105 coated with Pretreatment 1 for 6 minutes, and subsequently powder coated and Lockheed tested. a) shows the analysis performed on the outer outer region, b) the inner region

Pretreatment 2 - Fluorotitanic acid

SEM analysis has been carried out following a 3 min coating with fluorotitanic acid on alloy 3105. The analysis of the SEM images reveals a consistent surface on the whole, Figure 3.12a. EDX analysis does not indicate the presence of titanium on the surface of the aluminium, Figure 3.13. Upon magnification, the surface resembles that of Pretreatment 1 (fluorozirconic acid after 6 minutes of treatment). Pores, pits and rolling lines are all apparent, Figure 3.12b, c, d. However, charging of the pit edges is observed as for the etched sample of this alloy. A greater population of pits compared to the etched surface and following Pretreatment 1 is apparent, which may reflect what is expected to be the more aggressive etching nature of this acid. Further magnification reveals the appearance of a more sponge like texture than that of Pretreatment 1, Figure 3.14e, f, with a higher density of pores.

The corresponding SEM analysis for the same pretreatment, but this time following a 6 min coating on the same alloy, shows less charging of the hole edges. The surface closely resembles that following Pretreatment 1 after 6 min of exposure, Figure 3.14a. The holes appear less deep than those following 3 minutes of treatment, Figure 3.14b. Fewer holes are also visible at high magnification which may either be due to increased etching by the fluorotitanic acid removing surface material around the pores formed after 3 minutes or that a longer treatment time leads to a greater amount of coating deposit, which fills the in the pit voids created by the previous etching step/the initial Pretreatment stage (the 3 minutes of exposure discussed above). Interestingly, the rolling lines are also less apparent here than after 3 min exposure. This could be attributed to the etch action of Pretreatment 2 removing the surface layers, or indeed, coating depositing which is disguising the rolling lines. Figure 3.15 shows the EDX spot analysis, and clearly shows the presence of titanium after this longer treatment

time, whilst analysis of the area visible in Figure 3,12d, presented in Figure 3.13, does not conclusively indicate any titanium.

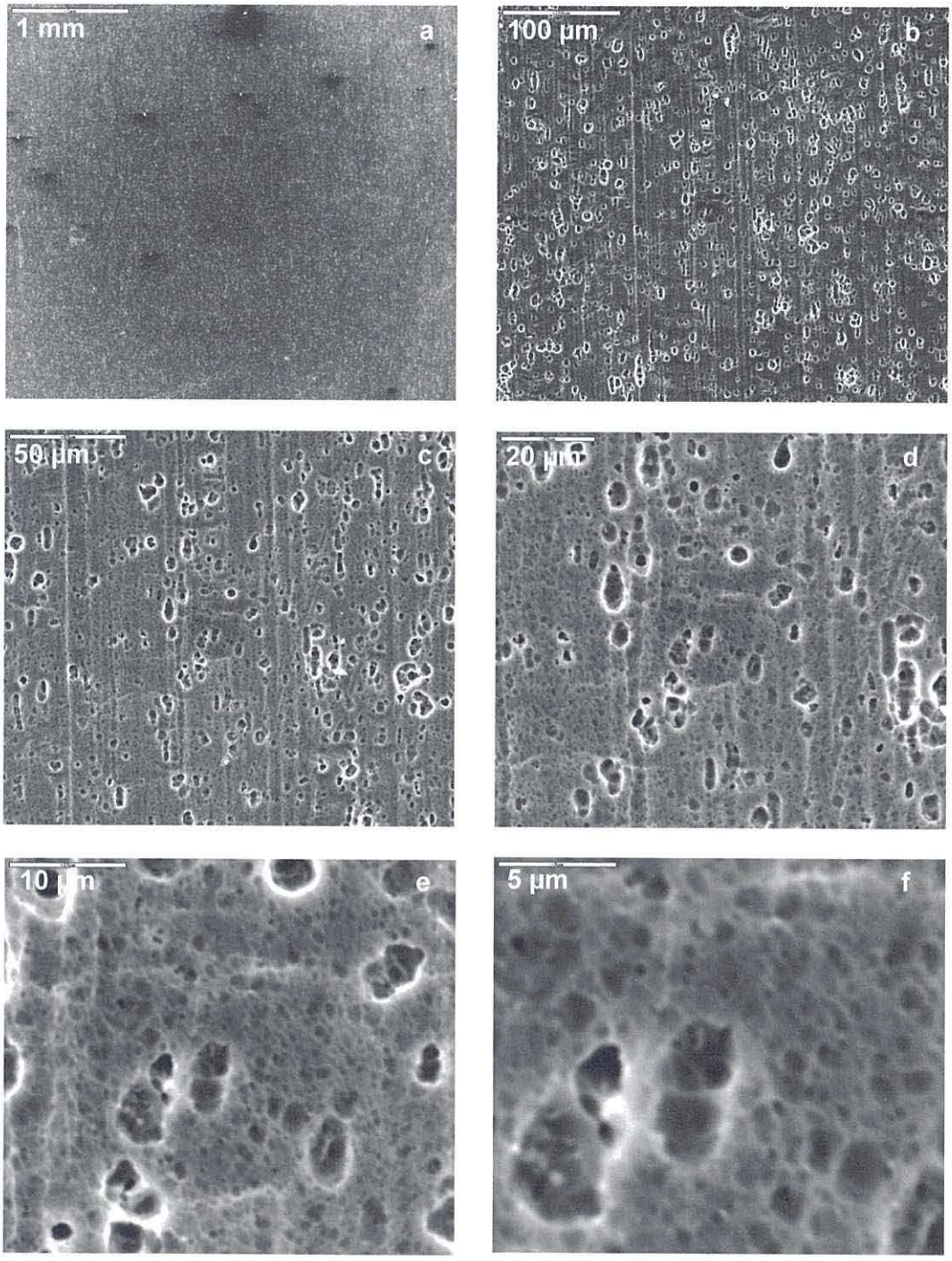

Figure 3.12 SEM images of alloy 3105 coated with Pretreatment 2 for 3 minutes

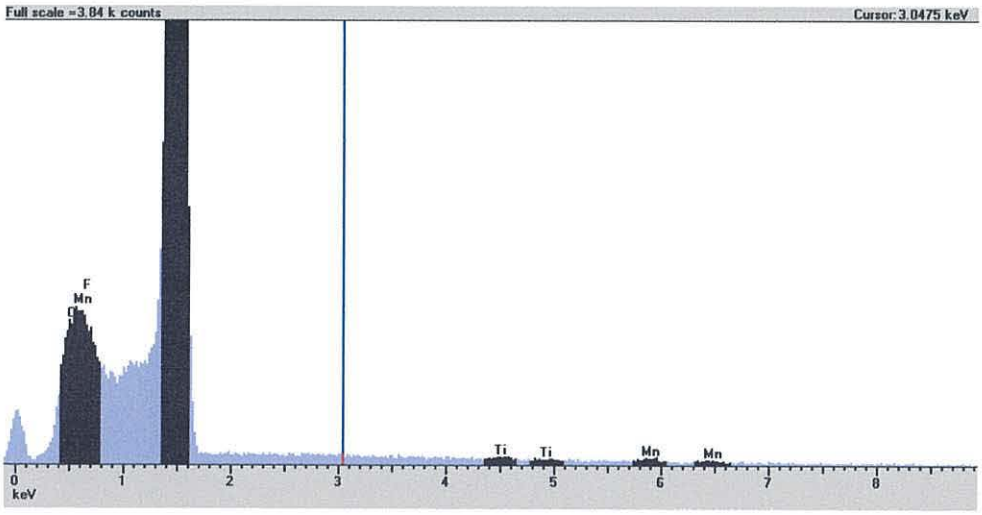

Figure 3.13 EDX analysis of alloy 3105 coated with Pretreatment 2 for 3 minutes, field of vision shown in Figure 3.12d

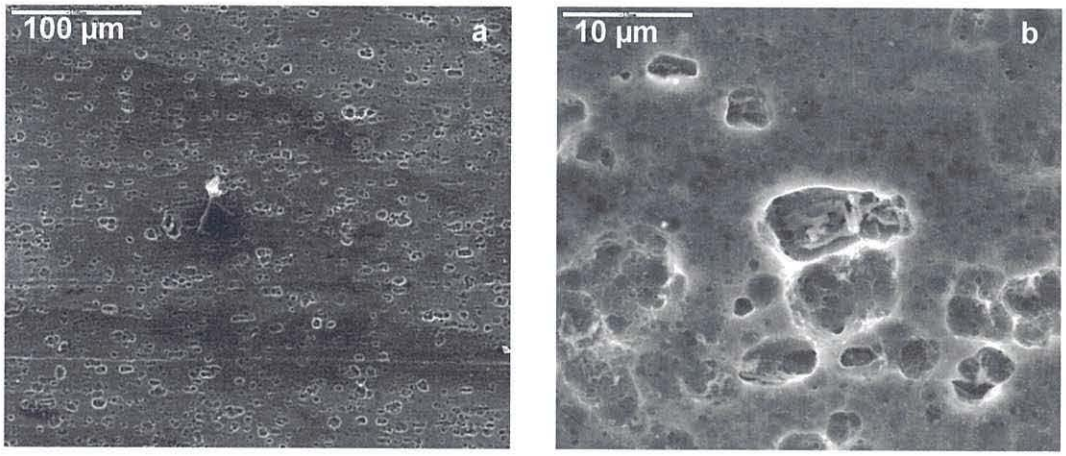

Figure 3.14 SEM images of alloy 3105 coated with Pretreatment 2 for 6 minutes

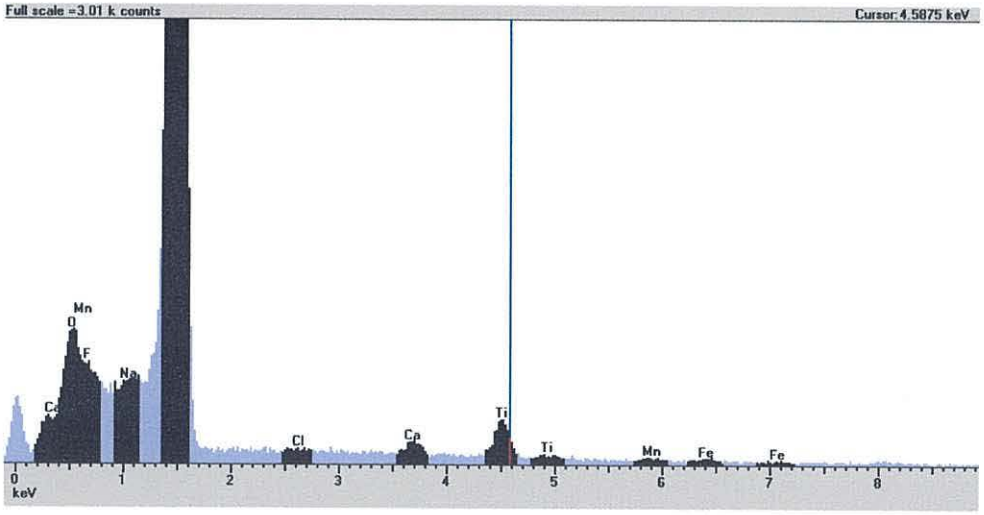

Figure 3.15 EDX analysis of alloy 3105 coated with Pretreatment 2 for 6 minutes, spot analysis

Cross sectional analysis of alloy 6063, coated with Pretreatment 2 for 6 minutes, by TEM has also been carried out. The data exhibit the structure of the aluminium substrate sub-surface, a thin aluminium oxide layer, the pretreatment layer, and finally a paint layer, Figure 3.16a, b, c. The titanium based treatment is visible as discrete particles of between 50 - 120 nm across, rather than a continuous layer.

In contrast to Pretreatment 1, which contains fluorozirconic acid, no paint is visible between the pretreatment layer and the oxide layer. Pretreatment 2 is attached to the aluminium oxide layer, with no penetration of the paint. This suggests better adhesion between the titanium pretreatment and the aluminium substrate. Nevertheless, detachment of the coating, assumed to be caused by the ultramicrotoming process, is evident on some of the sections examined, Figure 3.16c. This indicates that within this multilayer system, the adhesion is weakest between the pretreatment layer and the oxide layer. This may indicate that, in this format, this pretreatment is not suitable for long term aluminium corrosion protection.

EDX analysis of the ultramicrotomed sections of the coating on alloy 6063 confirms the presence of titanium and oxygen, as well as aluminium, Figure 3.17. A similar ratio of aluminium to titanium to oxygen is observed on the analysis of the ultramicrotomed sections of the coating on alloy 3105, Figure 3.18. In a similar manner to Pretreatment 1, this suggests that this coating exhibits one of the key parameters of a conversion coating in that aluminium is present in the corrosion coating along with the deposited metal (oxide) species. However, here again the delamination suggests that the coating is deposited as a separate layer on the outside of the metal surface. Silicon is also identified in the analysis of the 6063 alloy sample. This may be due to the impurities present in this particular alloy as discussed in Chapter 2. As mentioned during

discussions of Pretreatment 1, the copper and nickel peaks are most likely ascribed to the specimen holder.

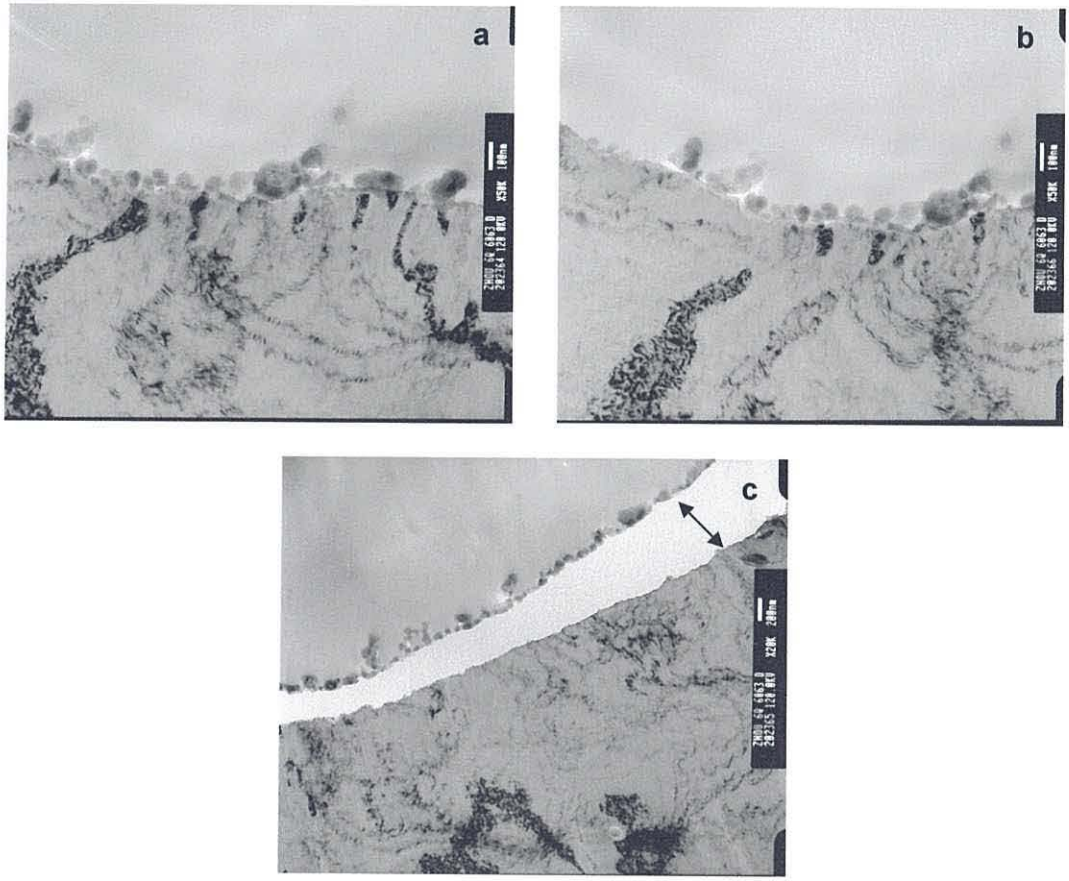

Figure 3.16 Ultramicrotomed cross sectional TEM images of alloy 6063 coated with Pretreatment 2 for 6 minutes, and subsequently powder coated, and Lockheed tested. Arrow shows detachment

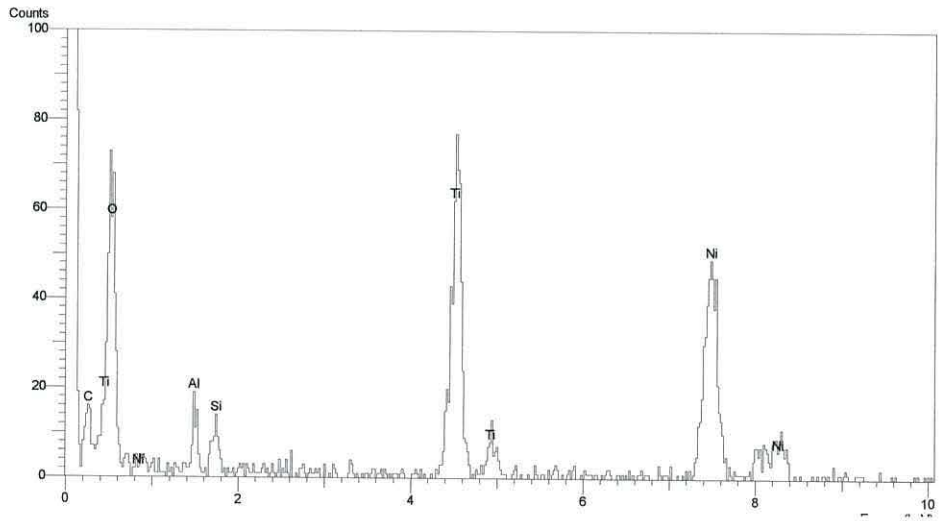

Figure 3.17 EDX analysis of the ultramicrotomed cross sections of alloy 6063 coated with Pretreatment 2 for 6 minutes, and subsequently powder coated, and Lockheed tested

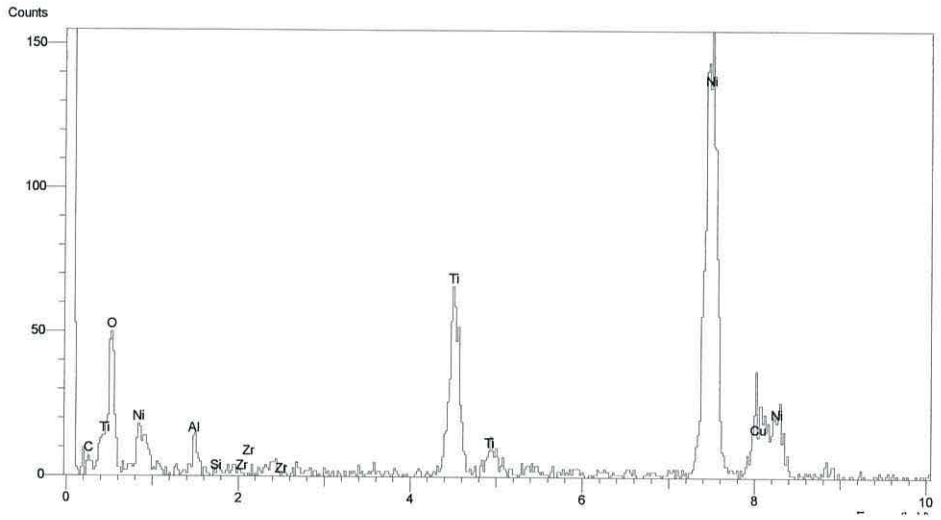

Figure 3.18 EDX analysis of the ultramicrotomed cross sections of alloy 3105 coated with Pretreatment 2 for 6 minutes, and subsequently powder coated, and Lockheed tested

Pretreatment 3 - Fluorozirconic and fluorotitanic acid

Pretreatment 3 investigated the effect of having both fluorozirconic and fluorotitanic acids present in the same solution. The SEM data show that following a 3 min coating on alloy 3105, at low magnification, there is some evidence that Pretreatment 3 does not give a consistent coverage, with a "marbling" effect being visible at the macro scale, Figure 3.19a. Considerably fewer holes are evident on the surface, Figure 3.19b, compared to Pretreatment 2. Instead, at the macro scale, the surface more closely resembles that following Pretreatment 1 after 6 minutes exposure. Also notable is that the rolling direction is less evident in these micrographs suggesting that further surface etching may have occurred, or that deposition is disguising these lines. The data also show that the holes that are present on this surface are larger than for Pretreatments 1 and 2 with hole diameters approaching 10 μm in size, Figure 3.19c, and with some charging apparent at the pit edges. The SEM data also show that a greater population density of pores (< 1.5 μm), Figure 3.19c, d, is also apparent for this pre-treatment when compared to Pretreatment 1. Finally, although the surface does not appear as glassy as Pretreatment 1, it does not exhibit the sponge-like texture observed following Pretreatment 2 for 3 minutes, but instead is more similar to the surface after Pretreatment 2 for 6 minutes.

The presence of zirconium is confirmed by EDX analysis, Figure 3.20. Further SEM analysis reveals that certain areas appear much darker on the surface of the substrate, Figure 3.21a. Closer magnification of these areas reveals cracking of a surface film which is assumed to be due to coating detachment, Figure 3.21b,c,d. As noted previously from Pretreatment 1, there was some evidence that darker areas are believed to be the result of a thicker deposit. Although quantitative analysis is difficult with this

technique, the EDX analysis of the darker regions of coating produced by Pretreatment 3 does suggest a relatively greater amount of zirconium and also the presence of titanium, Figure 3.22, compared to that of the neighbouring pitted, lighter area described earlier, EDX shown in Figure 3.20.

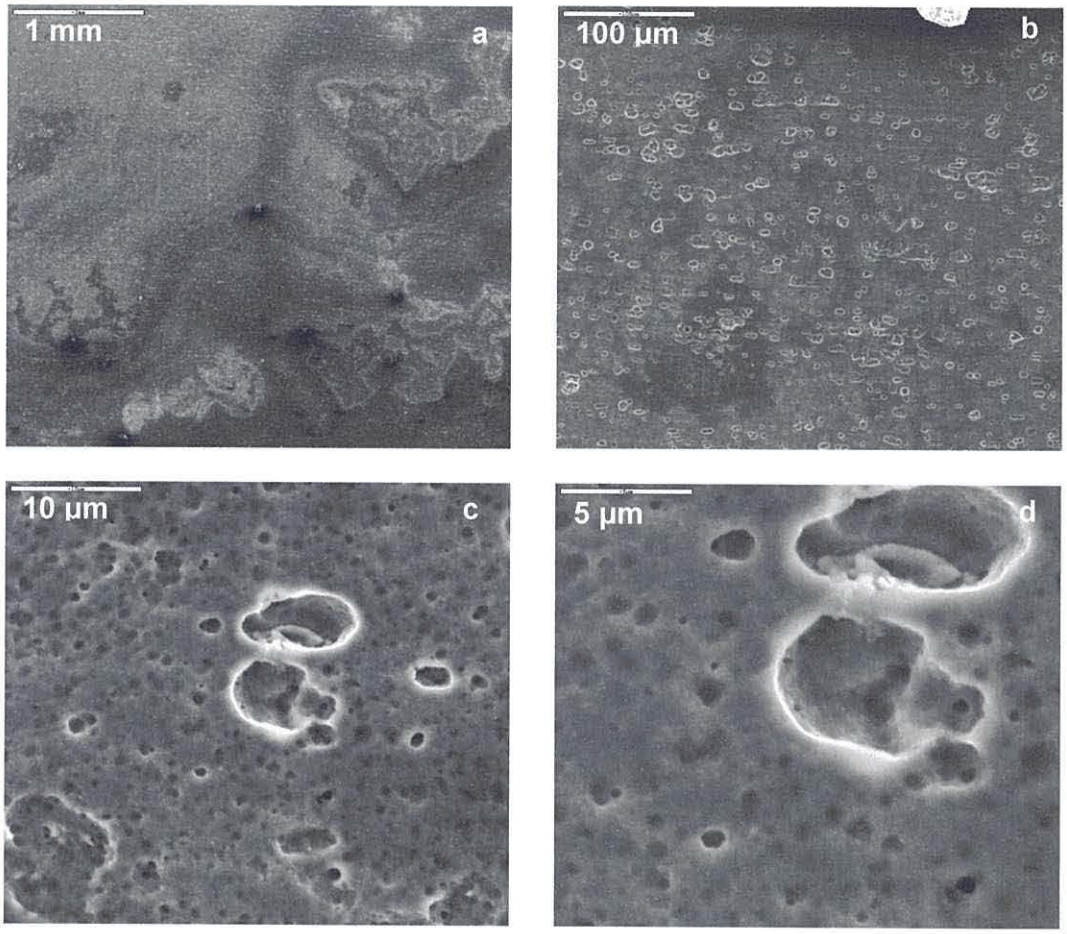

Figure 3.19 SEM images of alloy 3105 coated with Pretreatment 3 for 3 minutes showing (a) and (b) the macro-scale with darker and lighter areas and (c) and (d) the presence of holes and pores.

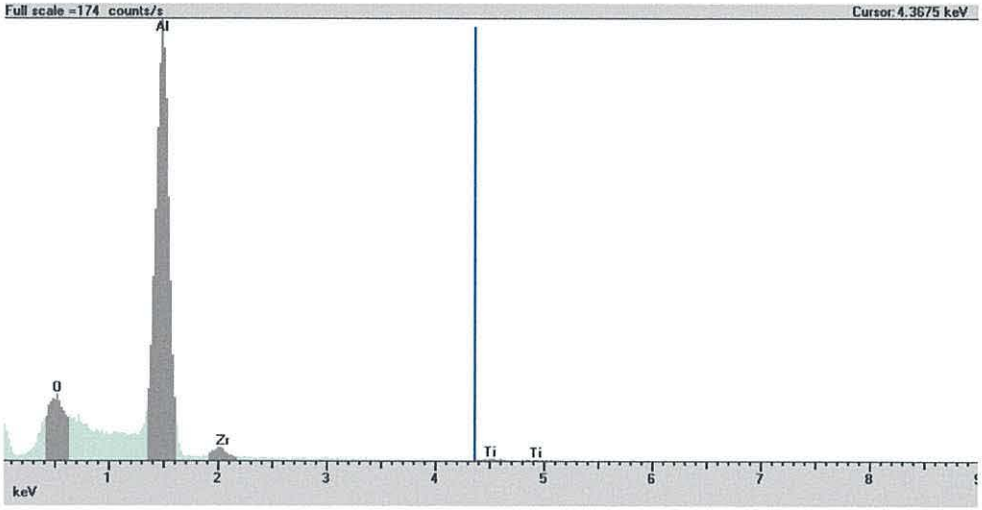

Figure 3.20 EDX analysis of, alloy 3105 coated with Pretreatment 3 for 3 minutes, field of vision shown in Figure 3.19c

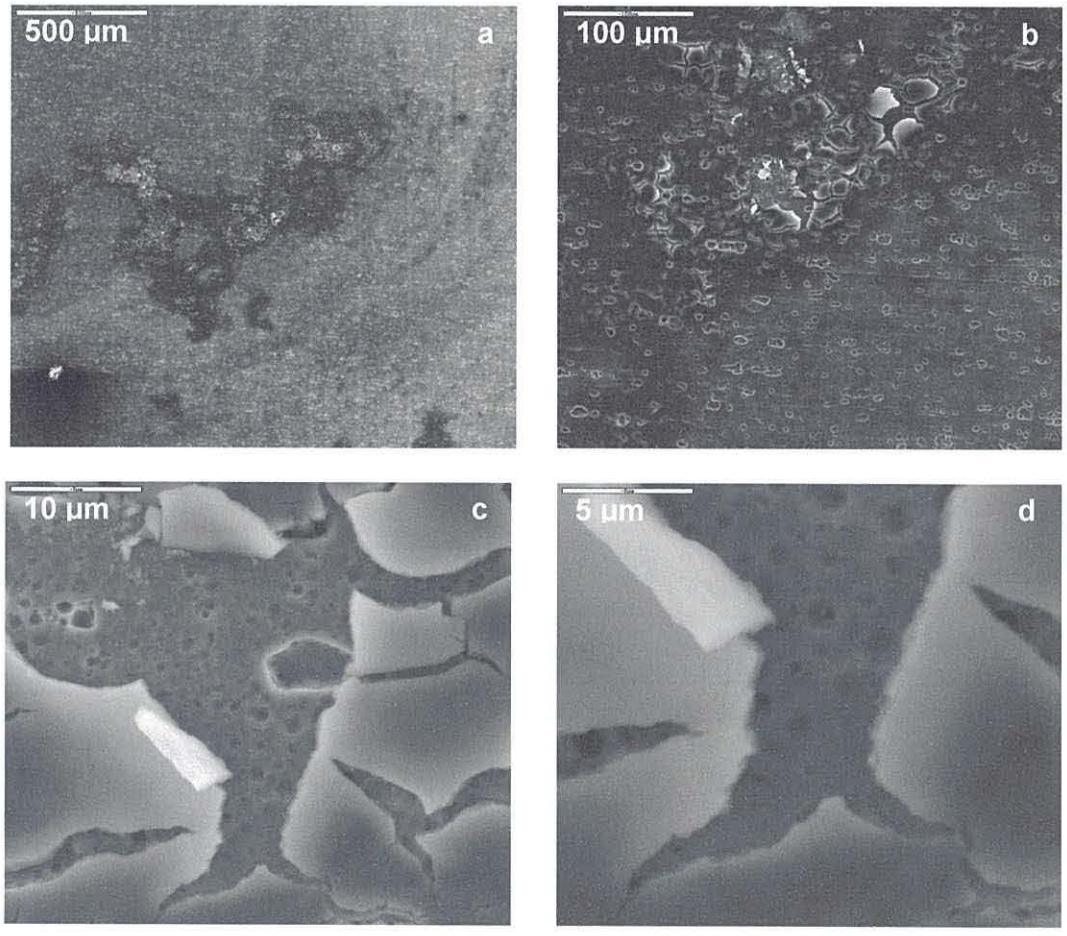

Figure 3.21 SEM images of alloy 3105 coated with Pretreatment 3 for 3 minutes, showing the darker areas of the coating

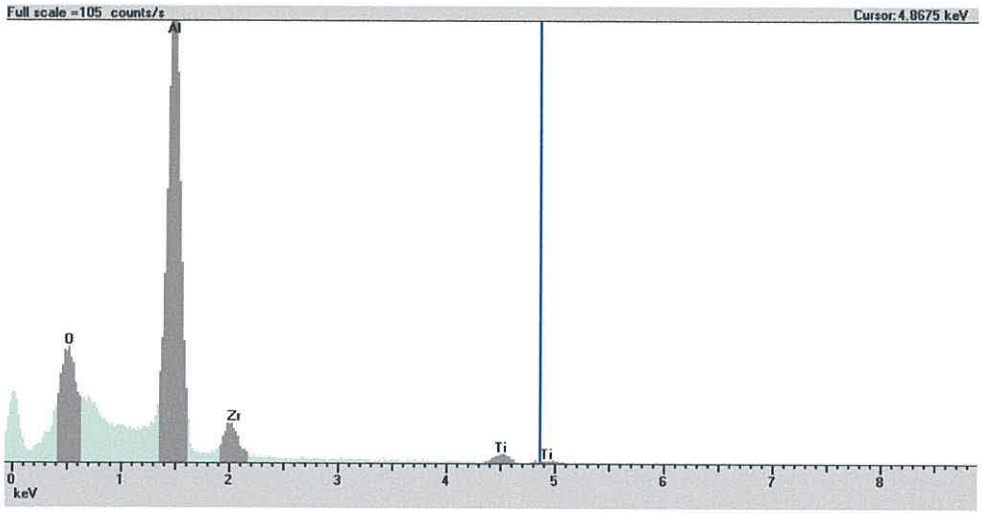

Figure 3.22 EDX analysis of alloy 3105 coated with Pretreatment 3 for 3 minutes, field of vision shown in Figure 3.21c

It could be that the cracking and detachment of the coating which is observed in this sample may be due to too thick a deposit.[7] Thus, it could be that the coating undergoes cracking during the drying process, leading to detachment from the substrate. The detached flakes of coating appear smooth, whilst visible between the cracks is the porous and pitted surface of the substrate, Figure 3.21b,c,d. The diminished rolling lines and indication of higher zirconium and titanium in areas of the coating may suggest a slightly thicker coating than that afforded by Pretreatment 2 after 3 minutes coating time.

SEM analysis following a longer 6 min coating on alloy 3105 gave a more uniform coating. Conversely to Pretreatment 2, a longer treatment time leads to a slightly more pitted surface than a treatment time of 3 minutes, Figure 3.23a, but with the pits appearing less deep, and the surface less porous, Figure 3.23b. This can be attributed to the competing etch and deposition reactions, both of which are more prominent following a greater exposure time, resulting in a greater number of pits caused by etching which are subsequently filled with deposition product. The EDX analysis of the

area shown in Figure 3.23b is similar to that presented in Figure 3.20 (of the area shown in Figure 3.19c).

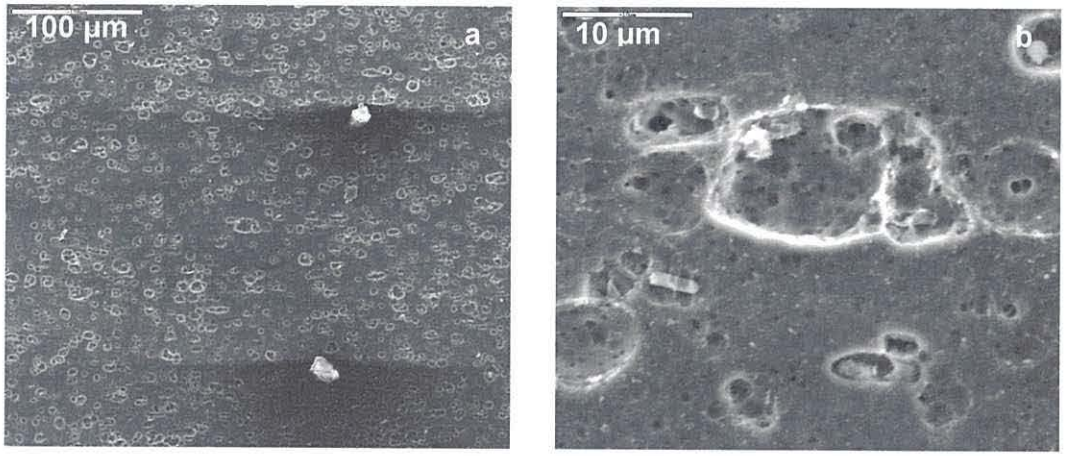

Figure 3.23 SEM images of alloy 3105 coated with Pretreatment 3 for 6 minutes

The cracking and flaking of the coating that were visible after a 3 minute treatment time are not observed here after 6 minutes exposure. Overall, the surface morphology appears to resemble that of the surface following exposure to Pretreatment 2 for 6 minutes.

From the higher resolution possible with TEM relative to SEM, cross-sectional analysis by TEM of Pretreatment 3 following a 6 min coating on alloy 6063 reveals that the coating is not continuous. Rather than discrete particles, agglomerations of deposits with dimensions up to 350 x 350 nm are apparent, Figure 3.24a,b,c,d. The coating appears attached to the substrate with no penetration of paint underneath the coating apparent. However, detachment of the coating is observed in some areas suggesting insufficient adhesion, Figure 3.25, Figure 3.26. However, where detachment has occurred, some of the deposited particles do appear to remain "attached" to the oxide layer, rather than the paint layer, indicating some improvement in adhesion between the coating and the metal oxide surface. EDX analysis an ultramicrotomed section of the

alloy has also been carried out. Analysis of the outer area of the pretreatment layer confirmed the presence of titanium and oxygen, and a smaller proportion of zirconium, as well as aluminium Figure 3.27. Analysis of the inner region showed the elements in similar proportion to that of the outer region. Evidence of carbon was found in both in the inner and outer region, but in much greater proportion on the inner region of the coating. The reason for the presence of carbon in the EDX analysis of these samples is not immediately clear as no organic polymer was included in this pre-treatment. However, the TEM grids used to support these samples have of a thin layer of carbon across one side of the sample holder, upon which the sample rests. It may be that the cross-section of this sample is thin enough in some regions for the EDX beam to penetrate the sample and register some carbon as well as the other elements. As noted

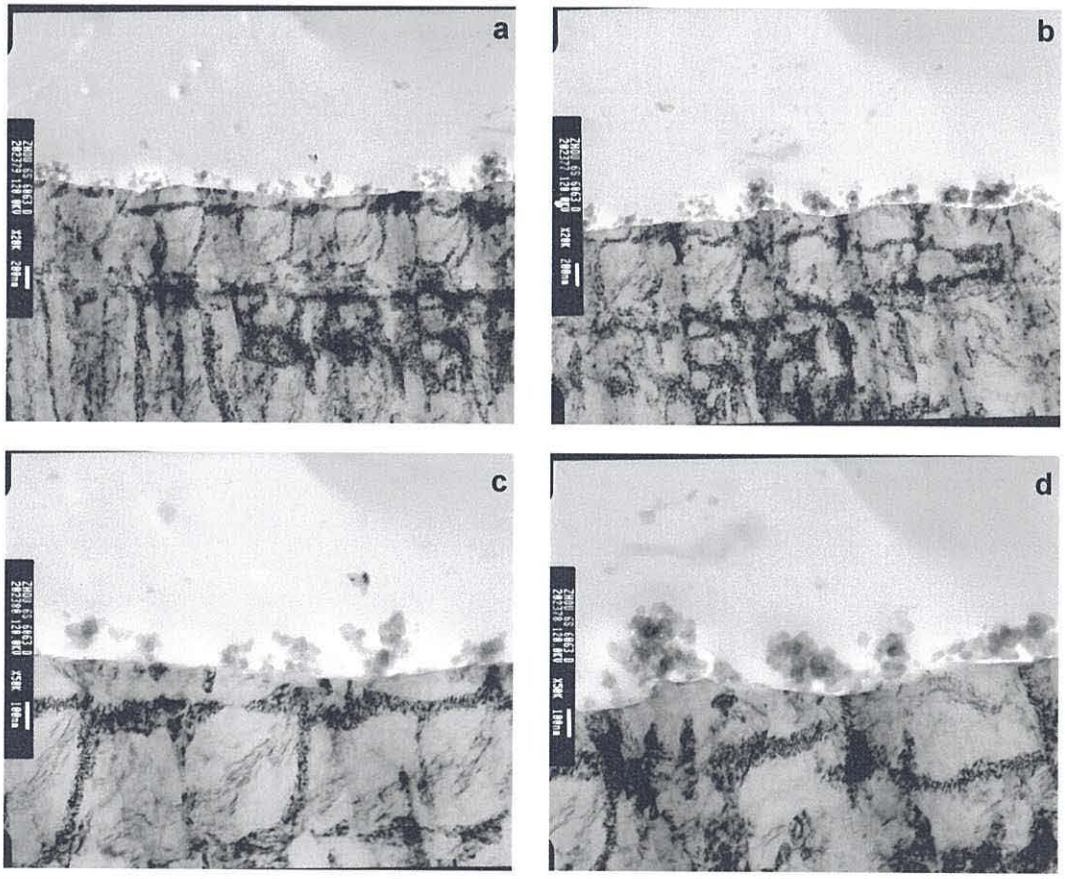

Figure 3.24 Ultramicrotomed cross sectional TEM images of alloy 6063 coated with Pretreatment 3 for 6 minutes, and subsequently powder coated, and Lockheed tested. Agglomeration of the treatment layer is evident

in the analysis performed on Pretreatment 2 on alloy 6063, silicon was also identified. EDX analysis of an ultramicrotomed section of alloy 3105 was also carried out, showing a similar proportion of titanium to zirconium, but at a lower proportion compared to that of the aluminium. This therefore may suggest less deposition on the 3105 alloy than the 6063 alloy.

Figure 3.25 Ultramicrotomed cross sectional TEM images of alloy 6063 coated with Pretreatment 2 for 6 minutes, and subsequently powder coated, and Lockheed tested. Delamination of the treatment layers can be seen, probably caused by the ultramicrotoming process

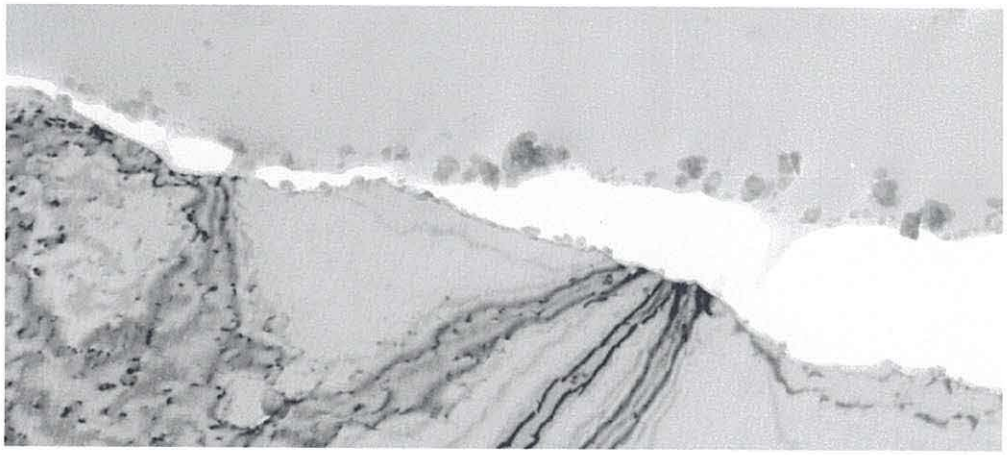

Figure 3.26 Close up of the image shown in Figure 3.25 to show deposited particles which have remained "attached" to the oxide layer, rather than the paint layer, indicating some improvement in adhesion

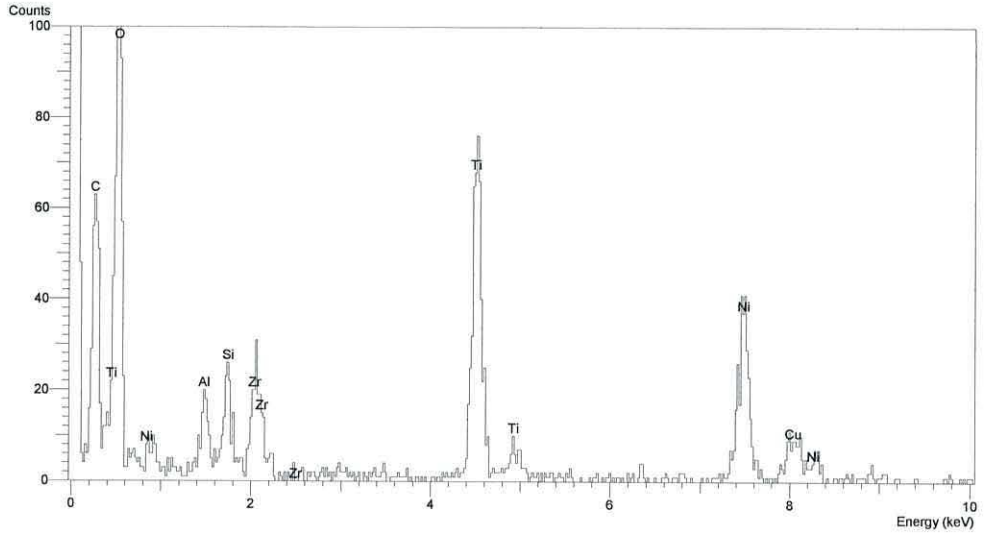

Figure 3.27 EDX analysis of the ultramicrotomed cross sections of alloy 6063 coated with Pretreatment 3 for 6 minutes, and subsequently powder coated, and Lockheed tested. The analysis of outer region of the coating is shown

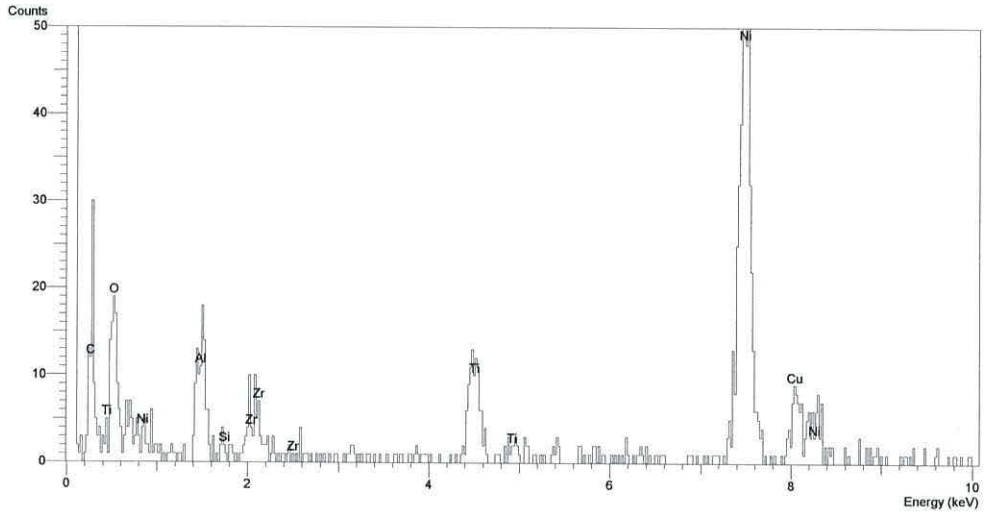

Figure 3.28 EDX analysis of the ultramicrotomed cross sections of alloy 6063 coated with Pretreatment 3 for 6 minutes, and subsequently powder coated, and Lockheed tested

Pretreatment 4 – Fluorozirconic acid, fluorotitanic acid, polyacrylic acid

Pretreatment 4 was a development on the previous coating by studying the addition of a polymer (in this case the water soluble polyanionic polyacrylic acid, PAA) alongside fluorozirconic and fluorotitanic acids. The SEM data show that the coating afforded by Pretreatment 4 gives good coverage after a coating time of 3 minutes on alloy 3105, Figure 3.31a. The population density of pits - holes ranging from 1.5 to 40 μm - is comparable to that following exposure to Pretreatment 3 for 3 minutes, and some similar darker regions can also be noted, Figure 3.31b. Again it is assumed that these darker areas are due to a greater deposition of the coating. However, in this case, further analysis of these dark areas at higher magnification did not reveal any flaking or cracking. It appears that the addition of the polyacrylic acid has prevented the shrinking and subsequent cracking and flaking of the coating, where the coating is concentrated. This could be due to the flocculating properties of the polyacrylic acid, structure shown in Figure 3.29.

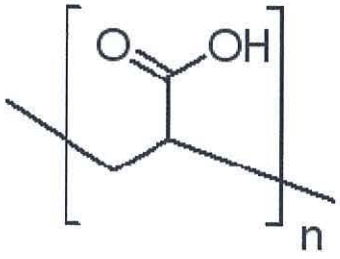

Figure 3.30 The structure of polyacrylic acid

Water soluble polyacrylic acid (i.e. the polymer without any cross linking of the polymer strands) is used commercially as a flocculating agent both in water treatment works and also as a soil conditioner (to reduce soil erosion).[10] Bridging flocculation of the type expected with polyacrylic acid occurs when segments of a polymer chain adsorb onto different particles which induces flocculation by linking the solid particles together.[11]

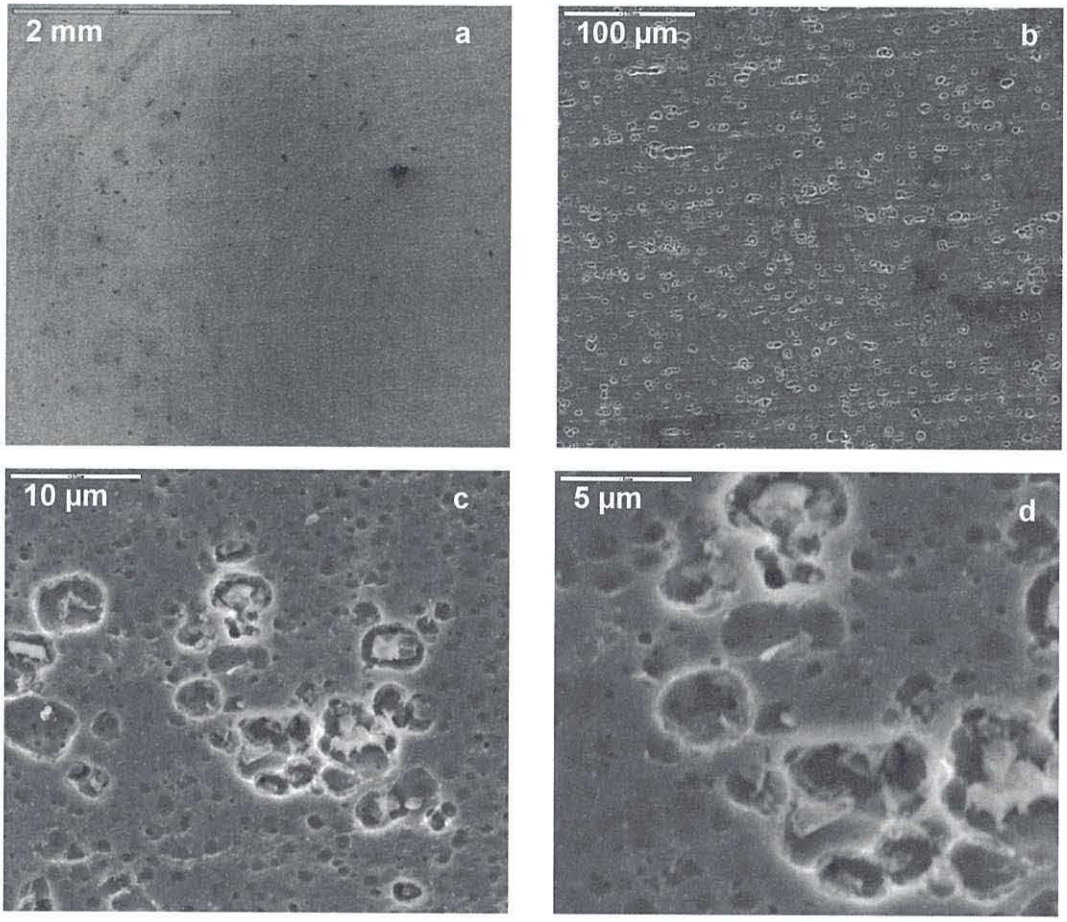

Figure 3.31 SEM images of alloy 3105 coated with Pretreatment 4 for 3 minutes

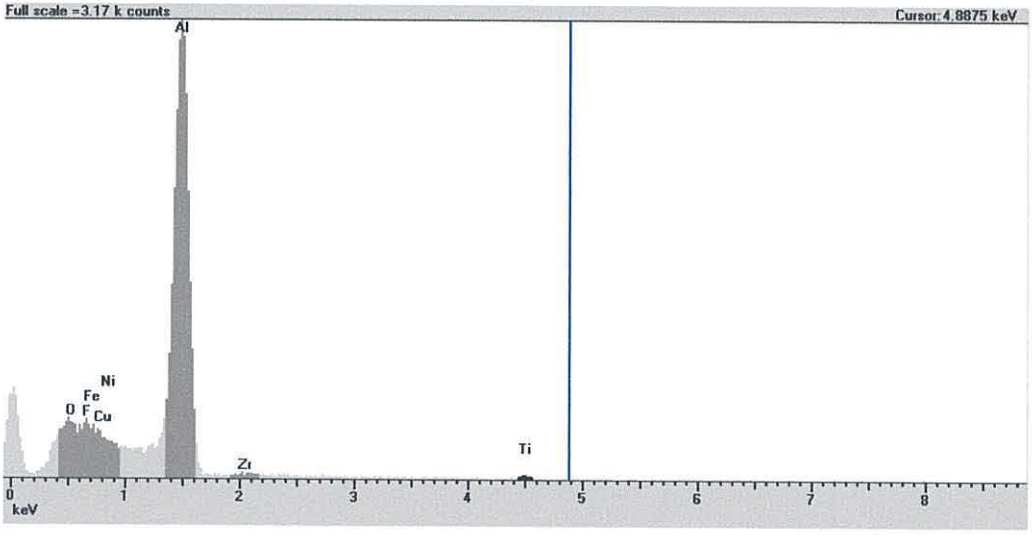

Figure 3.32 EDX analysis of Figure 3.31c, alloy 3105 coated with Pretreatment4 for 3 minutes. Analysis taken from field of vision shown in Figure 3.31c

It has also been suggested that hydrogen bonding from polyacrylic acid may also create a bridging effect that might cause flocculation.[12] From the data from this pre-treatment , it can also be noted that many of the pits visible contain deposits following this treatment type, Figure 3.31c,d. Corresponding EDX analysis of these deposits reveals weak signals for both the zirconium and titanium.

Further SEM data, Figure 3.33, show that increasing the treatment time to 6 minutes reveals new, fibrous deposits on the surface of the alloy which appear to be largely composed of carbon (from EDX analysis). This suggests a region of the surface which may be rich in polymer-based material such that these deposits could be due to flocs of the polyacrylic acid that have agglomerated. In addition, although some cracking of the surface is observed here, there appears to be no detachment, Figure 3.33a. As expected, the number of pits appears higher following the greater exposure time to the fluorozirconic and fluorotitanic acids, Figure 3.33a.

Analysis at higher magnification shows deposits within these pits, in these regions, Figure 3.33d. Magnification of the darker areas, depicted in Figure 3.33b,c, show that these holes have been filled almost completely. EDX analysis of the surface indicates zirconium and a weak signal for the titanium, Figure 3.34. Although still appearing porous in parts, Figure 3.33d, areas appear to resemble more as a glass than a foam type coating, Figure 3.33b,c.

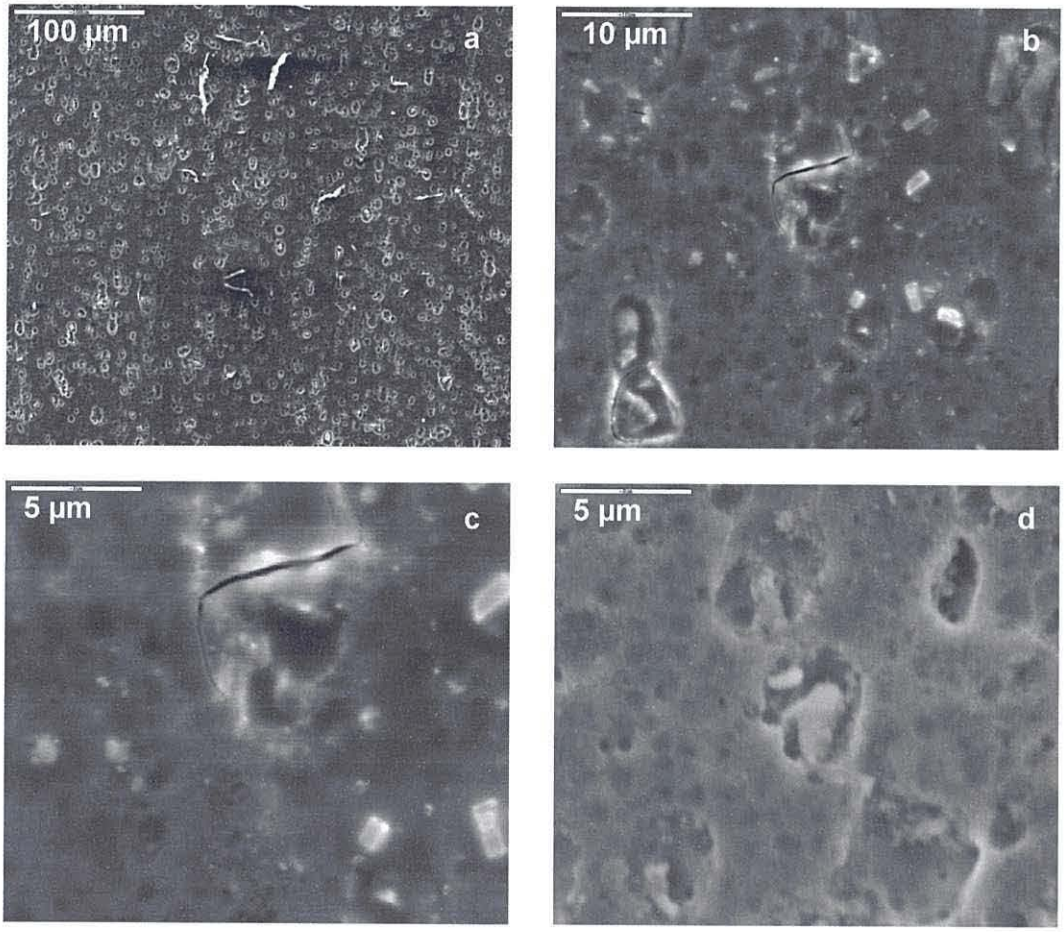

Figure 3.33 SEM images of alloy 3105 coated with Pretreatment 4 for 6 minutes

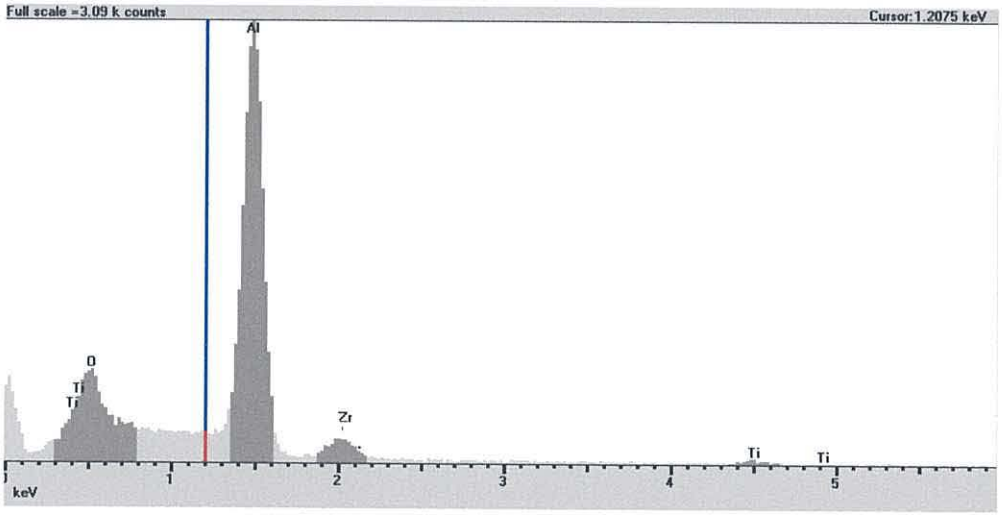

Figure 3.34 EDX analysis of alloy 3105 coated with Pretreatment 4 for 6 minutes Figure 3.33c

Further samples coated in Pretreatment 4 were subsequently powder coated and Lockheed tested, then prepared by ultramicrotomy for analysis by TEM. This revealed that Pretreatment 4 produced another coating composed of agglomerated particulate

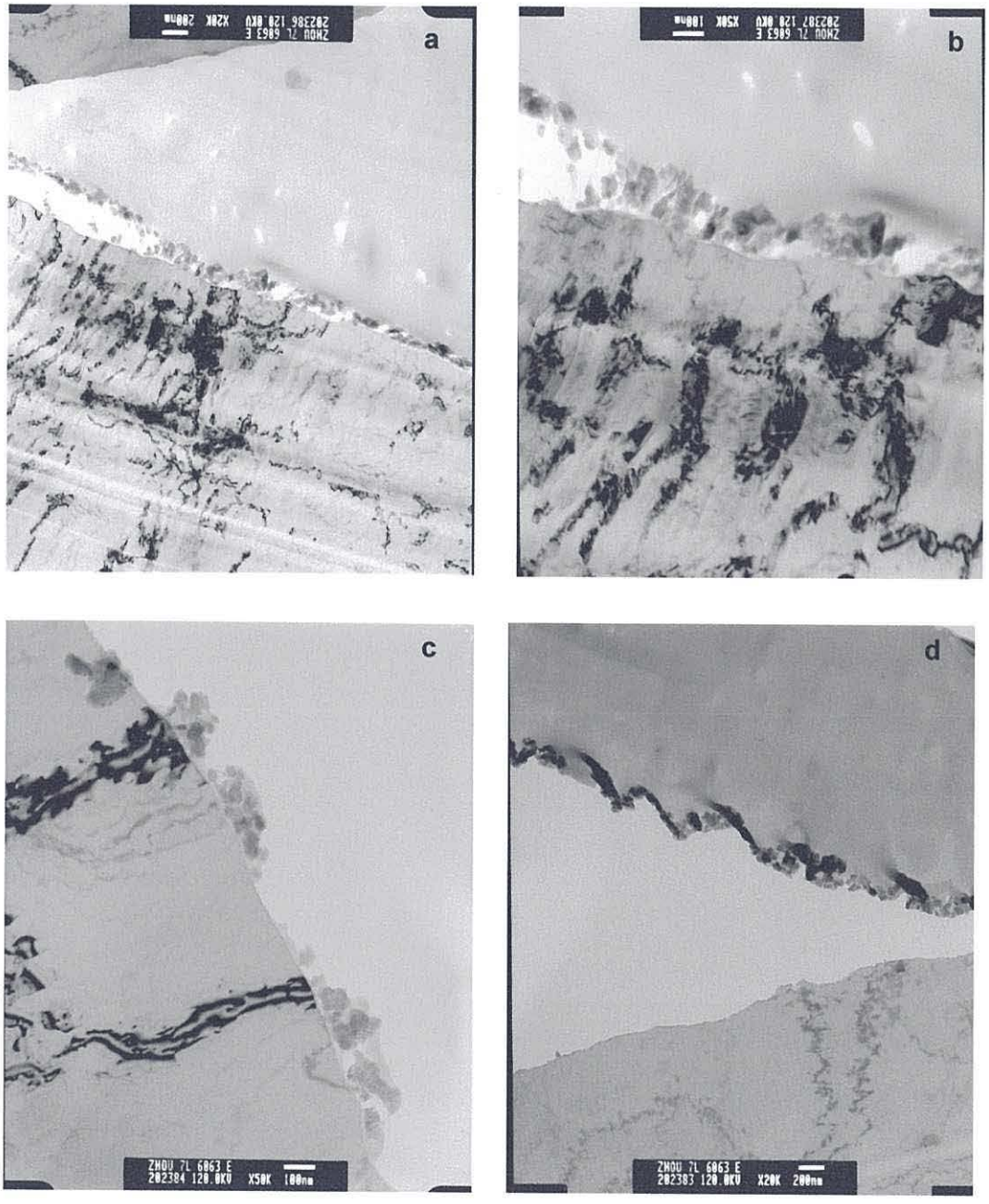

Figure 3.35 Ultramicrotomed cross sectional TEM images of alloy 6063 coated with Pretreatment 4 for 6 minutes, and subsequently powder coated, and Lockheed tested

deposits on the surface of the substrate following a 6 min coating on alloy 6063, Figure 3.35a,b,c. The agglomerated deposits range from 150 nm in thickness in some places to no deposit at all in other areas. Although no penetration of paint is observed in these samples there is evidence of detachment, Figure 3.35c,d. As in the case of Pretreatment 3 however, where detachment of the paint is observed, some of the deposited particles remain "attached" to the oxide layer, rather than the paint layer, indicating improved bonding of the pretreatment layer to the oxide, Figure 3.35c. The coating deposits also appear more continuous in these images, providing much more surface coverage than was observed for Pretreatment 3, suggesting a positive effect of the polyacrylic acid which is also in line with the SEM data for the 3105 alloy. EDX analysis of these ultramicrotomed sections has also been carried out and this confirms the presence of titanium, zirconium and oxygen, as well as aluminium, Figure 3.36. Inspection of the data, on going from the outer region of coating furthest from the aluminium substrate, to the middle of the coating and then to the inner region, closest to the aluminium, shows that, in the outer region, higher levels of carbon are apparent, which diminishes as the analysis of the coating approaches the substrate. This suggests that the carbon, attributed to the polyacrylic acid, is present at higher concentrations in the outermost parts of the coating.

TEM analysis of Pretreatment 4 on the AA3105 alloy reveals a continuous and thick coating, up to 400 nm in thickness, Figure 3.37. The coating appears to consist of a closely packed chain of regular discrete particles which are similar shape and size. The appearance of scalloping in areas is due to the aforementioned processing of the samples, compression resulting in rippling of the sample. However, evidence of a void where an intermetallic

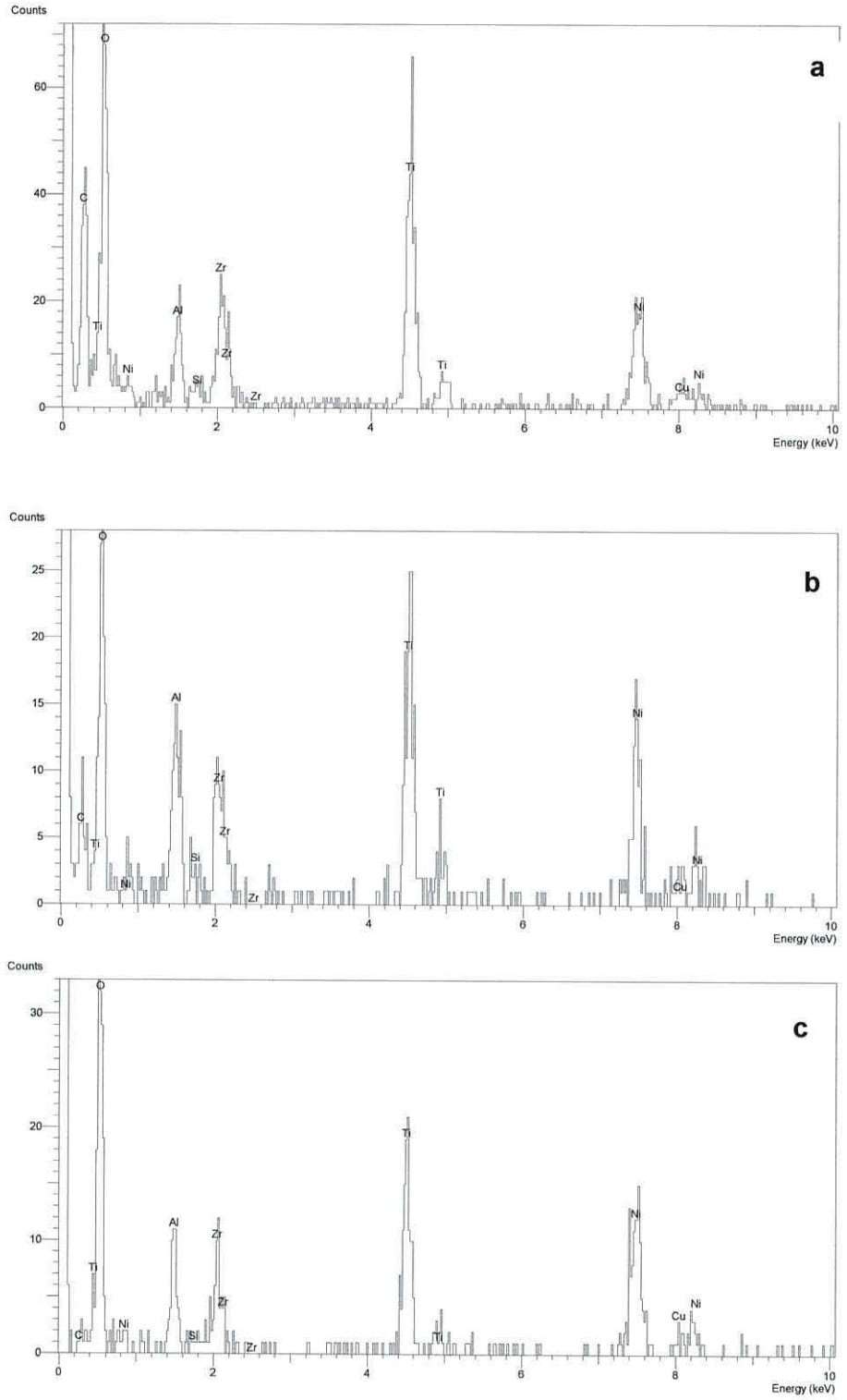

Figure 3.36 EDX analysis of the ultramicrotomed cross sections of alloy 6063 coated with Pretreatment 4 for 6 minutes, and subsequently powder coated, and Lockheed tested. a) shows the analysis performed on the outer region, b) the middle region, and c) the inner region

particle is assumed to have been removed and possibly a grain boundary are evident in Figure 3.37a.

EDX analysis of the ultramicrotomed sections has again been carried out and this confirms the presence of titanium, zirconium and oxygen, as well as aluminium in lone with the data for the 6063 alloy, Figure 3.38. Here again, higher levels of carbon where detected by EDX analysis of the outermost region of the pretreatment. This suggests that there appears to be a higher concentration of polyacrylic acid in the outermost layer of the coating. Whilst it is impossible to be absolutely certain of the role of the polymer during initial deposition in the coating process, these data suggests that more of the polymer remains in solution, then increasingly binds within the deposited material to hold the coating together as it grows.

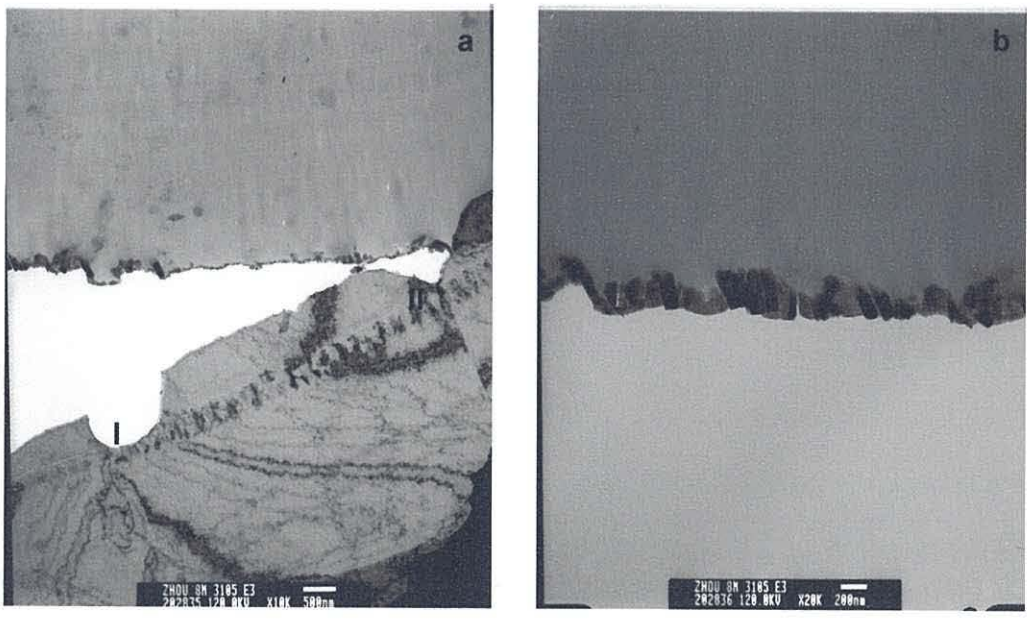

Figure 3.37 Ultramicrotomed cross sectional TEM images of alloy 3105 coated with Pretreatment 4 for 6 minutes, and subsequently powder coated, and Lockheed tested.

Overall, the polyacrylic acid appears to have provided an improved coating compared to Pretreatment 3 for both alloys 3105 and 6063. This is shown by a more even surface

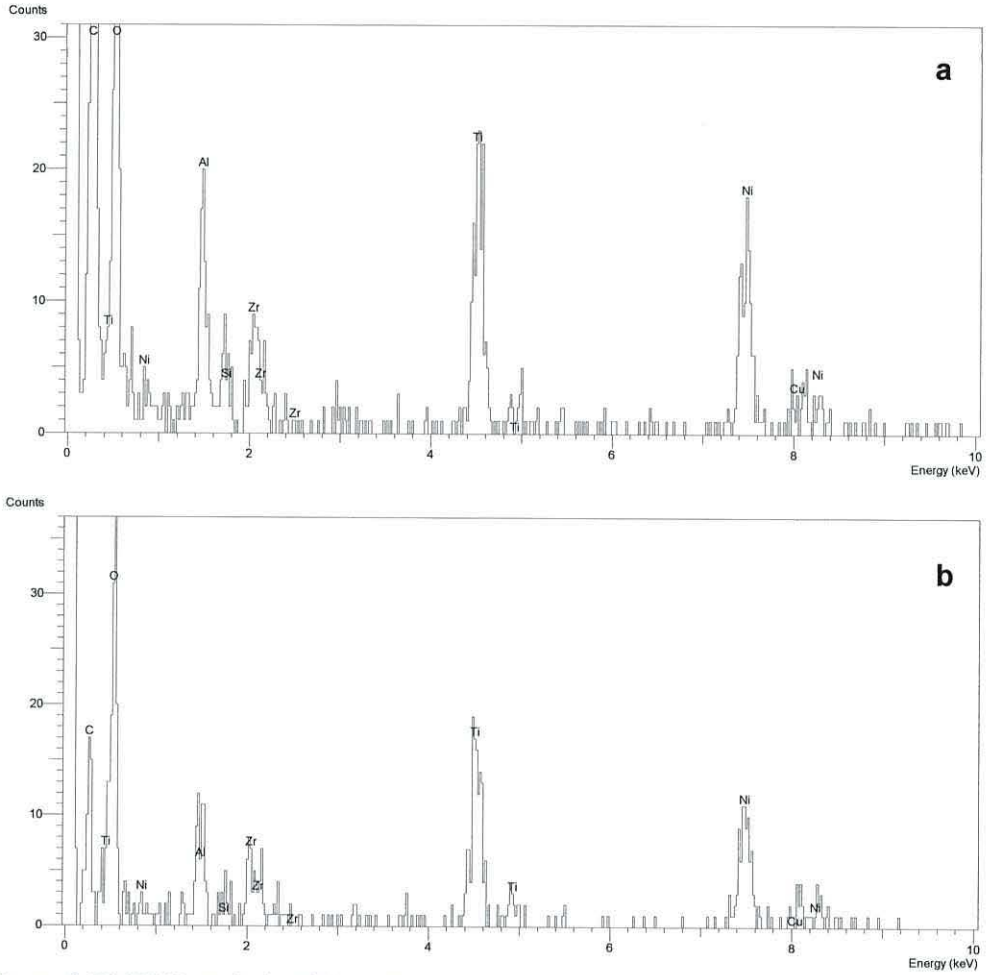

Figure 3.38 EDX analysis of the ultramicrotomed cross sections of alloy 3105 coated with Pretreatment 4 for 6 minutes, and subsequently powder coated and Lockheed tested. a) shows the analysis performed on the outer outer region, b) the inner region

coverage which is observed from SEM, with no detachment evident following 6 minute exposure time. In addition, greater surface area coverage is indicated from the TEM data. EDX of the ultramicrotomed coating sections as part of the TEM analysis suggests that the polyacrylic acid is within the coating suggesting that it does play an active role in this pre-treatment. However, the data also show that the concentration of the carbon (and thus presumably polymer as well) is not consistent throughout the coating with elevated levels of carbon observed towards the outside of the coating. This may possibly suggest the polymer is more important in the latter stages of the deposition process.

Pretreatment 5 Dilute Fluorozirconic, Fluorotitanic and Polyacrylic acid

Pretreatment 5 has been chosen because it contains the same materials in solution as Pretreatment 4, but these are present at 10 times lower concentration. The aim here has been to study the influence of concentration on the etch-deposition processes which are believed to lead to the coatings observed in these studies.

SEM data indicate that Pretreatment 5 gives a uniform coverage on alloy 3105 following a treatment time of 3 minutes. However, significantly less pitting was observed on the surface than with any of the other pretreatments, Figure 3.39a,b. Instead, the surface more closely resembles that of the etched surface discussed in Chapter 2. This is assumed to be due to the concentration of the main components in this pretreatment which would be expected to etch the aluminium surface (i.e, fluorozirconic and fluorotitanic acid) being 10 times less concentrated than in Pretreatment 4, making this pretreatment much less aggressive.

Although the density of pits on the treated surface is similar to that of the density of pits on the etched sample, less charging of the pit edges is evident. Upon further magnification, the surface appears similar to that following Pretreatment 2 after 3 minutes exposure. Interestingly, although less pitting is observed, this pre-treatment appears to give rise to a greater density of pores compared to the surface following Pretreatment 4, Figure 3.31c, which contained the same chemicals but of greater concentration. In addition, although the number of pores appeared increased, the pore size is smaller, approximately 0.25 - 1 μm, compared with 1 – 2 μm following Pretreatment 4. This could either be due to the weaker concentration of Pretreatment 5, which results in the etching process being less pronounced and/or the deposition processes exceeding surface etching, effectively filling in the pores.

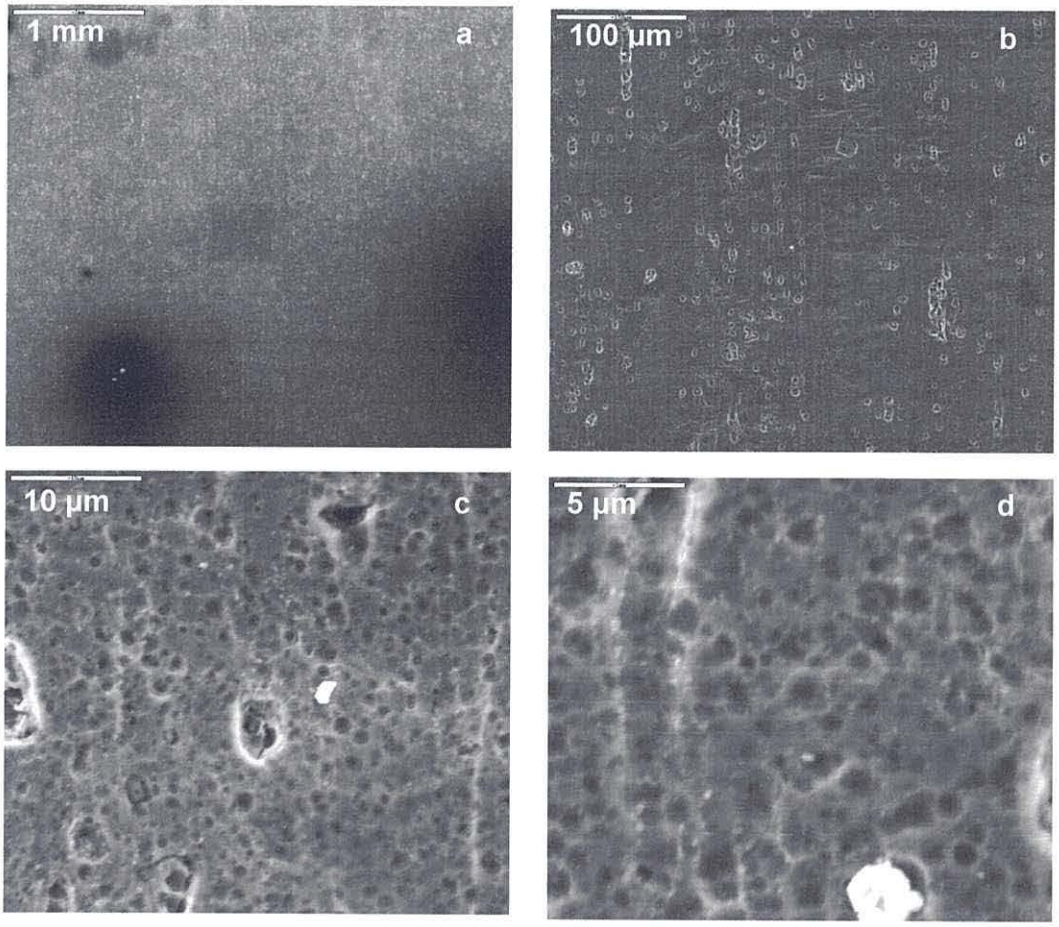

Figure 3.39 SEM images of alloy 3105 coated with Pretreatment 5 for 3 minutes

SEM analysis following a 6 min coating on alloy 3105 using Pretreatment 5, shows a greater amount of etching to the surface than following the 3 minute exposure which tends to suggest that it is the etch process that seems to dominate the resulting surface topography. However, the data also suggest a slightly thicker film, with the appearance of a "foam" type coating which suggests that increased deposition has also occurred with extended exposure to this pre-treatment solution.

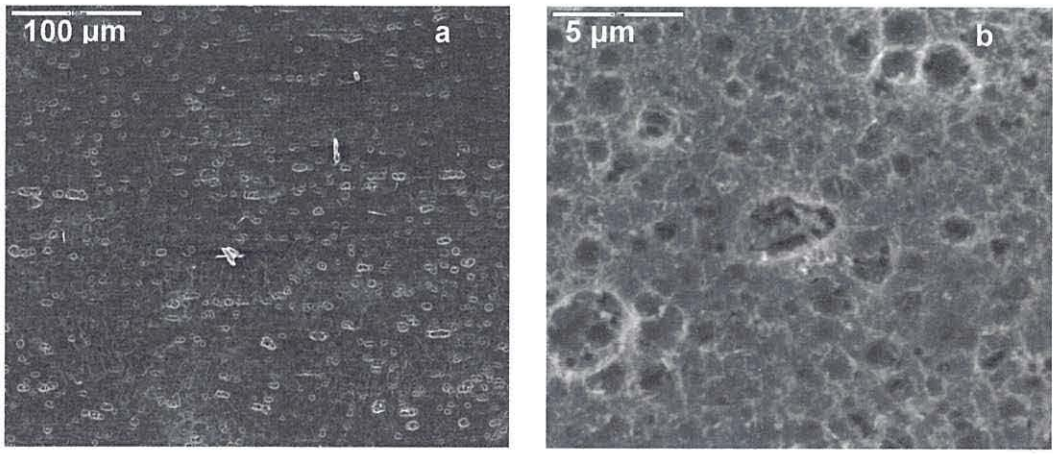

Figure 3.40 SEM images of alloy 3105 coated with Pretreatment 5 for 6 minutes

EDX analysis has also been carried out alongside the SEM studies and these data confirm the presence of Zr and Ti following both treatment times. However, due to the difficulties associated with quantitative EDX analysis, it is difficult to draw more conclusions from this data.

TEM data from ultramicrotomed sections of powder coated samples of alloy 6063 which have been exposed to Pretreatment 5 for 6 minutes are shown in Figure 3.41.

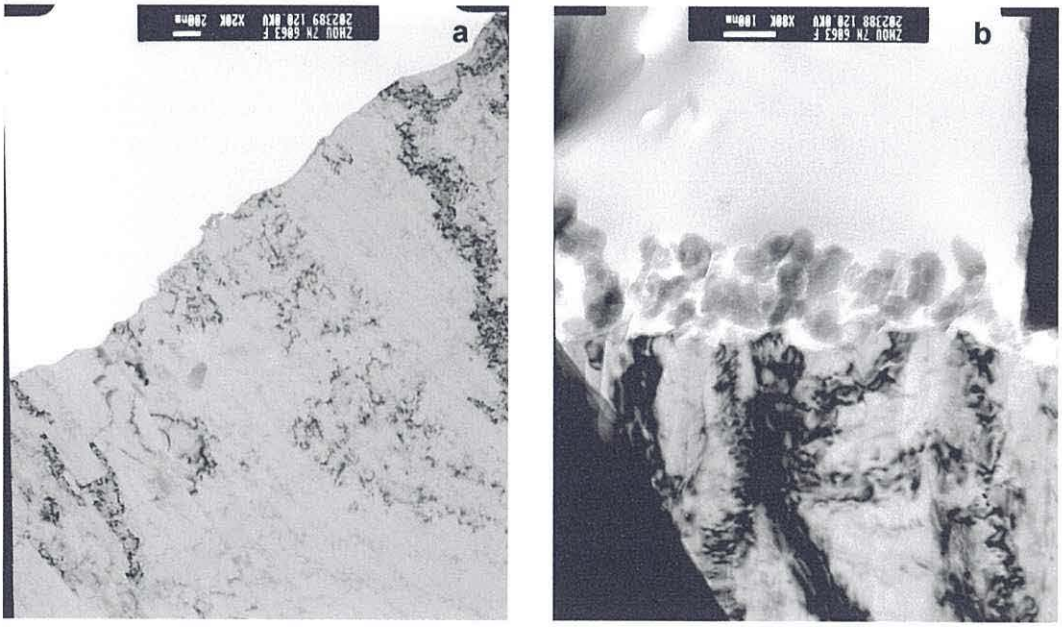

Figure 3.41 Ultramicrotomed cross sectional TEM images of alloy 6063 coated with Pretreatment 5 for 6 minutes, and subsequently powder coated, and Lockheed tested

Analysis of the TEM data for this coating shows that, although some agglomeration is still evident, this pretreatment results in a more continuous coating, Figure 3.41a,b. Although the lower concentration used in this pre-treatment appears to have improved the coating coverage, detachment of the paint layer has occurred in some areas, Figure 3.41a, suggesting poor adhesion.

Analysis by TEM of Pretreatment 5 on alloy 3105 following 6 minutes of exposure reveals a continuous coating of between 70 and 100 nm thickness, Figure 3.42. The morphology of the treatment layer is again more consistent than that produced by the other pretreatments, and appears as a continuous layer of particles which are similar in size and shape. The particles are to be roughly rectangular with the long axis oriented perpendicular to the aluminium surface which suggests that they may have grown in this vertical direction away from the surface. Occasional additional out-growths can also be observed developing from this initial coating layer (e.g. labelled I on Figure 3.42c).

Again these outgrowths appear to be perpendicular to the substrate suggesting additional coating growth beyond the initial deposition layer. In some areas, these out-growths resemble the agglomerated layer found on the AA6063 substrates treated with both fluorozirconic and fluorotitanic acid using Pretreatment 3. Rippling of the pretreatment and paint layers is evident in Figure 3.42a, which is attributed to the preparation of the cross sectional sample as discussed previously in this Chapter and is an artefact of the ultramicrotoming procedure. Finally some detachment is evident, Figure 3.42a, between the pretreatment coating and the aluminium substrate suggesting a weaker adhesion is present between these two layers. However, no penetration of paint has occurred in any of the data observed in these analyses.

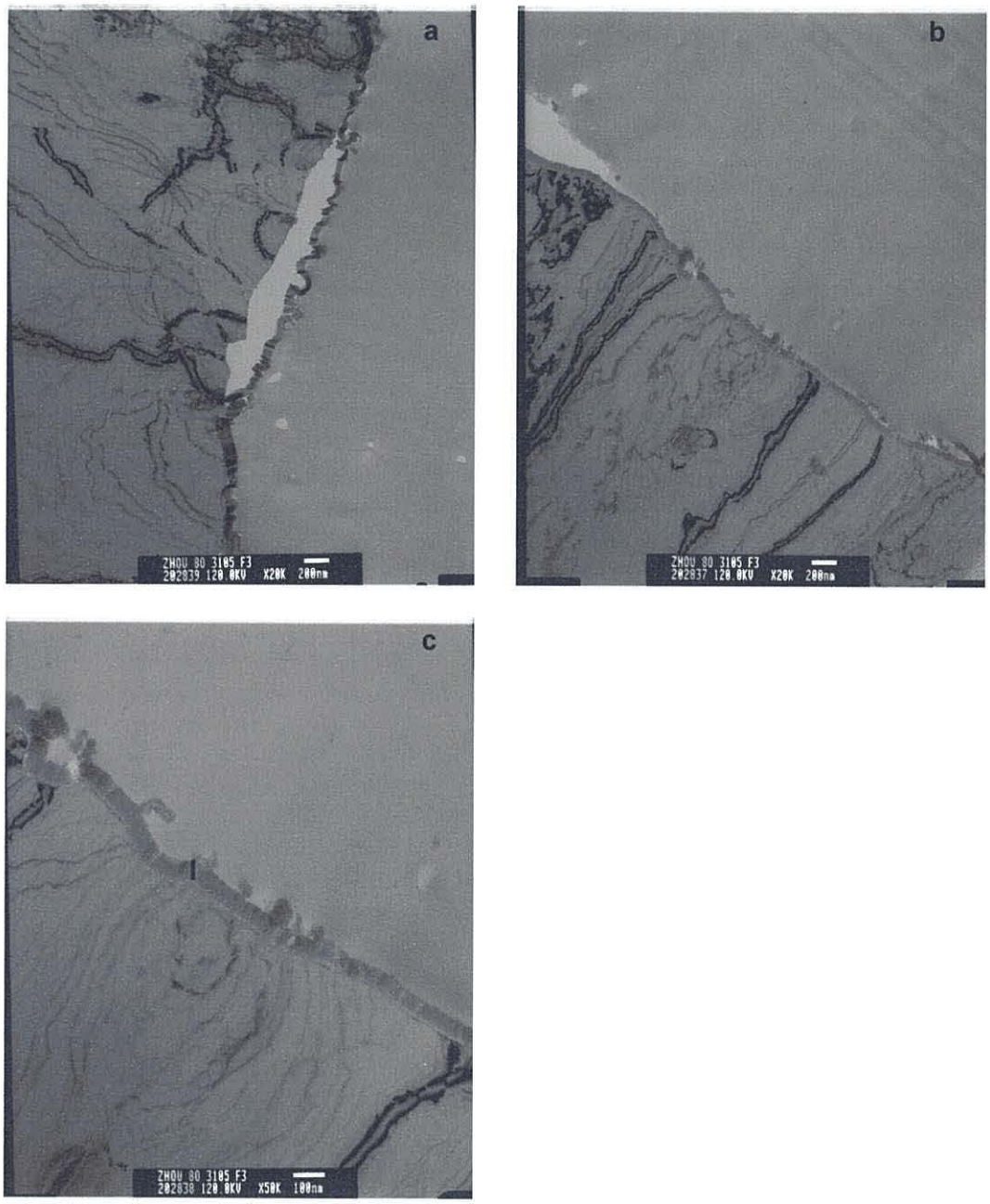

Figure 3.42 Ultramicrotomed cross sectional TEM images of alloy 3105 coated with Pretreatment 5 for 6 minutes, and subsequently powder coated, and Lockheed tested

Unfortunately, EDX analysis of these ultramicrotomed sections was not available. Overall, the reduced concentrations in Pretreatment 5 have changed the way that the aluminium etches giving rise to smaller pores and fewer pits compared with Pretreatment 4. However, the surface coverage on both alloys 3105 and 6063 appears good. There is some evidence for delamination of the coating which suggests that the

adhesion is still not sufficiently secure for this pre-treatment to afford long-term corrosion protection.

Pretreatment 6 - Fluorozirconic acid, Ammonium bifluoride and Polyacrylic acid

Pretreatment 6 has been chosen to compare the effects of Pretreatment 1 (fluorozirconic acid) with the addition of polyacrylic acid as a flocclating/binding agent but also in the presence of ammonium bifluoride as an additional etch agent.

Upon SEM analysis, it can be seen that Pretreatment 6 has not afforded a uniform coverage after 6 minutes. Instead, the coating observed appears patchy, with some lighter and darker regions, and darker, circular areas, Figure 3.43a. The data show that pits are less frequent on the surface. However, the pits which are present are greater in size than the previous pretreatments discussed, *ca.* 10 μm, Figure 3.43b,c,d,e,f. These pits also appear deeper in size than those on an etched surface (as discussed in Chapter 2) with the overall morphology appearing more "sponge" like. This could be due to the absence of the aggressive fluorotitanic acid and its replacement by ammonium bifluoride in this Pretreatment. No significant difference can be noted upon closer magnification of the darker areas compared to those of the lighter bulk of the surface, Figure 3.43e and f, but both show some evidence of a surface layer, indicated by I on Figure 3.43e,f. The presence of zirconium is suggested by EDX analysis but, here again, there is no observable difference noted between the dark and light regions, Figure 3.44a,b.

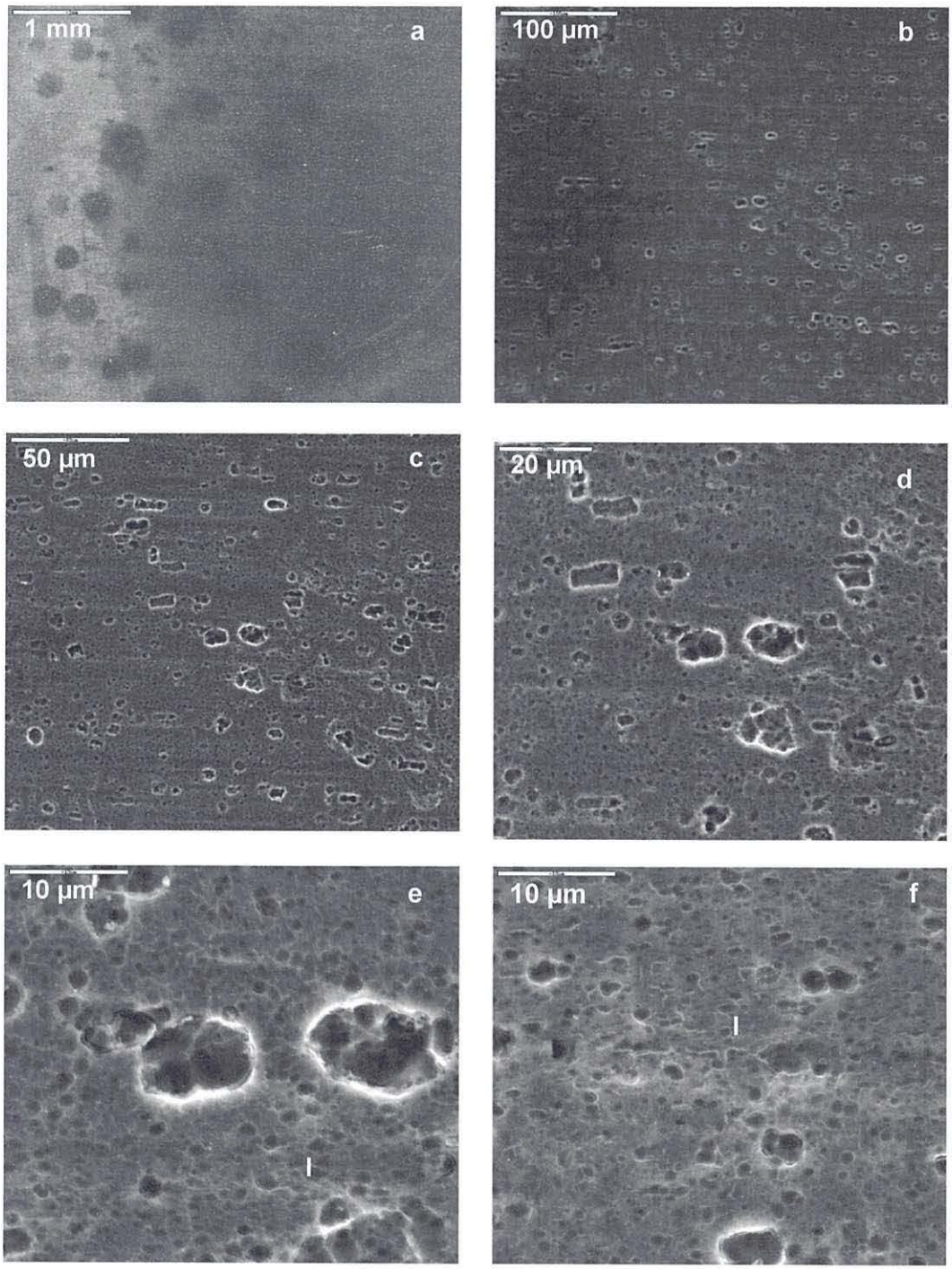

Figure 3.43 SEM images of alloy 3105 coated with Pretreatment 6 for 6 minutes. c), d), e), show magnifications of the lighter area visible in b), whilst f) is of the darker area in image b). I) indicates the surface layer features

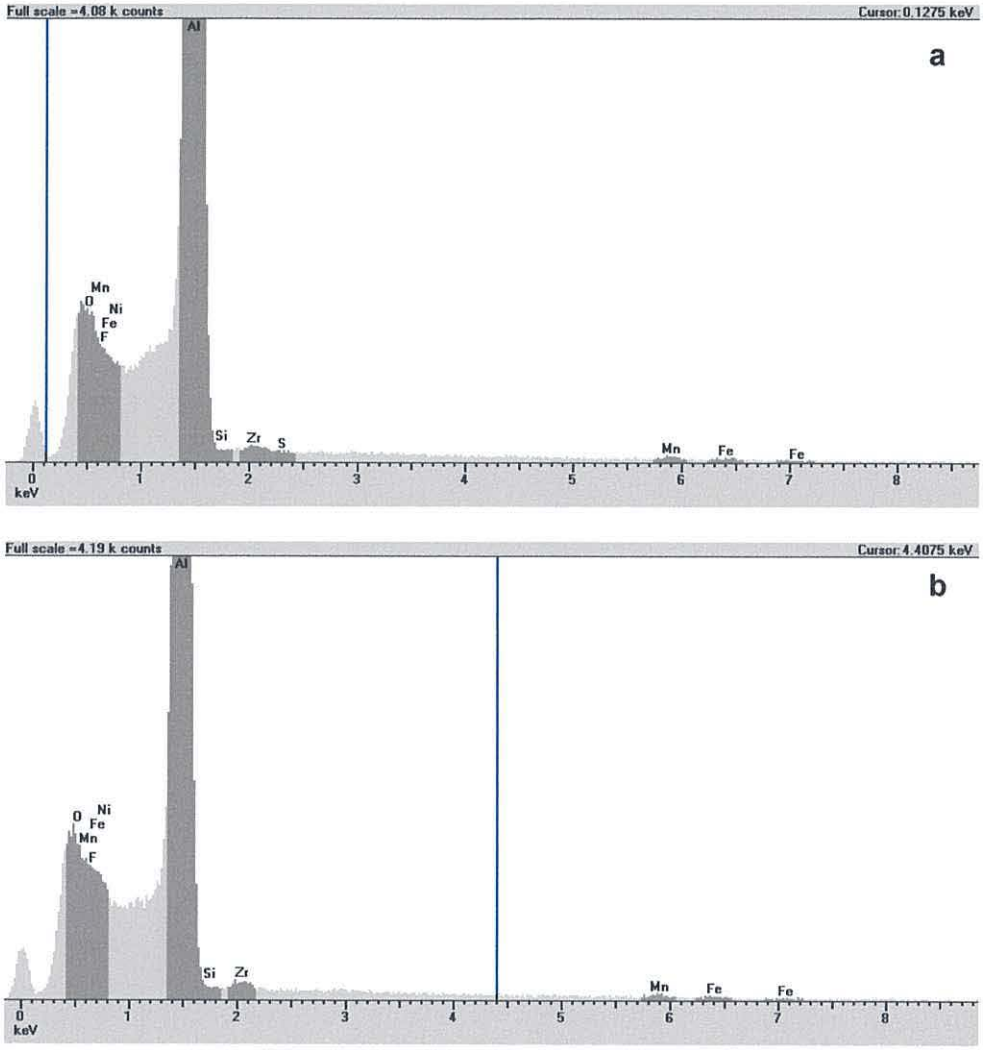

Figure 3.44 EDX analysis of alloy 3105 coated with Pretreatment 6 for 6 minutes, field of vision for a) shown in Figure 3.44e, field of vision for b) shown in Figure 3.44f

A non-uniform coating is also observed by SEM following Pretreatment 6 on alloy 6063 after 6 minutes of exposure, Figure 3.45, with lighter and darker patches apparent across the substrate surface as observed after 3 minutes exposure. On this alloy, the darker areas show no obvious pattern at low resolution on the SEM. Interestingly, the rolling lines remain apparent on this alloy which may suggest a lower etching power for this solution. The grain boundary lines and a number of intermetallic particles are visible at closer magnification, and it can be noted that areas immediately surrounding the

intermetallics also appear darker than the matrix, indicated by the arrows on Figure 3.45e.

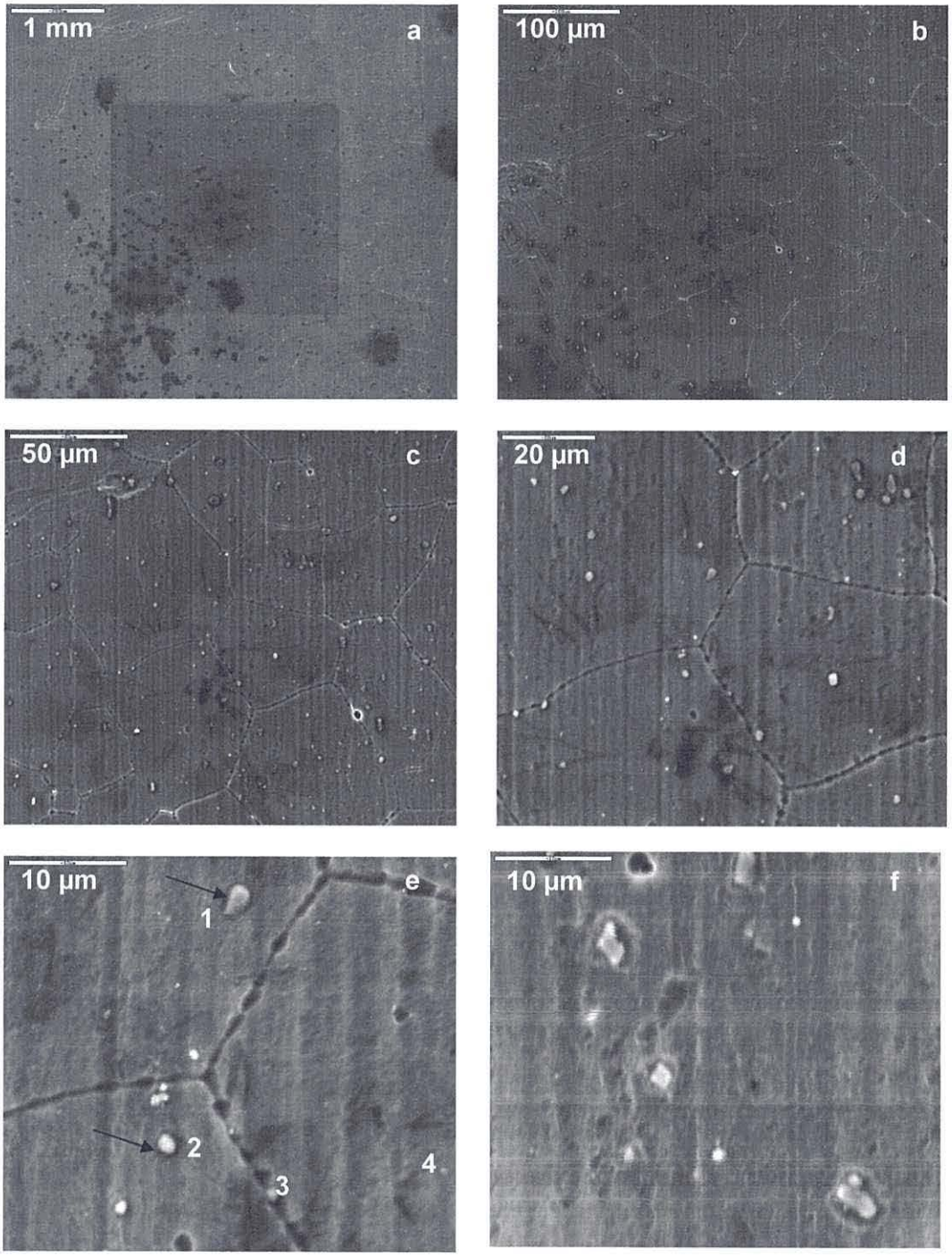

Figure 3.45 SEM images of alloy 6063 coated with Pretreatment 6 for 6 minutes. E shows a lighter area while F shows a darker area. The arrows indicate the dark areas surrounding the intermetallic particles

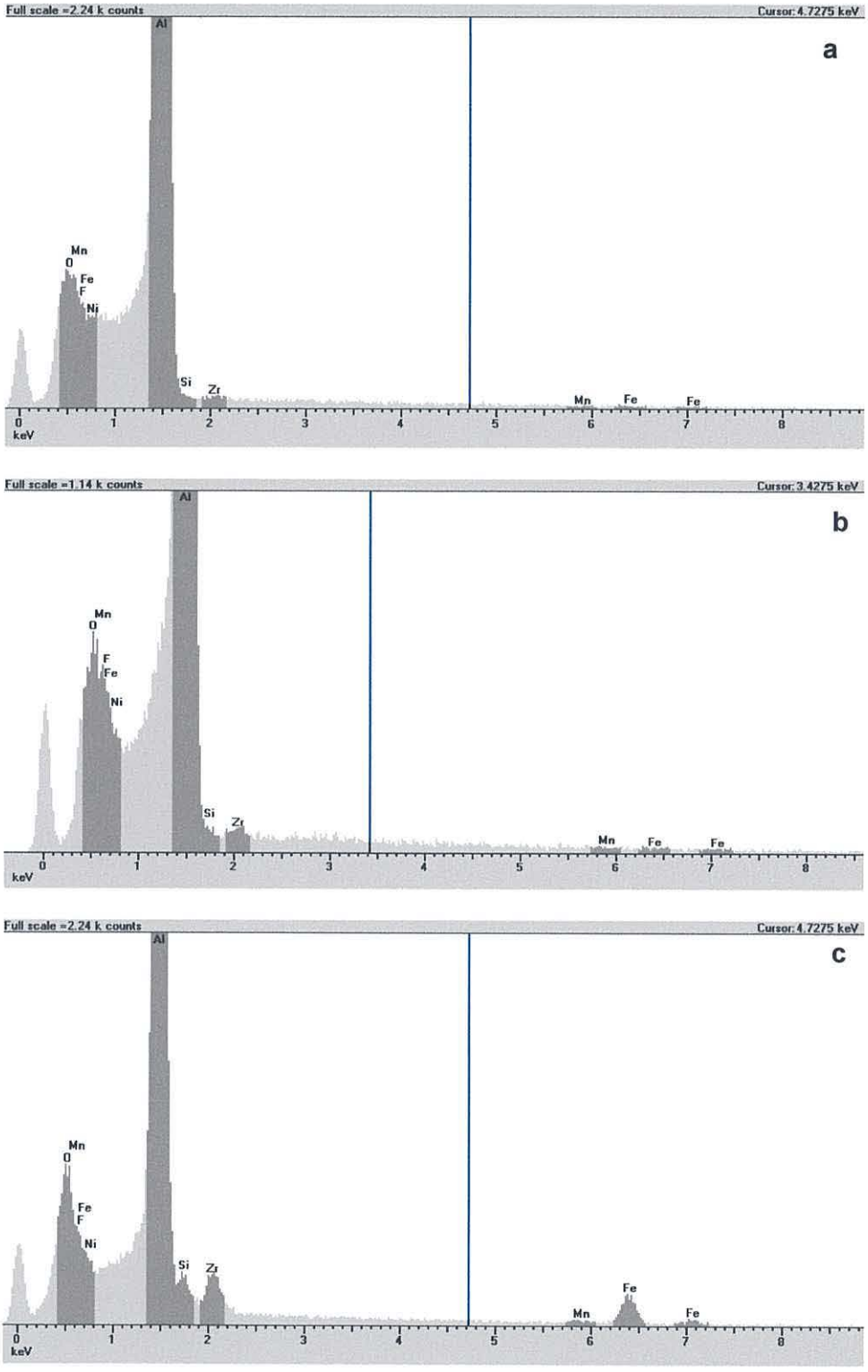

Figure 3.46 EDX analysis of alloy 6063 coated with Pretreatment 6 for 6 minutes, a) area shown in Figure 3.45e, b) area shown in Figure 3.45f, and c) showing spot analysis of particle I identified in Figure 3.45e

Further magnification does not reveal any significant differences in morphology between the light and larger dark regions. However, as discussed previously, EDX analysis suggests a more pronounced presence of zirconium in the darker areas which may suggest a thicker coating in these areas. Analysis of the intermetallic particles indicates the presence of manganese, iron and silica, and a high zirconium content compared with analysis of the matrix.

The suggestion from the SEM data of an uneven coating deposition by this pretreatment may indicate that the coating would not be a successful Pretreatment for corrosion resistance without further improvement to resolve this. On this basis, two further pre-treatment solutions have been assessed which have also used ammonium bifluoride within the solution.

Pretreatment 7 - Fluorozirconic acid, Fluorotitanic acid, Ammonium bifluoride and Polyacrylic acid

In the search for an improved chrome-free corrosion coating and based on the data collected from the earlier pretreatments, Pretreatment 7 has been chosen to compare the effects of a polymer (polyacrylic acid) along with fluorozirconic and fluorotitanic acids in the presence of ammonium biflluoride. Thus this solution can be considered as a modified version of Pretreatment 4 but with the addition of ammonium bifluoride as another etch agent.

Similarly to Pretreatment 6, SEM analysis indicates that Pretreatment 7 does not give a uniform coverage following 6 minutes exposure on alloy 3105, Figure 3.47a,b. Instead, there are light and dark areas as observed on earlier pretreatments. Indeed, dark, almost circular patterns are observed, around 400 μm in size which may be the result of drying processes. The surface shows both the presence of pits and pores with and larger pits from 1.5 to 40 μm across and smaller, spherical pores ranging from 0.25 to 1.5 μm in diameter, Figure 3.47c. Towards the centre regions of the dark circular areas, higher resolution analysis at further magnification reveals that the surface appears as a porous thick foam which is cracked in places, Figure 3.47d, e,f. Within these central areas, flaking of the surface coating is also apparent, Figure 3.49a,b,c,d. In the flaking areas, the coating appears to be a thin film rather than a foam-like type of material. Subsequent EDX analysis clearly indicates the presence of both zirconium and titanium in both the pitted and the flaking regions, providing similar analyses for both areas, Figure 3.49. Quantitative analysis using EDX is difficult to achieve but these data may possibly indicate a thicker coating in the darker regions (there is evidence of a link between darker shades and thicker coatings with some earlier pretreatments). Thus, the darkest areas may indicate the greatest coating deposition and, in turn, these data may suggest

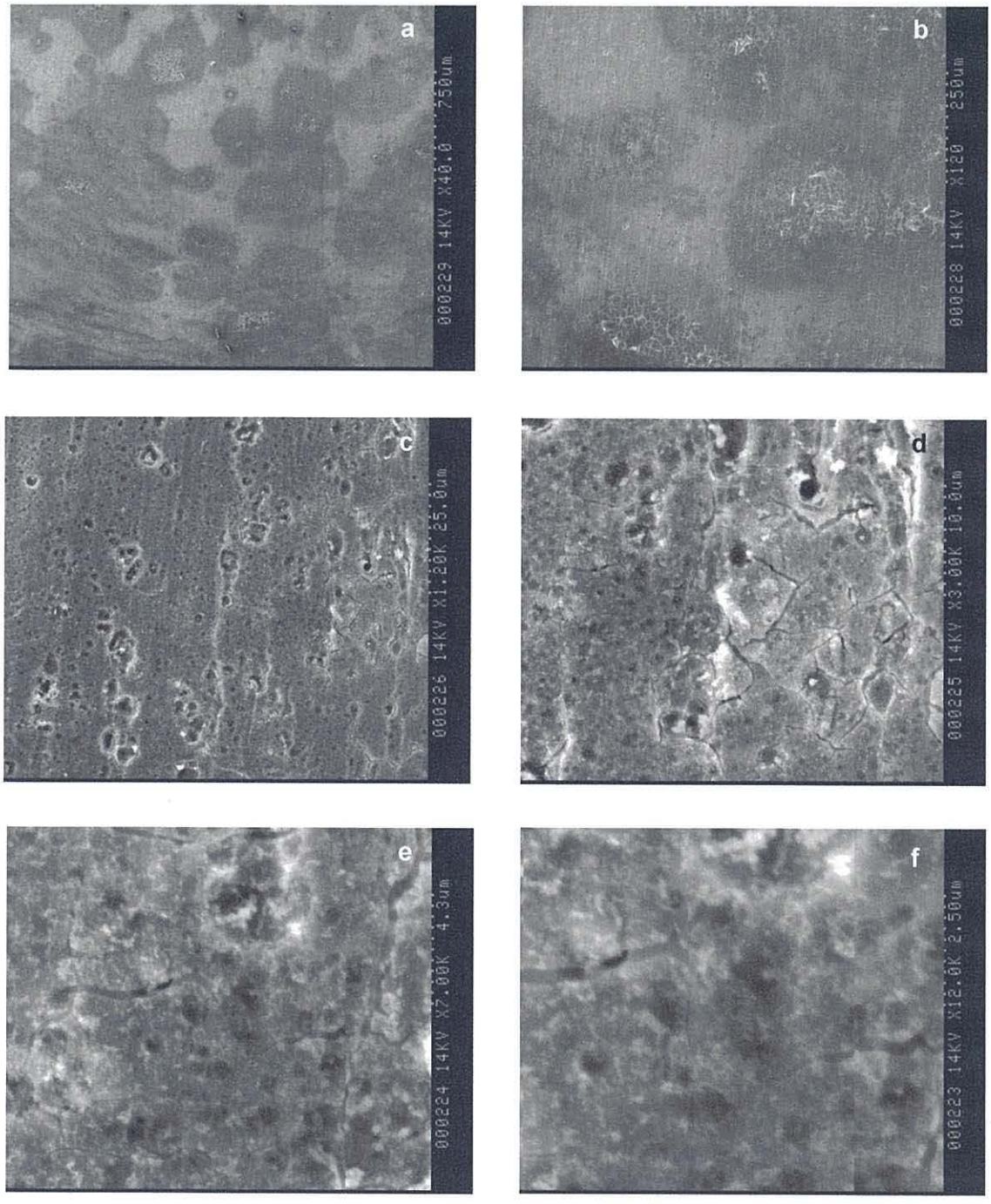

Figure 3.47 SEM images of alloy 3105 coated with Pretreatment7 for 6 minutes. c), d), e), f show the pitted regions, further images shown in Figure 3.48

an uneven coating for this pretreatment. This may be the cause of the detachment at the thickest central areas, where the coating appears to be more of a thin, dehydrated, film which has detached from the substrate.

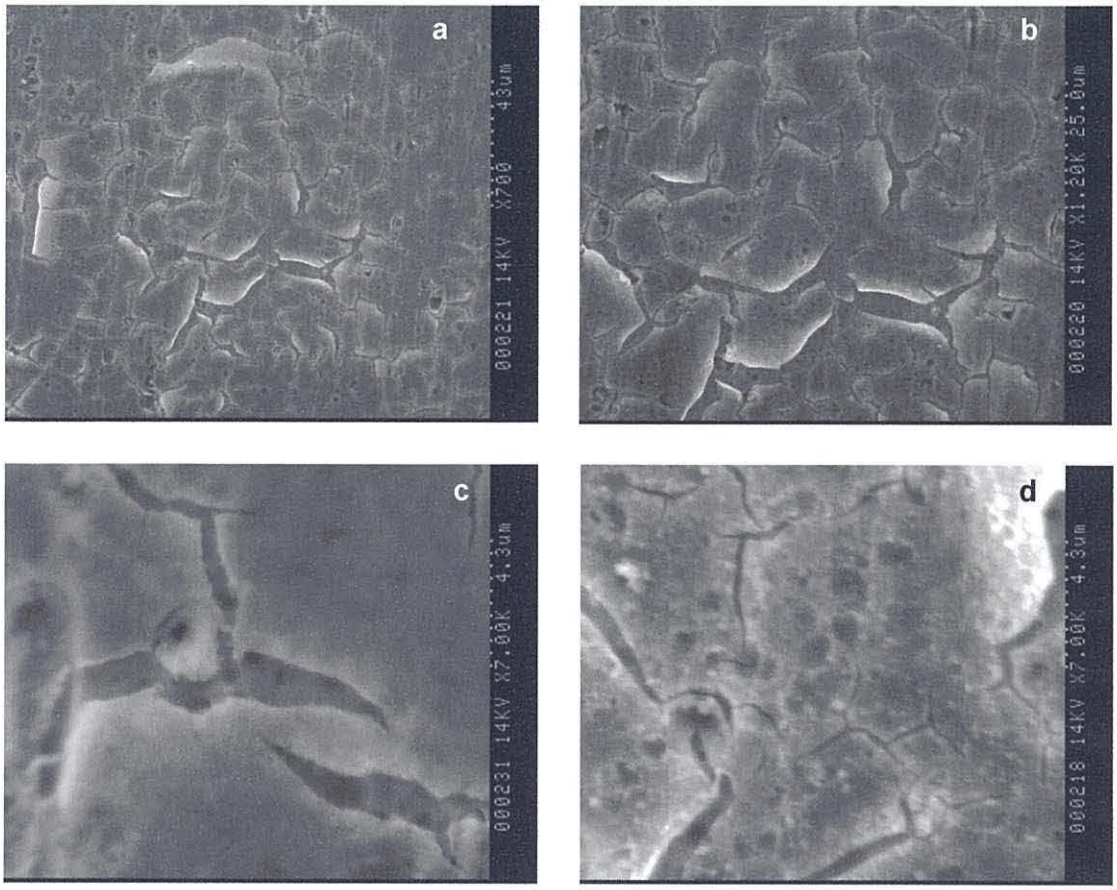

Figure 3.48 SEM images of alloy 3105 coated with Pretreatment 7 for 6 minutes showing the cracking of the coating. Further images are shown in Figure 3.47

Intermetallic particles are also visible on some parts of the substrate surface and these are evident by the dark area immediately surrounding them, Figure 3.50. In Pretreatment 1, this darkness was attributed to a greater deposition surrounding the particles and it was suggested that this might be due to their cathodic nature, resulting in preferential etching of the surrounding area. This preferential etching might be expected to produce a morphology which would "trap" solution close to the substrate surface creating localised conditions favourable for deposition leading to a thicker coating. Interestingly however, in the case of Pretreatment 7, in direct contrast to the data for Pretreatment 1, the SEM plan view data appears to show the coating is repelled by the

intermetallic particles. This could still be because of the cathodic nature of these particles but may indicate a charge reversal in the deposition process.

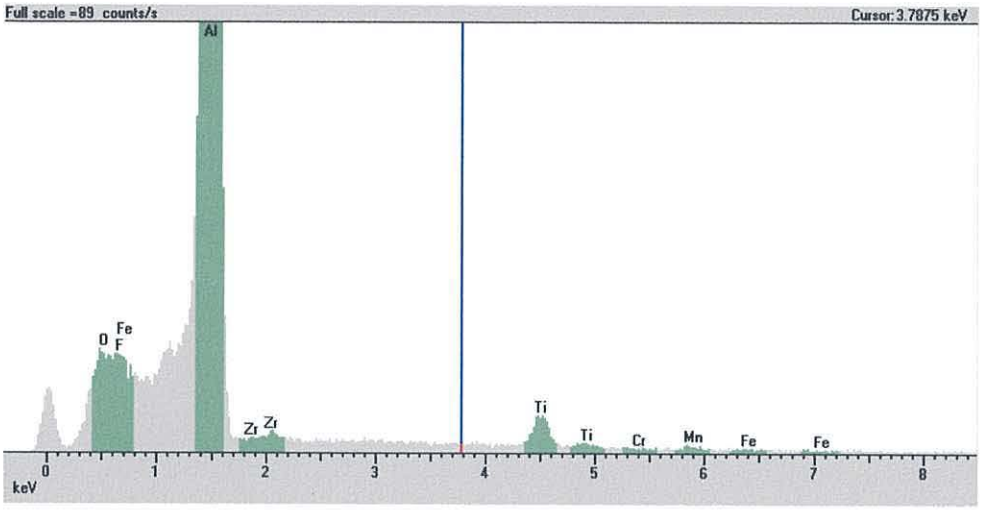

Figure 3.49 EDX analysis of, alloy 3105 coated with Pretreatment 7 for 3 minutes, field of vision shown in Figure 3.47c

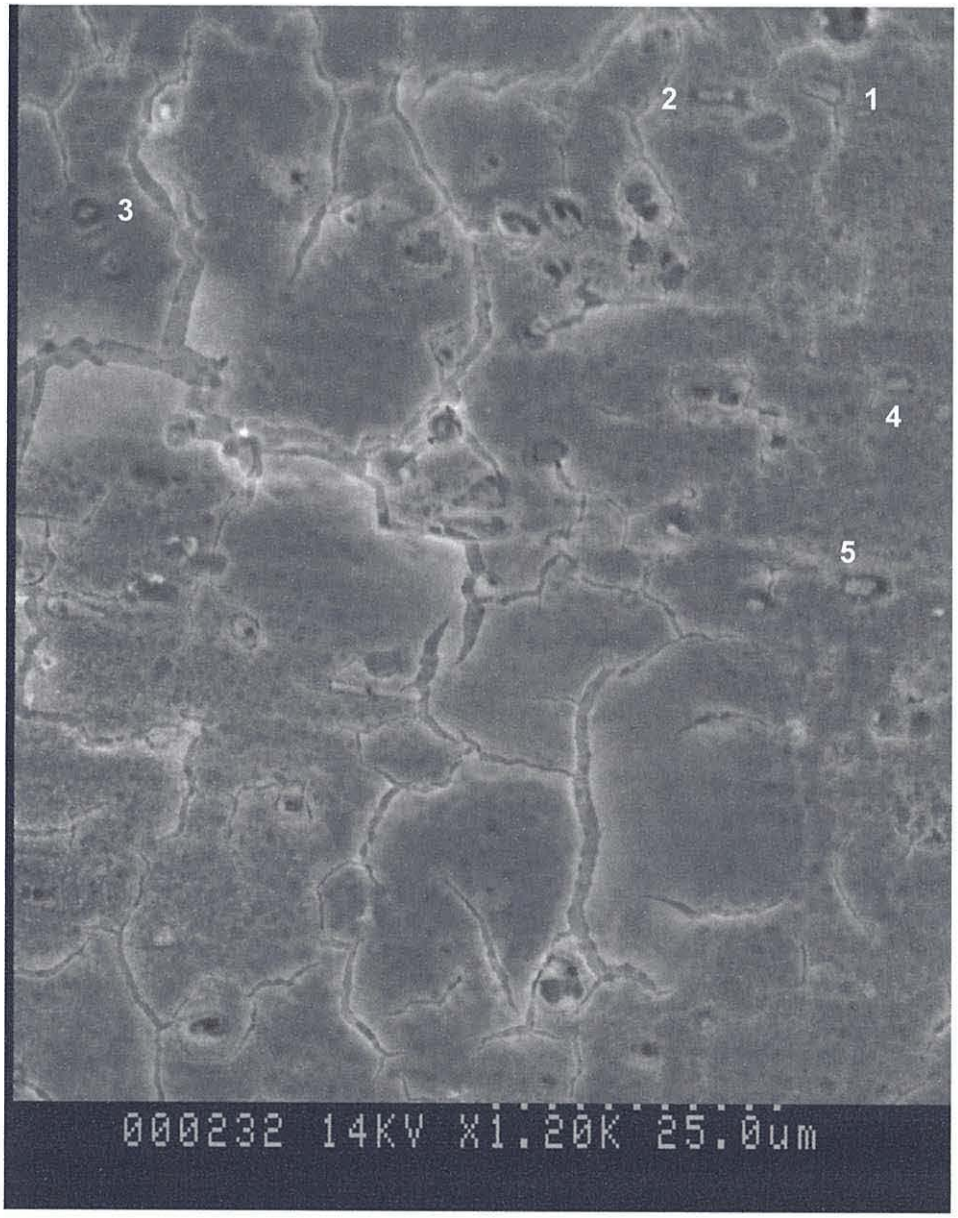

Figure 3.50 Enlarged SEM image of alloy 3105 coated with Pretreatment 7 for 6 minutes, showing the cracking of the coating and a number of intermetallic particles which have been numbered for clarity

On first inspection, the corresponding SEM data for alloy 6063 using Pretreatment 7 appears to show that this exhibits an extremely poor coating. The macro-scale images show flakes of film detaching from the surface, Figure 3.51a,b,c,d,e,f. Further magnification shows that the extrusion lines are still visible indicating that these have

not been removed by any etching processes. Intermetallic particles are also evident, and these show darkened areas surrounding them as in earlier SEM data, Figure 3.51c,e.

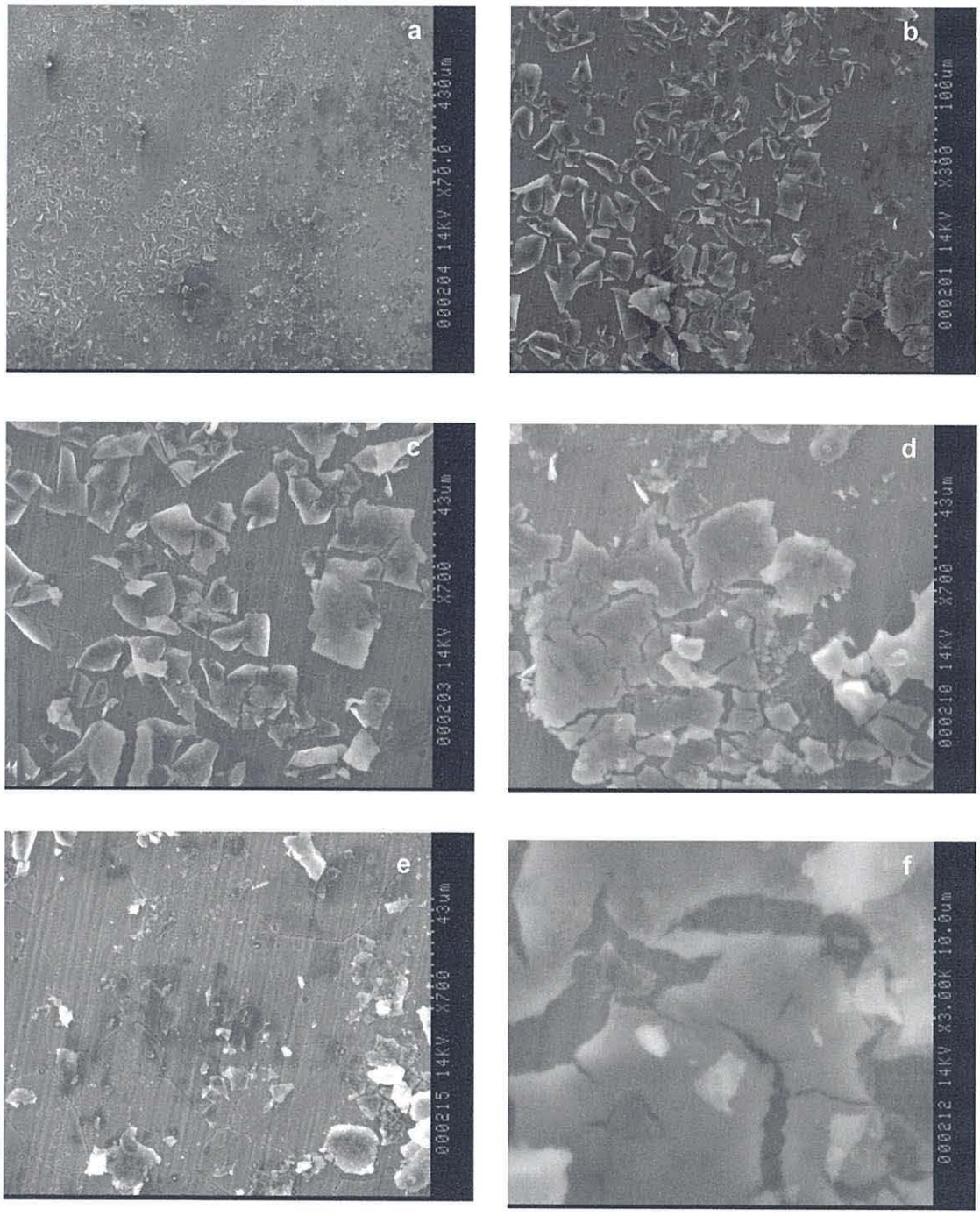

Figure 3.51 SEM images of alloy 6063 coated with Pretreatment 7 for 6 minutes.

Light and dark patches are also apparent on the substrate surface which is not involved with any of the delaminated flaky film.

If the coating is considered to be the flaking film, Figure 3.51b,c, then it is apparent that very little surface coverage is obtained in terms of film coverage on the metal substrate itself. Thus, this pre-treatment would not be considered a success. However, the light and dark areas which are observed on the metal substrate surface may indicate that the coating may have deposited in some areas where the flaking and detachment is not visible.

EDX analysis has been carried out and the analysis of the area shown in Figure 3.51b indicates the presence of both zirconium and titanium, Figure 3.52. However, it is difficult to conclusively determine which part of the coating or substrate these data refer to. It may be that too much coating has deposited on the surface in some areas and that this has caused the cracking and detachment which is observed by SEM. Equally, it could be the detached films or the substrate coating which gives rise to the strong signals upon EDX analysis.

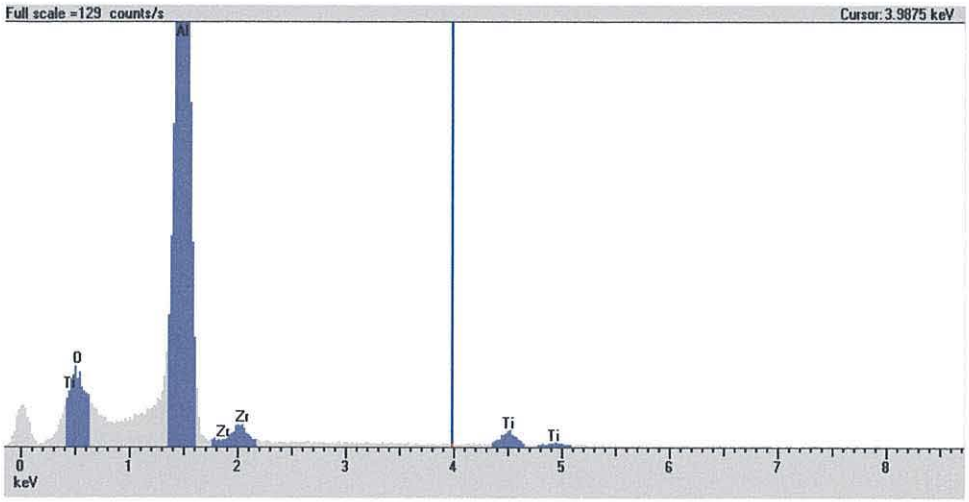

Figure 3.52 EDX analysis, alloy 6063 coated with Pretreatment 7 for 6 minutes, of the area shown Figure 3.51b

Overall, the SEM data for Pretreatment 7 suggest that this coating appears to deposit such a thick coating, that it cracks and detaches from the metal surface. In this context, it seems that the etch/deposition process is favoured too greatly in favour of the deposition, and the addition of the polyacrylic acid has not helped prevent the cracking as observed when added to Pretreatment 4 (*cf* Pretreatment 3 where the polyacrylic acid was not present). Thus it appears important for the development of a chrome-free corrosion coating that the layer is coherent with even coverage, but that the layer is thin enough to prevent it cracking and delaminating during subsequent processing steps (e.g. drying and powder coating).

Pretreatment 8 - Fluorozirconic acid, Fluorotitanic acid, Ammonium bifluoride and Polyacrylic acid

Following analysis of the data from Pretreatment 7, it was decided to choose a solution containing the same chemicals but with a greater concentration of polyacrylic acid to see if this could act as a more effective flocculating/binding agent for what was believed to be a thicker coating; this new solution is Pretreatment 8. The basis for this decision was that polyacrylic acid had previously been observed to reduce cracking, delamination and flaking in Pretreatment 4 (when compared with Pretreatment 3). However, the SEM data show that the addition of further polyacrylic acid to Pretreatment 8 has not achieved the same result when compared with Pretreatment 7. Instead, the coating produced from this Pretreatment actually appears to show more flaking and detachment than Pretreatment 7 at least at the macro-scale, Figure 3.53. Again darker and lighter regions are apparent. Also, circular patterns are evident with pits, where there seems to be a darkening (which as discussed earlier may possibly indicate a greater amount of deposit), towards the edges of the circles. Around the outside of this, the coating eventually gives way to cracking and detachment, Figure 3.53b,c. Although the additional polyacrylic acid has not completely prevented cracking, it has produced a different coating to that of the randomly detached, thin flakes of coating film as observed for Pretreatment 7. Furthermore, the coating produced by Pretreatment 8 appears to be a thick layer which has shrunk due to desolvation during the drying procedures leaving curled edges around the edges of the flakes, Figure 3.53e, Figure 3.54b. Interestingly, the areas between the circular regions are pitted, but otherwise resemble the morphology of the untreated alloy 3105, Figure 3.53d,f, Figure 3.54a, and not the etched alloy as would be expected should no coating have been deposited. This may indicate that the increased concentration of polyacrylic acid has interfered in some way with the etching process (perhaps by forming a surface layer of

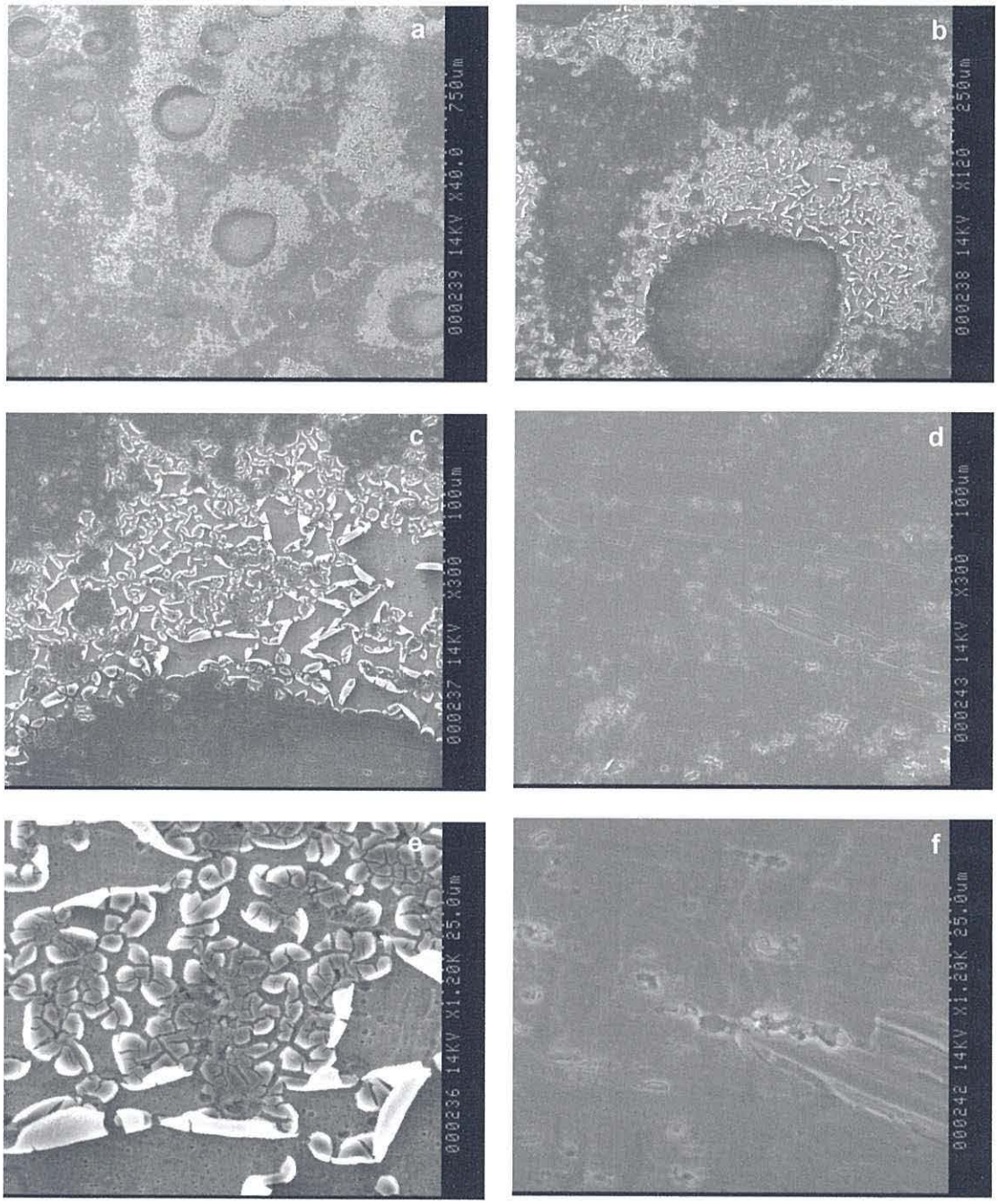

Figure 3.53 SEM images of alloy 3105 coated with Pretreatment 8 for 6 minutes. d shows a pitted region, further magnification presented in Figure 3.54

polymer to inhibit attack of the etchant species). This may suggest that too much polymer is present in this solution. However, the areas where coating has detached appear much lighter in contrast. This seems to indicate that the coating has deposited in these regions as normal but then delaminated leaving little coating behind. This is confirmed through EDX analysis, Figure 3.55. In addition, the darker coated surface, although showing pits, does not exhibit the pores that are visible where detachment has occurred, Figure 3.53f. This suggests that in the areas of coated surface deposition may have occurred within the pores to produce a film with a different morphology i.e. without pores, Figure 3.53e. Alternatively, a different etching process may have occurred in these regions.

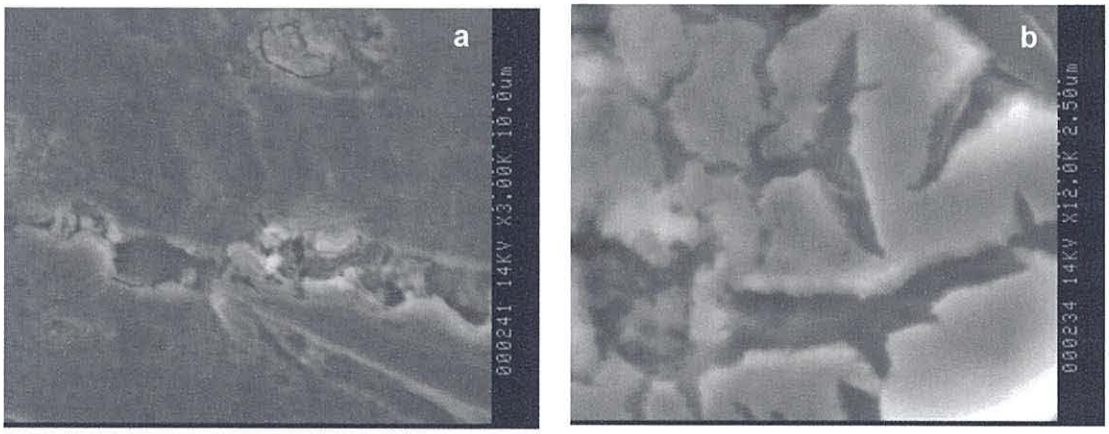

Figure 3.54 High magnification SEM images of alloy 3105 coated with Pretreatment 8 for 6 minutes

The reason for the circular patterns observed is less clear but it may possibly be that these patterns might be produced when a type of foam coating is produced on the substrate surface, possibly due to localised hydrogen formation. Thus, when the bubbles burst, coating is deposited, but this is denser at the circular area that was the interface between the bubble wall and the substrate, leading to the circular detachment observed.

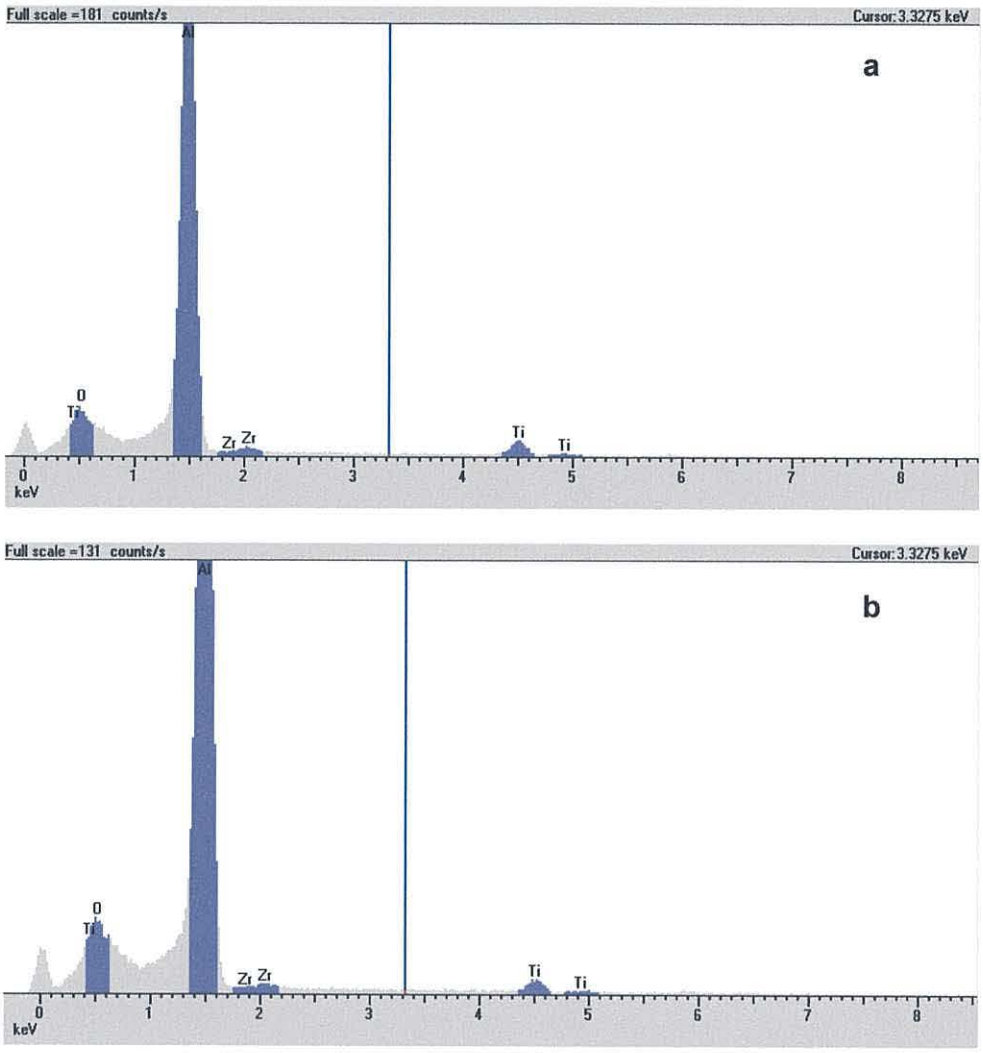

Figure 3.55 EDX analysis of alloy 3105 coated with Pretreatment 8 for 6 minutes. a) analysis of the region shown in Figure 3.54b, b) analysis of the region shown in Figure 53c

SEM data of the corresponding study of Pretreatment 8 on alloy 6063 also shows significant flaking and detachment, but without any obvious patterns as observed for alloy 3105, Figure 3.56a,b,c,d. Instead, on this alloy surface there is cracking throughout the coating, Figure 3.56c,e, and the areas that appear uncoated, Figure 3.57a,b, resemble an etched surface as might be expected. Thus, whilst the increased polymer concentration may not have solved the cracking and flaking of the coating for this alloy, equally, it does not appear to have had a negative effect either, relative to the lower concentration.

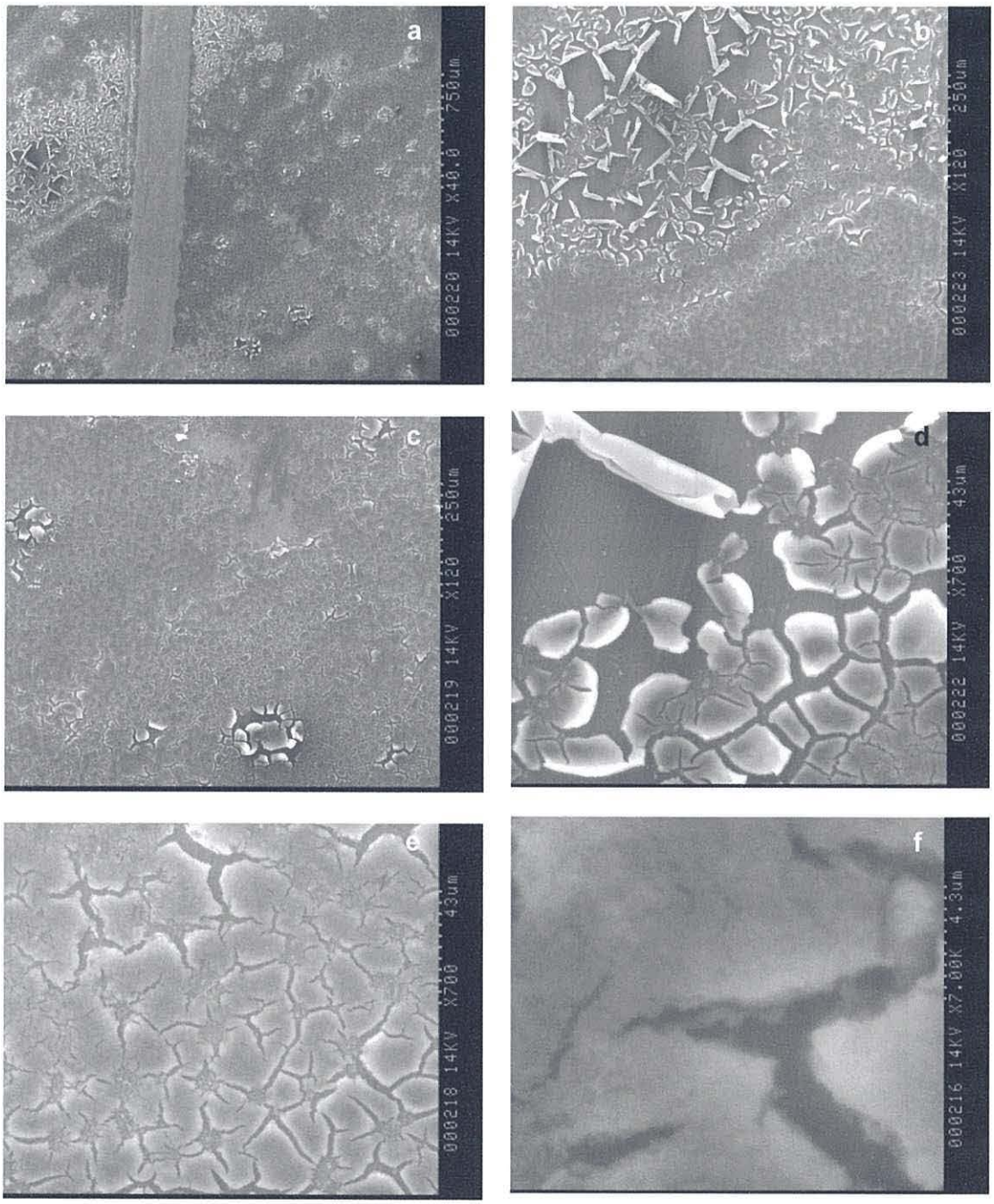

Figure 3.56 SEM images of alloy 6063 coated with Pretreatment 8 for 6 minutes. Images of uncoated regions are shown in Figure 3.57

Higher resolution images of this Pretreatment on alloy 6063 shows the presence of extrusion lines, intermetallic particles and grain boundaries suggesting that full etching of the surface layer of this alloy has not taken place during this pretreatment process.

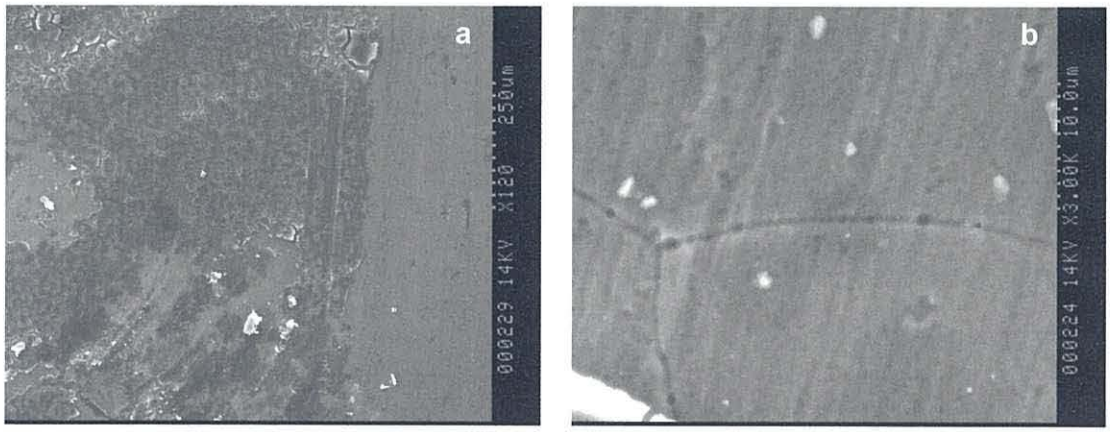

Figure 3.57 SEM images of alloy 6063 coated with Pretreatment 8 for 6 minutes, showing uncoated areas. Further images are shown in Figure 3.56

The EDX data suggest that both Zr and Ti are both present in what appears to be coated areas. However, it does not indicate that any zirconium or titanium is present in areas that appear uncoated, Figure 3.57b. Overall, this coating appears to most closely resemble that seen on alloy 3105, being thick and appearing to have dried and cracked, Figure 3.53e,f.

It can be concluded that the surface coverage of Pretreatment 8 is better on the 3105 alloy than on the 6063 alloy. However, the flaking and coating detachment on both alloys suggests that the coating would not be a successful pretreatment for corrosion resistance. These data suggest that, whilst it is clear that the use of the polyacrylic acid has benefits in terms of flocculating and binding the coating layer, this effect has limits with a key limit appearing to be the thickness of the coating layer. Thus, a revised target for this coating technology appears to be a thin coating with even and complete coverage and with good adhesion to both substrate and paint layers.

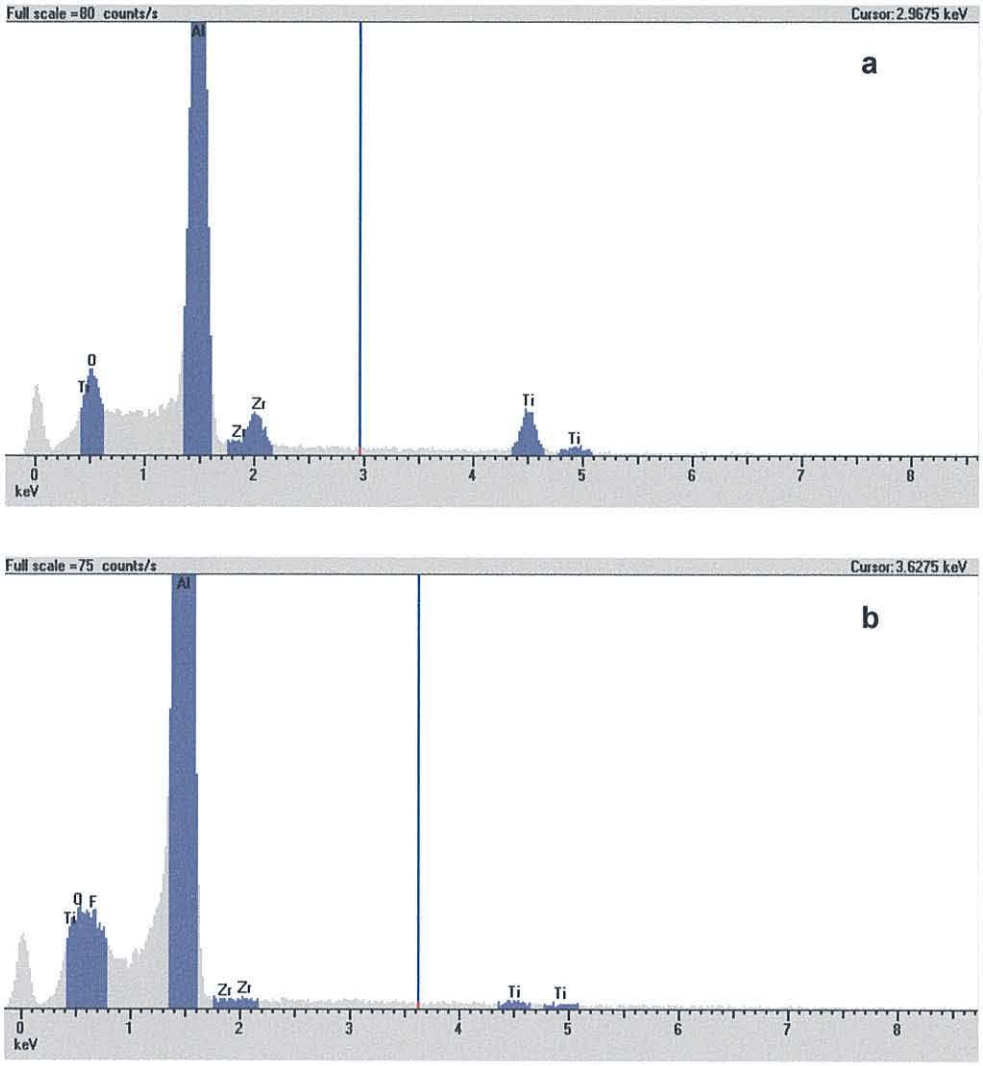

Figure 3.58 EDX analysis of alloy 6063 coated with Pretreatment 8 for 6 minutes. Image a) shows the field of vision shown in Figure 3.56a, and b) the field of vision shown in Figure 3.57b

Pretreatment 9 - Fluorozirconic acid, Fluorotitanic acid, Polyacrylic acid and Polyvinyl acetate

The penultimate pre-treatment tested in this section is made up of both fluorozirconic acid and fluorotitanic acids but, in this solution, two polymers have also been added. Polyacrylic acid (PAA) has been used because of its positive effects on previous coatings. However, polyvinyl acetate (PVA) has also been added to study whether this will give an additional benefit.

The SEM data for Pretreatment 9 shows that this appears to give a uniform coating on alloy 3105, Figure 3.59. Very little pitting is observed, and no charging is evident on what appear to be shallower pits than previously observed. This could be due to the weaker concentration of fluoride-containing chemicals in this Pretreatment which are expected to be responsible for the etching of the alloy surface. On closer magnification, the surface morphology is very porous and sponge like, making the coating appear thick. As stated for some of the earlier pretreatments, it may be that the coating has been deposited within the etch pits making them appear less apparent. Overall, this coating more closely resembles Pretreatment 5 and 6 than any of the others. Interestingly, these other pretreatments also had weaker concentration in terms of their fluoride-containing chemicals. This once again highlights the importance of the etching process within the etch-deposition balance that drives this type of pre-treatment technology.

The corresponding EDX analysis for this prereatment shows weak signals confirming the presence of titanium and zirconium, Figure 3.61.

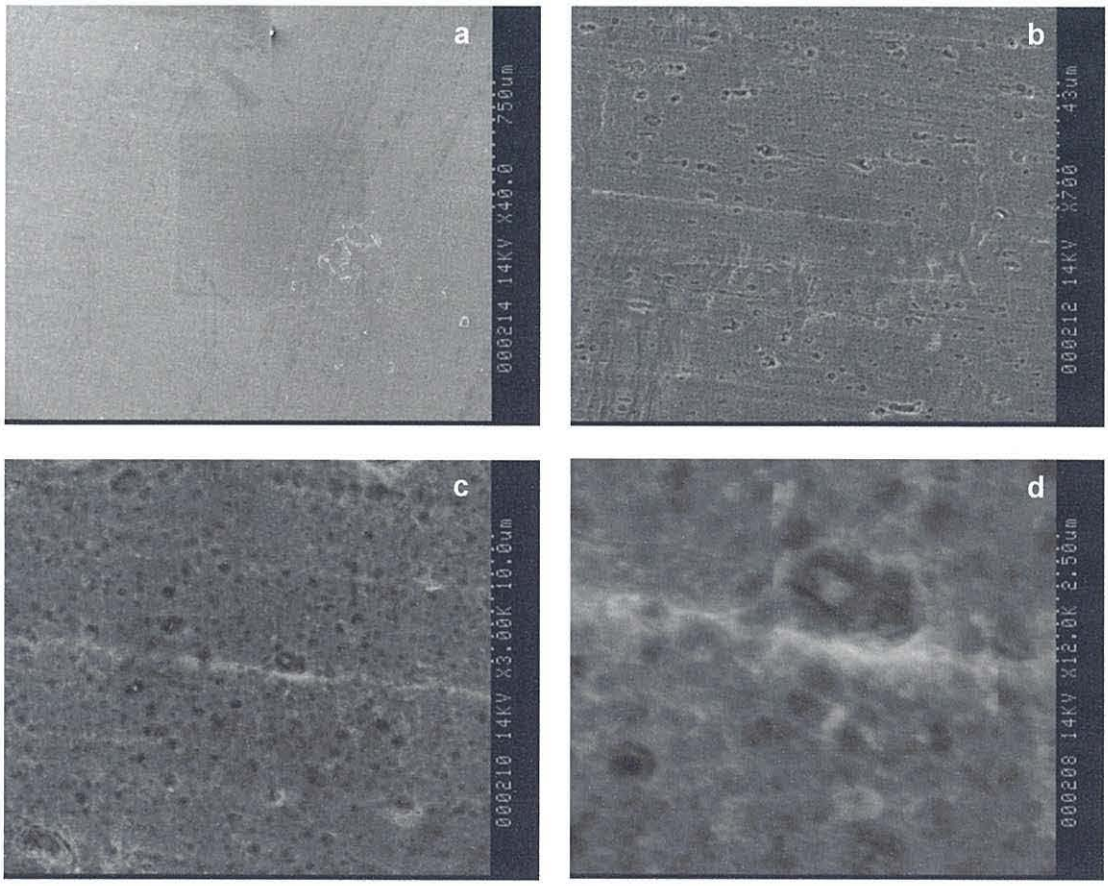

Figure 3.59 SEM images of alloy 3105 coated with Pretreatment 9 for 6 minutes

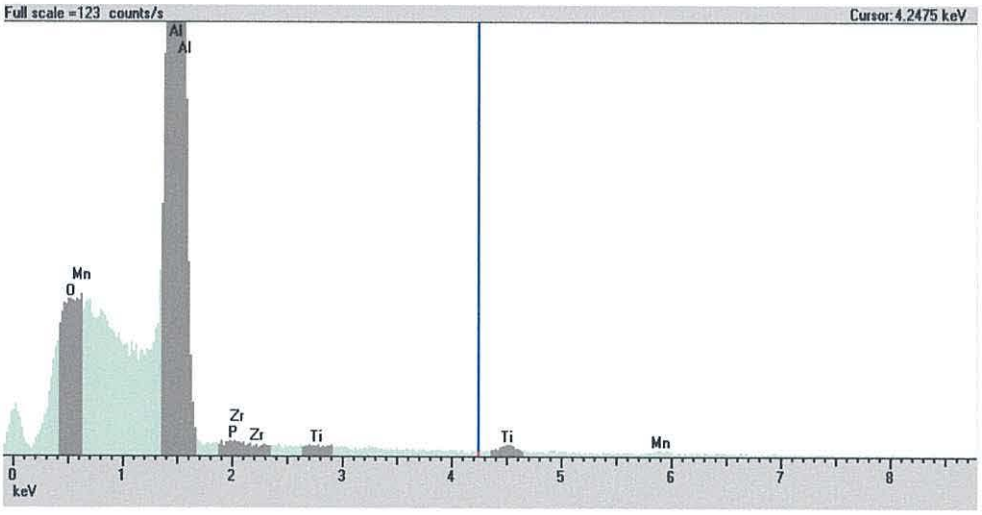

Figure 3.60 EDX analysis, alloy 3105 coated with Pretreatment 9 for 6 minutes, field of vision shown in Figure 3.59b

Pretreatment 9 has also been applied to alloy 6063. The coating deposited on this alloy does not appear as uniform as that observed on alloy 3105, Figure 3.61. For instance, there are some slightly darker and lighter regions observed although this is not as pronounced as in some earlier coatings. Some circular patterns are also evident here, but here again, these are not as apparent as observed on some of the previous pretreatments. In previous instances, there has been some evidence that these dark and light areas might be associated with differences in the thickness of the pretreatment coating.

For alloy 6063, closer magnification shows that the circular patterns show evidence of some cracking and slight detachment. In addition, the areas surrounding the cracked regions appear darker than the matrix. This has also been observed in earlier pretreatments and it may be that this is where the coating has become concentrated and thicker which has subsequently led to cracking, presumably during post- processing (e.g. drying and powder coating), Figure 3.61b. In regions where this coating is less evident due to the absence of cracks, is it difficult to ascertain what level of deposit has occurred. It is clear that some coating has been deposited because EDX analysis does show a signal for titanium and for zirconium, even if the latter signal is very weak, Figure 3.62. It should be noted here that the EDX technique is not best suited to the analysis of very thin films and even less so on metal substrates. The reason for this is that, in order to achieve resolution, the electron beam must be narrow and this is aided by increasing the accelerating voltage. Equally, in order to excite a reasonable number of elements in the Periodic Table, a higher accelerating voltage must be used (typically 14 kV in these measurements). However, the high accelerating voltage means that the incoming X-ray beam penetrates deeper into the surface exciting more of the bulk substrate than any thin surface coating.

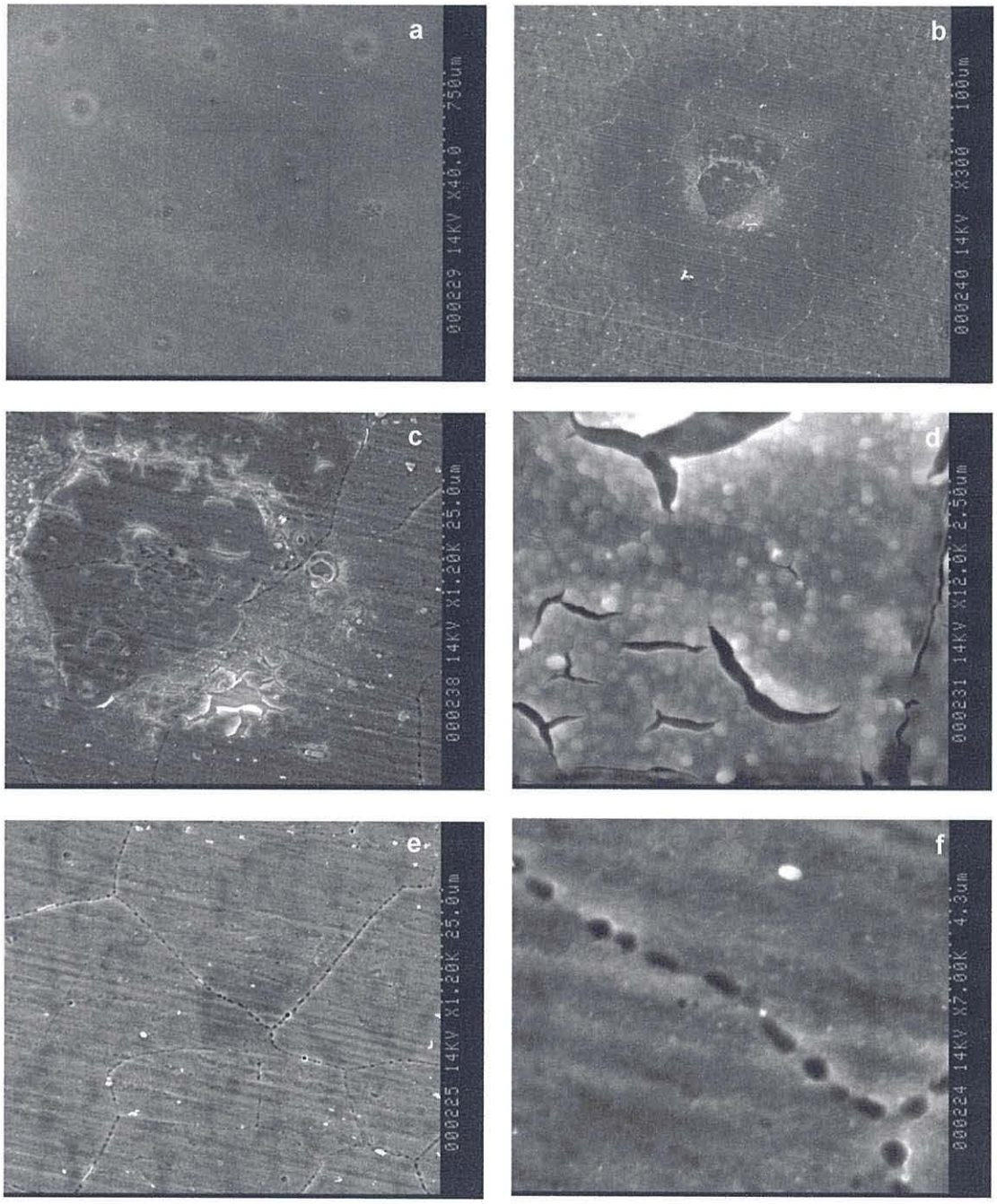

Figure 3.61 SEM images of alloy 6063 coated with Pretreatment 9 for 6 minutes

Thus, the weak signal for Zr observed here would probably appear more intense if EDX could be made more surface sensitive. This is the case in X-ray photoelectron spectroscopy (XPS) but the downside is that visualising the surface becomes much worse as a result. Spherical particles are evident in the coating shown in Figure 3.61d, and are also evident upon magnification of the area where coating is less evident, Figure 3.61f, suggesting coating deposition has occurred over the whole surface, with perhaps some concentration to produce a thicker coating in the circular areas.

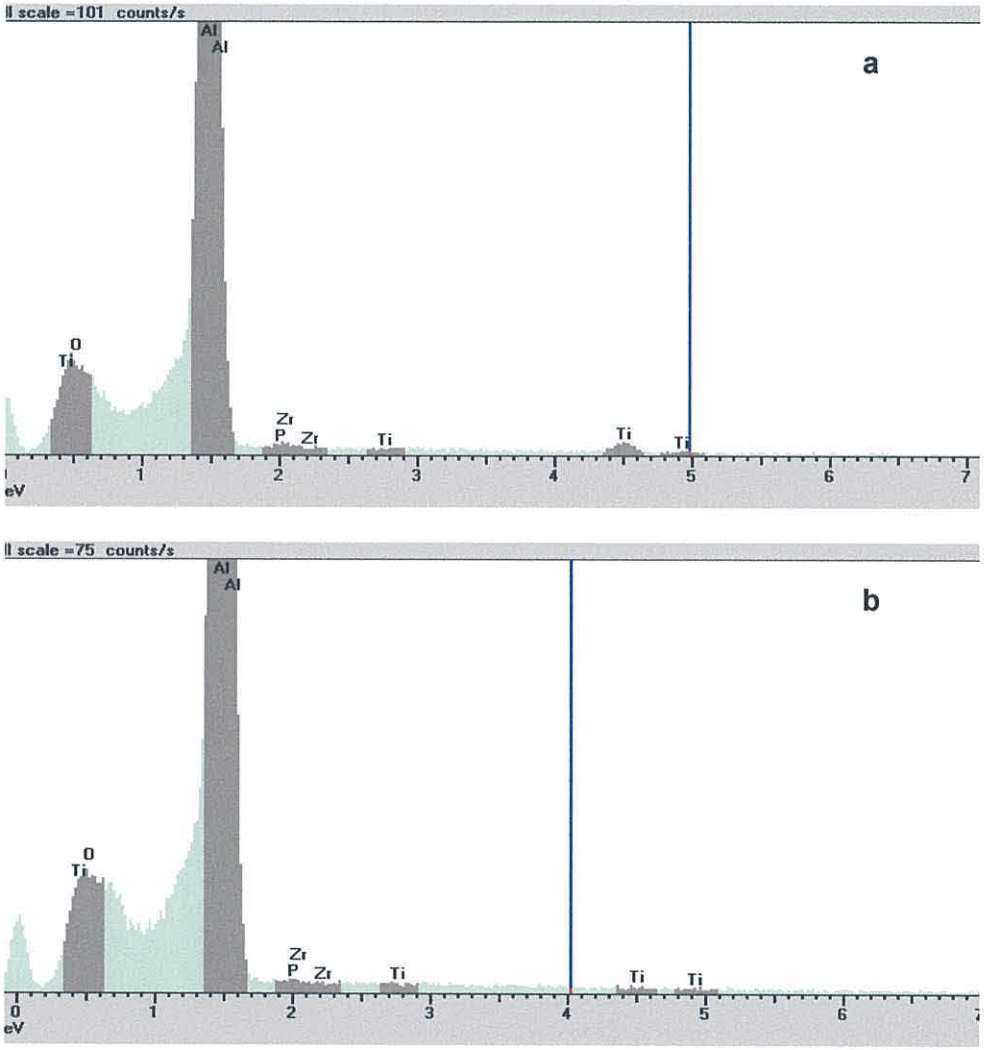

Figure 3.62 EDX analysis of alloy 6063 coated with Pretreatment 9 for 6 minutes. Field of vision for a) shown in Figure 3.61c, b) shown in Figure 3.61e

Although some cracking and slight detachment is evident, this is less significant than previously observed with other pretreatments, and the coating, from a plan view alone, appears promising. This implies that the addition of the PVA does have an additional benefit in producing a coating with good coverage, intra-coating binding and adhesion to the substrate.

Pretreatment 10 - Fluorozirconic acid, fluorotitanic acid and nickel sulfate

The final of the pre-treatments tested in this section (Pretreatment 10) is made up of fluorozirconic and fluorotitanic acids but wihout any polymers added. Instead, nickel sulfate has been added which should provide the coating with a faint colour. Colour has previously been an important spot check for commecial chromate coatings, ensuring even coverage of a given substrate.

The data show that coating afforded by Pretreatment 10 does not give a uniform coating on alloy 3105, Figure 3.63a. There are notable lighter and darker areas to the surface. Closer inspection shows that the surface appear lighter where flaking and detachment of the coating has occurred, Figure 3.65a,b. Darker patches are visible which exhibit a "marbling" effect, which is attributed to a thicker coating deposition. The bulk of the surface appears pitted, and further magnification reveals a thick, sponge like, texture with shallow pores, Figure 3.63b,c,d, similar to Preteatment 9. Examination of the substrate where coating has detached reveals a different morphology, which is porous but does not have the same thick sponge like texture, appearing "clean" and possibly "glass" like, Figure 3.65. This is more typical of the etched surface discussed previously in Chapter 2. Although quantitative analysis as previously mentioned is difficult using this technique, EDX analysis does indicate that there may be higher levels of titanium on the bulk of the surface, Figure 3.64, than at the regions where flaking and detachment has occurred, Figure 3.66 which is in line with the suggested delamination of the pretreatment discussed above.

.

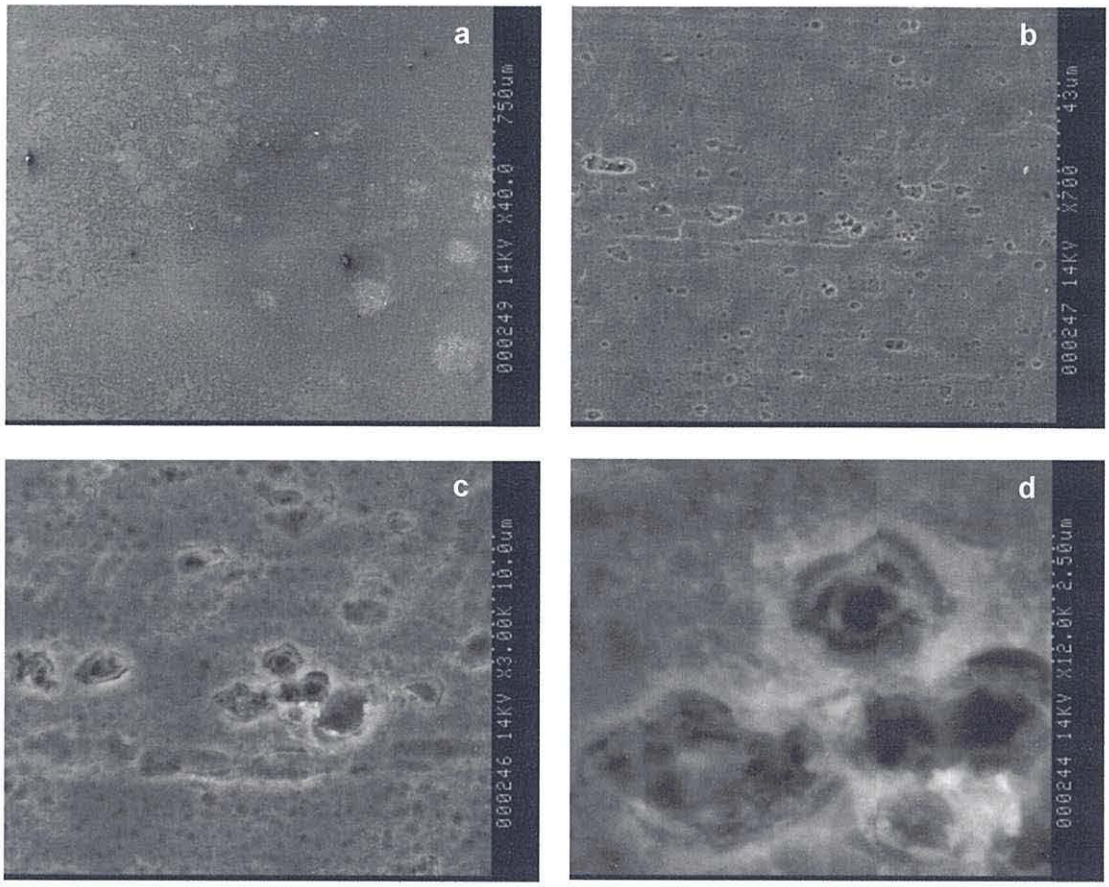

Figure 3.63 SEM images of alloy 3105 coated with Pretreatment 10 for 6 minutes.

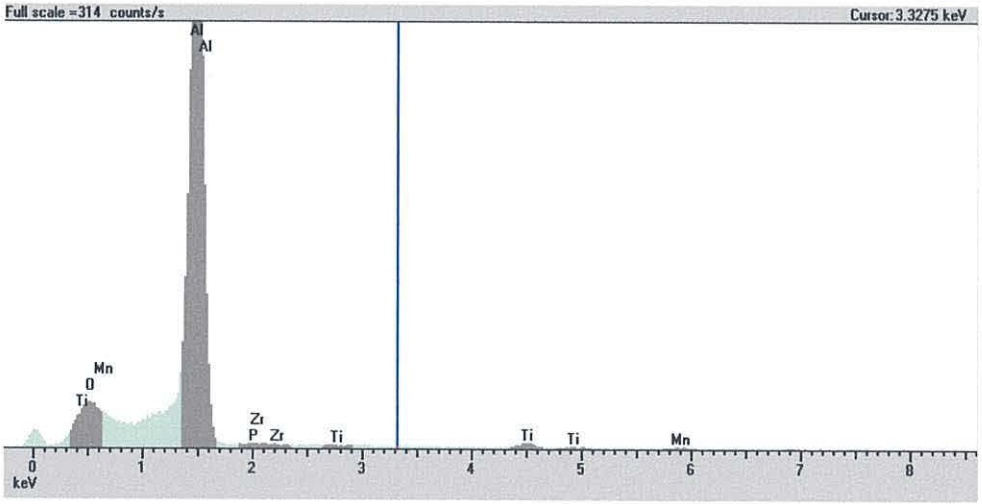

Figure 3.64 EDX analysis of, alloy 3105 coated with Pretreatment 10 for 6 minutes, field of vision shown in Figure 3.63c

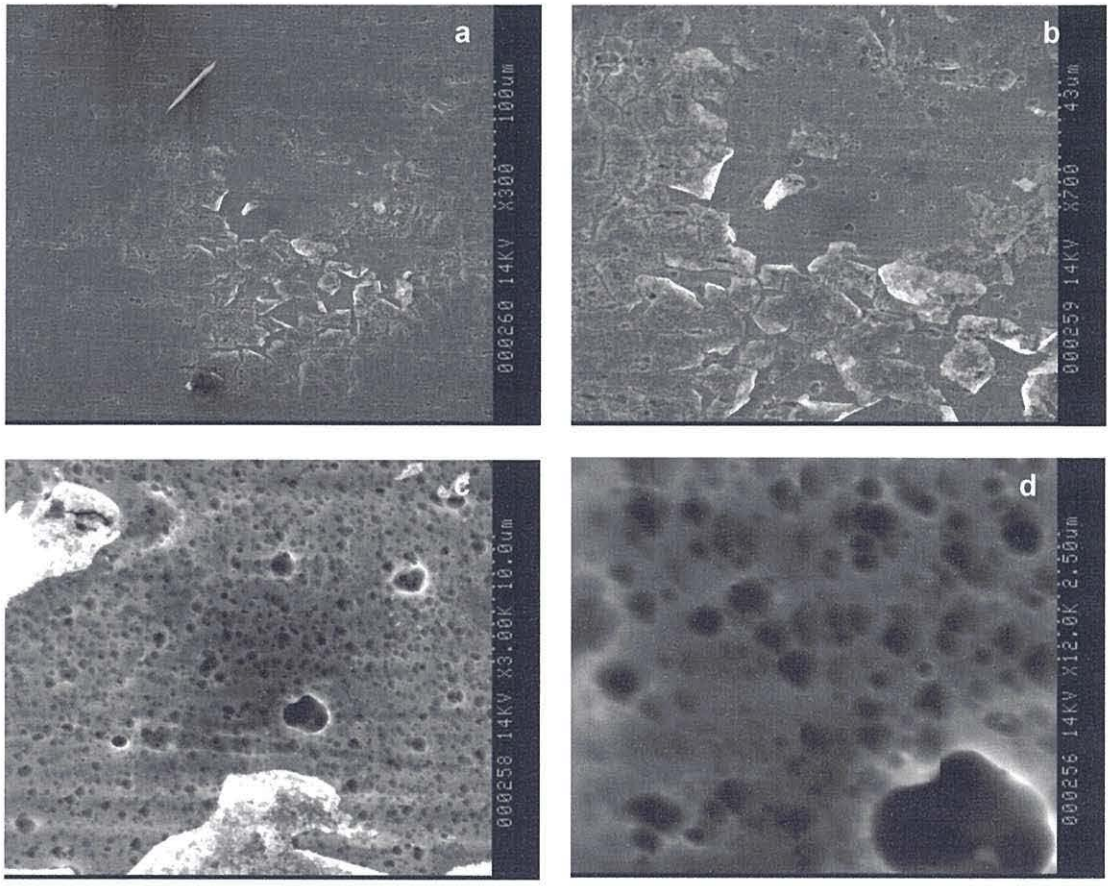

Figure 3.65 SEM images of areas of flaking and delamination for alloy 3105 coated with Pretreatment 10 for 6 minutes

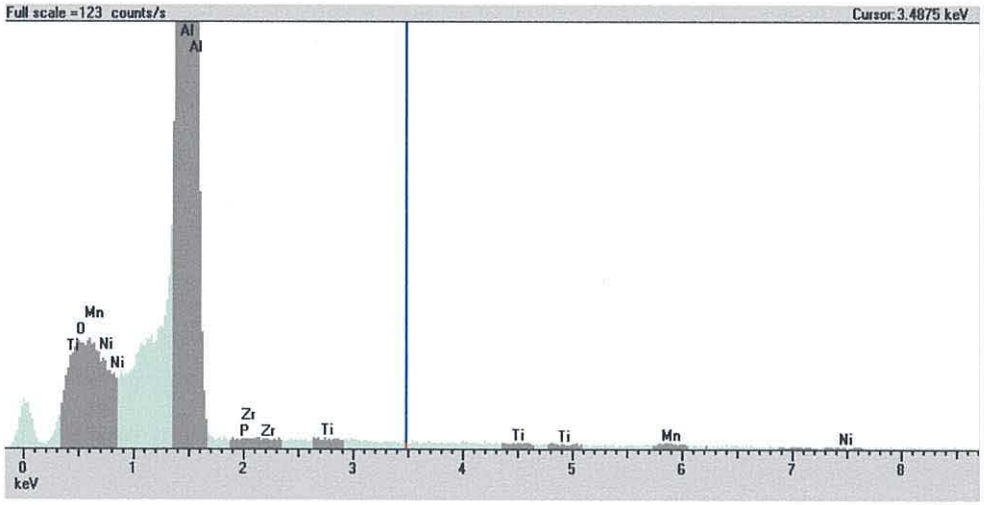

Figure 3.66 EDX analysis of alloy 3105 coated with Pretreatment 10 for 6 minutes. Field of vision shown in Figure 3.65d

SEM data have also been analysed for Pretreatment 10 on alloy 6063. In this case, the data show a distinctive patterned coating with the grain boundaries clearly visible across the surface. However no difference in morphology can be found between the darker and lighter areas by SEM, Figure 3.67 as for alloy 3105. In addition, for the 6063 alloy, a number of particles are visible on the surface at low magnification, Figure 3.67c,d, and these have been identified by EDX, Figure 3.68, to be intermetallic particles containing iron. Interestingly, at high magnification, a clear difference in morphology to that of the etched surface is noted. Scalloping is evident in some areas, with tiny spherical particles visible, Figure 3.69a-d. The dots are extremely small and are at the limit of the resolution of these images. Thus it is difficult to accurately measure them; however they appear to be of the order of tens of nanometers in diameter.

In general, it can be seen that the coating afforded by Pretreatment 10 does not provide a uniform coverage over the surface of the substrate. This is believed to be due to the absence of polymers in the bath solution and further illustrates the importance of these components in helping the coating to adhere both to the aluminium surface but also within the coating itself. The addition of the nickel sulphate was successful in applying a sheen to the metal substrate enabling the identification of coated from uncoated samples.

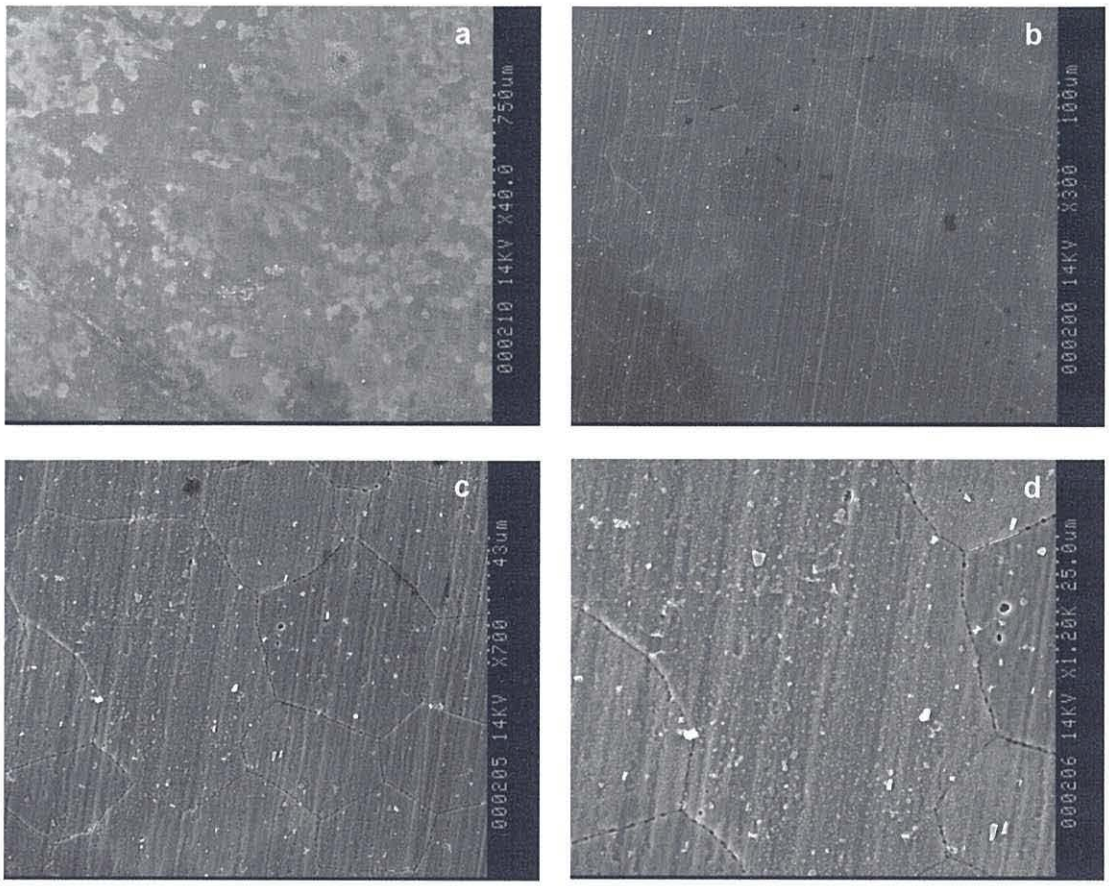

Figure 3.67 SEM images of alloy 6063 coated with Pretreatment P for 6 minutes. I identifies one of the intermetallics observed on the surface, analysed in Figure 3.68. Further images are shown in Figure 3.69

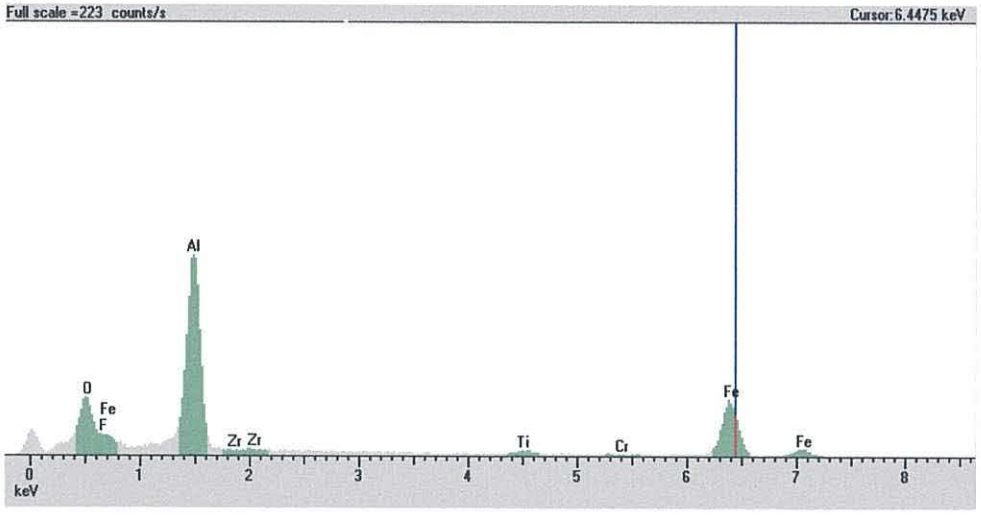

Figure 3.68 EDX analysis of the particle identified in Figure 3.67d on alloy 6063 coated with Pretreatment 10 for 6 minutes

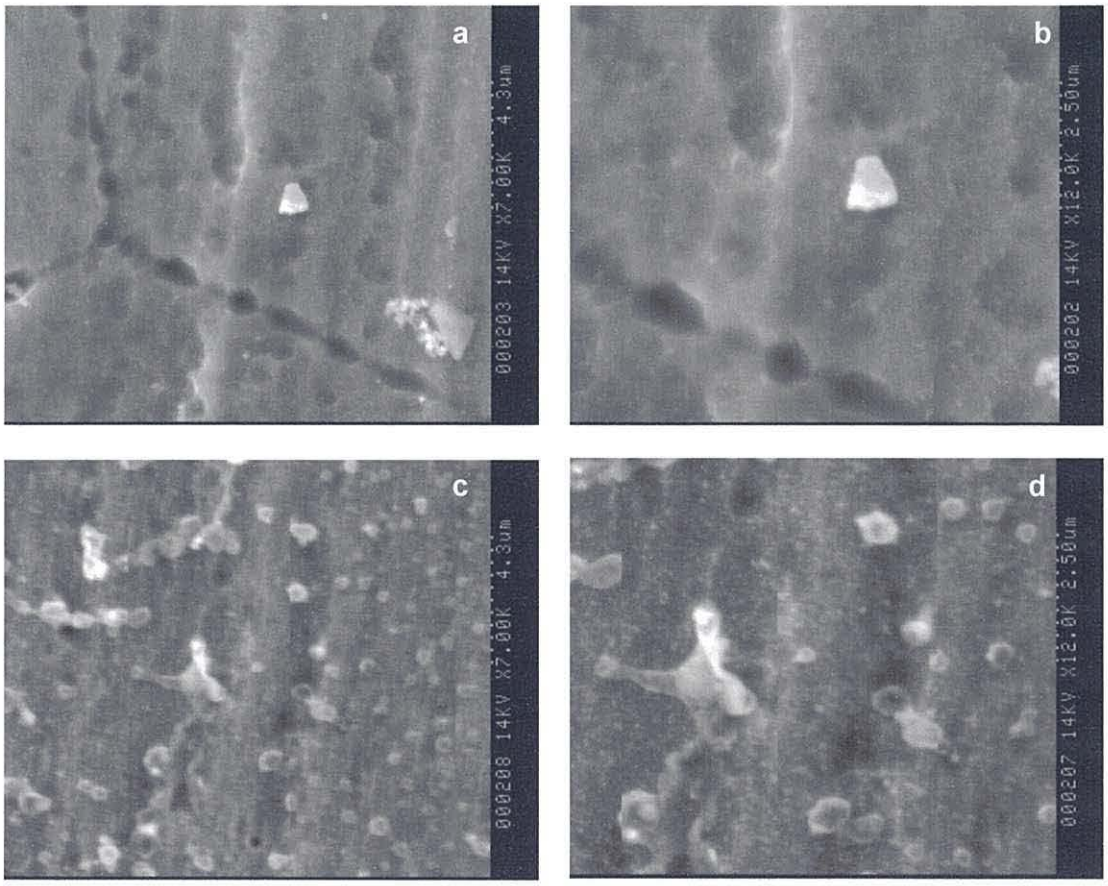

Figure 3.69 SEM images of alloy 6063 coated with Pretreatment 10 for 6 minutes. Further images are shown in Figure 3.67

Chromate Coating

A chromate pretreatment coating has been studied by SEM to compare with the data for the non-chrome treatments described in this chapter. Effectively, it can be considered as a control sample because it is known to reach the Qualicoat lifetime standard.

The chromate coating on alloy 3105 has been analysed after exposure to Almetron's commercial chrome phosphate system following a 6 min etch in AC133 (the latter described in Chapter 2). The 2 pack system; Kromal GA and Kromal GB, contains chromic acid, phosphoric acid and ammonium hydrogen fluoride solution. At low magnification, the coating appears uniform, Figure 3.71a. However closer magnification reveals that the coating is not uniform but that the morphology resembles a cracked mirror, Figure 3.71. This type of morphology has been described in literature as a morphology resembling the cracking of mud on the micrometer level.[13] A number of defects and deposits are evident. At very high resolution, tiny spherical particles are evident within the coating, Figure 3.71. EDX analysis of the coating indicates chromium, aluminium, and phosphorous, Figure 3.70, as does analysis of the deposits, Figure 3.72.

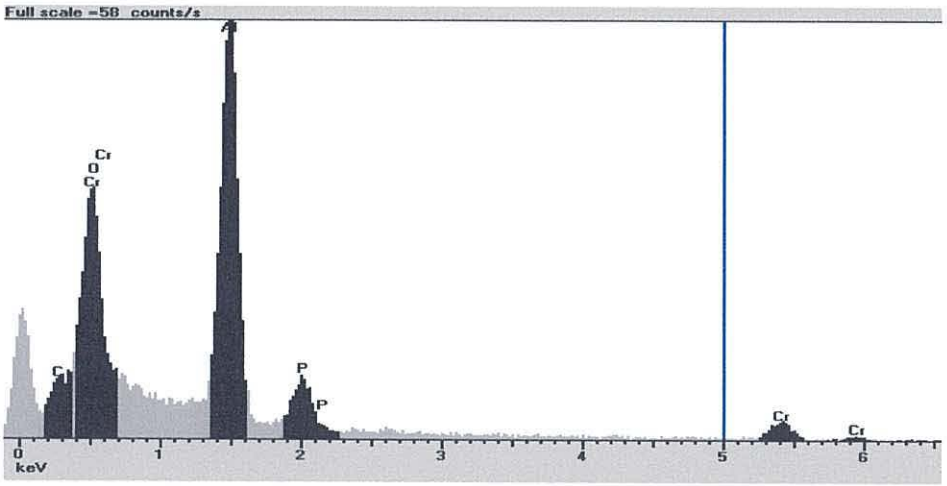

Figure 3.70 EDX analysis of alloy 3105 coated with chromate (chrome phosphate) for 3 minutes

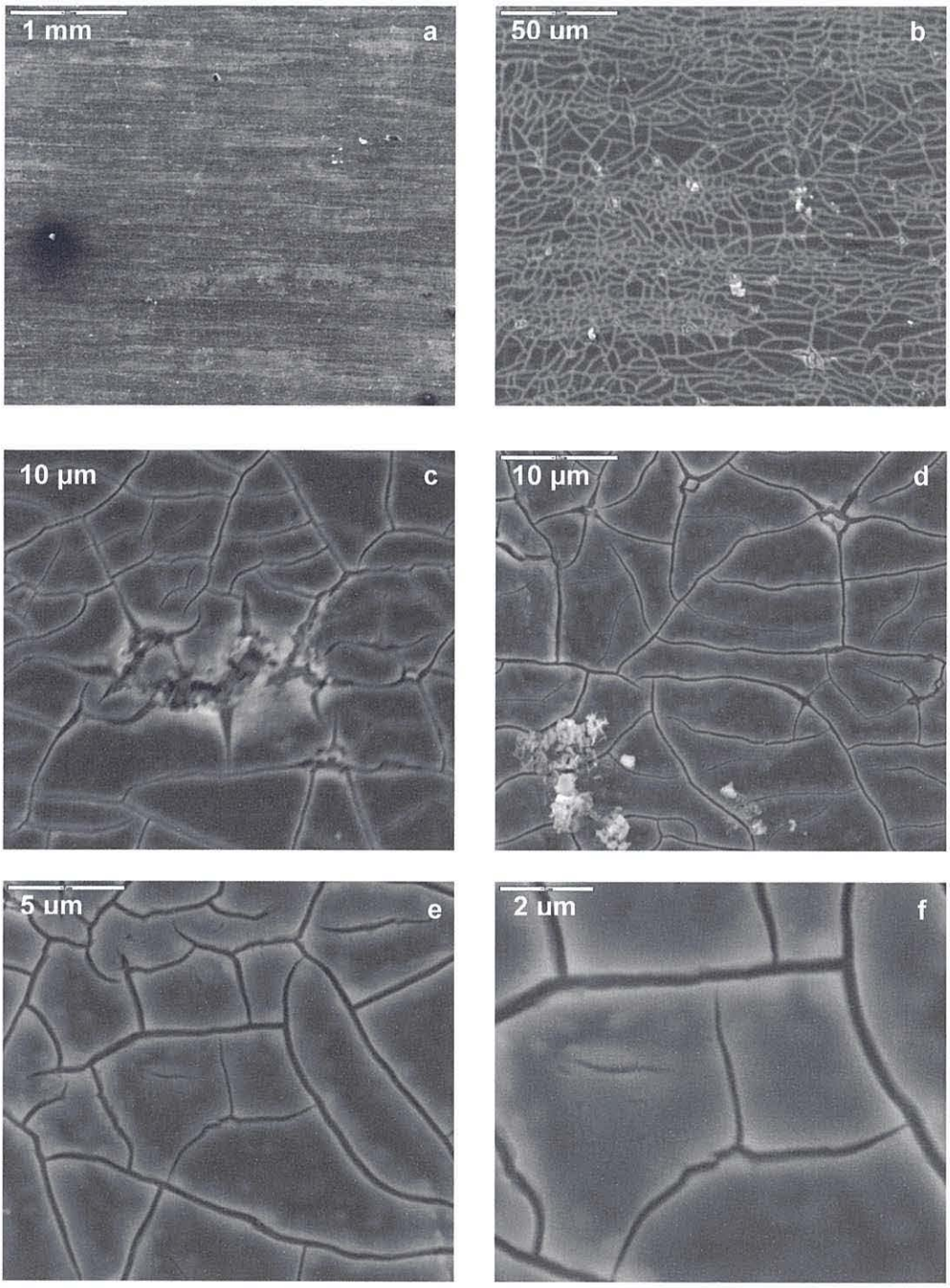

Figure 3.71 SEM images of alloy 3105 coated with chromate (chrome phosphate) for 3 minutes

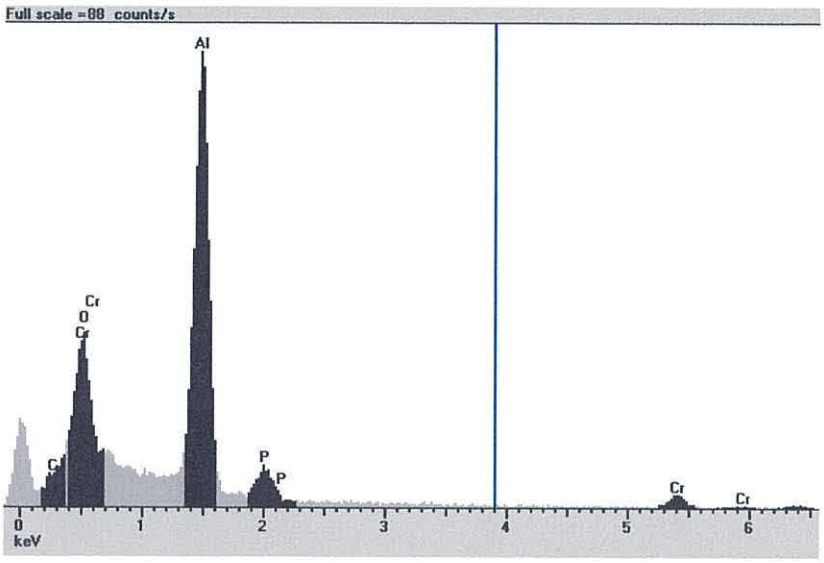

Figure 3.72 EDX analysis of deposits on alloy 3105 coated with chromate (chrome phosphate) for 3 minutes, deposit shown in Figure 3.71d

SEM analysis of the chromate coating was also examined after 6 min exposure on alloy 6063. At low magnification, the coating appears fairly uniform, Figure 3.73a. At higher magnification, again the cracked morphology is observed. However, cracking along the grain boundary is also evident for this alloy, Figure 3.73b,c,d. The extrusion die lines can also be made out in, Figure 3.73c,d,e, as well as the spherical particles evident in the coating on alloy 3105, Figure 3.73d,e,f. EDX analysis of the matrix, as expected, shows chromium, aluminium, and phosphorous and also manganese, Figure 3.74. At higher resolution, traces of iron are also observed, Figure 3.75, which is not unexpected, as intermetallic particles have been identified on this alloy type previously and discussed in Chapter 2. One of these particles, rod shaped, is identified by I on Figure 3.73f.

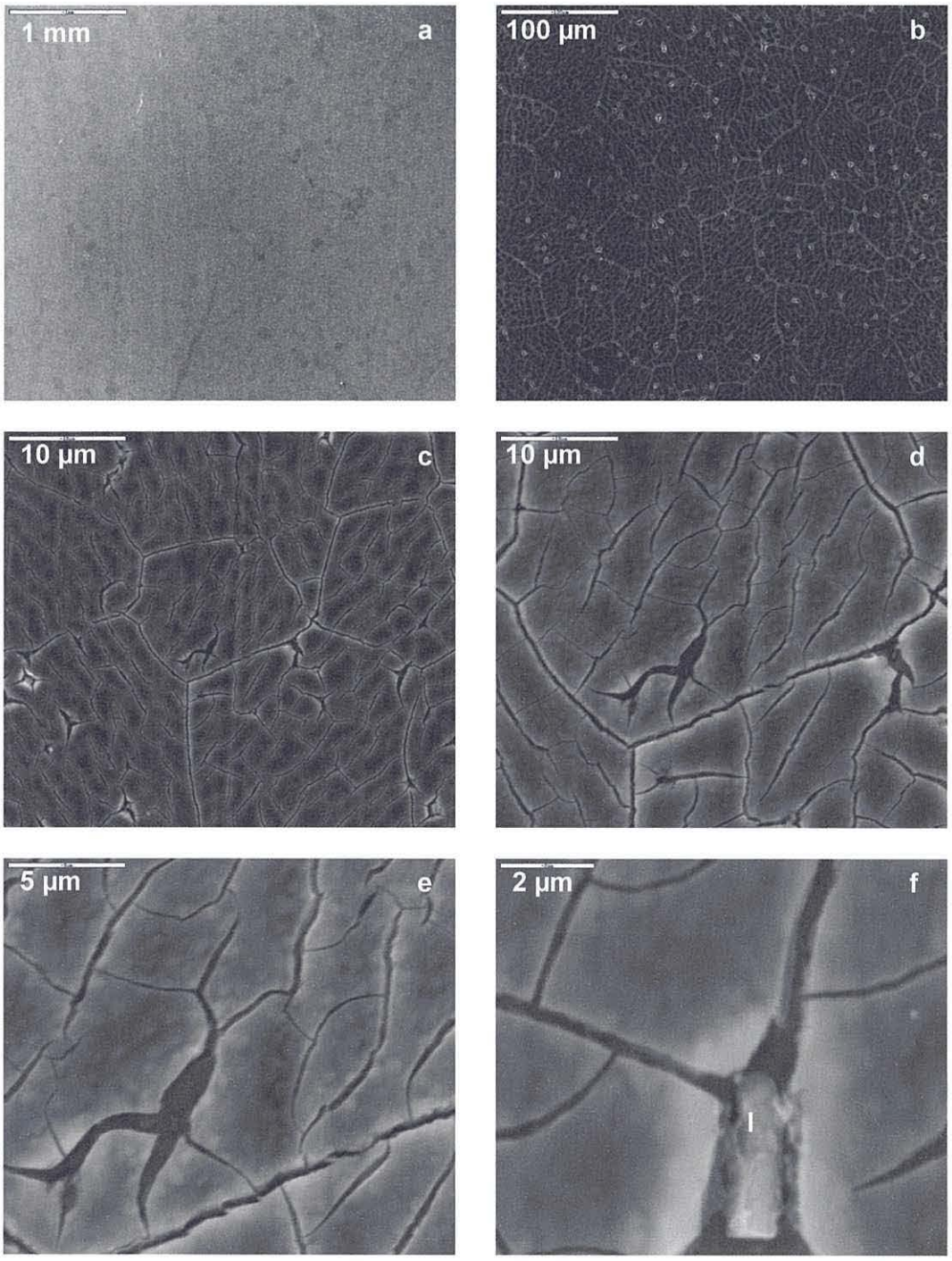

Figure 3.73 SEM images of alloy 6063 coated with chromate (chrome phosphate) for 6 minutes. I identifies an intermetallic particle

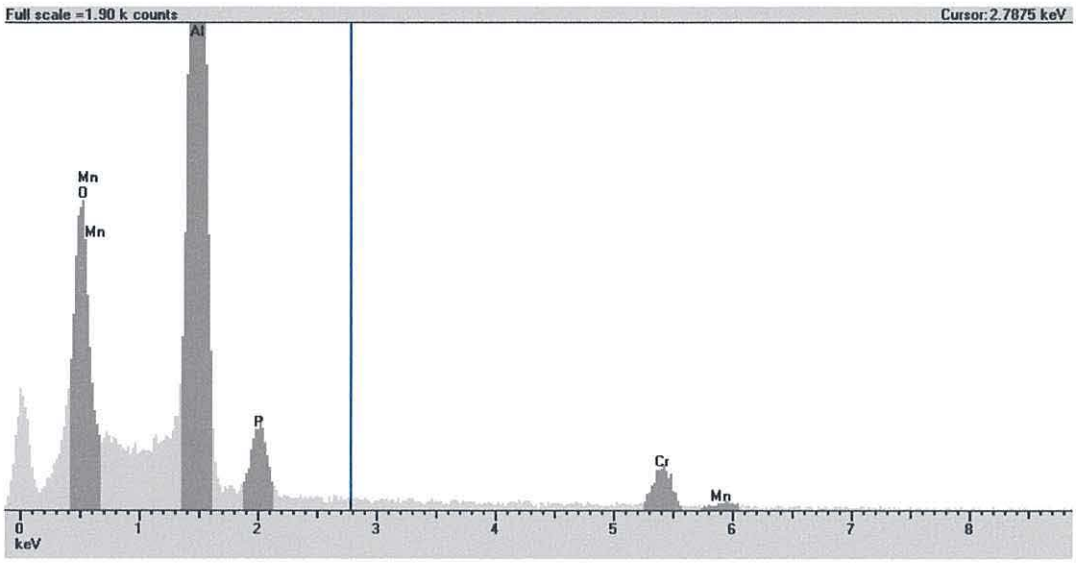

Figure 3.74 EDX analysis of alloy 6063 coated with chromate (chrome phosphate) for 6 minutes

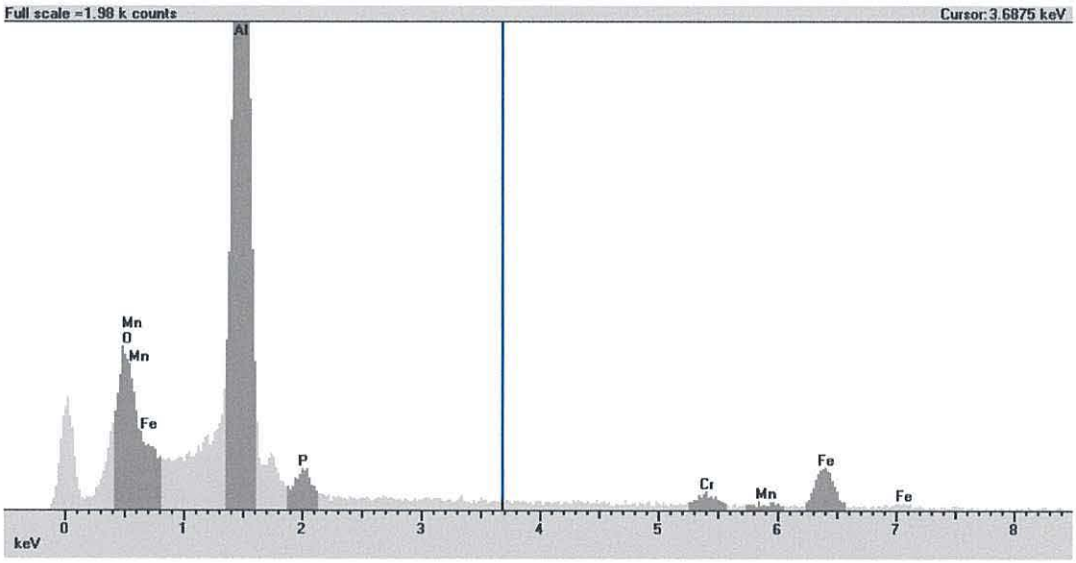

Figure 3.75 EDX analysis at high magnification of alloy 6063 coated with chromate (chrome phosphate) for 6 minutes

On comparing the chromate coating with the novel pretreatments discussed, it is immediately apparent that the chromate is a much more visible coating at the micrometer scale. The coatings observed for Pretreatments 1-6 do not resemble the chromate coating morphology. Upon examination of Pretreatment 7, however, the cracked morphology begins to appear, particularly on alloy 6063, and similar detachment to that following Pretreatment 7 has also been observed on a sample coated

with the chromate for 3 min, Figure 3.76. This cracked morphology is also visible on analysing Pretreatment 8.

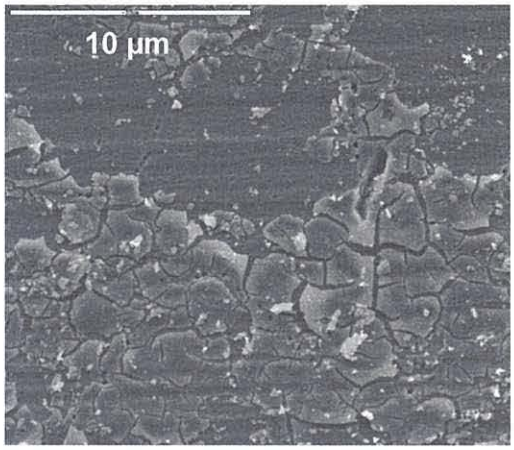

Figure 3.76 SEM image of alloy 6063 coated with chromate (chrome phosphate) for 3 minutes

Although showing a uniform coating, Pretreatment 9 also resembles the chromate coating at the micro level, in that it also exhibits tiny spherical particles within the coating. Pretreatment 10 has also been observed to have similar morphology at high resolution.

Conclusions

This chapter has described detailed microscopic investigations of a series of chrome-free pre-treatment solutions for the aluminium alloys 3105 and 6063. The solutions have been based around fluorozirconic and/or fluorotitanic acid which are believed to act in two ways during pre-treatment, by acting both as an etchant and also producing a deposit.

The data show that control over the etching power of the solutions is possible by varying the concentrations of fluoride. Additional problems have been observed with

uneven coverage and delamination of the coatings either from the aluminium substrate and/or from powder coated paint applied after the coating. Finally, there is evidence that, if the coating becomes too thick, it can crack and that this also appears to cause delamination. To combat these problems, the addition of polymers has been investigated. The first polymer (polyacrylic acid - PAA) appears to act as a flocculating and binding agent helping to produce more even coverage and to reduce delamination. However, the data show that it is possible to add too much of this material saturating the system which then interferes with the etching processes. The addition of a second polymer (PVA) seems to add an additional benefit presumably by complementing the PAA rather than working against it. In summary, there is clear evidence of the promise of some of these systems as a chrome-free corrosion protection technology for aluminium alloys.

References

(1) Luan, B.; Le, T.; Nagata, J. *Surface and Coatings Technology* **2004**, *186*, 431-443.

(2) Lunder, O.; Olsen, B.; Nisancioglu, K. *International Journal of Adhesion and Adhesives* **2002**, *22*, 143-150.

(3) Lunder, O.; Lapique, F.; Johnsen, B.; Nisancioglu, K. *International Journal of Adhesion and Adhesives* **2004**, *24*, 107-117.

(4) Critchlow, G. W.; Yendall, K. A.; Bahrani, D.; Quinn, A.; Andrews, F. *International Journal of Adhesion and Adhesives* **2006**, *26*, 419-453.

(5) Lunder, O., et al *Aluminium Surface Science and Technology proceedings* **1997**, 412-419.

(6) Ambat, R.; Davenport, A. J.; Scamans, G. M.; Afseth, A. *Corrosion Science, In Press, Corrected Proof.*

(7) Andreatta, F. *Aluminium Surface Science and Technology proceedings* **2005**, 168-172.

(8) Afseth, A.; Nordlien, J. H.; Scamans, G. M.; Nisancioglu, K. *Corrosion Science* **2001**, *43*, 2359-2377.

(9) Zhou, X.; Thompson, G. E.; Scamans, G. M. *Corrosion Science* **2003**, *45*, 1767-1777.

(10) Holliman, P. J., Clark, J.A., Williamson, J., Rowe, E. Jones, D.L., *Science of the Total Environment* **2005**, *336*, 12-24.

(11) Fan, A.; Turro, N. J.; Somasundaran, P. *Colloids and Surfaces A: Physicochemical and Engineering Aspects* **2000**, *162*, 141-148.

(12) Das, K. K.; Somasundaran, P. *Colloids and Surfaces A: Physicochemical and Engineering Aspects* **2003**, *223*, 17-25.

(13) Brown, G. M.; Shimizu, K.; Kobayashi, K.; Thompson, G. E.; Wood, G. C. *Corrosion Science* **1993**, *34*, 1045-1054.

4. Physical Testing

This chapter describes corrosion testing of the chrome-free pretreatments described in Chapter 3. These experiments have been carried out using industry-standard accelerated corrosion tests and the data have been compared between pretreatments and also correlated with the characterisation data to try to develop an understanding of how the different prereatments behave.

Thus, following application of the pretreatments as described in Chapter 3, physical testing was carried out to assess the corrosion protection offered by each treatment. Following application of the coating, three sets of samples were produced. The first were analysed by SEM and EDX, as described in Chapter 3. The second and third have been further treated by a subsequent process of one of two types of powder coating. Thus, the second group were powder coated with a clear lacquer and sent for independent Lockheed humidity testing by Innoval Technology Ltd. This group of samples were then used for TEM analysis as described in Chapter 3. The third group of pretreated panels were powder coated either with a beige polyester powder or the clear lacquer, and were then subjected to a series physical and accelerated corrosion tests. The data from this group of samples is described in this chapter.

As described in Chapter 3, the Lockheed humidity test is an accelerated corrosion test lasting 1000 h. This involves scribing the panels to expose the underlying pretreatment layer. The panels are scribed both parallel and perpendicular to the rolling/extrusion direction, before being inoculated with HCl and placed in a cabinet at 85 % relative humidity. The samples are removed and visually examined and scanned/photographed at intervals of 24, 250, 500 h and at 1000 h at the end of the test. To add context,

examination of the panels after 24 h is considered a good indication of an effective cleaning process. Thus, the absence of filiform corrosion at this stage is considered to suggest removal or deactivation of the surface active layer responsible for fast filiform corrosion.[1]

The industry approved Qualicoat test specifies that a cumulative infiltration of corrosion of a maximum 16 mm^2 is allowed over a scratch length of 10 cm, but the length of any single infiltration must not exceed 4 mm in order for a particular pretreatment to pass the test. In this thesis, the test panels have been examined and the greatest filament length noted. The results of this analysis are listed in Table 4.1.

The coatings show improvement in corrosion performance across the series of Pretreatments 1 to 5, as fluorozirconic acid and fluorotitanic acid were combined together, Figure 4.1, Figure 4.2. When polymer is added to the coating solution, the resulting samples outperform the reference chromate sample in this test (shown on Figure 4.3 Scanned images of sheet alloy 3105, pretreatment type noted, following 1000 h Lockheed testing. The pretreatment type is labelled on the relevant panelFigure 4.3, Figure 4.4). This is in good agreement with the observations made in Chapter 3, in which the data showed improvement in surface coverage and adhesion when polymer is added. In earlier discussions, this effect has been attributed to a presumed flocculating effect of the polyionic polymer helping the coating to adhere both within the coating layer and also to the surrounding substrates. These data support these assertions.

In addition, it is particularly notable that not only have the length of the filaments decreased in samples with Pretreatments 4 and 5, but the number of filaments has

[1] Communication with Geoff Scamans, Innoval Technologies

decreased significantly as well. This suggests that these coatings are particularly effective in preventing the initiation of corrosion as well as inhibiting its progress once started.

Pre treatment	Alloy			
	6063		3105	
	Lockheed	Acetic acid salt spray	Lockheed	Acetic acid salt spray
1	< 5	4 a	< 4	> 4 c
2	< 5	8 c, f	< 3	> 3 c, f
3	< 3	< 2	< 3	4 c, f
4	< 2	-	< 2	> 4
5	< 2	-	< 2	> 4
6	< 1	0	< 3	> 5 f
7	< 3	0	< 2	0
8	< 3	0	3x1	> 5 b,f
9	< 1	0	1x1	0
10	< 1	0	> 1	0
chromate	< 2	0	1x1	1 x 2

Table 4.1 Results of Lockheed and acetic acid salt spray testing. The length of the longest filament, or filaments, (mm) are noted. The table also includes data regarding visual inspection of corrosion events and these are listed using the following key:- a - loss of adhesion, b – blistering, c – corrosion, d – detachment, f – filiform, 3 x 1 – 3 filaments of 1 mm

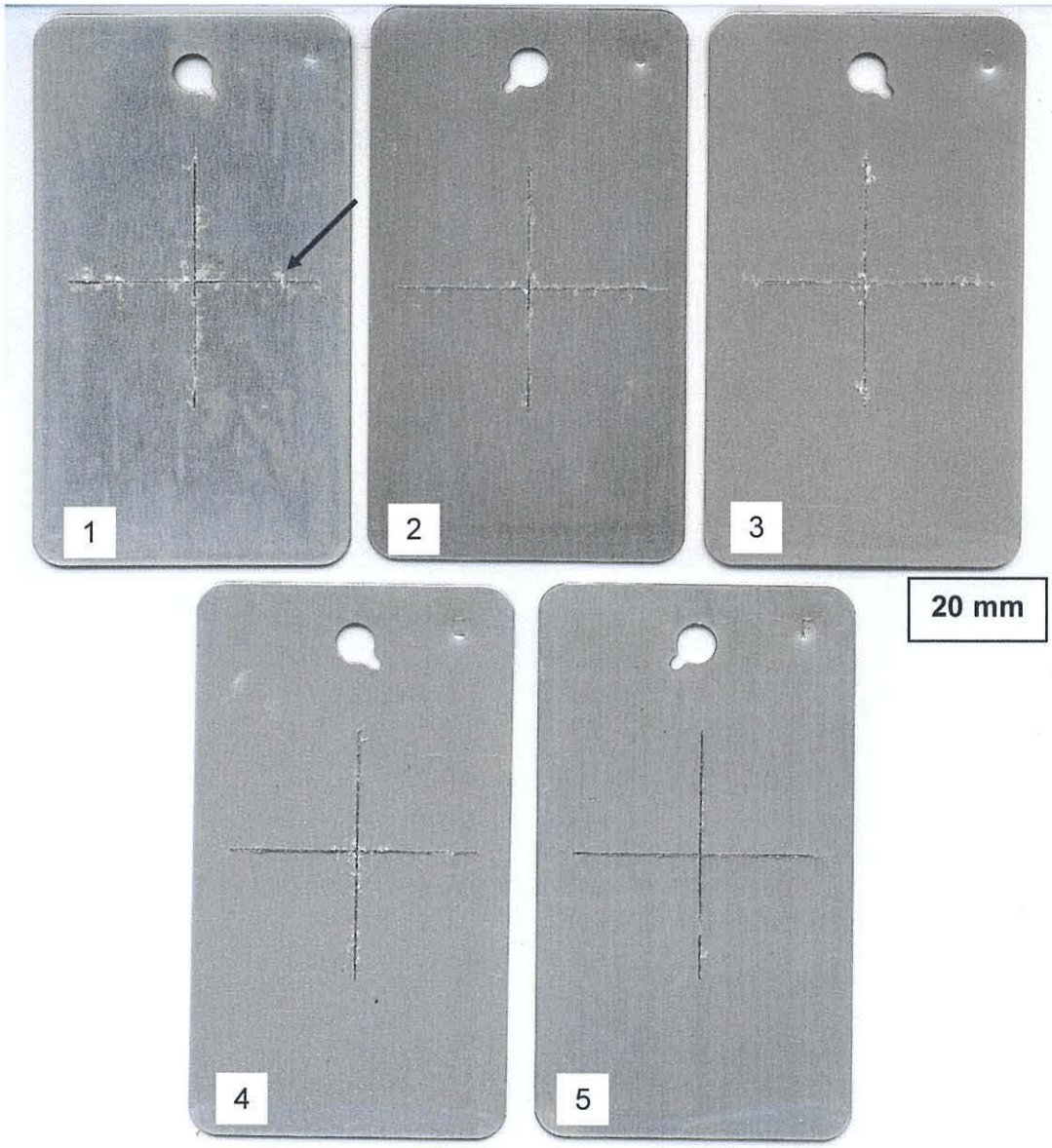

Figure 4.1 Scanned photographic images of sheet alloy 3105 showing the scoring marks in cross-wire arrangement. The filiform corrosion can be seen growing away from this. An example of filamentous corrosion is labelled with an arrow on Pretreatment 1 for clarity. The pretreatment type is labelled on the relevant panel. The data shown are following 1000 h Lockheed testing and clearly show a reduction in the number and length of filaments through the series Pretreatments 1 to 5

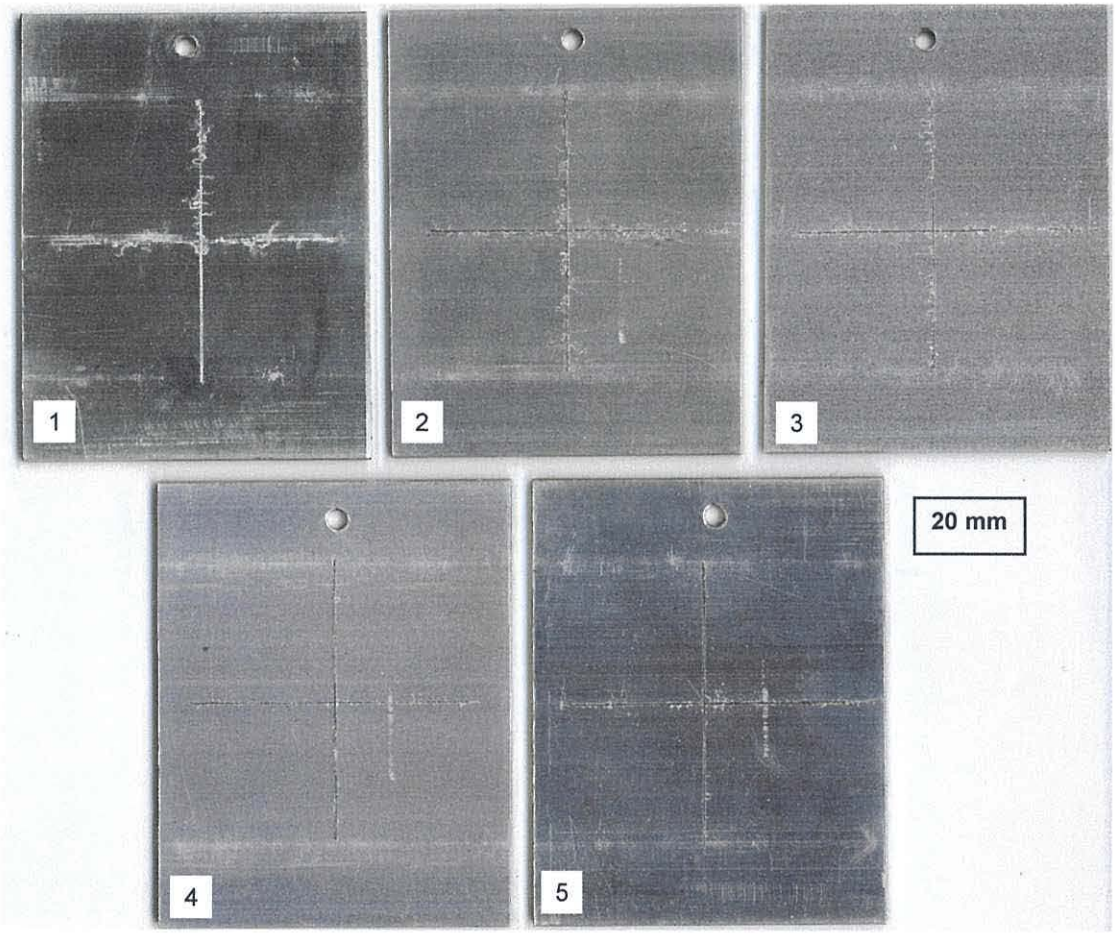

Figure 4.2 Scanned images of extruded alloy 6063, pretreatment type noted, following 1000 h Lockheed testing. The pretreatment type is labelled on the relevant panel

Pretreatment 6 also shows good performance. Indeed, very few filaments are observed on analysis of either of the alloys (3105 or 6063) following Pretreatments 6-10, Figure 4.3, Figure 4.4. However, Pretreatments 7 and 8 do show a slight decrease in corrosion performance, in that the length of the filaments has increased. This poorer performance for these two treatments types was also noted in the SEM analysis which indicated poor surface coverage along with some detachment of the pretreatment layer. Thus, the electron microscopy and corrosion testing data correlate very well for these samples.

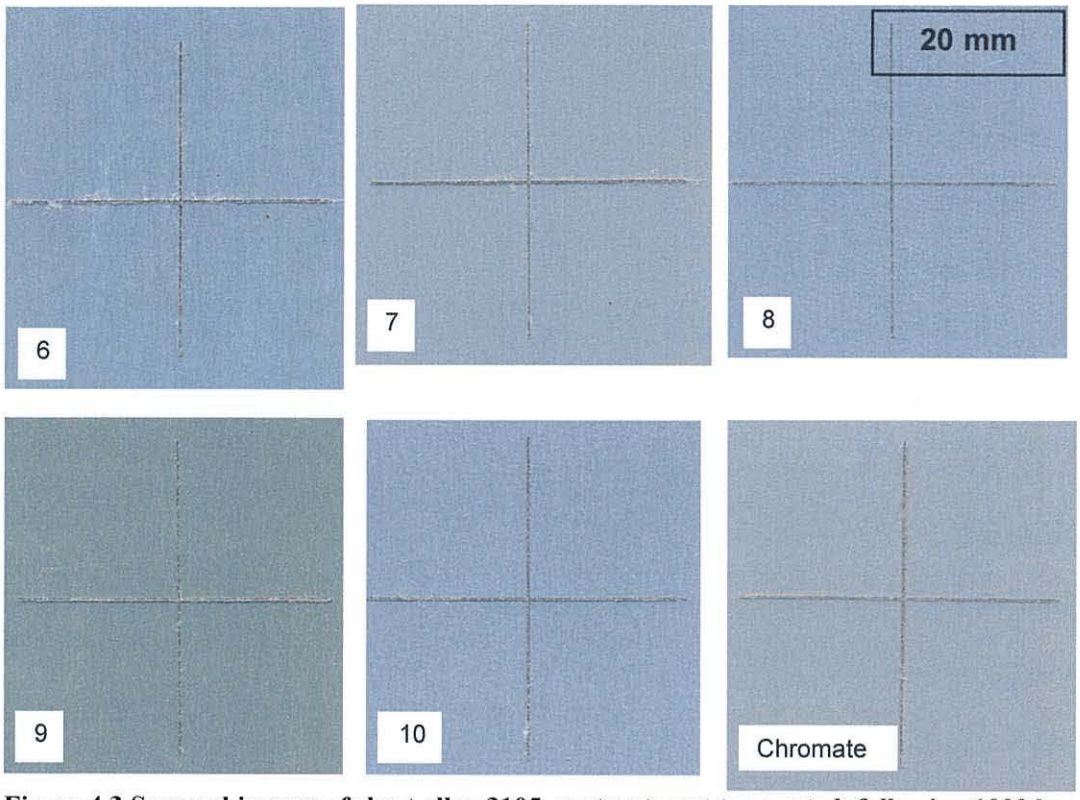

Figure 4.3 Scanned images of sheet alloy 3105, pretreatment type noted, following 1000 h Lockheed testing. The pretreatment type is labelled on the relevant panel

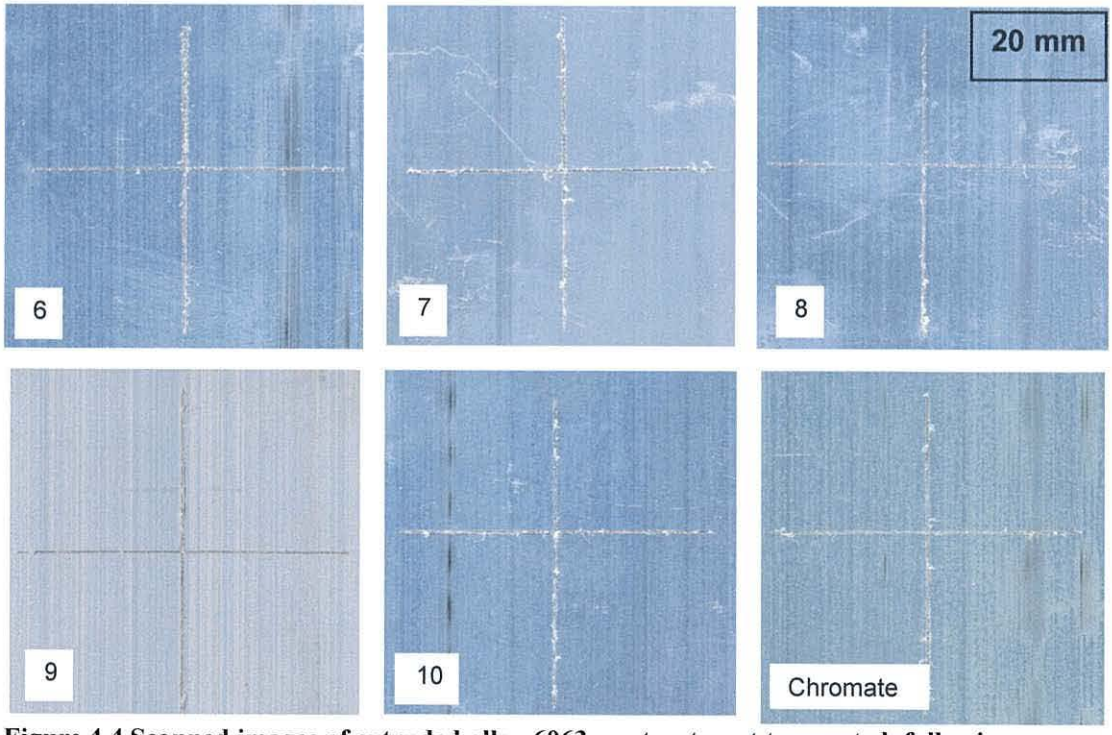

Figure 4.4 Scanned images of extruded alloy 6063, pretreatment type noted, following 1000 h Lockheed testing. The pretreatment type is labelled on the relevant panel

The best corrosion performance is observed for Pretreatments 9 and 10 and these samples show further improvements in a reduction in the number and length of filaments observed when compared to the previously best perfoming samples (Pretreaments 4, 5 and 6). This is again in line with the analysis of the pretreatment by SEM, which showed improved surface coverage compared to all other pretreatments examined in this thesis.

Acetic acid salt spray testing

The acetic acid salt spray test has been carried out at the Almetron Ltd laboratories, Wrecsam, for 1000 h according to Qualicoat specification. Two cross-cut incisions of width 1 mm have been cut into the powder coating diagonally across the sample in an X-shape, using a specific scratching tool, to expose the underlying pretreated metal. The panels have then been placed upright in a humidity chamber and exposed to mists of acetic acid and sodium chloride for 1000 h. Following this time period, the panels have been inspected for blistering, detachment and filaments of corrosion (filiform corrosion) in line with standard procedures, Table 4.1.

Pretreatments 1 to 5 did not perform well, showing both corrosion of the score site and filiform corrosion, Figure 4.5. The powder coating used in this test was the clear lacquer. Upon using the polyester powder coating for Pretreatments 6-10, a clear improvement is seen, with no corrosion, filiform, or detachment observed on alloy 6063, Figure 4.6. However, on alloy 3105, filiform corrosion and blistering is observed for samples with Pretreatment 8, and significant detachment on samples with Pretreatment 6, Figure 4.7. Pretreatments 7, 9 and 10 all performed better than the chromate control samples. Further testing of the pretreatments with different powder

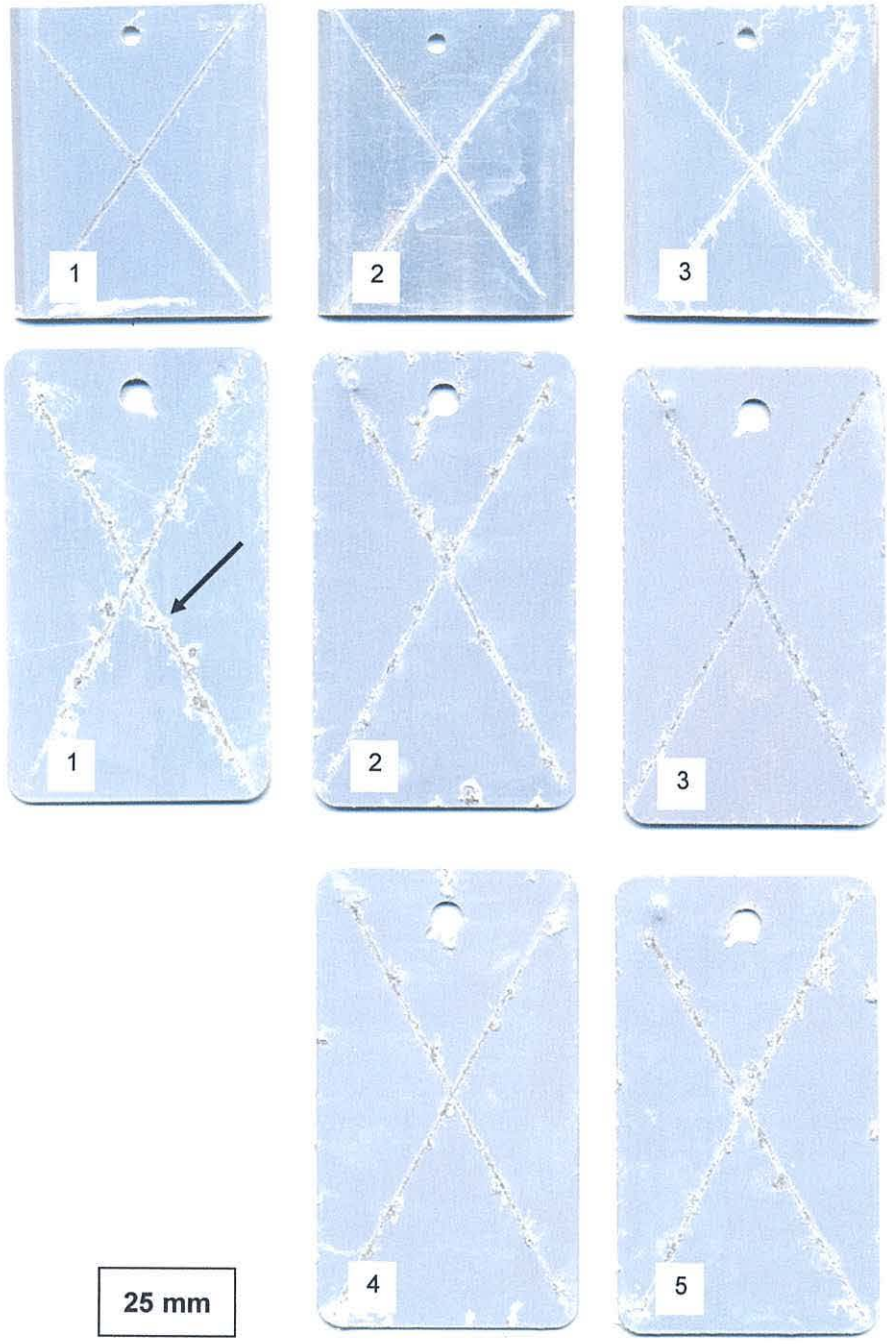

Figure 4.5 Scanned images of extruded alloy 6063 – top row, and sheet alloy 3105, pretreatment type noted, following 1000 h acetic acid salt spray testing. The images clearly show the scoring marks in an X-shape arrangement. Filiform corrosion can be seen growing away from this. An example of filamentous corrosion is labelled with an arrow on Pretreatment 1 for clarity. The scale bar is shown on the figure and the pretreatment type is labelled on the relevant panel

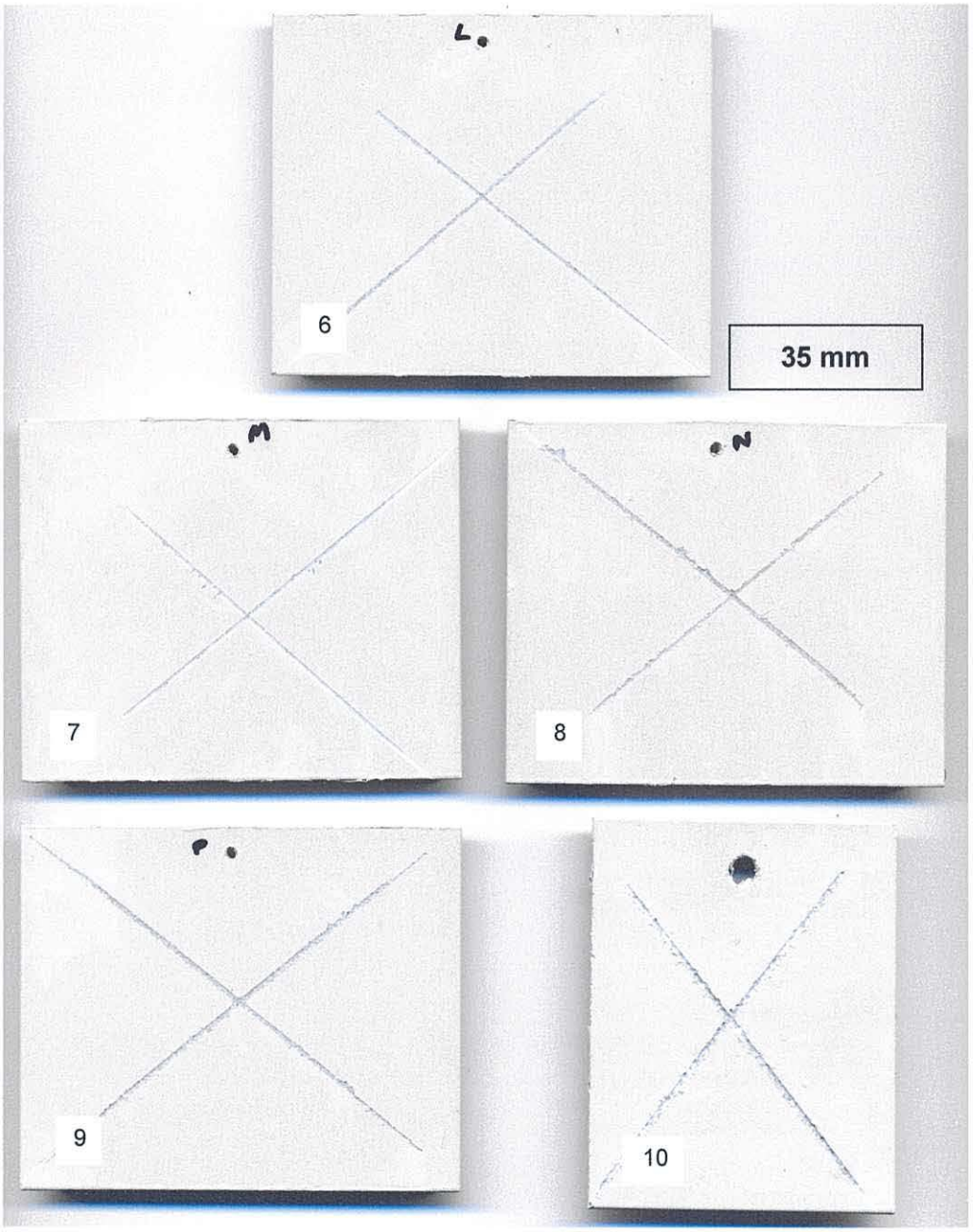

Figure 4.6 Scanned images of sheet alloy 3105 with pretreatment type labelled on the relevant panels. The date are shown following 1000 h acetic acid salt spray testing. The images clearly show the scoring marks in an X-shape arrangement. There is no filiform corrosion seen growing away from this. The scale bar is shown on the figure and the pretreatment type is labelled on the relevant panel

coatings would allow for greater reliance on the data, as the improvement noted in Pretreatments 6-10 could partially due to the powder coating used. Nonetheless, the data do show encouraging corrosion performance for the chrome-free coatings developed.

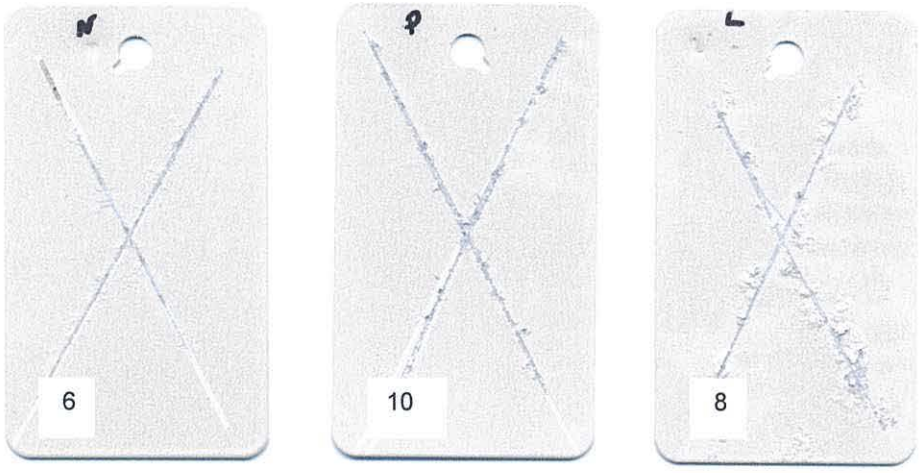

Figure 4.7 Scanned images of sheet alloy 3105, pretreatment type noted, following 1000 h acetic acid salt spray testing, showing filiform corrosion on Pretreatment 6, good performance from Pretreatment 10 and severe corrosion and detachment from Pretreatment 8

Physical Testing

Adhesion testing has been carried out according to Qualicoat specification, at the Kawneer Laboratories, Runcorn. These tests primarily indicate the adhesion of powder coating, rather than the corrosion protection offered by the pretreatment. However, if the adhesion is of a good standard, the pretreatment is less likely to be exposed to corrosion and thus more likely to last the 25 years required by industry standards. In addition, the cosmetic appearance of the aluminium is also very important, and the adhesion tests are indicators of the life of the appealing cosmetic appearance.

The tests include sawing and drilling and the cross hatching the panels, and these are carried out in order to observe detachment of the powder coating upon incision. The bend test is performed using a conical mandrel bend tester, which bends the panel placing strain at the apex of the bend, Figure 4.8. It is carried out to test the panels for coating cracking or detachment following deformation. An impact test is carried out to identify how the coating performs under a rapid deformation process, which involves dropping a hemispherical weight from a height to indent the metal sheet, Figure 4.9. The bend test and impact test have not been carried out on extrusion alloy 6063, as the thick nature of the extrusions is unsuitable for these tests.

It should be noted here that all the pretreatments passed all the physical tests, showing no loss of adhesion or detachment, with only one exception of Pretreatment 6, which has failed in adhesion following the impact test. For this pretreatment, the powder coating at the area of the impact has detached almost completely from the metal panel, Figure 4.9. This result makes Pretreatment 6 a fail, and would not be suitable for commercial use.

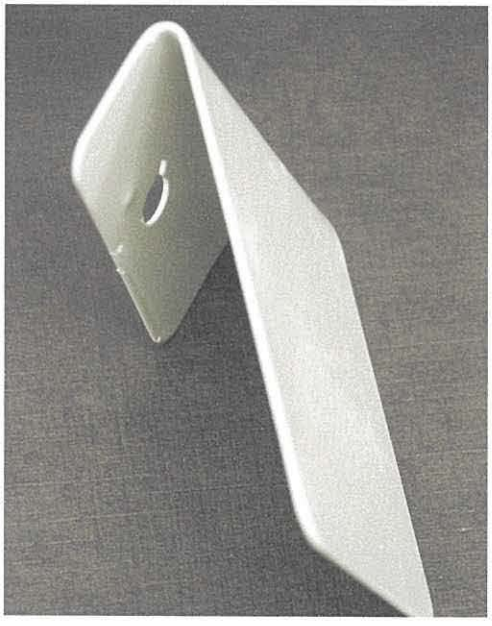

Figure 4.8 Image of alloy 3105 Q panel having undergone a bend test

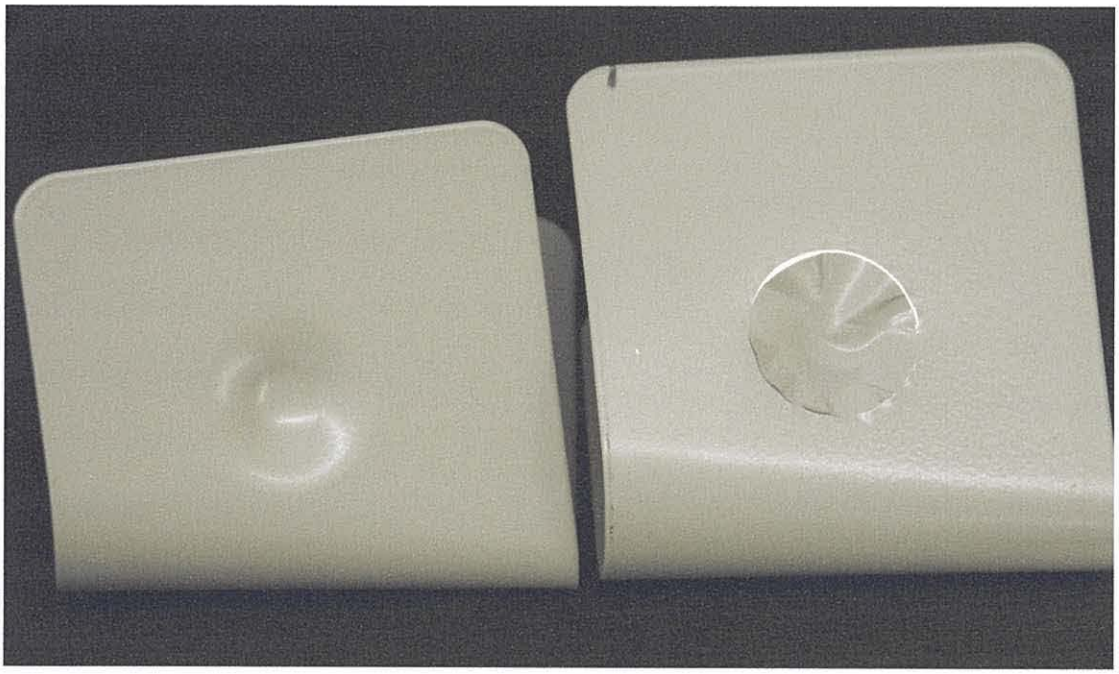

Figure 4.9 Images of alloy 3105 Q panel having undergone the impact test. The panel on the right has been coated with Pretreatment 6, and shows detachment at the indented area

In conclusion, from the Lockheed and acetic acid salt spray corrosion tests, Pretreatments 6, 9 and 10 stand out as excellent performers in terms of corrosion resistance. The results are in good agreement with the observations made in Chapter 3. However, the physical testing suggests that Pretreatment 6 does not show adequate adhesion, leaving Pretreatments 9 and 10 as the most likely potential corrosion pretreatments for commercial use. Unfortunately, due to lack of time, TEM analysis of Pretreatment 6 has not been possible at the time of producing this thesis. However, this would be very valuable data in the context of the physical data results and would be expected to show detachment. Such cross sectional analysis would indicate the reason for the insufficient adhesion, i.e. weakness at the pretreatment – substrate interface, or powder coating – pretreatment interface.

5. Electrochemistry

It has been reported that aluminium corrosion proceeds by local electrochemical cells comprising of anodic and cathodic reactions occurring simultaneously at the metal surface.[1] These reactions are generally the accepted mechanism of aluminium corrosion. In addition, it is believed that the anodic dissolution of aluminium occurs in two ways, through the movement of aluminium ions through the surface oxide film, and indirectly through consecutive oxide film formation and dissolution.

In the context of corrosion prevention, the pretreatments applied to the aluminium surface are designed to act as a barrier to prevent corrosion. Thus, measuring the extent to which any surface barrier layer acts to prevent the transfer of electrons (e-), and hence prevent the movement of ions through the film can be a useful tool to assess the efficacy of corrosion protection. As stated above, it has been reported that the processes taking place at electrolyte-metal surfaces are often governed by localised electrochemical reactions.[2] It is also known that recording the response of the coated aluminium surfaces to an applied potential can be performed by cyclic voltammetry,[3] using a three electrode approach. Thus, this type of experimental approach allows for rapid measurements, and can be used to determine when, and to what extent, surface-localised processes such as oxidation and reduction occur. A disadvantage is that an "averaged" response is obtained which relates to the whole electrode surface being studied, but it remains a useful guide. In this chapter, cyclic voltametry (CV) will be used to assess selected pretreatments developed in Chapter 3.

The three electrode system is very widely used in electrochemical measurements.[4] In such a system, the electrode where the reactions of interest are investigated is termed

the working electrode. The second electrode is the counter electrode, and the third is the reference electrode, which is contained in a separate compartment. In a typical experiment, current flows between the working and the counter electrodes, with the potential of the working electrode held relative to the reference electrode. In this experimental design, the reference electrode is used to provide a stable and fixed potential so that when a voltage is applied, the drop in potential between the working electrode and the solution is precisely defined. It is this potential difference that is the driving force for the electrochemical processes to take place at the interface. In this system, the dependence of current relates to the chemical reaction occurring at the surface of the working electrode as follows:-

$$\mathbf{E = (\phi_m - \phi_s) + iR + (\phi_s - \phi_{REF})} \qquad \textbf{Equation 5.1}^3$$

where $(\phi_m - \phi_s)$ is the driving force, iR is the voltage drop, and $(\phi_s - \phi_{REF})$ refers to the potential drop at the reference electrode/solution interface (fixed by the chemical composition of the reference electrode).[3]

Cyclic and linear voltammetry are widely used techniques for electrochemical measurement.[4] The techniques depend on diffusion to transport material to the electrode surface. In a typical experiment, the potential of the working electrode is swept from one voltage (E_1) to a second voltage (E_2). These voltages are chosen as points above and below the active region of interest. In cyclic voltammetry, when the potential reaches E_2 the voltage sweep is reversed either back to E_1 or an alternate potential E_3; hence the cyclic nature of the voltage sweep lends the technique its name, Figure 5.1.

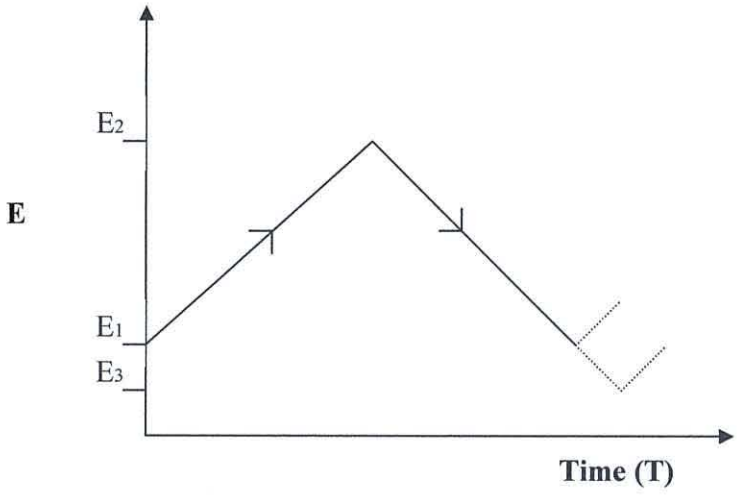

Figure 5.1 Potential-time profile of cyclic voltammetry

In a typical CV experiment, initially, no current passes because the applied potential is not sufficient to result in electron transfer. However, as the potential is swept to more oxidising potentials, electron transfer can be induced and, if it is, current is passed. For a general charge transfer reaction:

$$R_{(aq)} - ne_{(m)} \longleftrightarrow O_{(aq)} \qquad \textbf{Equation 5.2}^{3}$$

Nernst showed that the potential established under equilibrium conditions is given by

$$Ee = E^{\theta} + \frac{RT}{nF}\ln\frac{[O]}{[R]} \qquad \textbf{Equation 5.3}^{3}$$

where the equilibrium potential (E_e) of the electrode results from the standard electrode potential (E^{θ}) of the reaction and the concentrations of O, oxidation, and R, reduction, at the electrode surface, which, under equilibrium concentrations, are the same as their values in bulk solution. R is the universal gas constant ($J.K^{-1}.mol^{-1}$), T is the absolute temperature (K) and F is the Faraday constant ($C.mol^{-1}$).

Thus, the charge applied causes electron exchange which, in turn, alters the oxidation state of the relevant species present at the electrode surface. In the experiments presented in this Chapter, investigations have been carried out into the nature of the

corrosion pretreatment on the aluminium. In this case, the observed data show that oxidation processes are occurring showing loss of electrons from the coatings to the working electrode.

The overall aim of this Chapter is to carry out electrochemical studies of selected pretreatments which appear to exhibit a range of corrosion resistance by other exposure or physical testing methods. By analysing the data and examining the extent or ease of oxidation of a particular coating, it is hoped that it will be possible to develop insights into the corrosion resistance of different aluminium pretreatments.

Thus, the experiments described in this chapter have been designed using the knowledge developed in Chapter 3 and 4 where studies of solution-based corrosion testing have been described. Thus, as in the case of corrosion testing in solution, chromate coated and etched aluminium samples have been examined initially, to determine if the resistance offered by chromate is evident using these electrochemical techniques. In addition, in order to accelerate the corrosion process to bring the timescale of these experiments within practical limits, a sodium chloride solution acidified to pH 3.1-3.3 with acetic acid has been chosen as the test solution. It must also be noted that electrochemical techniques such as CV are highly dependant on the area of the working electrode. This can result in significant variation in data between repeat samples because, although the same experimental set up is used, it is impossible to reproduce exactly the same area of electrode surface to be exposed to solution. However, important trends can be identified between different samples when observed over several samples. In this Chapter, it is therefore theses trends that are investigated and discussed.

The first sample to be investigated is alloy 3105 which has been etched for 6 mins in AC133 solution, which has been discussed in Chapter 2. Thus, this sample is essentially aluminium alloy which has had the surface oxide and aluminium sub-surface layer removed and where a thin layer of surface aluminium oxide will have reformed in air following the etch. The measurements are all taken at a scan rate of 50 mV/s against a saturated Calomel electrode. The cyclic voltammograms (CV) for four repeat samples show oxidation occurring at less than -0.82 V with peak current readings ranging from 4.1×10^{-4} to 2.38×10^{-5} A, Figure 5.2. Following 24 h in the corrosive solution, the general trend observed is an increase in the height of the oxidation peaks, with the peak current readings increased by approximately one order of magnitude. The area of the peaks, which represent the charge at the surface, and hence the change to the surface – which could be associated with damage such as corrosion, also indicate an increase of the order of ten times, Figure 5.2. Oxidation is observed to occur at potentials less than 0.81 V. This implies that, after the alloy has been left in the corrosion solution, the oxidative corrosion processes measured by CV become more pronounced. This is entirely in line with what might be expected by removal of the surface aluminium layer which would otherwise be expected to reduce corrosion processes. Thus it would appear that the oxide barrier film, which was largely removed during etching, has diminished further in the acidic-chloride solution, offering less resistance to the transfer of electrons. This etched sample may be considered a baseline of high corrosion to be compared with later samples.

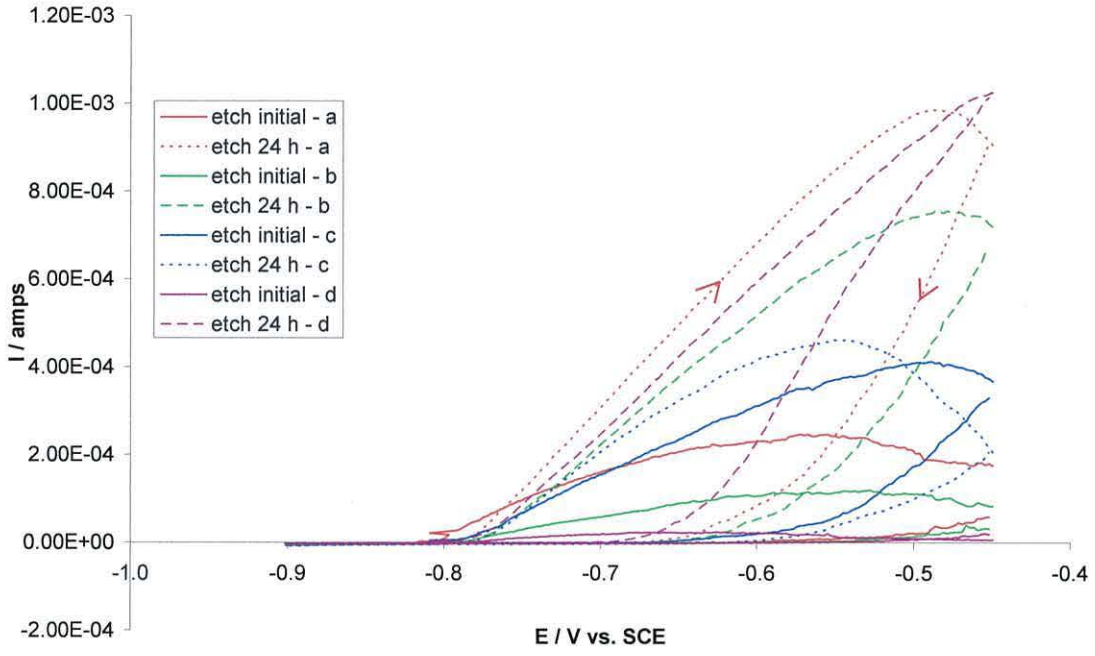

Figure 5.2 CV data for etched aluminium alloy 3105 initially and after 24 h in acidified sodium chloride with four replicate samples (a, b, c, d)

By comparison, the cyclic voltammograms for a chromate-coated surface of alloy 3105 show slightly smaller response peaks initially, with the peak current readings ranging from 1.76 x 10^{-4} to 4.49 x 10^{-5} A, Figure 5.3. However, following 24 h in the corrosive solution, the peak current readings ranged from 4.15 x 10^{-4} to 1.13 x 10^{-4} A, showing a slight increase compared to the initial data. An increase in the charge was noted, Figure 5.5.

As for the etched sample, the data for the chromate-coated sample show an increase in current after 24 h in the acidic-chloride solution, which implies that the surface of this substrate has been altered to become more susceptible to oxidative corrosion over time in the same way as the etched sample. However, in the case of the chromate coated sample, the effect is much less severe, suggesting greater resistance to corrosion which is attributed to the chromate coating.

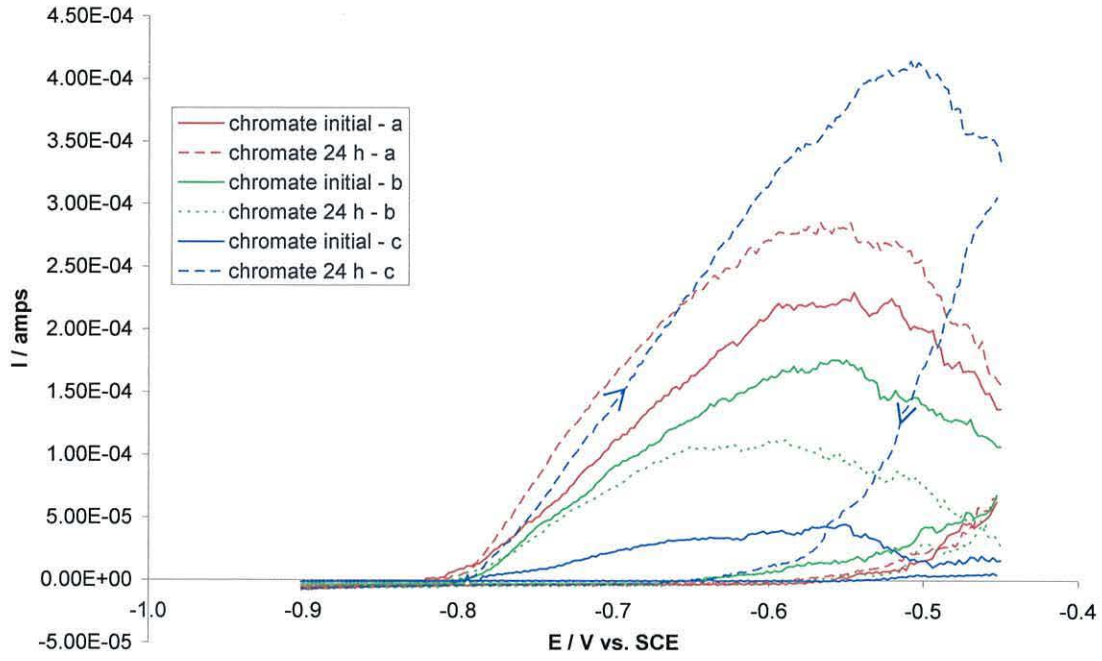

Figure 5.3 CV data for chromate-coated alloy 3105 initially, and after 24 h in acidified sodium chloride with three replicate samples (a, b, c)

Thus, directly comparing the CV readings and the peak area of the CV (which represents the charge) between the etched and chromate-coated samples, it is immediately obvious that oxidation occurs to a much greater extent (a factor of 10) on the etched samples following immersion in the solution for 24 h, Figure 5.4. This indicates that the chromate-conversion coating does still function as a corrosion protection layer even after exposure to an accelerated corrosion solution which may be considered to be in part due to the initial barrier nature of the oxide coating but then over time due to the well–known, "self-healing" nature of chromate coatings. Thus, the CV experiments proved to be a valuable tool in evaluating the surface coating for corrosion resistance.

The etched samples also show a greater increase in charge after 24h compared to initially, with the etched sample showing the greater charge after 24 h, Figure 5.5.

However, significant error margins are obtained with these charge readings, and reliance cannot be placed with confidence on the charge value/change in charge value.

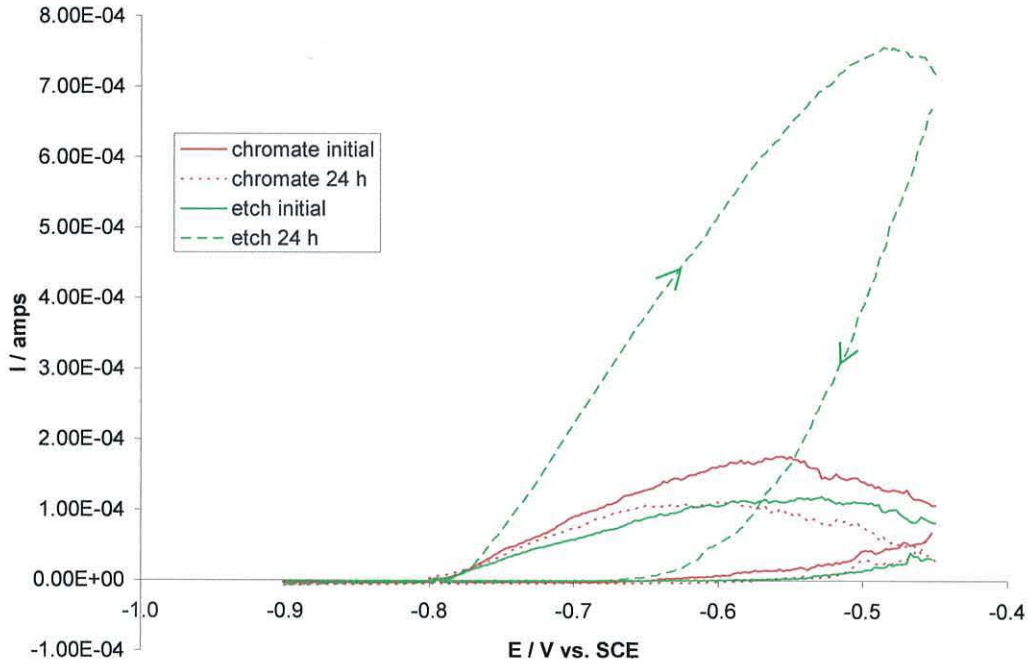

Figure 5.4 Typical CV data produced for chromate coated (red) and etched alloy 3105 (green) initially, and after 24 h in acidified sodium chloride

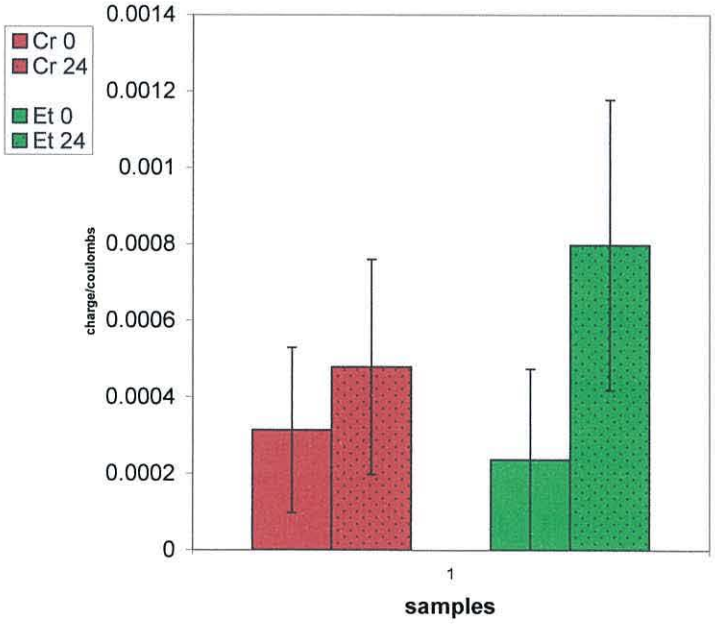

Figure 5.5 Average charge measured following CV for chromate coated (red) and etched alloy 3105 (green) initially, and after 24 h in acidified sodium chloride

As this was a favourable result, showing clearly a difference in the size and change in the oxidation peaks between the chromate and etched sample, some of the other aluminium corrosion protection pretreatments described in Chapter 3 and 4 have also been examined and the data is presented in the following section.

Pretreatments 1, 5, 9 and 10 have been selected. Pretreatment 1 is the worst performing of these pretreatments in terms of it's corrosion resistance, and has been selected to investigate whether this performance is reflected in these tests. By comparison, Pretreatment 5 exhibits marked improvements in corrosion performance compared to Pretreatment 1, with both Pretreatments 9 and 10 performing similarly to each other and the best of the pretreatments examined in this thesis. Again, these pretreatments have been selected to ascertain whether corresponding results are obtained with this technique.

The cyclic voltammograms for aluminium alloy 3105 surfaces treated with Pretreatment 9 show initial oxidation peaks larger than those of the etched samples with peak current readings reaching between 9.79×10^{-4} and 4.43×10^{-4} A. Following 24 h in the corrosive solution, a clear reduction in the size of the oxidation peak is observed with peak currents ranging from 4.2×10^{-4} to 6×10^{-5} A measured, compared to the initial readings obtained for this sample. Associated with this change is a general reduction in the charge measured to values, Figure 5.9. In this instance, Pretreatment 9 was studied because it gave amongst the best corrosion performance during the accelerated chemical and physical testing described in Chapters 3 and 4. Thus, these data are important in supporting the accelerated corrosion data because they imply that the corrosion effects actually decrease after 24h in acidic-chloride solution. These phenomena are clearly different to those observed for the etched aluminium alloy, and do not replicate the

trend observed for the chromate coated sample, suggesting that the mechanism in which this coating protects against corrosion is different. However, if the size of the corrosion peak is accepted as an indication of susceptibility towards corrosion, after ageing – or submersion in corrosive solution for 24 h, it can be concluded that Pretreatment 9 performs comparatively to the chromate coated samples, which are known to be effective in preventing corrosion (discussed in Chapter 1).

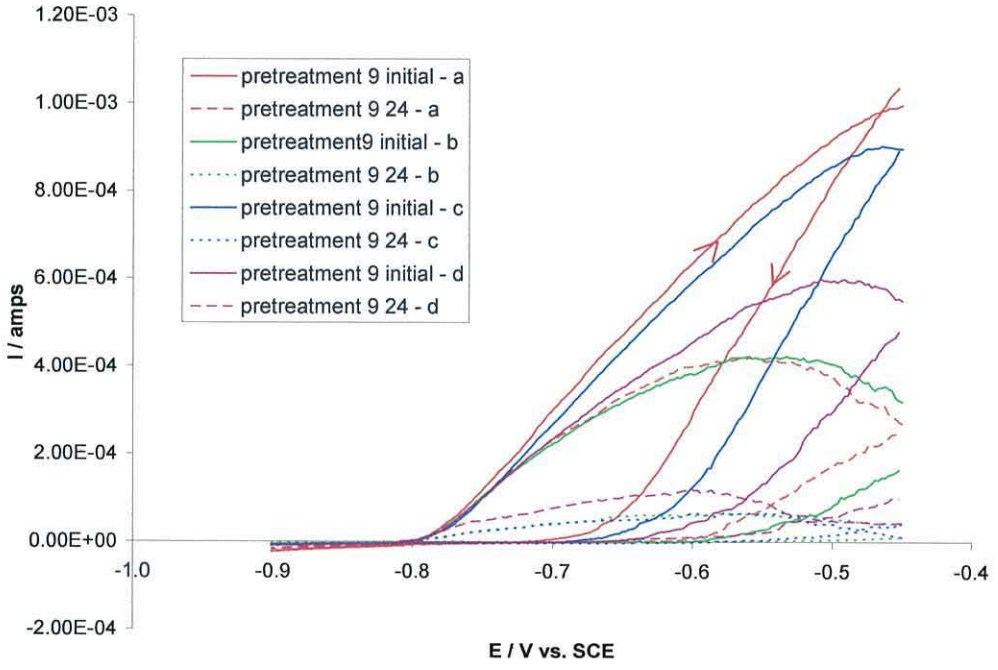

Figure 5.6 CV data for aluminium alloy 3105 coated in Pretreatment 9, initially, and after 24 h in acidified sodium chloride. with four replicate samples (a, b, c, d)

Pretreatment 10 does not show an overall trend, with two of the four samples showing a decrease in oxidation peak measurements, and two showing an increase in oxidation peak measurements. The initial oxidation measurements show peak values ranging from 4.03×10^{-4} to 6.47×10^{-5} A, and the measurements after 24 h range from 2.17×10^{-4} to 1.59×10^{-4} A, on average showing a reduction. The charge values are similar for both the initial and 24 h measurements, Figure 5.9.

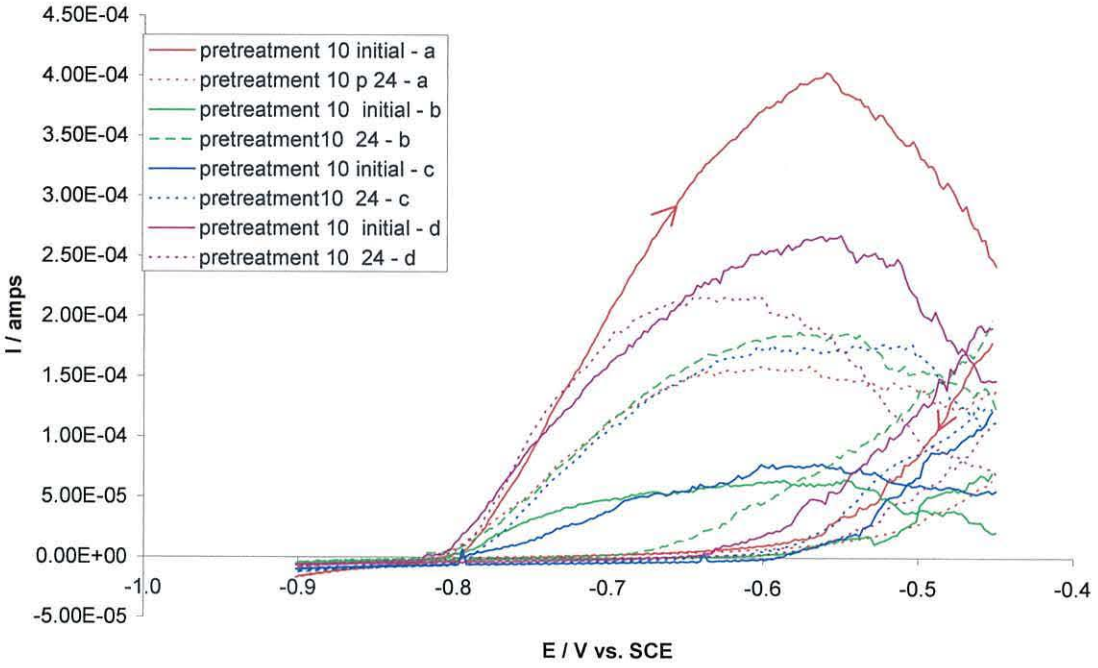

Figure 5.7 CVs of aluminium alloy 3105 coated in Pretreatment 10 initially, and after 24 h in acidified sodium chloride with four replicate samples (a, b, c, d)

Pretreatment 5 gave similar results to those of Pretreatment 9. Typical data for Pretreatments 9, 10, 5 and 1 are presented in Figure 5.8. The initial oxidation measurements show peak values ranging from 8.24 x 10^{-4} to 3.62 x 10^{-4} A, and the measurements after 24 h range from 1.89 x 10^{-4} to 9.87 x 10^{-5} A. The measurements for 24 h are smaller than those for Pretreatment 9, and comparable to the chromate coated sample, which would suggest, on the assumption discussed relating oxidation to corrosion, that Pretreatment 5 performs better that Pretreatment 9 in preventing corrosion after 24 h. However the charge measured showed a general increase rather than a decrease, Figure 5.9, which again is similar trend to the chromate samples, but is more in line with the magnitude of the etched samples.

Pretreatment 1 showed initial oxidation peaks ranging between 5.87 x 10^{-4} and 2.52 x 10^{-4} amp initially. Similarly to Pretreatments 9 and 5, the size of the peaks clearly

reduce following 24 h exposure in the corrosive solution, with peak oxidation values of between 1.89 x 10^{-4} and 9.87 x 10^{-5} A measured. A general reduction in the charge measured is also observed.

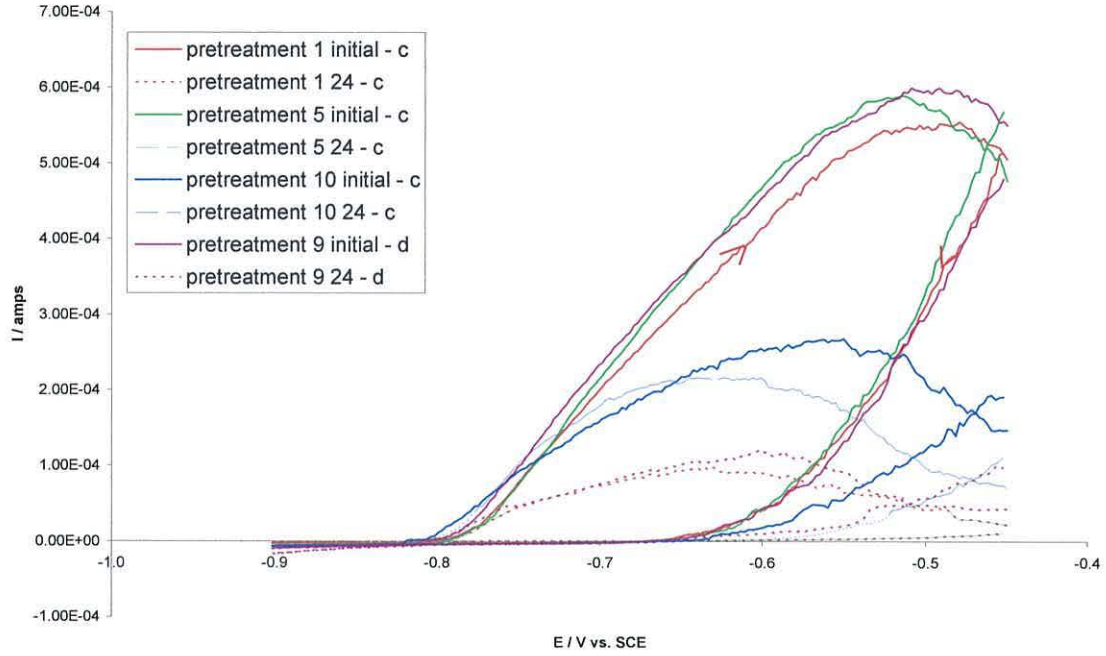

Figure 5.8 Typical CV data produced for Pretreatments 1, 5, 9 and 10, initially, and after 24 h in acidified sodium chloride

Overall, the results suggest that Pretreatment 10 is the best at corrosion protection of the four pretreatments examined, due to its smaller oxidation peaks, Figure 5.8, which is in line with the data presented in Chapter 4. In contrast to the other pretreatments (9, 5, and 1), Pretreatment 10 did not show the same trend of reducing charge size following 24 h in the corrosive solution. However a greater number of samples would need to be analysed to confirm a definite trend.

In terms of examining the charge on the samples, the change to the surface, Pretreatment 5 is the weakest performer, showing both an increase in charge after 24 h, which suggests breakdown of the coating, and the greatest charge measured overall.

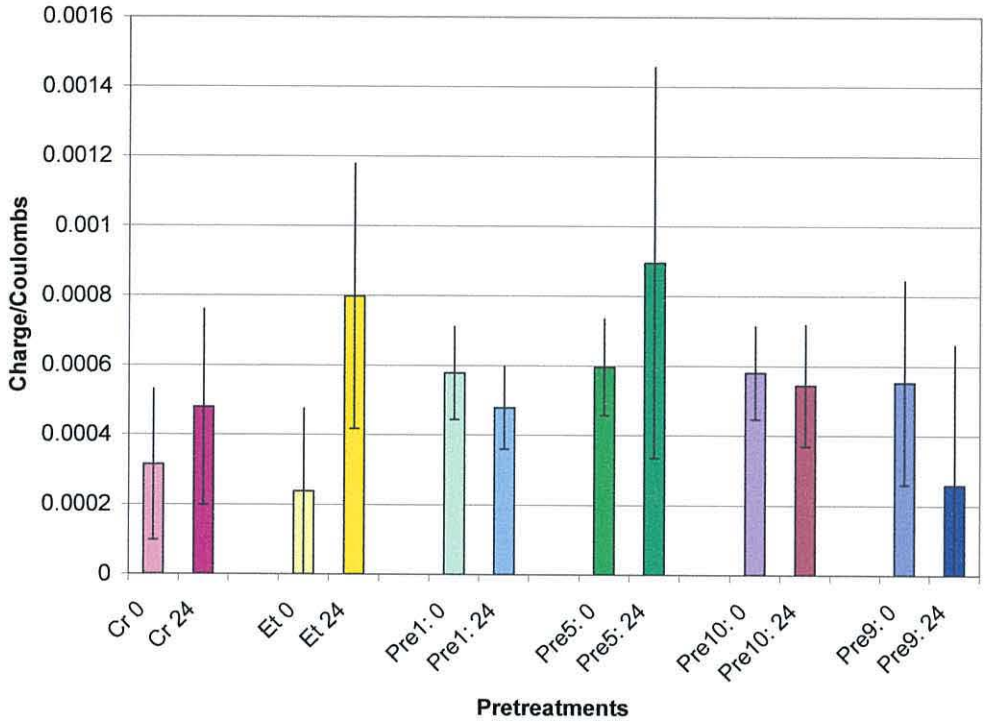

Figure 5.9 Average charge measured following CV on treated aluminium substrates initially, and after 24 h in acidified sodium chloride

Thus, in considering the information presented in Chapters 3 and 4, the results obtained from the electrochemical experiments correlate best for the best performing pretreatment as might be expected. The differences in performance of the other pretreatments may be the result of the fact that this is a different technique to the other methods of analysis. CV is very sensitive to the nature of the surface and provides averaged data across the surface exposed to the solution. By comparison, the other techniques used (e.g. microscopy or Qualicoat testing) can take into account that one substrate may give a variable response across its surface. Thus, from the CV measurements Pretreatment 1 (the worst performing pretreatment by Qualicoat testing) behaves worse than Pretreatment 5 initially, but better by CV after 24 h, suggesting that, here again, it would be preferable to run additional samples to confirm these trends.

References

(1) Moon, S.-I. P. S.-M. *J Solid State Electrochem* **2000**, *4*, 267-272.
(2) Van Gils, S.; Melendres, C. A.; Terryn, H.; Stijns, E. *Thin Solid Films The 3rd International Conference on Spectroscopic Ellipsometry* **2004**, *455-456*, 742-746.
(3) Fisher, A. C. *Electrode Dynamics*; 1 ed.; Oxford University Press, 1996.
(4) A. J. Bard, L. R. F. *Electrochemical methods: Fundamentals and applications*; 2nd ed.; New York: John Wiley, 2001.

6. Corrosive Solutions

This chapter describes the corrosion of aluminium in various solutions with the aim of developing an accelerated corrosion test to more rapidly screen pre-treatment procedures. The underlying reason for this has been to reduce the time taken to identify promising pre-treatments which otherwise would require a testing procedure such as the 1000 hours salt-spray test. The Chapter begins by reviewing the relevant literature. The experimental design process is then described in detail including the process to develop a short accelerated corrosion screening test, along with the application of these procedures to test the protective properties of some potential new coatings.

As stated in the Introduction to this thesis, it is well known that the surface layer of aluminium oxide on aluminium metal exhibits amphoteric behaviour, and is susceptible to both acid and alkali attack, producing either $[Al(OH_2)_6]^{3+}$ or $[Al(OH)_4]^{-1}$.[1] It is also known that the extent of corrosion is dependant on parameters such pH, tempertature, nature and concentration of anions, and oxygen concentration.[2-4] Furthermore, it has been reported that, in non-oxidising acidic solutions, a porous oxide film is formed,[5] which can act as a barrier to corrosion. Indeed, even when this surface oxide film is stable, the presence of aggressive ions such as chloride are known to cause extensive, localised attack.[5] It has been suggested that adsorption of chloride ions at defects in the oxide film is the initial step in this process with the subsequent formation of aluminium oxide chloride water soluble complexes[5] which, in turn, produces characteristic crystallographic pitting.[2]

Previous work has reported studies of changes in the aluminium oxide surface layer on different alloys to investigate the effects of corrosive aqueous solutions on this layer and

thus on corrosion. For instance, the pitting tendency of aluminium in aqueous perchlorate solutions has been reported to be less pronounced than chloride solutions.[2] However, the presence of chloride has been reported in oxide films following exposure to perchlorate which suggests that these ions have undergone transformation to chloride which presumably must be associated with a reduction process with electron capture presumably arising from aluminium oxidation.[2]

Studies by Van Gils[4] and co-workers have described the changes in the oxide layer on alloy 1050 following immersion in hydrochloric and sulphuric acid. Two types of oxide layer were studied, an electro-polished layer, and a barrier oxide layer produced by anodising. The changes were observed by *in situ* spectroscopic ellipsometry (VISSE), which provided information regarding the surface thickness and roughness. Parallel experiments measuring open circuit potential provided corresponding electrochemical data. It was found that both anodic films showed similar features; a decrease in thickness over time in both solutions, with a slight increase in nanoscale roughness observed following immersion in sulphuric acid. The films showed an initial decrease in the oxide thickness which was followed by an increase, which then levelled off. These data were in agreement with the open circuit potential measurements which showed a decrease initially, before a small increase before finally reaching a steady state. The slight increase in surface roughness observed on the sulphate immersed sample was attributed to pitting of the surface. Thus, under the acidic conditions present in the sulphate solution, these workers stated that they believed that Al^{3+} and $Al(OH)_3$ should reach an equilibrium, and that hydrous oxides should precipitate at the surface leading to an increase in thickness of the film. For the sulphate immersed sample, the thickness was assigned to the adsorption of sulphate ions and this was further evidenced from IR data. By comparison, the increase in roughness in the

chloride solution was much greater, due to the increased pitting caused by the chloride ion. In this work, both the elipsometry and electrochemical techniques showed good concurrence, suggesting that the change in thickness could be closely related to the electrochemical processes. Thus, the change in open circuit potential could be directly related to surface oxide growth and dissolution. These workers reported that dissolution corresponded to a change in V_{OC} in the cathodic direction, caused by low pH. By comparison, growth was indicated by change in V_{OC} in the anodic direction.

Cabot *et al.* have reported that the pitting corrosion of aluminium in chloride solutions takes place as a crystallographic etching at low anodic potentials, while at higher anodic potentials polished hemispherical pits tend to appear.[6] These workers studied single-phase, pure aluminium and found that it exhibited intrinsic inter-granular attack. Thus, where general corrosion occurred, no pitting was evident but the corrosion rate was greater at the grain boundaries. These experiments showed that this was followed by pit nucleation in the grain boundaries and within the grains, but with preferential pit growth along the boundaries to form fissures.

Further studies by Wiersma and Herbert looked at the etching of aluminium at elevated temperatures.[7] They discussed that etching in hot chloride solutions at temperatures above 60 °C, which resulted in crystallographic etch pits during initial attack. These workers reported that their data showed that the pit walls grew in five directions simultaneously, this being each if the four faces of the pit, and the 5th the face of the substrate – creating the depth of the pit. Thus, the depth of the pits was half of the width at the surface. Lin and workers showed that as the pit width increased to around 1 μm, a change in the pit morphology occurred and that the pits transformed into etch tunnels.[8] This was considered a special type of pitting corrosion in which simultaneous

dissolution and passivation on adjacent surfaces, and sustained balance between these two processes took place. At below 60 °C however, the formation of macro-pits of circular shape dominated, and the pit walls were composed of faceted surfaces which presumably is the result of a reduced rate of etching at lower temperatures.[7]

As well as investigations into the accelerating effect of some chemicals on the corrosion of aluminium, various chemicals have been studied to investigate their inhibiting effect on aluminium corrosion. To date, the literature shows that additions have generally been made in one of two ways: to the surface oxide, through the application of a coating, or directly to the corrosive solutions. For instance, Metikosae-Hukovicâ *et al.* have investigated the effect of various aliphatic and aromatic amines and nitrogen heterocyclic compounds.[5] They showed that the inhibitory action observed for these compounds was related to factors such as type of adsorption, the charge distribution on the adsorbing molecule and the type of interaction between the adsorbate and the metallic surface. As an example, one type of pyrrole studied was added to hydrochloric acid and potentiodynamic and impedance experiments were carried out.[5] It was found that no change to anodic polarization curves occurred on addition of the pyrrole, but the cathodic current densities decreased. The hydrogen evolution reaction, a cathodic process, was not affected, which implied that the inhibitory action of the pyrrole was through the improvement of the barrier characteristics of the oxide layer, which did not suppress the reduction processes.

In an industrial context, mercaptoacetic acid and its derivatives are often used for corrosion inhibition in the oil field industry.[9] To understand the influence of these compounds on corrosion performance, the addition of this acid to HCl was studied in the context of corrosion inhibition on aluminium by weight loss and hydrogen

evolution.[9] The data showed that severe pitting corrosion and black corrosion products were visible on the aluminium coupons used. It was found that the addition of mercaptoacetic acid actually increased the weight loss of the aluminium coupons. A corresponding hydrogen evolution investigation also revealed greater hydrogen gas evolution with increasing mercaptoacetic acid concentration. The volume of evolution increased slowly with time before eventually becoming linear. In this case, the pattern of gas evolution was considered to be due to initial protection of the oxide film.

In summary, corrosion in various solutions has indicted that acidity and chloride ions play an important role in the corrosion attack on aluminium, which may be inhibited or exacerbated by the addition of further chemicals. In the remainder of this Chapter, studies of the corrosion of aluminium (coated, etched and as received) in a variety of solutions (varying pH and chloride ion concentration) will be discussed. The addition of inorganic films to the surface of the aluminium, as described in Chapter 3, will be investigated to identify any corrosion protection phenomena using these accelerated corrosion tests.

Corrosive solution screening test – development

This section will describe the development of an accelerated corrosion test for aluminium. The aim of this work has been to develop a valid, reproducible, but rapid test be able to assess the corrosion protection offered by potential new pre-treatments in a short period of time. Any accelerated corrosion test suffers from the fact that the data must be extrapolated over often very extended time periods (typically up to 25 years). As such, the data will naturally suffer from errors associated with this. However, in this context, the aim here has not been to develop an absolute test of corrosion protection but rather a rapid, simple screening test to trial new corrosion-protection coatings. As part of the experimental design, the application of a powder coating to the pretreated substrates has been avoided to limit variables and to reduce the sample processing time. In addition, a typical chromate-conversion coating has been used as a reference due to its known corrosion protection properties. Etched and untreated aluminium samples have also been included in the experiments to quantify the chromate coating protection. The trends in weight loss and appearance – i.e. the physical and visual affects of corrosion attack, have been used as end-points to examine corrosion protection in each case.

The experiments have involved immersing the treated aluminium coupons into various aqueous solutions, which would be expected to initiate corrosion effects at different rates in the different solutions. The aim of this was to identify a suitable corrosive medium which would provide consistent data over a reasonable timescale. A further requirement of the new test has been that trends evident from the protective properties of the chromate coating on aluminium in the selected medium should be easily identifiable and differentiated clearly against trends observed for the etched and bare aluminium substrates. Following this, the aim has been to test novel pretreatments with

replicates in the selected medium. Novel pretreatments which compare favourably to the chromate coating should then be considered to impart good corrosion resistance, and then further investigated with longer term testing.

Corrosive solution screening test - results

A series of aqueous-based solutions have been trialled as potential corrosion solutions. The solutions include tap water, deionised water, sodium hydroxide, ammonium chloride, acetic acid, sodium chloride, hydrochloric acid, AC133 acid cleaner (this being an Almetron product containing phosphoric acid and fluoride in water), and Machu Test solution. The Machu Test solution is a solution specified by Qualicoat for testing coatings, and contains sodium chloride, glacial acetic acid and hydrogen peroxide. For the standard Machu Test, the pretreated surface is powder-coated, and is scored using a metal tool to reveal the protective coating i.e the pretreatment, under scrutiny. The substrate is then submerged in the Machu solution for 48 h. The extent of detachment and/or blistering of the powder coated paint at the score site (or elsewhere) are then used to judge the quality of the pretreatment in preventing corrosion from developing from the score site under the powder paint.

After submerging the samples in the various solutions, they were examined for changes in weight and appearance due to corrosion attack at different intervals, depending on the severity of the attack.

Corrosion in Water

Aluminium samples, alloy 3105, have been examined after having been placed in either deionised (DI) water or in tap water for a total time of 36 days. The samples were

initially treated in one of four ways: as received, etched, chromate coated, or chromate-coated with a score through the coating. The data show that some visible patches, which may have indicated etching, are apparent to the naked eye on both chromate coated and etched samples after ten days. The samples have been examined in plan view using optical microscopy with epi-illumination. Both dark field and bright field imaging has been used to image any colour changes as accurately as possible. Typically, images have been recorded at 50 x magnification. Optical images of the chromate coated samples are presented in Figure 6.1, showing distortion in the rolling direction following corrosion in the (tap) water, and also showing darkened areas assumed to be pit holes. The etched and as received samples show some brown discolouration. The optical images for the as received samples show this distortion in the rolling direction following corrosion in the (tap) water, and also show a brown discolouration surrounding the dark pit holes in the bright field images, Figure 6.2. The score area on the chromate coated samples does not appear significant, with no additional visible changes apparent compared to the samples that were without scoring.

Weight measurements on the substrates prior and after the 36 days water treatment reveal only a slight weight loss for the as received sample in tap water only; and this was less than 4 % loss of the original weight. This suggests that the pitting observed was superficial on the remaining samples analysed. The pH of deionised water (pH 5) and tap water (pH 7.3) are both within the passive range of the Pourbaix diagram for aluminium (as discussed in Chapter 1) and thus would not be expected to cause significant corrosion. However, tap water typically contains more ions than DI water, such as fluoride, chloride and copper, although at low concentrations. Such ions are known to be aggressive towards aluminium and promote corrosion. Thus, these ions could be the cause of the slight weight loss observed on the as received sample.

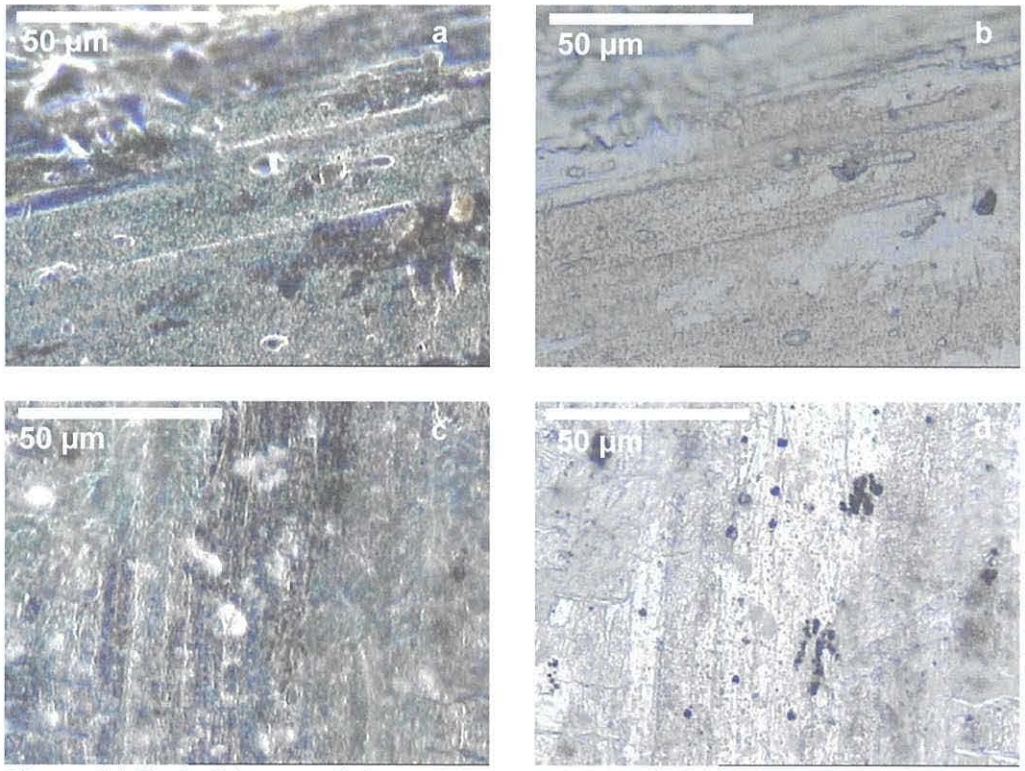

Figure 6.1 Optical images of chromate coated alloy 3105 a) dark field and b) bright field, both prior to corrosion treatment. c) dark field and d) bright field, both after 16 h in tap water

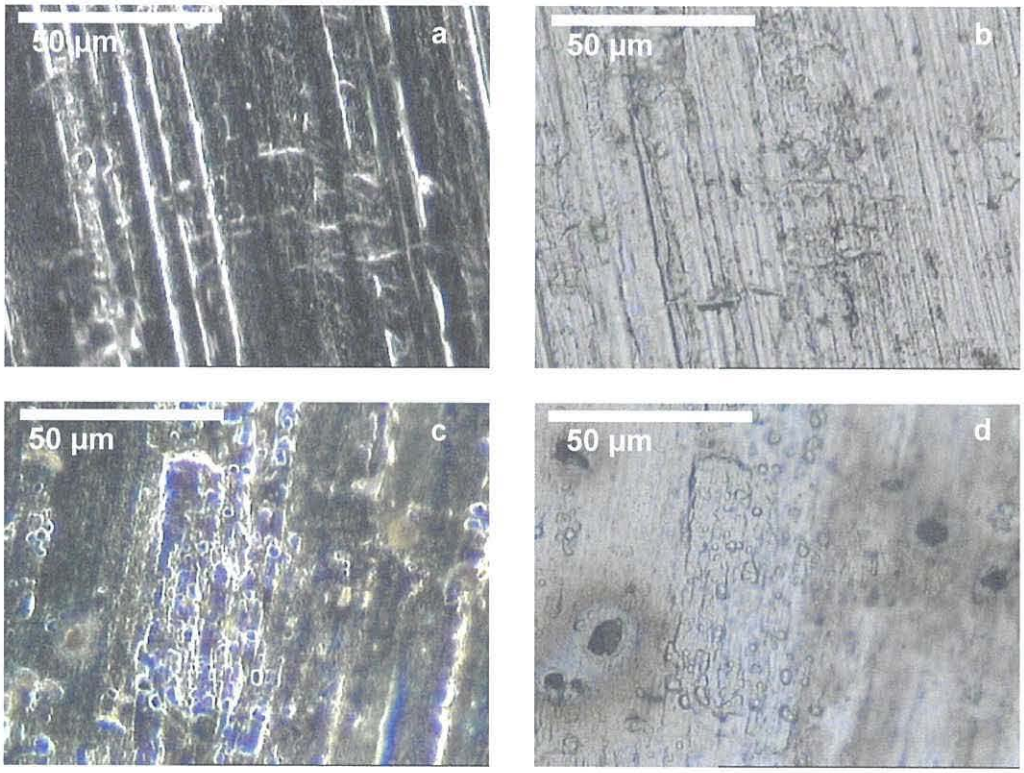

Figure 6.2 Optical images of untreated alloy 3105 a) dark field and b) bright field, both prior to corrosion treatment. c) dark field and d) bright field, both after 16 h in tap water

However, although pitting was observed, neither tap or DI water are suitable as potential corrosion test solutions as there is insufficient variation in response between the different substrates to give differentiated test results for different pre-treatments.

Sodium hydroxide

The corrosion of three types of samples in 1M NaOH has been investigated; etched aluminium, air dried chromate-coated aluminium, and oven dried chromate coated aluminium. The data showing the mass remaining in these sample types after fixed time intervals are shown in Figure 6.3. The substrates have been examined and weighed after 10 minute intervals in solution. This process was repeated three times (30 min total time), and again after a further 60 min, Figure 6.3, before being left overnight. Similar weight loss values for all three treatment types are observed, with blackening of the surface observed after 60 min. This blackening is believed to be the result of smut which was loosely attached to the surface and was removable by a deionised water rinse. This smut is assumed to be the insoluble etch products produced during alkaline etching which have previously been discussed in Chapter 2. All the samples dissolved completely overnight in the sodium hydroxide solution. With a pH of 12.8, this sodium hydroxide solution would be expected to be highly corrosive towards aluminium due to the pH lying outside the passive region of the Pourbaix diagram. Thus, corrosion of the etched sample is expected. Similar weight loss values for the chromate coated samples following the intervals suggests that the chromate coating does not offer resistance to the alkaline solution. As all samples were dissolved equally (and totally over 12 h), no differentiation was observed between treatments either visually or by weight loss, ruling out sodium hydroxide as a suitable corrosive solution for the experiment in mind.

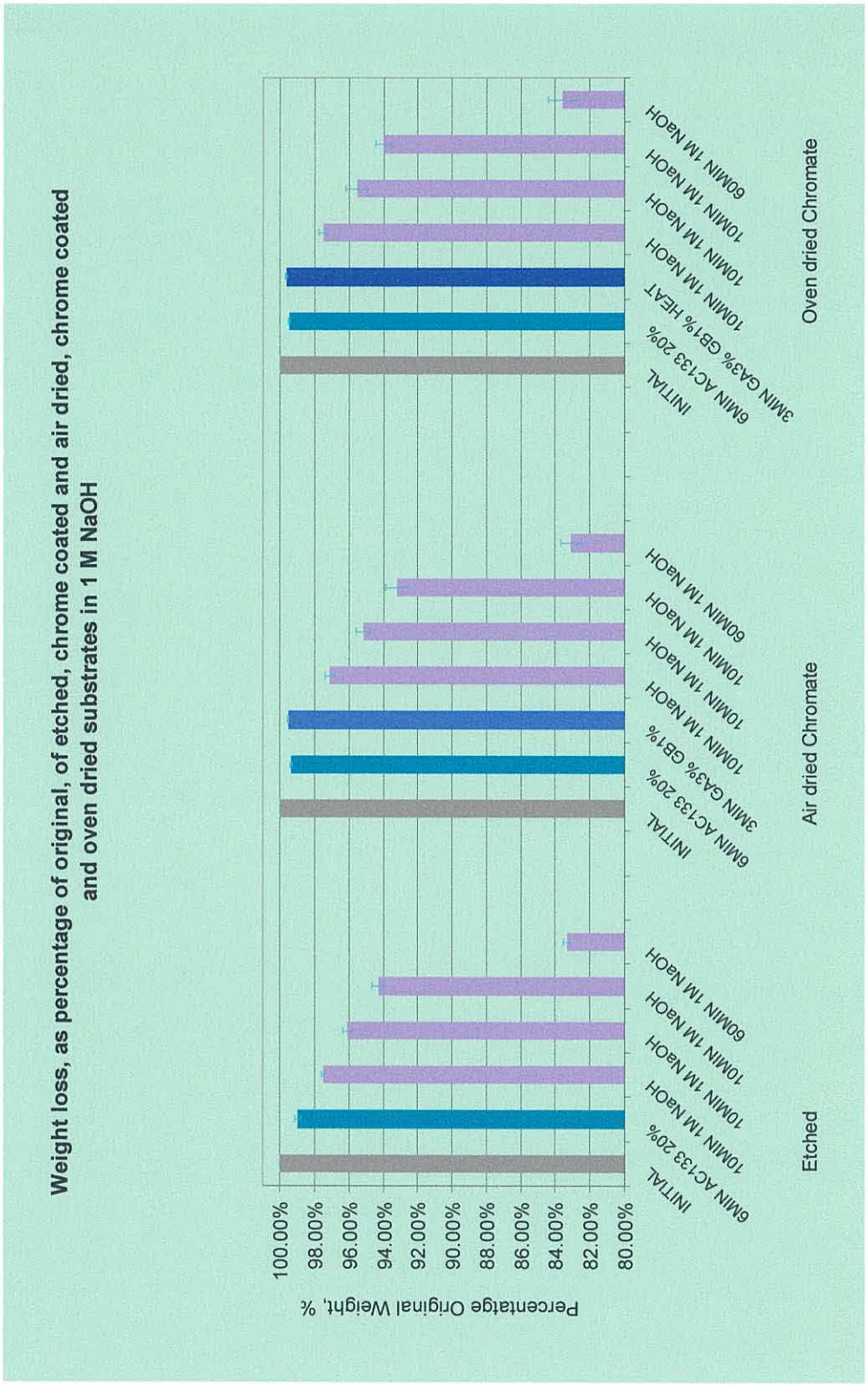

Figure 6.3 Data showing mass remaining at fixed time periods for aluminium samples treated with NaOH

Ammonium chloride

The corrosion of etched aluminium substrates have been investigated in 1 molar ammonium chloride. By comparison with the data presented for NaOH, these etched aluminium substrates that have been treated in 1M NH_4Cl over the same time period show significantly less weight loss. The average remaining weight for the samples treated with NH_4Cl was 97.5 ± 0.2 % after 90 min compared to 83.3 ± 0.2 % in the NaOH. This is in line with the expected result as the pH of ammonium chloride is 5.7, which is within the passive range of the Pourbaix diagram. This is similar to the pH of deionised water. However, the increased concentration of chloride in the ammonium chloride solution is assumed to be the cause of the small weight loss observed during the short exposure time. As the weight loss observed was low for the etched sample, and would be expected to be less for the chromate for a favourable result, this solution was ruled out as the weight loss was not sufficiently great.

Acetic acid

Corrosion tests have also carried out on both etched aluminium and air dried chromate-coated aluminium in solutions of 5M acetic acid. Although no significant weight loss has been evident after 40 days, pitting of the chromate coated sample is observed by optical microscopy following less than 24 h immersion in acetic acid, Figure 6.4. Although acetic acid contains no chloride or other small ions, its pH of 2.7 is in the lower pH corrosion range for aluminium according to the Pourbaix diagram. However, with a pKa of 4.8, acetic acid is considered a weak acid, and it is this weak acidic nature of the acetic acid that is therefore assumed to be the cause of the pitting that has been observed but has caused little weight loss.

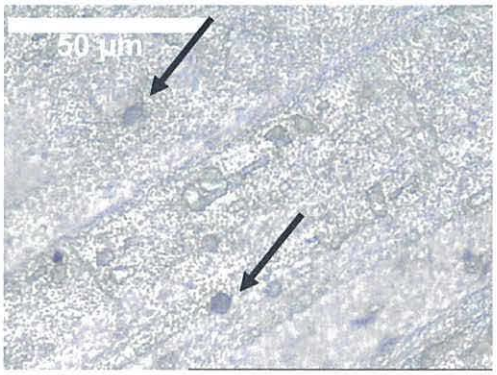

Figure 6.4 Optical microscope image, bright field, of chromate coated alloy 3105, following 24 h in 5 M. The arrows show examples of the pits observed

Sodium chloride solution

A solution of 1M NaCl results in variations of less than 2 % of the initial weight loss over a period of 3 weeks for etched and air dried chromate-coated aluminium alloy 3105 samples. Sodium chloride has a pH of 5.5 which is in the passive range for aluminium according to the Pourbaix diagram. However this solution contains a significant concentration of chloride ions, which, as discussed previously, are very aggressive towards aluminium. Thus it would have been expected for the presence of these chloride ions to cause significant pitting, but at this pH, only superficial pitting is observed over this time period.

Hydrochloric Acid

Concentrated HCl, (12 M) has also been investigated and this solution has been found to corrode etched aluminium and air dried chromate-coated aluminium alloy 3105 to 60 ± 17 % and 70 ± 4 % of the original weight in 40 min, Figure 6.5. By comparison, 6M HCl dissolved most samples in less than 10 minutes.

Following these initial experiments, the corrosion of etched aluminium and chromate coated, oven dried aluminium substrates has also been tested in 1M HCl with visual

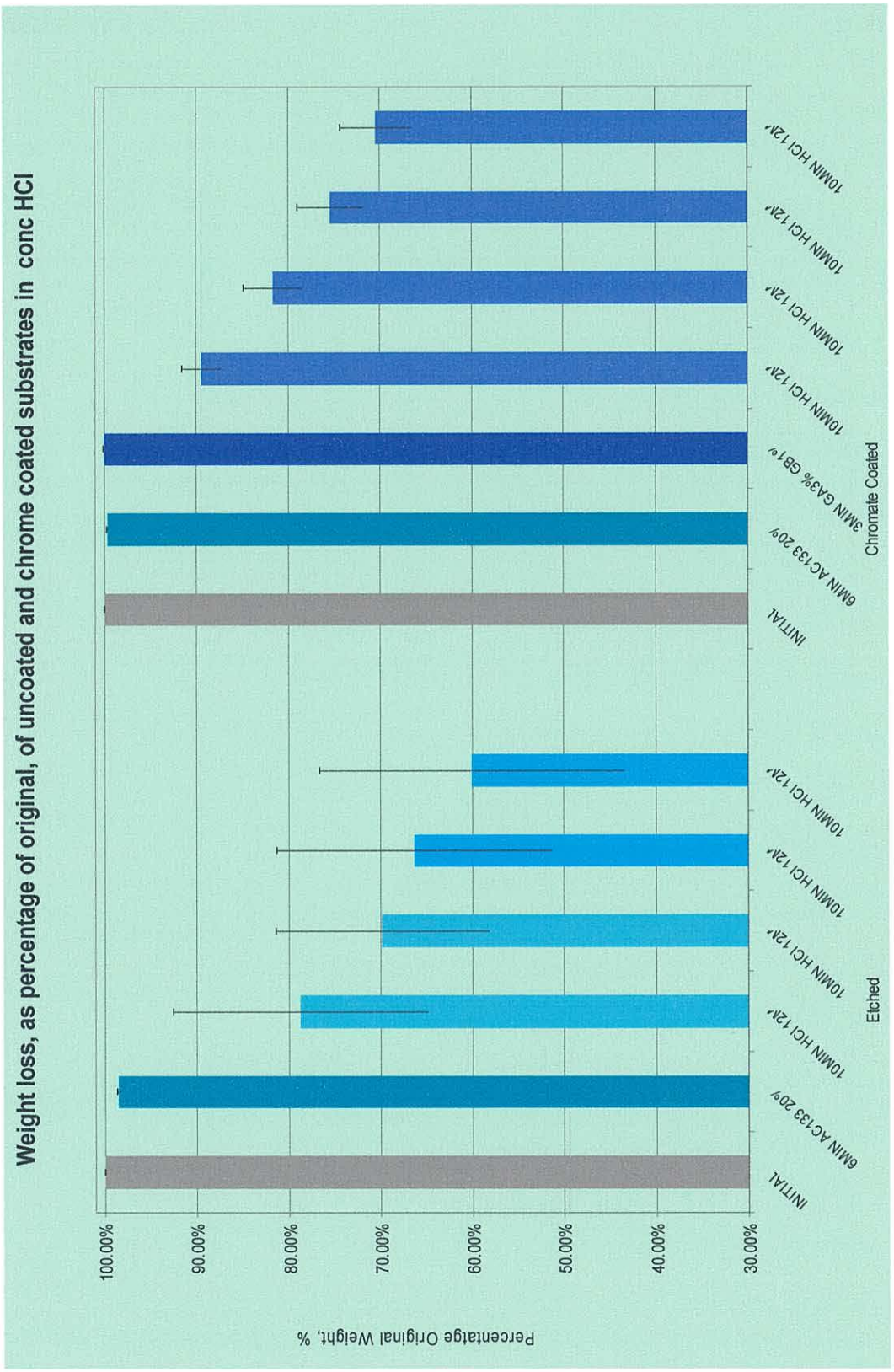

Figure 6.5 Data showing mass remaining at fixed time periods for aluminium samples treated with 12M HCl

examination (by eye and by optical microscopy) and weight loss measurements taken after 1, 2 and 3 h intervals. The data give percentage masses of the original weight of 99.5 ± 0.3 and 99.8 ± 0.2 after 3 hours exposure, respectively. However, after a further 24 h interval in solution, these values have been reduced to 46 ± 4 and 49 ± 9 %, respectively, with both samples completely dissolving after 48 h. In all cases here, the HCl solutions are highly acidic (pH < 1); i.e. well outside the passive region of the Pourbaix diagram for aluminium.

Different surface corrosion morphologies have been observed between the etched and chromate coated substrates. The etched metal shows a uniformly rough surface, with crystallographic etch pits appearing at the aluminium grain boundaries. Scanning electron microscopy, Figure 6.6, shows the morphology of these samples after exposure to HCl and it is clear that there has been a vast change in the morphology of the previously largely flat aluminium surface. The data show that large voids have been created within the surface and sub-surface of the aluminium metal as material has been dissolved and removed by the HCl. This has left behind a remaining skeleton of aluminium particles giving the surface an extremely roughened appearance. The data suggest that once the surface coating of a particular crystallite of aluminium has been breached, rapid dissolution of that crystallite takes place.

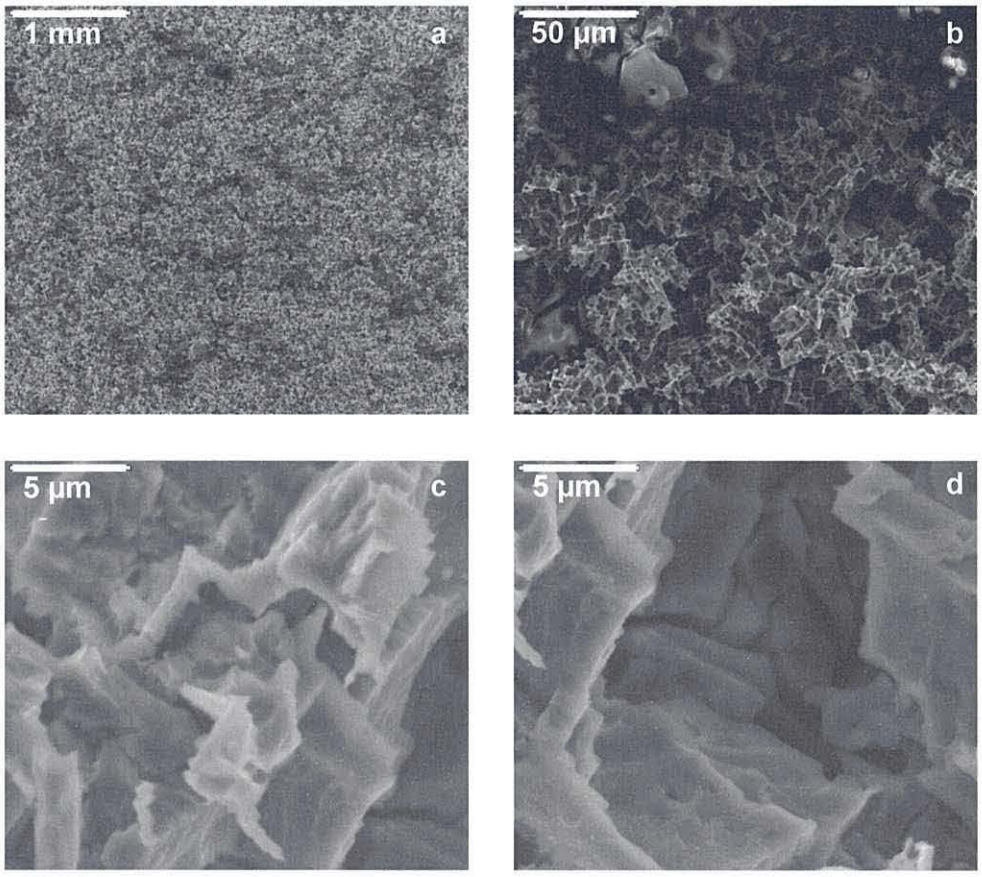

Figure 6.6 SEM images of uncoated alloy 3105, after 24 h in 1M HCl showing a highly roughened surface

By comparison, scanning electron microscopy of the chromate-coated surface which has been exposed to HCl also shows areas where the surface appears to have been breached in a similar manner to the uncoated alloy. However, there are also areas that resemble flat "islands", that have been left relatively unaffected by the etching, Figure 6.7. These "islands" appear in distinctive and regular lines across what would once have been the surface of the metal. It is assumed that the "islands" are areas of the chromate coating that have remained intact and which have resisted attack from the HCl. There is some evidence, (although it is not possible to be absolute due to the significant extent of aluminium etching), that the areas of un-etched surface may resemble a pattern of approximately parallel lines which might be attributed to the rolling direction.

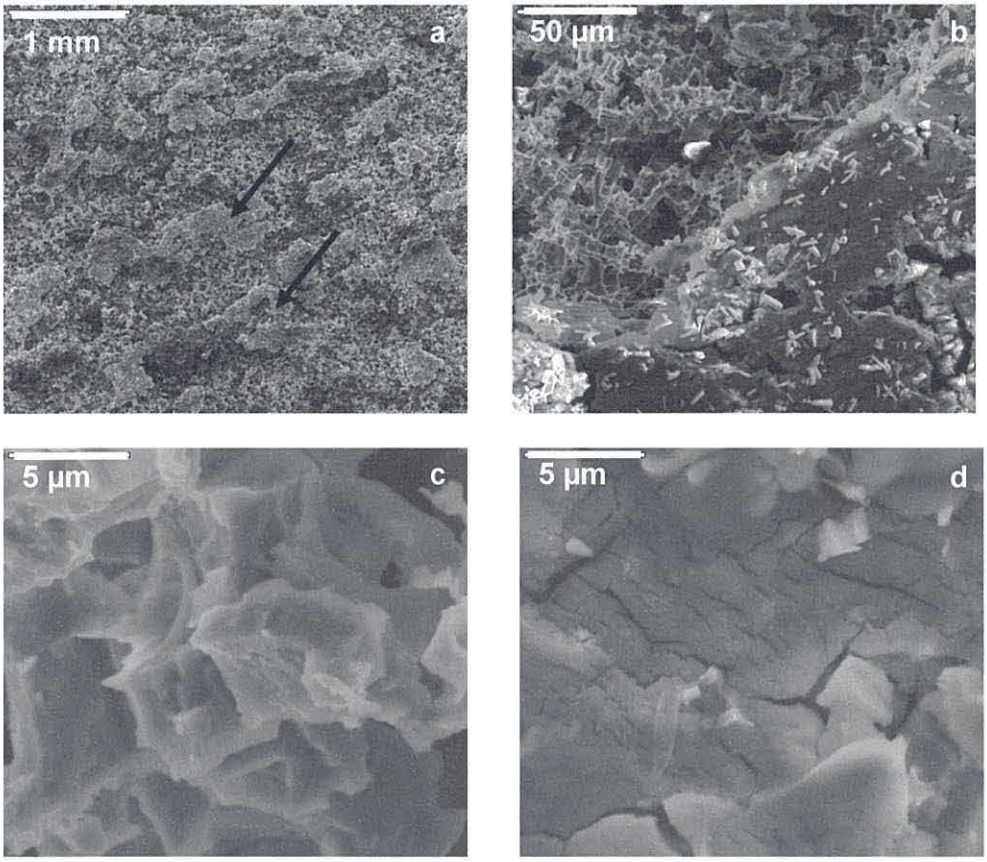

Figure 6.7 SEM images of chromate coated Al, after 24h in 1M HCl. The arrows show examples of "islands" where corrosion does not appear to have taken place

The complete change in morphology observed in these samples has been observed previously in powdered aluminium samples which have been exposed to HCl.[10] Furthermore, the production of the crystallographic etch pits may be due to the exothermic nature of the reaction, which has been reported to cause localised temperatures exceeding 60 °C at the surface where the reaction takes place.[3] Thus, this excess of energy in combination with the acidic, aqueous environment would certainly allow for dissolution but potentially for some deposition as well (effectively a process of Ostwald ripening). Alternatively, the edge pits may simply arise from dissolution of surrounding, more vulnerable material with the particles which remain being left largely intact.

In association with the SEM work, different EDX spectra were recorded for the various substrates. The EDX data show predominantly aluminium and oxygen peaks for the uncoated aluminium substrate which has been treated with HCl, Figure 6.8. This is as expected with the electropositive aluminium being expected to become rapidly oxidized as well as being dissolved during the etching process. Interestingly, the chromate-coated sample still shows clear evidence of chromium and phosphorus remaining on the coated sample after HCl treatment which supports the assumption that there is chromate-containing material still present after HCl treatment, Figure 6.9.

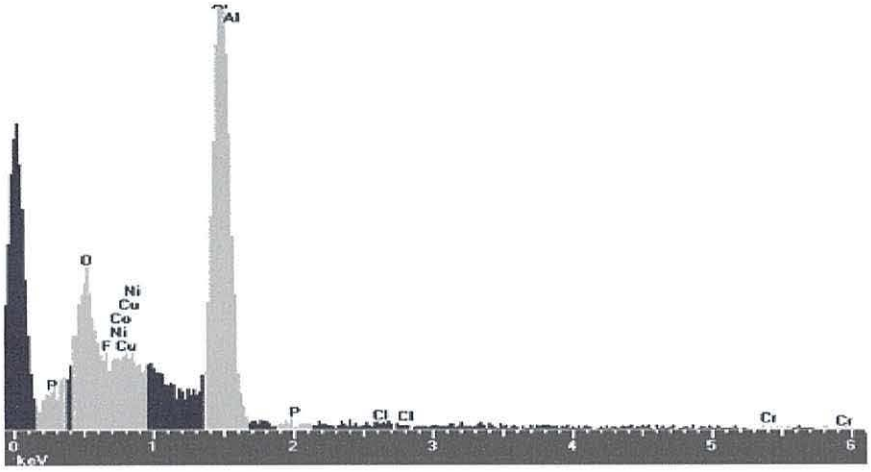

Figure 6.8 EDX analysis of etched alloy 3105, after 24h in 1M HCl showing Al and O peaks

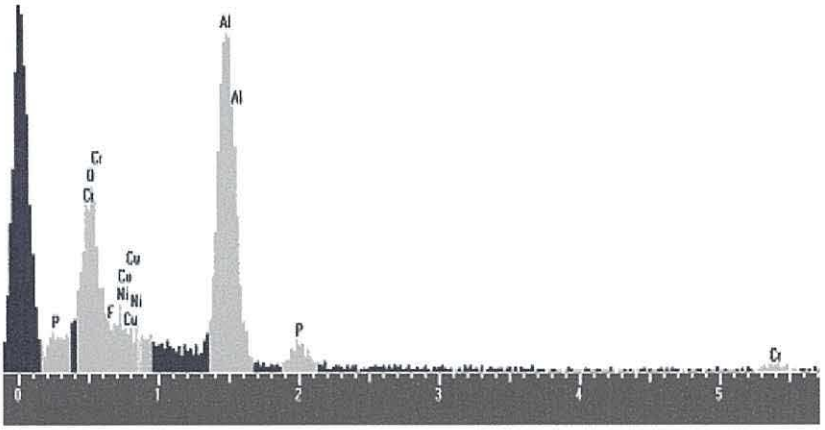

Figure 6.9 EDX analysis of chromate coated alloy 3105, after 24h in 1M HCl showing Cr and P peaks in addition to Al and O peaks

X-ray diffraction data have also been collected on the samples to investigate the possibility that there might be new crystalline material present in the samples. The data confirm that aluminium metal dominates the XRD data as expected, Figure 6.10. There are also new low intensity peaks present in the uncoated sample but it has not been possible to positively identify these and assign them to a specific phase due to the small number of peaks and their low intensity. However, these additional peaks do seem to appear diminished in the data of the chromate coated substrate, Figure 6.11. What is also clear from the data for the chromate coated sample is that there is no evidence for a crystalline, chromate containing conversion coating which is in agreement with the literature which states this material is amorphous.[11]

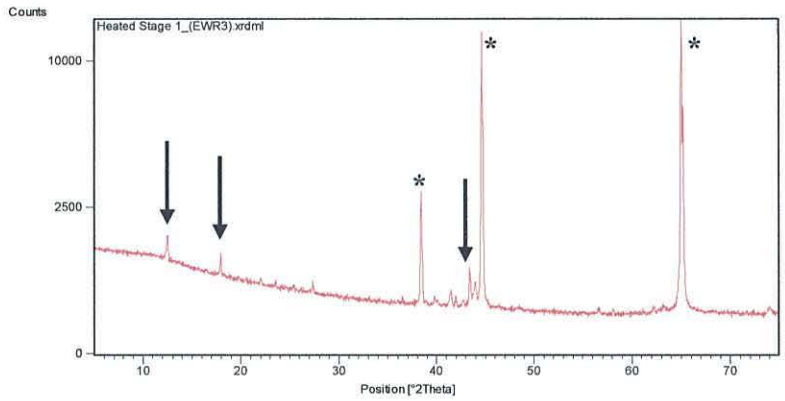

Figure 6.10 XRD of etched alloy 3105, after 24h in 1M HCl. Arrows denote diffraction lines for new phase. Aluminium metal diffraction lines are labelled by *

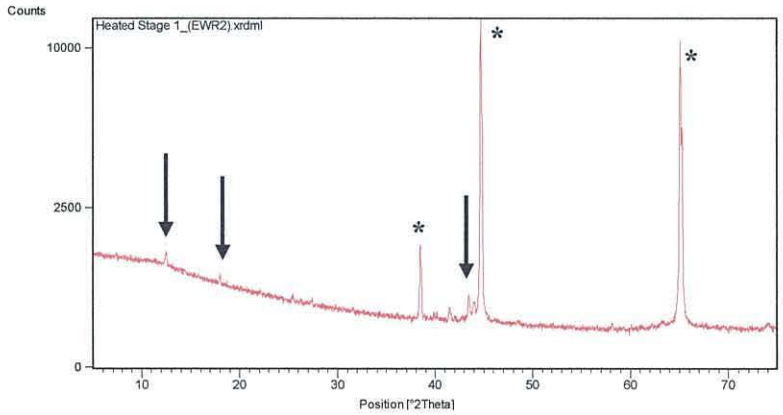

Figure 6.11 XRD of chromate coated alloy 3105, after 24h in 1M HCl. Arrows denote diffraction lines for new phase. Aluminium metal diffraction lines are labelled by *

Etch solution AC133

Samples of alloy 3105 have also been immersed in AC133 solution, a commercial etch and proprietary product of Almetron Ltd, the commercial sponsors of this EPSRC CASE award project. For these samples - etched, chromate coated and air dried, chromate-coated and oven dried - three intervals of 10 min exposure in 20% AC133 (i.e. 30 min total), results in a slight loss of weight for all samples. The resulting masses remaining (shown as a percentage of their initial weight) are 98.5% ± 0.4, 98.8% ± 3, 99.3% ± 1, respectively. Thus, there is no measurable difference between the samples after this short time exposure. However, increasing the exposure time of the samples to AC133 for up to 18 h results in reduced sample masses of 76% ± 1, 79% ± 6, 73% ± 4 %. Here, although the data remain the same within error, it may be that some slight differences are beginning to emerge after this longer exposure time.

In these samples, a black coating on the surface of the substrates is apparent after 1 h, which is loosely attached to the substrate and, as such, can be washed off during the DI rinse. Again, this is assumed to be the insoluble etch products. The optical microscopy shows that a significantly different type of corrosion appears to have occurred on the surface when comparing the morphology to that of the substrates exposed to HCl, Figure 6.12 The surface morphology in this case is rounded and not crystalline; there are no sharp edges in these images which were present for the HCl samples. Instead, the surface resembles the scalloped topography produced by alkaline etching[12,13] discussed in Chapter 2, more than the crystallographic etching produced by the HCl.

The optical microscopy data is supported by the SEM data, Figure 6.13, which also show a scalloped morphology over the substrate surface, the scallops appearing to

overlap, one on to another. Again there is no evidence of the sharp edge residual material observed after HCl exposure.

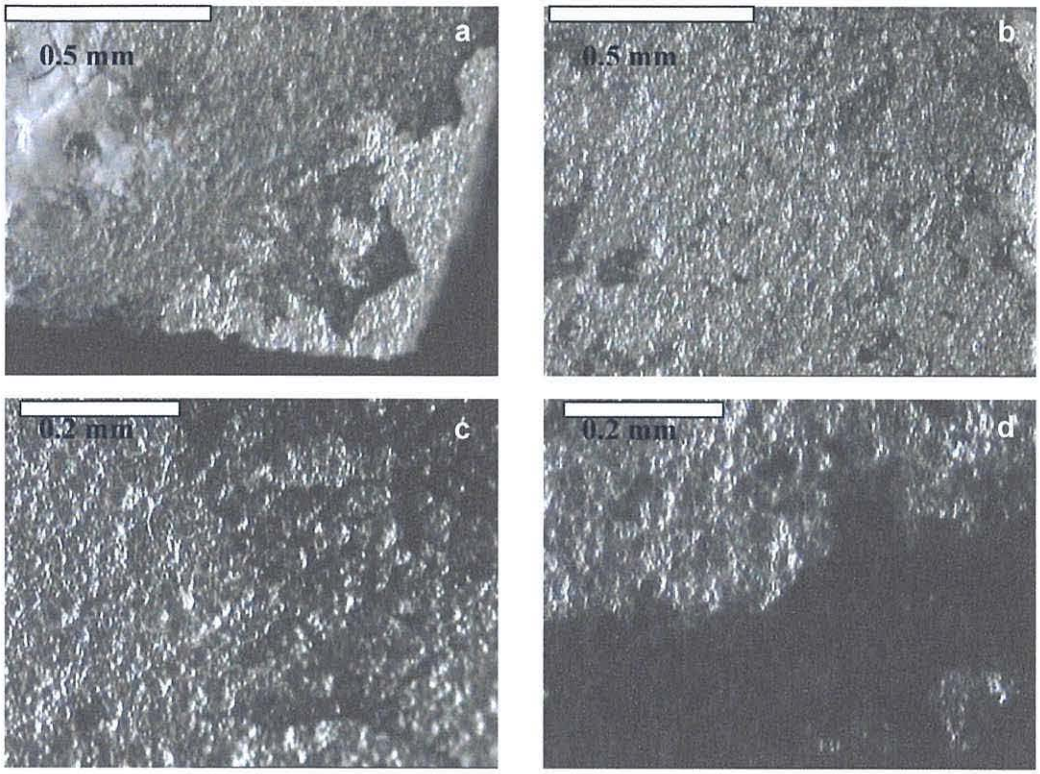

Figure 6.12 Optical microscopy, bright field, of chromate coated, oven dried alloy 3015, after 10 minutes in AC133. (Top are 5 x magnification and bottom are 10 x magnification)

EDX analysis has also been carried out on the chromate coated sample before, and after treatment with AC133 for 72 h. The data show that, before the sample is exposed to AC133, there is clear evidence of chromium and phosphorus in addition to aluminium and oxygen, Figure 6.14. In addition, evidence of a further peak has been attributed to gallium, which is an impurity in the 3015 alloy. By comparison to that observed following HCl corrosion, after exposure to AC133, no chromium or phosphorus peaks are present, Figure 6.15. This suggests that the chromate coating is completely removed by the AC133 solution and thus would no longer offer significant protection against corrosion in the etch bath.

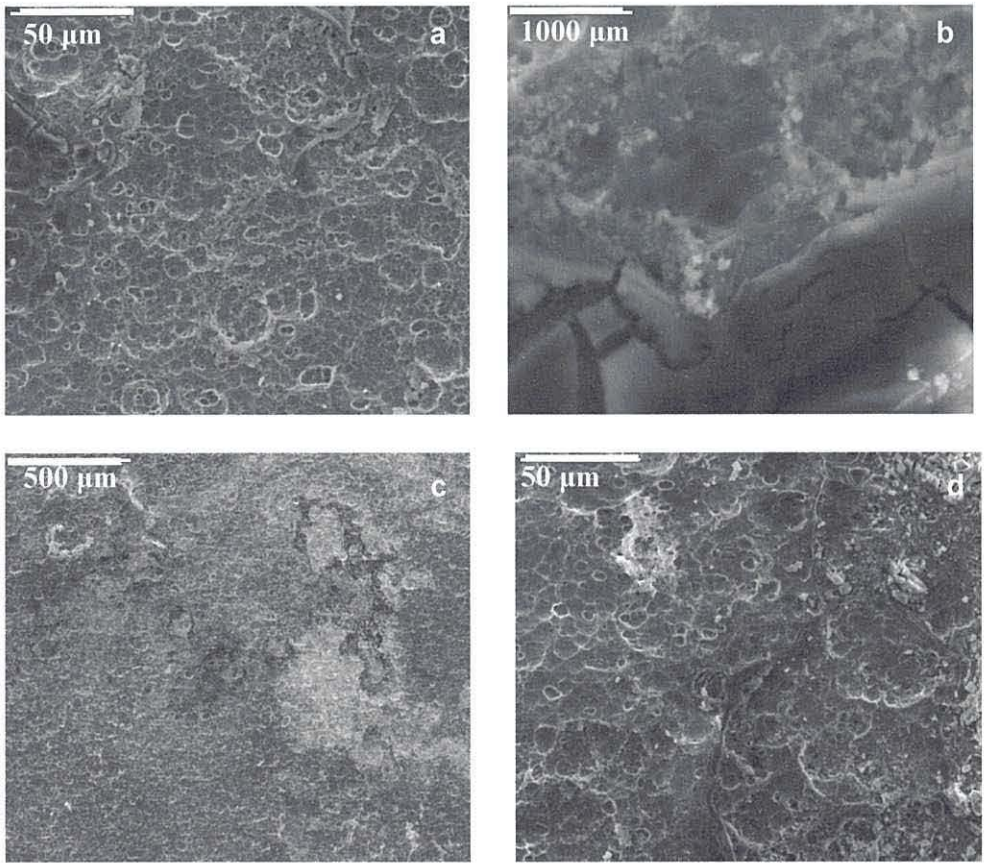

Figure 6.13 SEM images of chromated, oven dried aluminium, after 72 h in AC133

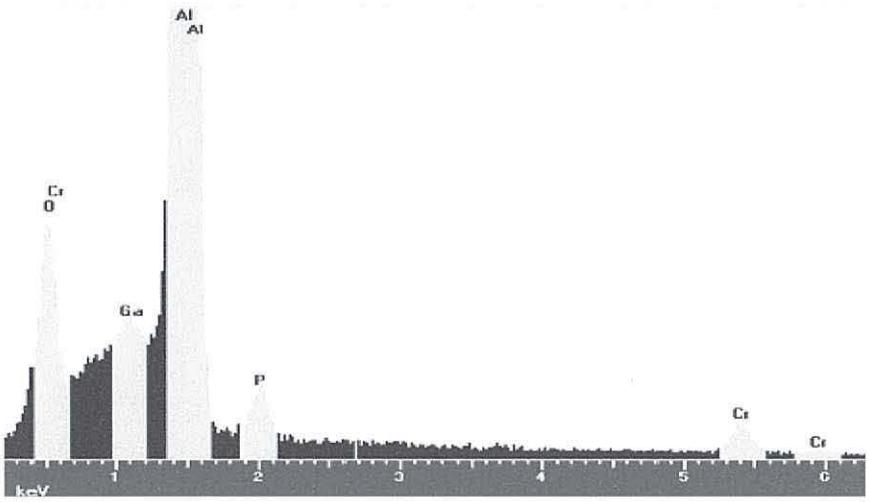

Figure 6.14 EDX analysis of chromate coated, oven dried alloy 3105, prior to corrosion in AC133

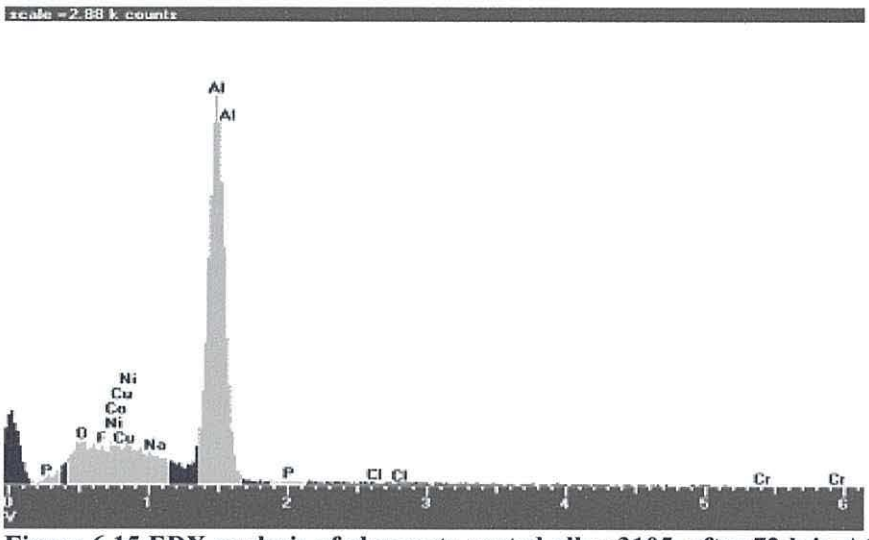

Figure 6.15 EDX analysis of chromate coated alloy 3105, after 72 h in AC133 showing the absence of Cr and P

X-ray diffraction of the samples has also been carried out after the substrate has been exposed to AC133. The data resemble that of the uncoated substrate exposed to HCl, rather than the coated substrate, Figure 6.16. Thus, it would appear that any changes to the surface arise either from non-crystalline material or from the loss of small amounts of crystalline material (aluminium metal) from a bulk substrate of the same phase.

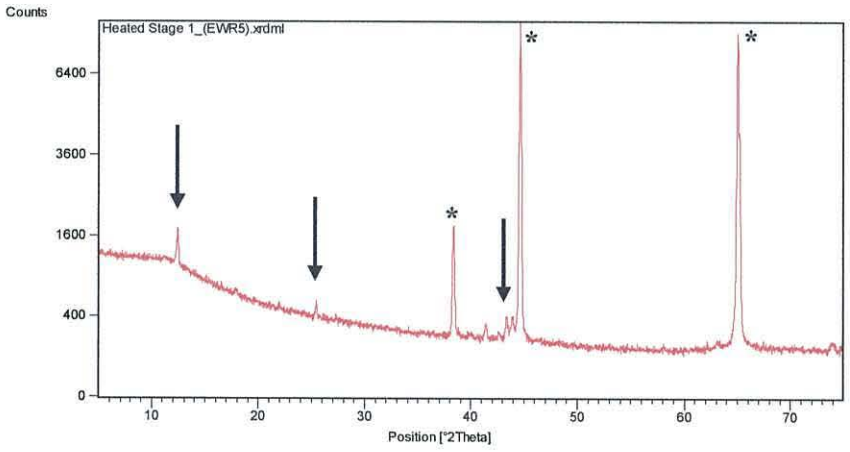

Figure 6.16 XRD of chromate coated, oven dried alloy 3105, after 72 h in AC133. Arrows denote diffraction lines for new phase. Aluminium metal diffraction lines are labelled by *

Machu Solution

The final solution that has been investigated is the Machu solution. This solution contains sodium chloride, glacial acetic acid and hydrogen peroxide. As received and oven dried chromate coated 3105 samples have been placed in Machu solution for 12 hours. After this exposure time, the substrate resulting masses (as a percentage of initial weight) are 86% ± 1.5 and 98.4% ± 0.2%. Optical micrographs of the substrate after exposure to Machu solution are shown in Figure 6.17 showing clear corrosion damage of the surface. This is a promising result because it shows that, in this corrosive solution, the chromate-coated sample shows corrosion resistance that is measurable against the untreated aluminium substrate. This is perhaps to be is expected due to the use of Machu solution by Qualicoat as part of their pretreatment testing. Due to this difference in weight loss between the coated and uncoated substrates in this solution, and the weight loss shown in 12 h, the Machu solution has been further investigated to ascertain it's potential in testing the corrosion resistance of other pretreatments.

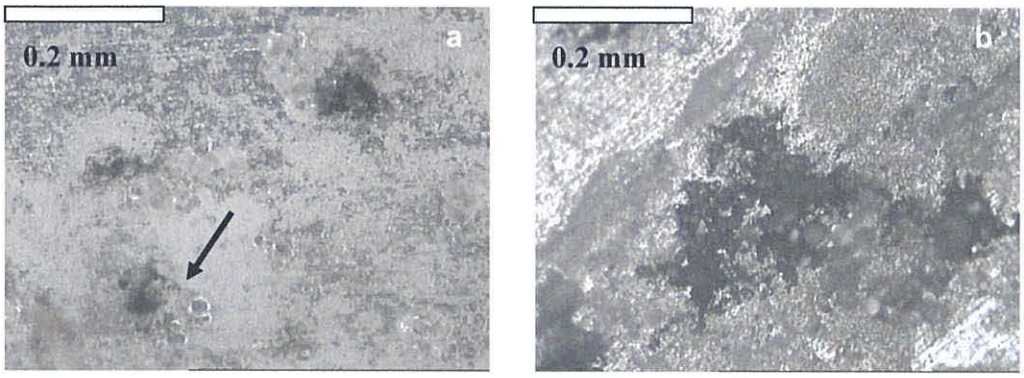

Figure 6.17 Optical microscopy, bright field and dark field, of "as received" alloy 3105 after 12 h in Machu Test solution. (10 x magnification). Arrow shows example of pitting

Thus, a further set of experiments have been designed using as received aluminium, etched aluminium, etched and oven dried aluminium, and oven-dried, chromate coated aluminium. The experiment has been designed to assess the corrosion resistance of these different substrates in Machu solution for various periods of time up to 168 hours. The results of the corrosion damage, or weight loss are presented in Figure 6.18. As

might be expected, the chromate coated samples show the lowest weight loss and hence the least corrosion over time. Interestingly, the untreated substrates show the second best corrosion performance in terms of weight loss, which is probably due to the natural oxide coating formed on aluminium during production. However, when this oxide coating is removed, as in the etched samples, the weight loss increases as the corrosion resistance decreases. The process of oven drying the etched samples, in general, has improved the corrosion resistance, which is assumed to be due to a thicker oxide coating, caused by the heat treatment in an oxygen-containing atmosphere. In addition to weight loss data, it is also evident from visual inspection that the etched samples underwent greatest corrosion, Figure 6.19.

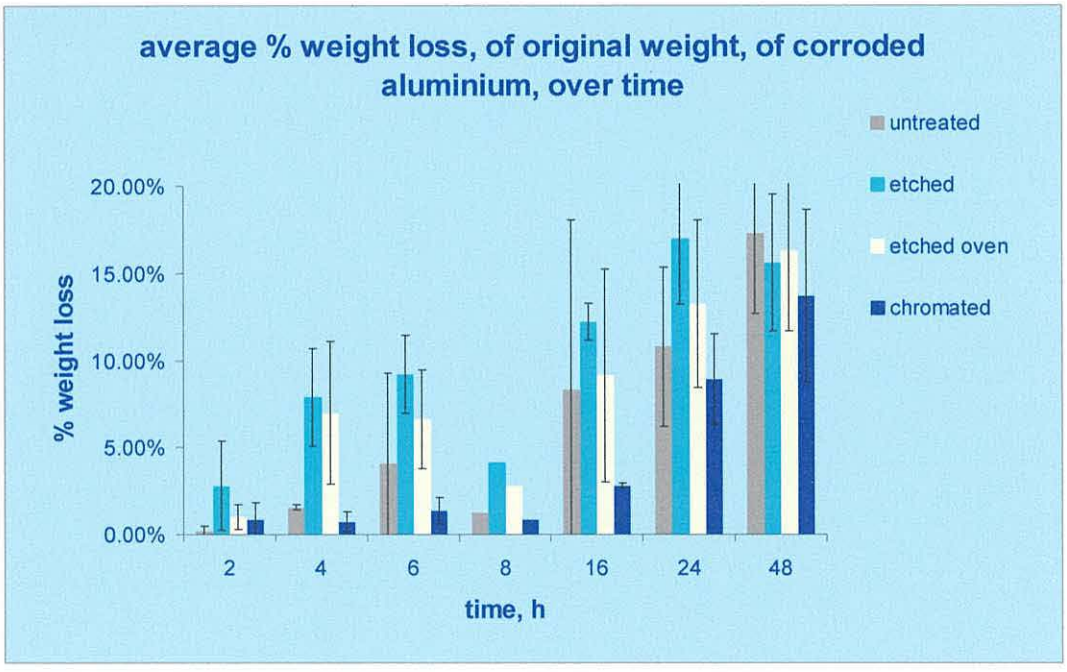

Figure 6.18 Graph of weight loss following corrosion in Machu salt containing solution

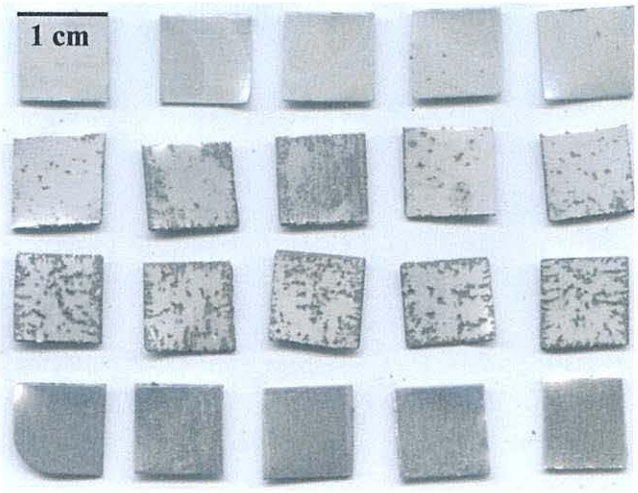

Figure 6.19 Samples following 4 h corrosion in Machu acidic salt containing solution. Treatments are as follows top – bottom rows: chromate coated, etched and oven dried, etched, as received. All substrates shown are alloy 3105

Figure 6.20 Corroded chromate coated alloy 3105 samples following 72 h in Machu acidic salt containing solution. Cut-edge corrosion is visible at the edges

Interestingly, ICP analysis did not indicate any additional chromate in the solutions which had been used to treat the chromate-coated samples, although this may reflect the very small concentrations of chromate likely to be present in a complex solution matrix. Also, when the chromate coated panels do show evidence of corrosion, it appears to occur mainly at the edges of the substrates, Figure 6.20. This type of cut-edge corrosion suggests that the chromate coating on the face of the substrate resists attack by the corrosive solution.

As the greatest difference in corrosion between the etched and chromate coated samples is observed following 16 h of immersion in the Machu solution, the pretreatments previously described in Chapter 3 have been corroded and examined for weight loss

following 16 h in this solution, to assess their performance in this screening test compared to the other testing performed. It has been observed from the previous tests and analysis that the pre-treatments have exhibited corrosion protection categorised as follows: Pretreatment 1 is the worst performing pretreatment, Pretreatment 5 shows a marked improvement compared to Pretreatment 1, with both Pretreatments 9 and 10 performing well. However, that the data from the 16 h corrosion in Machu solution, Figure 6.21, show some discrepancies between this accelerated test and the data reported in Chapters 3 and 4. Pretreatment 6 gives the closest weight loss to the chromate coating, with Pretreatment 1 the next best performing pretreatment. In line with the data from Chapters 3 and 4, Pretreatments 9, 10 and 5 all perform better than the etched and oven dried substrates, with Pretreatment 8 matching the etched and oven dried substrates' performance. Pretreatment 2 performs worse than all of the etched samples, Pretreatments 3, 4 and 7 perform slightly worse than the etched sample.

These data illustrate that this accelerated test does produce data which are broadly comparable to the more extended tests detailed in Chapter 4. However, as might be expected when such an abbreviated test is used, there are some potentially "false" positives (e.g. Pretreatment 1). Overall, the new test can be said to be a success based on the fact that, out of ten pretreatments, it has correctly identified three as being worthy of further study (Pretreatments 5, 9 and 10) whilst also carrying forward Pretreatments 1 and 6 which would subsequently be eliminated following the more detailed and extended testing. Nonetheless, this represents a halving of the number of samples for extended testing which was the original aim of developing this screening procedure.

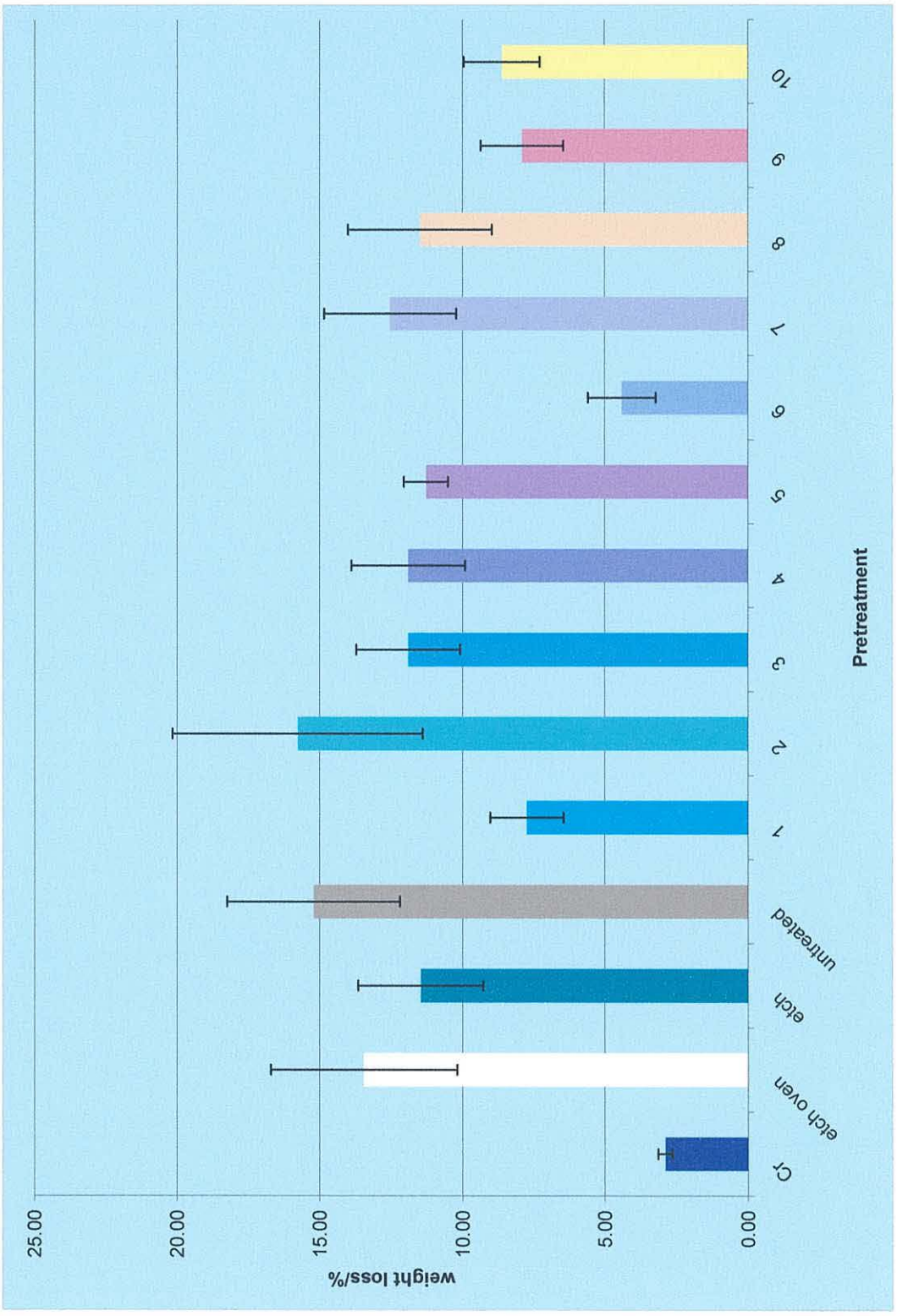

Figure 6.21 Graph showing the weight loss (as a percentage of the original weight) of aluminium alloy 3105 substrates coated with various pretreatments, in Machu solution after 16 h

Unfortunately, time constraints have not allowed for further studies in this area. However, it would be interesting to test the pretreatments following the Qualicoat Machu test specifications – i.e. with a powder coating, scored to expose the pretreatment, to see whether the test results are in agreement with the screening test discussed here, or if they indicate similar results to those of the physical testing although this might extend the test periods beyond the short-term timescale desired from this screening procedure.

Interestingly, when considering the data from this chapter as a whole, the chromate coating does not resist attack in many aqueous solutions, suggesting that either the approach of submerging pretreated panels in solution is too aggressive, or that the pretreatments should be tested along with the powder coating, scored to expose the pretreatment. Another alternative would be to test the pretreatments in mists or humidity of different environments, to eliminate the further variable of the added powder coating, and to more closely resemble the final use of the aluminium extrusions, which should not be in aqueous environments. However, these processes would probably complicate the testing procedures too much for this to be considered a rapid screening test.

References

(1) Shriver, D. F., Atkins, P.W. , Langford, C H., *Inorganic Chemistry*; 2nd ed.; Oxford Uni. Press, 1995.

(2) Van Gheem, E.; Vereecken, J.; Le Pen, C. *Journal of Applied Electrochemistry* **2002**, *32*, 1193-1200.

(3) Na, K.-H.; Pyun, S.-I. *Corrosion Science* **2007**, *49*, 2663-2675.

(4) Van Gils, S.; Melendres, C. A.; Terryn, H.; Stijns, E. *Thin Solid Films The 3rd International Conference on Spectroscopic Ellipsometry* **2004**, *455-456*, 742-746.

(5) Metikos/-e-Hukovica, M., Babica, R., Grubac, Z,. *Journal of Applied Electrochemistry* **1998**, *28*, 433-439.

(6) Cabot, P. L.; Centellas, F. A.; Garrido, J. A.; Perez, E.; Vidal, H. *Electrochimica Acta* **1991**, *36*, 179-187.

(7) Wiersma, B. J., Herbert, K.R., *Journal of the Electrochemical Society* **1991**, *138*, 48.

(8) Lin, W., Tu, G.C., Lin, C.F., Peng, Y.M., *Corrosion Science* **1997**, *39*, 1531.

(9) Abiola, O. K.; Oforka, N. C.; Angaye, S. S. *Materials Letters* **2004**, *58*, 3461-3466.

(10) Holliman, P. J., Hughes, D.D. *Physical Chemistry Chemical Physics* **1999**, *1*, 4091-4097.

(11) Brown, G. M.; Shimizu, K.; Kobayashi, K.; Thompson, G. E.; Wood, G. C. *Corrosion Science* **1993**, *34*, 1045-1054.

(12) Lunder, O.; Lapique, F.; Johnsen, B.; Nisancioglu, K. *International Journal of Adhesion and Adhesives* **2004**, *24*, 107-117.

(13) Lunder, O.; Walmsley, J. C.; Mack, P.; Nisancioglu, K. *Corrosion Science* **2005**, *47*, 1604-1624.

7. Experimental

Aluminium alloys

Alloy 3105 panels were purchased from Q - Panel Lab Products, Bolton, (alloy 3105 H24, 0.6 mm thickness), with the following percentage elemental composition: Al, 97.07-95.95; Cr, 0.2; Cu, 0.3; Fe, 0.7; Mn, 0.3-0.8; Mg, 0.2-0.8; Si, 0.6; Ti, 0.1; Zn, 0.4; others (total) – 0.15).

The 6063 aluminium extrusions were gifted by Kawneer, Runcorn, and were produced to the commercial specifications detailed in Chapter 1 for aluminium extrusions.

Panels for SEM, EDX, AFM, electrochemical or corrosion solution testing were cut into 10 x 10 mm sections. Prior to use, all substrates were acetone degreased for 30 seconds, oven dried at 90 °C for 10 minutes and then dessicator cooled for a minimum of 30 minutes.

Surface preparation

Surface preparation was carried out to Qualicoat specifications, which were applied to the etched, and chromate-coated samples. The degree of etching specified for extruded sections such as those studied in this project is 1 g m^{-2}. However, Almetron Ltd, Wrecsam, specify 2 g m^{-2}, and hence this weight loss has been adhered to in this work. The chromate coatings applied in this thesis are classified as chromate-phosphate conversion coatings, with an application weight between 0.6 and 1.5 g m^{-2}. Plastic or stainless steel equipment was used throughout.

Acid Etch AC133

The acid cleaner used throughout this thesis is a commercial acid cleaner AC133, gifted by Almetron Ltd, which consists of ammonium hydrogen fluoride (ammonium bifluoride) and phosphoric acid. The technical data sheet advises a concentration of around 5 % bath strength for weight loss of > 2 g m^{-2}, in around 5 min, which corresponds to a fluoride strength of over 1,000 mg l^{-1}. For the small 10 x 10 mm aluminium coupons produced for the SEM, TEM, AFM, electrochemical and corrosive solution screening tests, the actual AC133 concentration used was 20 % by weight to achieve weight loss of > 2 g $^{-2}$ in 6 min.

Etch times were normally 6 minutes, followed by a DI rinse with reference samples being weighed before and after etching to confirm adequate weight loss to ensure a chemically clean surface. Etch baths were discarded after three cycles.

Chromating

Chromate coatings were produced from a commercial 2 pack system gifted by Almetron Ltd, Wrecsam; Kromal GA and Kromal GB. These solutions contain chromic acid, phosphoric acid and ammonium hydrogen fluoride. The coating process followed etching immediately (following a DI rinse). Operating conditions used were 3% GA, 1 % GB, at room temperature, for 3 minutes, followed by a DI rinse, to produce a coating of between 0.6 and 1.5 g m^{-2} as specified by Qualicoat. Samples were weighed when dry, either oven dried at 140°C or air dried as described in the thesis, and baths were discarded after three cycles.

Pretreatment solutions

The pretreatments described in Chapter 3 were prepared from the following chemicals sourced from Aldrich with the concentration of the component chemicals in g l^{-1}:

Pretreatment ($g\ l^{-)1}$	H_2F_6Zr	H_2F_6Ti	NH_4HF_2	PAA	PVA	$NiSO_4$	pH
1	7.56						1.85
2		8.375					0.76
3	3.48	8.375					0.88
4	3.48	8.375		0.17			0.94
5	0.348	0.8375		0.02			1.41
6	2.52		0.4	0.19			1.97
7	2.52	5.25	0.4	0.19			1.78
8	2.52	5.25	0.4	1			1.93
9	2.52	5.25		0.25	0.1		2.11
10	2.52	5.25				3.5	2.09

Powder Coating

Powder coating was carried out with a hand held electrostatic powder coating gun in a custom built booth. Polyester clear and beige powders were gifted by Almteron.

Instrumentation/Characterisation Techniques

Scanning electron microscopy (SEM) was measured at 10 kV on a Hitachi S-520 SEM. EDX was measured on the same instrument at 10 kV or 14 kV with an Oxford Instruments 7497 EDX with Link ISIS computer software. Prior to analysis, samples were placed on conductive carbon tape on an aluminium stub.

Optical microscopy was carried out using a Leica DMLM Microscope, with a Mercury Hg 50 light source and daylight filter, with normal optics for both bright and dark field

observation. Images were recorded using a Digital JVC colour video camera using Win TV2K software.

AFM measurements were carried out on a Digital Instruments NanoScope 3100, with NanoScope 7.10 software used for analysis.

TEM analysis was carried out by Dr Xiarang Zhou in the Corrosion Protection Centre at Manchester University. Prior to analysis, sections were cut from the panels following Lockheed testing. Ultramicrotomed sections were prepared using a Leica 2 Archocut instrument, producing nominal sections of 10 nm (30-40 nm real). A diamond knife was used to prepare the cross sections, at 0.3 μm s^{-1}, with a glass knife used for trimming. A Jeol 2000 FX2 TEM instrument was used at 120 kV, a vacuum of 10^{-7} Torr giving a spatial resolution of 0.2 nm. The EDX probe used, Oxford Instruments, has a 20 nm spot size.

X-ray powder diffraction was carried out using Ni-filtered Cu Kα1 radiation (λ = 1.54051 Å) on a X'Pert PRO theta-theta diffractometer (PANalytical Ltd) at 45 kV and 35 mA. Data was collected using X'pert Industry and analysed using Highscore software packages (PANalytical Ltd). Samples were analyzed in continuous scan mode (counting 10s per 0.010 °2θ) between 5 and 75 °2θ.

ICP analysis was carried out using a Jobin Yvon emission JY138 Ultrace instrument. Calibration was by in house standards prepared from Analar grade stock solution.

Physical Testing

Adhesion testing was carried out in line with Qualicoat specifications, at the Kawneer Laboratories, Runcorn with details listed below. Inspection for detachment also included attempting to remove the powder coating with a sharp instrument.

Sawing and drilling

These tests were carried out on both alloy types. One drill hole was produced on each panel tested, and a saw indentation to the edge of the panel, extending 1 cm, through the panel was also produced. The powder coating was examined for cracking, or detachment/chips, as a measure of adhesion.

Cross-hatching test

The powder coating was deformed in a cross-hatch pattern, using a specific cross-hatch tool at spacings of 5 mm, in both the vertical and horizontal direction to produce a cross-hatched grid. The tape-pull adhesion test was then carried out by applying Scotch 610 tape firmly to the cross-hatched area. The tape was then pulled off sharply at right angles to the plane of the panel after 1 minute. The powder coating was then examined for cracking and detachment.

Bend test

The bend test was carried out using a Conical Mandrel bend tester. This test was performed on alloy 3015 only, as the thickness of the 6063 extrusion prevented this test from being possible. The 3105 alloy panels were placed in the mandrel and bent over the mandrel. The powder coating was inspected for cracking and detachment.

Impact test

The impact test was carried out using a hemispherical weight of 1 kg dropped from a height of 0.5 m onto the metal panel, causing an indent at the area of impact The powder coating was inspected, both sides, for evidence of cracking or detachment. Here, as for the bend test, the thickness of the 6063 extrusion prevented this test from being possible valuable, as the impact did not produce an indent in these thick extrusions.

Acetic acid salt spray testing

This test was carried out according to Qualicoat specification, at the Almetron Ltd laboratories, Wrecsam. Two cross-cut incisions of width 1 mm were cut into the powder coating, using a specific scratching tool, to expose the underlying pretreated metal. The panels were then placed upright in a humidity chamber and exposed to mists of glacial acetic acid, 7.5 ml l^{-1} and 50 g l^{-1} sodium chloride for 1000 h. The panels were inspected for blistering, detachment and filaments of corrosion – filiform corrosion.

Lockheed testing

Lockheed humidity testing was carried out at the Innoval Laboratories, Banbury. Panels were scribed to expose the underlying pretreatment both parallel and perpendicular to the rolling/extrusion direction, before being inoculated with 16 % HCl and placed in a cabinet at 85 % relative humidity. The samples were removed, visually examined and scanned/photographed at intervals of 24, 250, 500 h and finally at 1000 h at which point the test was complete. Samples were then sent to Dr X Zhou, Manchester University. Corrosion Protection Centre for TEM analysis as described above.

Electrochemical methods

All measurements were performed using an AUTOLAB ECO CHEMIE IME663. The analysis was carried out with a three-electrode cell, Figure 7.1, using a saturated calomel reference electrode and a platinum counter electrode. Prior to use, the cell was cleaned using a 50:50 mixture of concentrated H_2SO_4:HNO_3 followed by rinsing in deionised water (nominal resistivity > 18 MΩ cm at 25 °C), cleaning in a steam bath, and drying in the oven. The working electrode was the 10 x 10 mm aluminium substrate, prepared according to the etch / pretreatments previously described. The sodium chloride solution, 0.5 g\l, was acidified to pH 3.1-3.3 with acetic acid. The measurements were all taken at a scan rate of 50 mV s^{-1}.

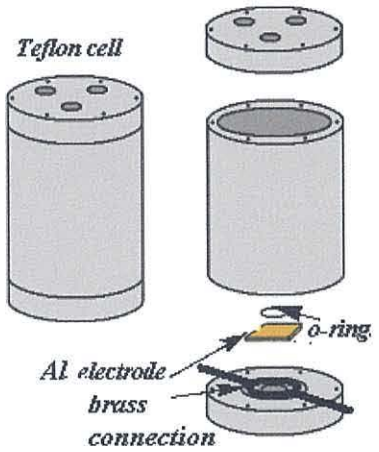

Figure 7.1 A pictorial representation of the home made Teflon electrochemical cell

Corrosion in various solutions

Solutions were prepared to concentrations as specified below and in Chapter 6, and 20 ml of the appropriate solution was placed in an plastic beaker, with one aluminium sample per container. Chrome coated, both air and oven dried, etched and as received samples, prepared to the specifications already described, were used for comparison, and five replicates of each made. Where scoring is mentioned, this was carried out by use of a sharp instrument. At various times, depending on the corrosive nature of the

solution, and specified in the discussion, samples would be removed, rinsed with DI, and left to dry in air, before being weighed.

The corrosive solutions used were:-

- Concentrated HCl (12 M)
- HCl (6 M)
- HCl (1 M)
- NaCl (1 M)
- CH_3COOH (5 M)
- NH_4Cl (1 M)
- NaOH (1 M)
- 20 % AC133 – commercial reagent containing ammonium hydrogen fluoride and phosphoric acid
- Machu Solution – This solution was prepared based on an accelerated corrosion test specified by Qualicoat for pretreated painted panels, lasting 48 hours. The actual method adopted involved making a solution containing NaCl (50 g l^{-1}), glacial CH_3COOH (10 ml l^{-1}), and 60 % H_2O_2 (4 ml l^{-1}).
- Deionised and tap water

8. Conclusions

This thesis describes studies of the development of novel, chrome-free pretreatments for the corrosion protection of aluminium. This is a challenging task because chromate based coatings have been used for many years for corrosion treatment of aluminium, and also because the desired working lifetime for any such coating is 25 years. This extended time period not only makes severe demands on the coating but also complicates coating assessment because accelerated corrosion tests are required. The thesis describes how, as well as investigating the new pretreatments *via* microscopic techniques and accelerated corrosion testing, their electrochemical behaviour has also been examined by cyclic voltammetry, and a rapid screening test has been developed and assessed against the information already acquired.

In summary, Chapter 1 puts the research carried out in this thesis into context by describing the background of how aluminium is made and the different aluminium alloys including their composition, uses and the corrosion issues associated with some of these alloys. This chapter also includes a review of published research into chrome-free coatings for aluminium and includes some examples of the characterisation of these coatings which provides useful data for comparison with the new coatings described in this thesis.

Following on from this, the thesis is organised in the logical manner in which the problem of coating development was approached. Thus, Chapter 2 begins the research by describing the preparation steps necessary to ensure adequate and consistent preparation of the alloys before any pretreatments can be applied. This chapter describes a detailed study of the etching and subsequent morphology of both alloys

3105 and 6063. The data show that the commercial etch solution, AC133, appears to etch both alloys effectively over a short time period suitable for commercial processing (6 min). The data also show interesting comparisons in behaviour between the two alloys which are believed to be associated with differences in alloy composition and processing history prior to etching. Firstly, for alloy 3105, an interesting morphology consisting of pitting rather than scalloping is observed after etching with AC133. This pitted morphology has not been reported before in the literature for this alloy and it is hoped that this will be a suitable substrate for subsequent coating pretreatment. For alloy 6063, a similar pitted morphology was observed along with grain boundries. However, much less etching was apparent for alloy 6063 after 6 min exposure to AC133 compared to alloy 3105 which may be related to the composition of this alloy.

Chapter 3 describes the development of chrome-free pretreatments for alloys 3105 and 6063. The coatings are believed to be based on a sol gel type process using fluorozirconic and/or fluorotitanic acid as precursors. The coatings appear to involve both etch and deposition processes occurring simultaneously. Thus, the data show that precursor concentration is important to prevent over etching of the surface. This chapter also describes the analysis of the pretreatments, obtained using SEM, TEM and EDX techniques. The TEM data suggest that the process of ultramicrotoming causes detachment of the Pretreatments 1-5, either from the metal oxide itself, or by detachment between the pretreatment and the paint layer which suggests that coating adhesion is insufficient for any of these coatings to be effective in the long term. However, general improvement is observed with each pretreatment (in the order 1-5). The corresponding SEM data for these pretreatments also suggest uneven coverage across the alloy surfaces. By comparision, the SEM and EDX data for Pretreatments 6-10 are more promising which suggests that the addition of polymers to the precursor

solution is important. These polymers are believed to act as flocculating agents to bring the coating particles together to improve coverage. In line with these assertions, the data indicate that Pretreatment 9 which contains two different polymers provides the most uniform coating, with Pretreatment 10 also providing good surface coverage with limited flaking.

In agreement with the information obtained from Chapter 3, the accelerated corrosion testing described in Chapter 4 reveals improvement in corrosion performance from Pretreatment 1 through to 5. Pretreatments 6-10 perform generally well in corrosion testing, with Pretreatments 6, 9 and 10 showing excellent results. However, whilst showing little filiform corrosion in the accelerated corrosion testing, Pretreatments 6 showed adhesion failure in the physical testing, possibly indicating poor adhesion with the powder paint coating. Thus, the best corrosion performance is observed for Pretreatments 9 and 10 which is in line with the data from Chapter 3.

Chapter 5 reveals that the results obtained from the electrochemical experiments provide some interesting data which do show an enhanced corrosion protection for chrome-based coatings. However, the data for the new pretreatments do not correlate as would have been expected when considering the results from Chapters 3 and 4. This may suggest a different mechanism of corrosion protection in the new pretreatments compared to chrome based systems where self-healing is known to occur.

The attempts to develop a novel and much more rapid pretreatment screening procedure described in Chapter 6 did not show comparable results to those in Chapters 2 and 3. Instead, this new procedure indicated that Pretreatments 1 and 6 were likely to be the best performers. By definition, any method of accelerated corrosion testing must be

subject to errors as there is such a large extrapolation in time and this effect must get larger, the shorter the time period used. Given the errors observed here, this new testing method may not be the best method to screen coatings initially before subsequent longer term testing.

Time constraints has limited the extent of research presented in this thesis, and there are many avenues for further work to be carried out. TEM analysis of all the pretreatments investigated, both on alloy 3105 and 6063, and in particular these alloys in their as received and etched conditions, would be extremely interesting to examine and would provide further valuable information about the etching effect on morpholgy of AC133, the changes in morphology between the etching process and pretreatment application. Investigating Pretreatments 6-10 would give insight into how the pretreatments bond to the metal substrate and further information on adhesion. In particular, the bonding of Pretreatments 9 and 10 - and whether detachment has occurred - would be of great value, and might prove that evidence of adhesion following the processes carried out to prepare the TEM is a critical test in seeking an effective pretreatment.

Further investigations into different etch solutions, their composition and resulting morphology would also be of interest, in particular the effect of phosphoric acid, which is not typically used in etch treatments, sulphuric acid and nitric acid being more widely used. It has already been noted that the etch used, AC133, does not provide a morphology typical to that discussed in literature, which may be related to the fluoride content of the etch. Given that promising pretreatments have been identified, examining some of the pretreatments following different etch processes would also be valuable in assessing the optimisation of the pretreatment application process as a whole.

From the data presented in Chapter 4, two possible pretreatments stand out in terms of corrosion protection, Pretreatment 9 and 10. From an SEM perspective, Pretreatment 9 appears to be the most successful, exhibiting the best surface coverage from this plan view analysis. Further development of these pretreatments for commercial use would include bath life/chemical consumption analysis. The benefits of additional chemicals could also be investigated, such as surfactants, which might prove critical in providing more uniform surface coverage for Pretreatment 10. If this were found to be the case, it would indicate that the surface may not be adequately wetted during coating which may indicate that there is scope for further etch development as discussed earlier.

Overall, although the additional electrochemical testing and rapid screening test have not provided directly correlating information with the earlier chapters compared with the accelerated corrosion testing required by industry, Pretreatments 9 and 10 provide excellent corrosion protection results, and it is believed that both of these coatings should be suitable for commercial use. On this basis, the industrial partner of the CASE award (Almetron Ltd) is currently optimising and assessing bath life for these pretreatments, and will shortly be applying for independent approval by Qualicoat.